Analysis and modelling of Morphodynamics of the Yangtze Estuary

Chu, Ao

DOI
10.4233/uuid:068a1257-dfc2-4389-964e-f665aa5cb213

Publication date
2019

Document Version
Final published version

Citation (APA)
Chu, A. (2019). *Analysis and modelling of Morphodynamics of the Yangtze Estuary*. [Dissertation (TU Delft), Delft University of Technology]. https://doi.org/10.4233/uuid:068a1257-dfc2-4389-964e-f665aa5cb213

Analysis and modelling of Morphodynamics of the Yangtze Estuary

Analysis and modelling of Morphodynamics of the Yangtze Estuary

PROEFSCHRIFT

ter verkrijging van de graad van doctor
aan de Technische Universiteit Delft
op gezag van de Rector Magnificus prof.dr.ir. T.H.J.J van der Hagen
voorzitter van het College voor Promoties,
in het openbaar te verdedigen op woensdag 03 juli 2019 om 15:00 uur

door

Ao CHU
Master of science in Hydraulic Engineering, IHE, Delft
geboren te Shanghai, China

Dit manuscript is goedgekeurd door de promotoren:
Prof. dr. ir. Z.B. Wang
Prof. dr. ir. S.G.J. Aarninkhof

Samenstelling promotiecommissie:

Rector Magnificus	voorzitter
Prof. dr. ir. Z.B. Wang	Technische Universiteit Delft, promotor
Prof. dr. ir. S.G.J. Aarninkhof	Technische Universiteit Delft, promotor

Onafhankelijke leden:

Prof. dr. ir. M.J.F. Stive	Technische Universiteit Delft
Prof. dr. ir. J.D. Pietrzak	Technische Universiteit Delft
Prof. dr. Y.P. Chen	Hohai University, China
Prof. dr. ir. P. Hoekstra	Universiteit Utrecht

Other member:

Prof. dr. ir. H.J de Vriend	Technische Universiteit Delft

This research has been financially supported by the National Nature Science Foundation of China (No. 51620105005), the National R&D Projects of China (No. 2017YFC0405401), the Lamminga Fund of Delft University of Technology and the China Scholar Council, and KNAW (No. PSA-SA-E-02).

Cover picture: air view of the diversion head of the Deep Draft Channel project under construction. Image from Yangtze Estuary Water Administration Bureau, MOC.

ISBN: 978-94-6366-191-1

Summary

The flow and sediment transport in the Yangtze Estuary are intrinsically complex because various processes and mechanisms are involved on a large range of temporal and spatial scales. In this thesis the interaction of river discharge and tidal wave with the corresponding sediment transport in the Yangtze Estuary is investigated. The objective is to gain further understanding of the processes and mechanisms dominating the sediment transport in the estuary. Based on the understanding of flow and sediment transport, a morphodynamic model is established and tested to simulate the morphological change of the Yangtze Estuary.

Supported by a literature survey reviewing previous studies, the observed data (including water levels, currents, salinity, sediment concentration, sediment samples, etc.) at various stations under different conditions (spring/neap tide, dry/wet season, etc.) are first analyzed to investigate the characteristics of flow and sediment transport in the Yangtze Estuary. Subsequently, a process-based model based on Delft3D is set up for the estuary. After being calibrated and validated against measurements under various conditions, the model is used to simulate the sediment transport at the mouth bar of the Yangtze Estuary. Scenarios of model simulations are designed to account for different combinations of processes and mechanisms contributing to sediment transport. The results demonstrate that taking salinity processes into consideration is a prerequisite to understand how fine sediment has been trapped in the mouth bar area of the Yangtze Estuary in the last half century. It is also concluded that flocculation of fine-grained sediment in suspension enhances the sediment deposition in the mouth bar area. The net effect of all sediment transport processes is typical sedimentation in the wet season and erosion in the dry season, with net deposition annually. A decreasing trend in the annual net deposition has recently become visible. The deposition rate at present is down to 1/3 of the magnitude in the past.

According to the results of the process-based flow model study, a morphodynamic model for the estuary requires to be three-dimensional and needs to include processes of salinity, flocculation of fine-grained sediment, etc., besides the primary driving forces of river discharge and tides. It is too time-consuming and unpractical to apply a 3D morphodynamic model of the Yangtze Estuary for long-term simulations. Therefore, a model input reduction for tides and river discharges is used to reduce the computational effort. However, as is different from most previous studies, the large river discharge from the Yangtze River results in a significant residual flow velocity in the estuary. This gives two complications for model input reduction: (1) the influence

of residual flow on the schematization of the morphological tide (Chapter 5); (2) an extra dimension of varying discharge (Chapter 6). Regarding the first aspect, the approach of Van de Kreeke and Robaczewska (VDK&R, 1993) for the residual coarse sediment transport with negligible residual flow velocity is extended to the estuarine environment with remarkable residual flow velocity induced by river discharge, even though we know that the fine sediment is dominating in the study area. The analytical expression of VDK&R (1993) indicates the interactions of M_2 & M_0, M_2 & M_4 and the triad interaction of M_2, M_4 & M_6 yielding a long-term residual coarse sediment flux. As a consequence, the representative tide only consisting of M_2, M_4 and M_6 might be applicable for the coastal environment with a negligible (with respect to M_2) M_0. The present analytical solution reveals that other interactions of tidal current constituents also contribute to the residual sediment flux, especially the interactions of all tidal constituents with M_0 and the triad interactions of (M_2, S_2 & MS_4), (M_2, N_2 & MN_4) and (M_2, K_1 & O_1). Therefore, the tides consisting of M_2, S_2, N_2, M_4, MS_4, MN_4, M_6, K_1 & O_1 and other important constituents should be included in tidal input reduction for the Yangtze Estuary morphodynamic model. Although such a conclusion on tidal force input reduction is (usually) for coarse sediment, it is also applicable for fine sediment transport in the study area. Regarding the second aspect, the classic method (Latteux, 1995) to determine a representative tide is also applied to the Yangtze Estuary morphodynamic model with varying discharge from upstream. The sediment transport rate in the estuary shows large variations with different discharges from upstream. This reveals that the variation of discharge is another free parameter for the model input reduction of such a morphodynamic model, which is proposed by the multi-discharge levels with their probability of occurrence to be reduced.

For morphodynamic modelling of the Yangtze Estuary, the modified parallel Mor-Merge (MM) approach (Roelvink, 2006) with multiple discharge levels and a full spring-neap tidal water level series is applied together with the Morphological acceleration Factor (MorFac). This approach is first tested by comparing the MM model result with the result of the Quasi Real Time (QRT) model of the Yangtze Estuary for the period of 1998-1999. The result indicates that the MM model reasonably captures the erosion and sedimentation features of the QRT simulation. The number of discharge levels, required to drive the morphodynamic model, follows from the balance between computational effort and accuracy. A schematization with six discharge levels is recommended for the Yangtze Estuary case. The Yangtze Estuary morphodynamic model is further applied to hind cast the bathymetry changes from 1965 to 1986. The model results for a smaller value of MorFac seem more pronounced than those for larger values. Several important features are represented by the model, but large discrepancies

between model results and measurements are also observed, especially in cases with larger values of MorFac. Apart from the value of MorFac, the morphodynamic model results are sensitive to the bottom boundary condition for the sediment transport, i.e. the bed composition. As the parallel technique is used in the MM approach, the sequence of discharge levels or the seasonal variation cannot be considered. Thus, the presented Yangtze Estuary morphodynamic model is designed for long-term simulations. Although the morphodynamic modelling for the Yangtze Estuary is feasible with the present MM approach, it indicates that such morphodynamic modelling for estuaries requires more research efforts before practical application.

Samenvatting

Stroom-en sedimenttransporten in de monding van de Yangtze Rivier zijn intrinsiek complex omdat hierbij op grote temporele en ruimtelijke schalen verschillende processen en mechanismen betrokken zijn. In deze thesis wordt de interactie onderzocht van rivierafvoer en getijdebeweging met het bijbehorende sedimenttransport in het estuarium van de Yangtze. Het doel is om meer inzicht te krijgen in de processen en mechanismen die het sedimenttransport in de monding domineren. Gebaseerd op het begrip van stroom- en sediment-transport, wordt een morfodynamisch model geconstrueerd en getest om de morfologische verandering in het estuarium van de Yangtze te simuleren.

Ondersteund door literatuurstudie van eerder onderzoek, zijn op de eerste plaats de waargenomen gegevens (waaronder: waterniveau, stromingen, zoutgehalte, sediment concentratie, sedimentmonsters, enz.) op verschillende meetstations onder verschillende condities (zoals springvloed/doodtij, droog/nat seizoen, enz.) geanalyseerd om de kenmerken van stroom- en sedimenttransport in het estuarium van de Yangtze te onderzoeken. Vervolgens wordt een op Delft3D gebaseerd procesmodel opgezet voor het estuarium. Na te zijn gekalibreerd en gevalideerd met metingen onder verschillende omstandigheden, wordt het model gebruikt om het sedimenttransport te simuleren bij de“mouth bar” van het estuarium van de Yangtze. Scenario's van modelsimulaties zijn ontworpen, rekening houdend met de verschillende combinaties van processen en mechanismen die bijdragen aan het sedimenttransport. De resultaten tonen aan dat in achtname van processen, gerelateerd aan het lokale zoutgehalte, voorwaarden zijn om te begrijpen hoe het fijne sediment in de afgelopen 50 jaar gevangen is in de gebied van de “mouth bar” van het estuarium van de Yangtze. Ook wordt geconcludeerd dat vlokvorming van fijnkorrelig sediment in suspensie de sedimentdepositie in het “mouth bar” gebied vergroot. Het netto-effect van alle sedimenttransport processen is over het algemeen sedimentatie in het natte seizoen en erosie in het droge seizoen, met een jaarlijkse netto depositie. Een dalende tendens in de jaarlijkse netto depositie is recentelijk zichtbaar geworden. De depositie graad is momenteel gedaald tot 1/3 van de omvang in het verleden.

Volgens de resultaten van de studie van de op het betreffende processen gebaseerde stroommodel, is het noodzakelijk dat een morfodynamisch model drie-dimensionaal moet zijn, inclusief processen van zoutgehalte, vlokvorming van fijnkorrelig sediment, enz., naast de primaire krachten van rivierafvoer en getijden. Het is te tijdrovend en te

onpraktisch om een 3D morfodynamisch model van het estuarium van de Yangtze toe te passen voor lange-termijn simulaties. Daarom is een gereduceerd model ingevoerd voor getijden en rivierafvoer om de computationele tijd te beperken. Echter, anders dan in eerdere studies, resulteert de rivierafvoer van de Yangtze Rivier in een significante reststroom-snelheid in het estuarium. Dit geeft twee complicaties voor de reductie van de model-input: (1) de invloed van de reststroom op de schematizatie van het morfologisch getij (Hoofdstuk 5); (2) een extra dimensie van variërende afvoer (Hoofdstuk 6). Met betrekking tot het eerste aspect, wordt de aanpak van Van De Kreeke en Robaczewska (VDK. & R., 1993) voor het overblijvend grove sedimenttransport met een verwaarloosbare reststroom-snelheid uitgebreid tot de estuariene omgeving, met als gevolg een opmerkelijke reststroom-snelheid, te weeg gebracht door de rivier afvoer, ook al weten we dat het fijne sediment in het studiegebied domineert. De analytische formulering van VDK. & R. (1993) geeft de interacties aan van M_2 & M_0, M_2 & M_4 en de drievoudige interactie van M_2, M_4 & M_6, resulterend in een lange termijn fluctuatie van resterend grof sediment. Het representatieve getij, slechts bestaande uit M_2, M_4 en M_6, kan daardoor van toepassing zijn voor de kustomgeving, met een verwaarloosbaar effect van (m.b.t. M_2) M_0. De huidige analytische oplossing laat zien dat andere interacties van bestanddelen van de getijdestroom ook bijdragen aan de residuele sediment flutuatie, met name de interacties van alle getijde bestanddelen met M_0 en de drievoudige interacties van (M_2, S_2 & MS_4), (M_2, N_2 & MN_4) en (M_2, K_1 & O_1). Daarom, zouden de getijden, bestaande uit M_2, S_2, N_2, M_4 M_4, Mn_4, M_6, K_1 & O_1 en andere belangrijke bestanddelen, moeten worden opgenomen in de getijde input reductie voor het morfodynamisch model van het estuarium van de Yangtze Rivier. Hoewel een dergelijke conclusie over de getijde input reductie meestal grof sediment betreft, is deze ook toepasbaar voor het fijn sedimenttransport in het studiegebied. Met betrekking tot het tweede aspect, de klassieke methode (Latteux, 1995) om het representatieve getijde te bepalen wordt ook toegepast op het morfodynamisch model voor het estuarium van de Yangtze met variabele stroomopwaartse afvoer. De mate van het sedimenttransport in de monding toont grote variatie in verschillende stroomopwaartse afvoer. Hieruit blijkt dat variatie van afvoer een andere vrije parameter is voor de gereduceerde model-input van een dergelijk morfodynamisch model, welk wordt voorgesteld door de veelvoudige afvoer- niveaus met een verlaagde waarschijnlijkheid van voorkomen.

Voor de morfodynamisch modellering van het estuarium van de Yangtze, wordt de gewijzigde parallelle “Mor-Merge” (MM) benadering (Roelvink, 2006) met meerdere afvoerniveaus en een volledige spring-doodtij waterniveau-serie toegepast samen met de “Morphological acceleration Factor”(MorFac). Deze aanpak wordt eerst getest door

vergelijking van het resultaat van het MM model met het resultaat van het “Quasi Real TIME”(QRT) model van het estuarium van de Yangtze Rivier voor de periode van 1998-1999. Het resultaat geeft aan dat het MM model redelijkerwijs de kenmerken van erosie en sedimentatie van de QRT simulatie vastlegt. Het aantal afvoerniveaus, welke vereist zijn voor het aansturen van het morfodynamisch model, komt voort uit het evenwicht tussen computationele inspanning en nauwkeurigheid. Een schematisatie met zes afvoer niveaus wordt aanbevolen voor het estuarium van de Yangtze case. Het morfodynamische model voor het estuarium van de Yangtze wordt verder toegepast op de hindcast van de bathymetrische veranderingen van 1965 tot 1986. De resultaten van het model m.b.t. een kleinere waarde van MorFac lijken meer uitgesproken dan de resultaten voor de hogere waarden. Diverse belangrijke eigenschappen worden vertegenwoordigd door het model, maar grote discrepanties tussen model resultaten en metingen worden ook waargenomen, vooral in gevallen met hogere waarden van MorFac. Afgezien van de waarde van MorFac, zijn de resultaten van het morfodynamische model gevoelig voor de basis-grensvoorwaarde van het sediment transport, dat wil zeggen, de samenstelling van de rivierbedding. Als de parallelle techniek wordt gebruikt in de MM-benadering, kan de volgorde van de afvoerniveaus of de seizoensgebonden variatie niet worden overwogen. Zo is het voorgestelde morfodynamische model voor het estuarium van de Yangtze ontworpen voor lange-termijn simulaties. Hoewel de morfodynamische modellering voor het estuarium van de Yangtze haalbaar is met de huidige MM-benadering, geeft het ook aan dat een dergelijke morfodynamische modellering voor riviermondingen in het algemeen meer onderzoek vereist alvorens het universeel toepasbaar is.

Contents

1 Introduction

1.1 Estuarine morphology

Large parts of the coastlines in the world are interrupted by semi-enclosed water bodies. When connecting one or more rivers to the sea, such water bodies are called estuaries. Depending on one's point of view, estuaries can be divided into different categories. The essential features and processes used as criteria will lead to classification schemes. The most commonly adopted definition is that of Cameron and Pritchard (1963) with the statement of '***An estuary is a semi-enclosed coastal body of water which has free connection to the open sea and within which sea water is measurably diluted with fresh water derived from land drainage***'. Estuaries are surrounded by the densest population areas, as 22 of the 32 largest cities in the world are located around estuaries (Ross, 1995). Therefore, estuaries attract a variety of human activities, e.g. navigation, land reclamation, fishing & aquaculture and mining. Many estuaries provide habitats for a large number of organisms and support very high productivity, forming unique ecosystems. An example is the Yangtze Estuary (see Figure 1.1), study area of this research.

In order to properly manage estuarine systems, it is important to understand their physical functioning and to be able to predict the impacts of human interference, such as upstream dam building, and changing natural forces, such as land subsidence and accelerated sea level rise. These impacts lead to changes in the topography of the estuary. The systematic study of features (land forms) of alluvial sediment shaped by water motion in an estuary is known as *estuarine morphology*. Changing morphological features will also feed back onto the water motion, as shown in Figure 1.2. The evolution of morphological features due to their dynamic interaction with the hydrodynamic forcing, including climatic, geological, biological and anthropogenic conditions, is called *morphodynamics* (De Vriend et al., 1993a). From Figure 1.2 we can find that *sediment transport* is the link between the forcing and the morphological changes.

From a sediment transport point of view Dalrymple et al. (1992) have defined two types of estuaries: wave-dominated and tide-dominated (Figure 1.3). According to their definition, the Yangtze Estuary can be defined as the tide-dominated estuary: as a result of the strong tidal currents (maximum speed exceeds 2 m/s) relative to the wave effects, the mouth area generally contains *tidal sand bars* which are aligned with the current, and around which the sediment circulates. In the case of the Yangtze Estuary, the most important tidal sandbars occur on the shallow fringe of the estuary. This is called mouth bar, because it constitutes an obstacle to navigation. The research presented herein focuses on the sediment transport processes in this mouth bar area.

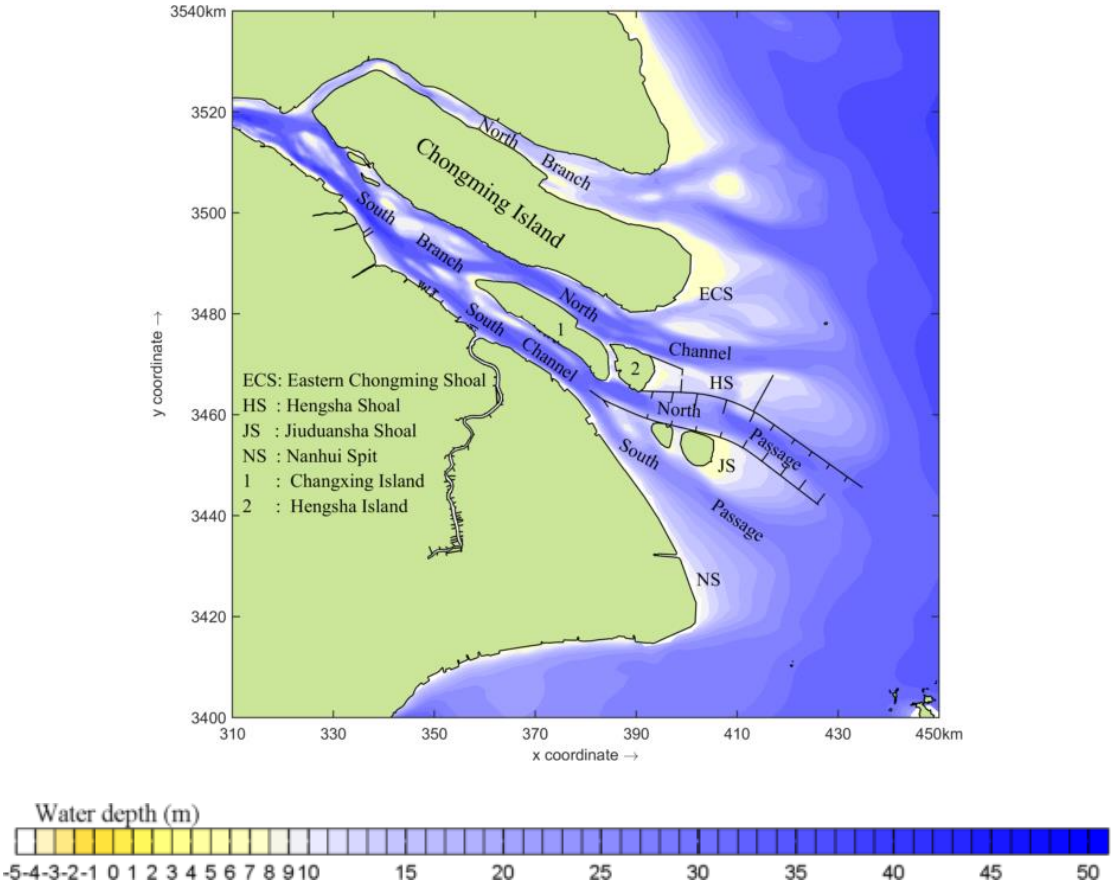

Fig.1.1 The layout of the Yangtze Estuary

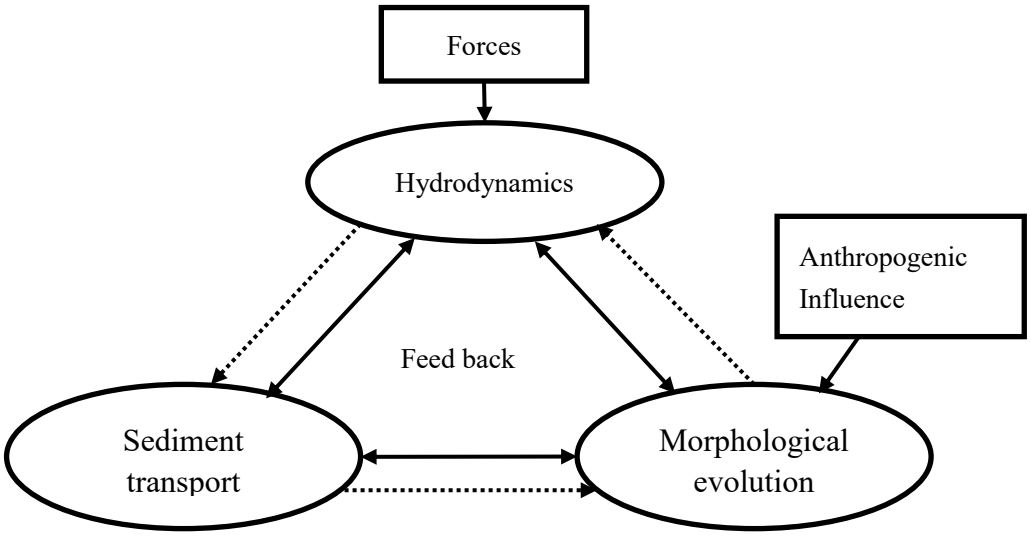

Fig.1.2 Sketch of the morphodynamics loop

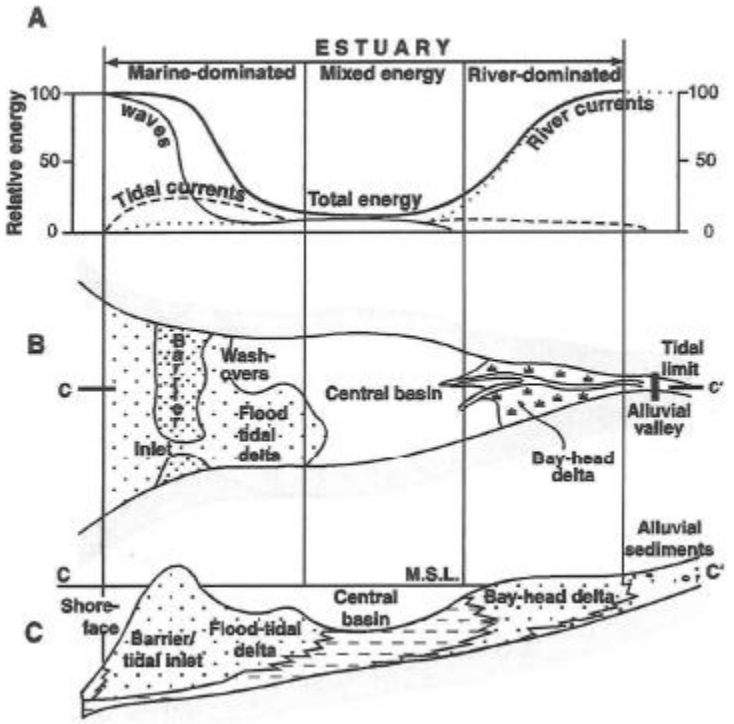

Fig.1.3a Distribution of (A) relative energy, (B) morphological components and (C) sedimentary faces in a longitudinal section within an idealized wave dominated (microtidal) estuary. (original from Dalrymple et al., 1992)

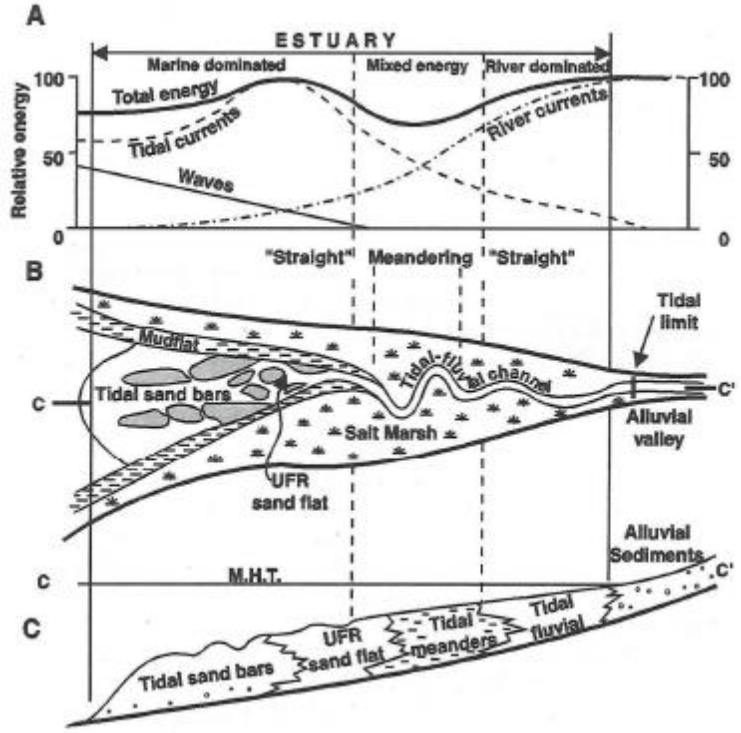

Fig.1.3b Distribution of (A) relative energy, (B) morphological components and (C) sedimentary faces in a longitudinal section within an idealized tide dominated estuary. (originally from Dalrymple et al., 1992)

1.2 Mouth bar of the Yangtze Estuary

1.2.1 Mouth bar in a narrow sense

The Yangtze Estuary (see Figure 1.1) is an estuary characterized by ample river flow & sediment and obvious tidal influence. The morphology of the estuary is characterized by three level bifurcations and four outlets, with well-developed shoals alternating channels, stretching sandbar and sub-aqueous delta. The dynamic altering between the river runoff and tidal current are the main factors influencing the morphological processes of Yangtze Estuary.

A mouth bar is a bar in a river that is typically created in the middle of a channel in a river delta (Edmonds and Slingerland, 2007). As the flow diverges near the ocean, sediment settles out in the channel and creates an incipient mouth bar. As flow is routed around the incipient bar, additional sediment is deposited on the incipient bar. This continued process results in the formation of a full-fledged mouth bar, which causes the channel to bifurcate (Edmonds and Slingerland, 2007).

In the Yangtze Estuary the term mouth bar refers to the particular shallow parts at the river mouth of the Yangtze. As shown in Figure 1.1, there are 3 shoals and 4 channels at the mouth of the estuary. The North Branch (NB) and the North Channel (NC) are separated by the Chongming East Shoal (CMES). The Hengsha Shoal (HSS) separates the NC and the North Passage (NP) and the Jiuduansha Shoal (JDSS) separates the NP and the South Passage (SP). The mouth bar of the Yangtze Estuary often refers to the shallow parts in the main channels (NC, NP and SP). The water depth above the bar is relatively small in comparison with the depth in upper or lower reaches. Therefore, the water depth above the mouth bar is a key accessibility factor for seagoing vessels to Shanghai Port and other inland ports along the Yangtze River.

Based on historical bathymetry measurements, Chen (1998) points out that the water depth above the mouth bar varies along the channels, as well as the length of the shoals. The shallowest part along the NC varied from 6.1 m (1842) to 9.3 m (1865). The third bifurcation of the estuary, dividing SC into NP and SP, occurred around 1960. The shallowest area along the NP varied from 7.1 m (1960) to 8.9 m (1977). The smallest water depth in the SP varied from 7.5 m (1970) to 8.3 m (1963). The sediment along the channels mainly consists of fine particles with gentle slope. This means that the shallow parts cover a long distance along the channels. Table 1.1 lists the length of shoal with a depth smaller than 9 m, 10 m, 11m or 12 m in the main channels. Clearly, these elongated shallow areas constitute a bottleneck for navigation in the estuary.

The main harbors of Shanghai Port are located along the South Branch (SB) and the Huangpu River. Although the water depth along the NC is sufficient as an access channel, the route via the NC to those harbors is uneconomic (Gao, 2008). Therefore, the channels in the SP and NP are the main entrances to the inland ports. The channel in the SP used to be the main access channel before the 1980's. In last three decades, a new generation of vessels with large capacity was developed and became the principal

means of marine transportation. The conditions (water depth and width) of access channel in the SP became insufficient for the new vessels and the heavy traffic. Meanwhile, large sedimentation occurred along the SP due to fluid mud deposition and a southward expansion of the JDSS in 1970's and early 1980's (Yun, 2004). During typhoon Forrest (8310) period, the large sedimentation in the SP almost silted up the 9 m draft channel in 1983 (Chen, 1998). Therefore, the main navigation channel was forced to be shifted to the NP.

Table 1.1 The length of shoals along outlets of the Yangtze Estuary (Chen, 1998)

Outlets	Length of shoals along the outlets (km)			
	Depth<9m	Depth<10m	Depth<11m	Depth<12m
NC	30	34	37	39
NP		43	53	58
SP	44.7(6.7+38)	56	60	64

At present, the NP is the main entrance to Shanghai Port and the other ports along the Yangtze River. Figure 1.4a (blue line) shows the location of the navigation channel along the NP with water depth in 1998 shown in Figure 1.4b. Obviously the water depth at the section of 18~35 km (referred to the land side start point of the navigation channel) was less than 8 m in 1998.

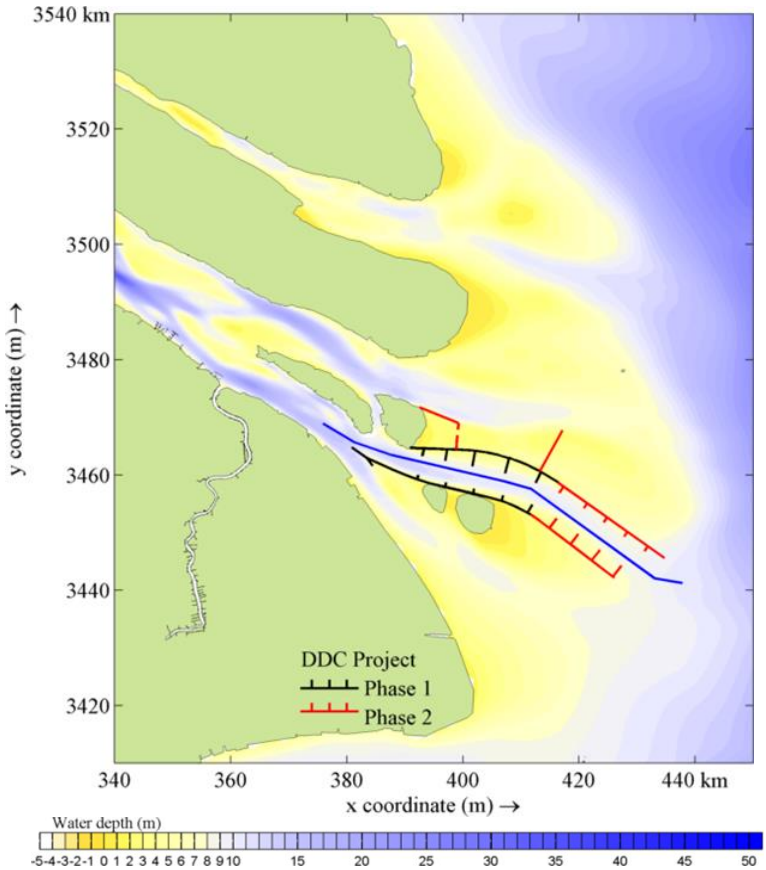

Fig.1.4a Sketch of the improvement project of the Deep-Draft Channel of the Yangtze Estuary (black and red lines indicating the training dikes and the attached groins; blue line indicating the location of the water depth profile measured in Feb. 1998)

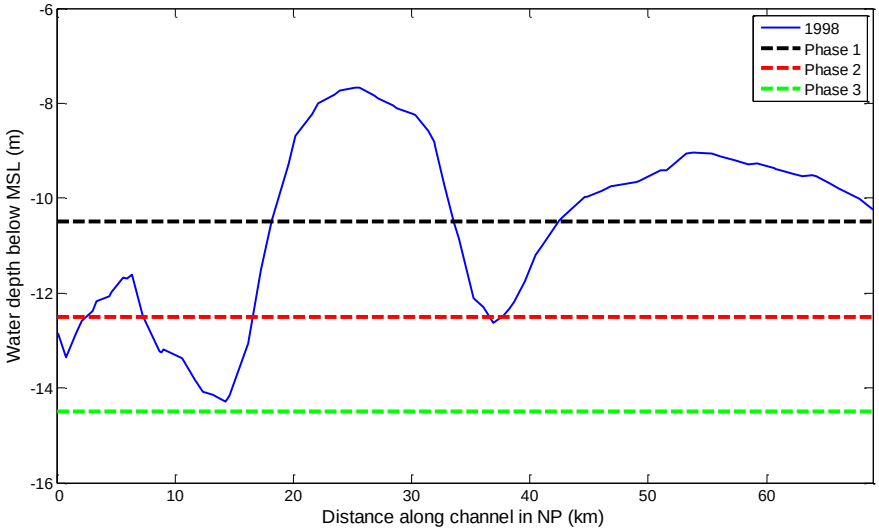

Fig.1.4b Water depth along the navigation channel in NP of the Yangtze Estuary (from land side to sea; location of the channel indicated by the blue line in Figure 1.4a; dashed lines: envisaged water depth after different phases)

Due to the existence of the shallow part (mouth bar) in the NP, the water depth of the navigation channel could only be used up to 8~9 m draft, which was insufficient for the ever-increasing demands of the new-generation vessels. Therefore, an improvement project, the Deep-Draft Channel (DDC) of the Yangtze Estuary, was implemented from 1998. The project consists of a combination of control dams at the head of the south dam, training dams, groins and channel dredging, as shown in Figure 1.4a. The purpose of this project is to increase the navigation depth from 8 m to 14.5 m. The dams and groins were constructed between 1998 to 2004, in two consecutive phases (indicated in Figure 1.4a by the black and red lines, respectively). The required water depth (10.5 m for the first phase and 12.5 m for the second phase) in the channel was achieved by capital dredging and maintenance dredging (see Figure 1.4b). The main construction work of the third phase is dredging the channel to 14.5 m depth.

The engineering work of the project seems to work well, in that the required water depth is achieved. However, Tan et al. (2009) point out that the sedimentation along the channel was quite high. During the first phase of construction (1998-2002), the annual dredging amount was about 15-20 million m^3 whereas the prediction was 14 million m^3. During the second phase (2003-2008), the annual amount of 60 million m^3 was twice the predicted value. Since 2008 the annual dredging amount has increased to 80-90 million m^3, whereas the prediction was 30 million m^3.

1.2.2 Mouth bar in a broad sense

In a broad sense, the *mouth bar* is the shallow area at a river mouth blocking the connection of the sea and the upstream reach, where the water depth is larger than that above the bars. Thus, a longitudinal profile shows a hump at the mouth bar and deeper parts at both ends. The part with the small water depth is the mouth bar in a broad sense.

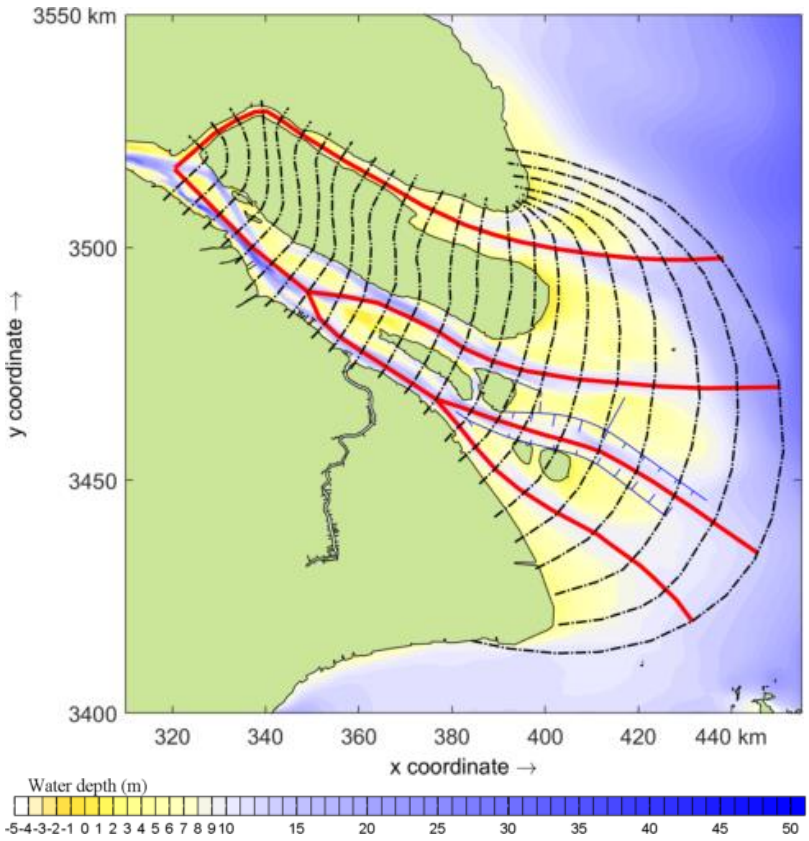

Fig.1.5a The sketch of cross-sections in the Yangtze Estuary (blue lines: the training dikes and the attached groins; red line: the location of the channel centerlines; black dashed lines: location of cross-sections)

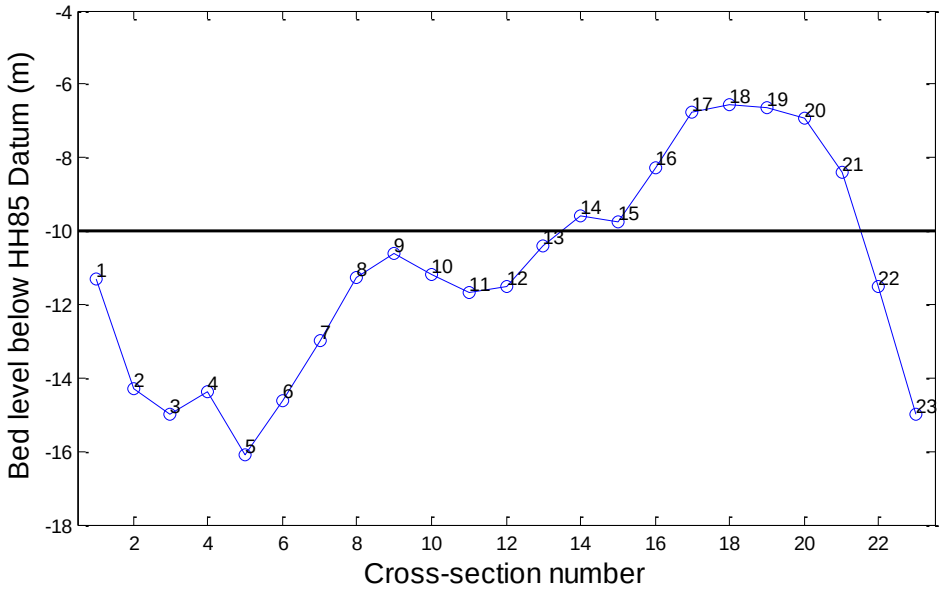

Fig.1.5b Mean bed level height below HH85 datum at cross-sections in the Yangtze Estuary (1998)

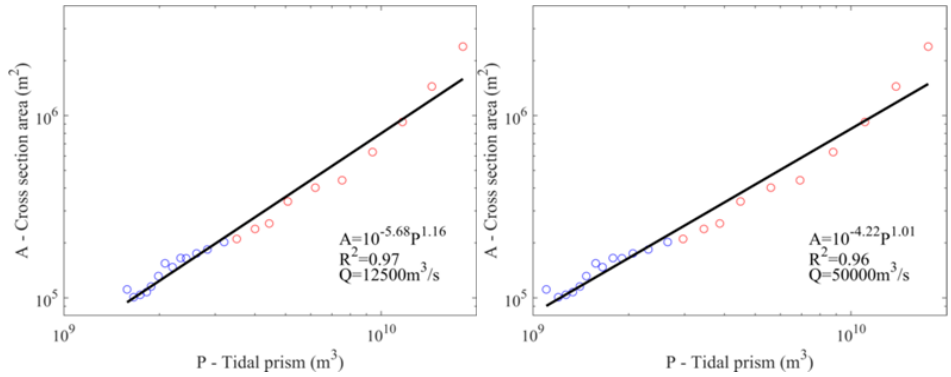

Fig.1.5c P-A relationship of the Yangtze Estuary (A: cross-sectional area below local mean water level; P: tidal prism during spring tide; blue: cross-sections 1-14; red: cross-sections 15-23)

To identify the mouth bar in a broad sense, 23 cross-sections in the Yangtze Estuary are chosen to calculate the mean bed level. Figure 1.5a shows the location of these cross-sections. They are approximately perpendicular to the channel's centerlines (red lines in Figure 1.5a), and about 5-6 km apart. Each cross-section is further divided into smaller segments. The area and depth of each segment are calculated based on observed bathymetry. The mean bed level of each cross-section is obtained by area-weighted averaging. The results in Figure 1.5b show that there is a distinct hump between the 14th and the 21th cross-section. Consequently, the mouth bar of the Yangtze Estuary here refers to the area between the 14th and the 21th cross-sections.

It may be argued that this shallow part results from the divergence of the estuary. If so, and there is no difference in sediment characteristics, the P-A relationship (i.e. the relationship between the tidal prism and the cross-sectional area) should be the same for all cross-sections. In the case of the Yangtze Estuary, however, Figure 1.5c shows that that the cross-sectional areas around the mouth bar (red points) are below the fit line. This means that the existence of the shallow part, mouth bar, is not only due to the divergence of the estuary: there must also be a difference in sediment characteristics and/or physical processes.

1.3 Objectives and research questions

Present understanding of the morphodynamic evolution of estuaries and the ability to predict it are still limited, because of its complexity and because of the wide range of time- and space-scales involved. The sketch of a tide-dominated estuary (Figure 1.6) outlines the sediment transport around the mouth bar of the estuary. The external forces and disturbances due to human activities are summarized in Table 1.2. It shows that all-natural forces and human activities finally attribute into three kinds of net transport mechanism: mean flow, tidal asymmetry induced transport and transport due to gravitational circulation (Shen et al., 2001). Therefore, investigating the sediment transport due to these mechanisms must give insight into the morphodynamics of the mouth bar of the Yangtze Estuary.

The ultimate objective of this study is to develop and test improved methods and modelling approaches for the prediction of estuarine morphology on spatial scales of several dozens of kilometers and time scales of decades. In this study the following objectives are emphasized:

- Acquiring better knowledge of forcing processes behind the sediment transport around the mouth bar in the Yangtze Estuary
- Reducing the important forcing processes to "representative" forcing conditions with comparable long-term net sediment transport rate and patterns
- Improving the prediction capabilities concerning the morphological evolution of the mouth bar by using process-based numerical models

These objectives are translated into the following research questions:

- Which forcing processes/mechanisms relevant to the sediment transport need to be included in the morphological model of the Yangtze Estuary?
- To what extent can the complexity of the processes/mechanisms underlying the morphological development of the Yangtze Estuary be reduced?
- How can morphodynamic models be applied practically to the Yangtze Estuary?

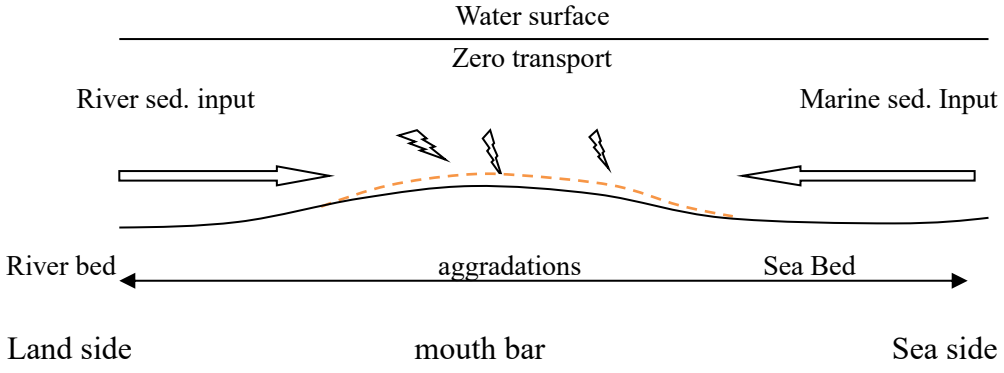

Fig.1.6 Sketch of sediment transport process around the mouth bar

Table 1.2 Processes and mechanisms for sediment transport around the mouth bar

Originate	Process	Mechanism	Direction
Fluvial	Discharge	Mean flow	To Sea
Marine	Tides	Asymmetry	To land
	Salinity	Gravitational circulation	To land
		Flocculation	With flow
	Wave	Stirring/mixing	With flow
Meteorology	Wind/Storm	Residual/mixing	Wind direction
Anthropic	Structures/Dredge&dump	Change in regimes	With flow
	Water deviation		With flow
Climate	Sea level rise	Mean flow	With flow

1.4 Research approach and thesis structure

In order to set up a morphodynamic model for the Yangtze Estuary, it is essential to identify the processes/mechanisms playing a significant role in the sediment transport. A direct way to do so would be to separately consider the transport due to individual process/mechanism. However, the physical processes in the Yangtze Estuary are complicated and interact with each other. It is hard to isolate contribution to the transport due to a certain individual process. Once a validated model is available, model simulations can be performed with the selected physical process/mechanism disabled, in order to identify which process dominates the sediment transport. Furthermore, input reduction and model reduction can be applied to establish a practically applicable morphodynamic model. Thus, the answers to the above research questions can be achieved.

The structure of the thesis reflects the objectives listed above. Chapter 2 first gives the general condition of the estuary, the detailed information of the mouth bar area and a review of relevant previous research. Chapter 3 describes the set-up, calibration and validation of a process-based model for the estuary. The calibrated and validated process-based model for the estuary is applied to investigate the mechanisms/processes contributing to sediment transport in Chapter 4. Chapter 5 presents the analytical expression to establish the residual sediment transport in case of a significant river discharge. The expression is further applied to study the residual sediment transport in the Yangtze Estuary. Based on the results from Chapters 4 and 5, a process-based morphodynamic model for estuaries with a large river input (discharge and sediment load) is proposed in Chapter 6, based on the Mor-merge method with multi-discharge levels. Chapter 7 discusses the present approach to morphological modelling of the Yangtze Estuary, summarizes the conclusions of the thesis and gives recommendations for further research.

2. General condition of the Yangtze Estuary

2.1 Yangtze Estuary

The Yangtze River is the largest river in China, with a total length of 6,300 km and a catchment area of 1.8 million km^2. The Yangtze Estuary is the partly enclosed water body through which the Yangtze River (Figure 2.1) flows into the East China Sea. The estuary forms a transition zone between river environments and ocean environments and is subject to both marine influence, such as tides, waves and the saline water intrusion, and fluvial influences, such as flows of fresh water and sediment.

Fig.2.1 Sketch of the Yangtze River Basin
(from http://en.wikipedia.org/wiki/File:Map_of_the_Yangtze_River.gif)

The influence of the ocean (tidal water level fluctuation) can reach up to Datong, the tidal limit in the dry season. Therefore, the region from Datong to the sea (Figure 2.2) is regarded as the estuary. Based on the hydrodynamic characteristics, the estuary can be divided into three segments. The upper segment is the river section between the tidal limit (Datong) and tidal current limit in the wet season (Jiangyin). In this segment, the water level varies with the tide, but the current is in seaward direction most of the time (note that the tidal current limit can be up to Nanjing in the dry season). The middle segment is the river estuary, from Jiangyin to the river mouth at 122° E. It is a transition zone with interaction between riverine and marine forces. The current in this segment is mainly collinear. The most seaward segment is the shore area near the mouth, from 122° E to about 123° E, usually the location of the freshwater plume front (Shen et al., 2001). In this segment the marine influences are dominant and there is small influence of the river discharge. The tidal current is typically rotational.

Datong gauging station is the most downstream integrated hydrological station along the Yangtze River. The catchment area upstream of this station is about 1.7 million km^2, accounting for 95% of the total catchment area. Therefore, the measured discharge and sediment transport at this station can be referred to as inputs to the estuary.

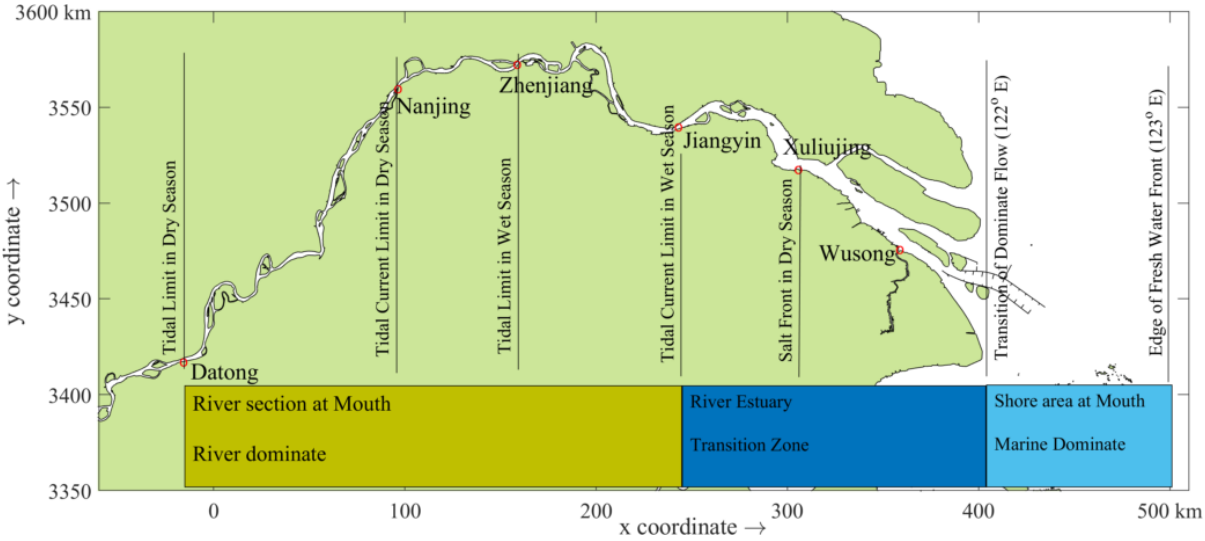

Fig.2.2 Yangtze Estuary segments (after Shen et al., 2001)

2.2 Hydrodynamics

2.2.1 River discharge

The daily mean and the yearly average discharge at Datong from 1950 to 2017 are shown in Figure 2.3. We can observe that the long-term average discharge in this period is about 28,400 m^3/s with a mean annual runoff of 896 billion m^3. Figure 2.3 also shows the large fluctuation of the yearly average discharge from the long-term mean, without a clear trend over the last half century. A spectral analysis of the yearly mean discharge shows that it varies in time, with a period of about 10 years (Shen et al., 2001). The maximum recorded discharge of 92,600 m^3/s occurred on Aug. 1st 1954, the minimum was 4,620 m^3/s on Jan. 31st 1979 (Chen, 1998). The ratio between maximum and minimum daily mean discharge is about 20, which is small compared to those of other rivers, e.g. 447 of the Yellow River, 30 of the Nile River and 26.8 of the Mississippi River (Chen, 1998).

The temporal variation of the discharge within a year can be observed from the long-term monthly mean discharge at Datong (Table 2.1). About 71% of the annual runoff occurs in the flood season (May ~ October) and about 29% in the dry season. July is the wettest month, accounting for about 15% of the annual runoff. January and February are the driest months with about 3% of the annual runoff each.

The TGD (Three Gorges Dam) was constructed from 1998 to 2003, and causes change in the discharge distribution over the year. Figure 2.4 shows the monthly mean discharges before and after the TGD constructed. As the manipulation of the TGD is to impound water in the reservoir in flood season and to use this water generate power in the other period. Therefore, the increase of discharge in the dry season (in January, February and March) and the decrease in the wet season (from May to October) are clearly visible.

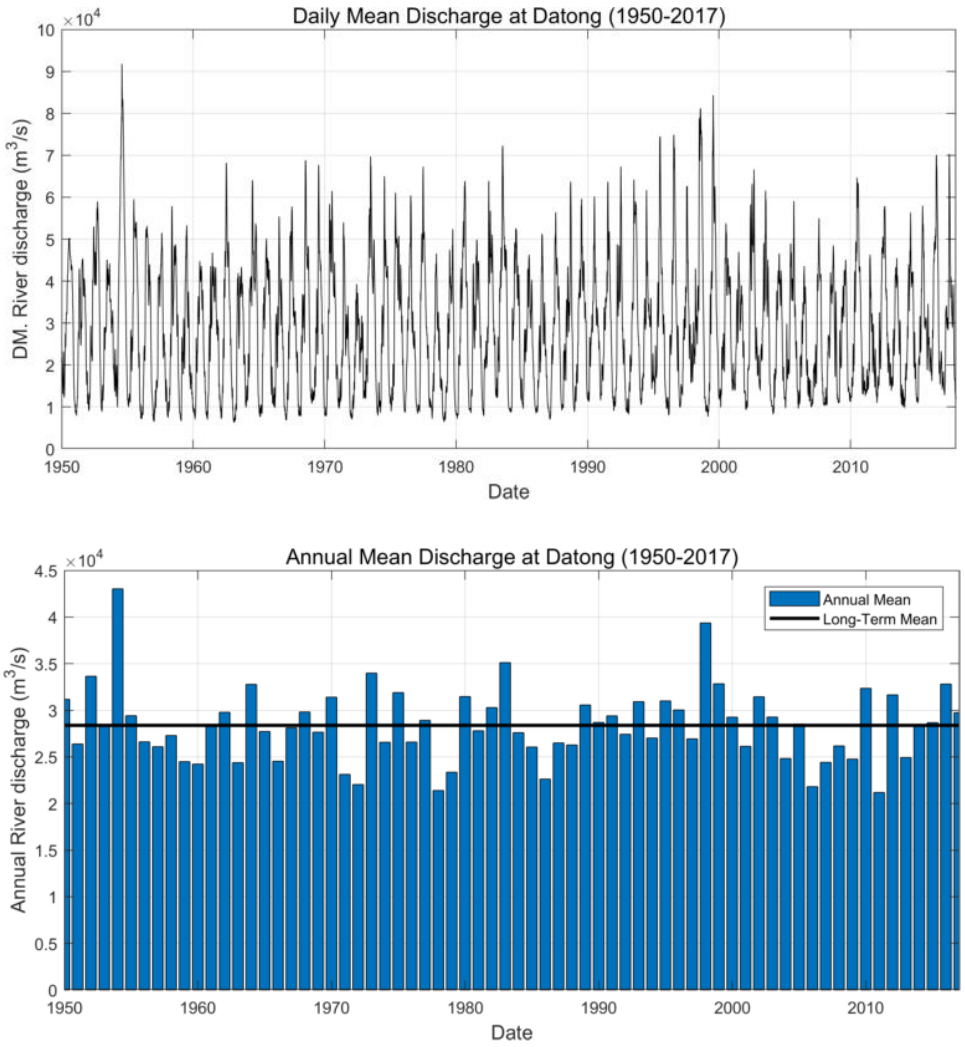

Fig.2.3 Top: daily mean discharge; Bottom: yearly average discharge, black thick line indicates the long-term average discharge (Datong 1950 -2017)

Table 2.1 The monthly mean discharge (m^3/s) at Datong (1950-2017)

	Month												Mean
	1	2	3	4	5	6	7	8	9	10	11	12	
Max	24700	22500	32500	39500	51800	60600	75200	84200	71300	51600	35800	23100	-
Year	1998	1998	1998	1992	1975	1954	1954	1954	1954	1952	1952	1982	-
Min	7220	6730	7980	12800	19900	27200	32800	25900	18900	15000	13200	8310	-
Year	1979	1963	1963	1963	2007	1969	1972	1971	2006	2006	1956	1956	-
Mean	11100	12000	16400	23900	33400	40100	49700	43900	40100	32500	22700	14200	28400
Runoff(%)	3.3	3.2	4.9	6.9	10.0	11.6	14.9	13.1	11.6	9.7	6.6	4.2	-

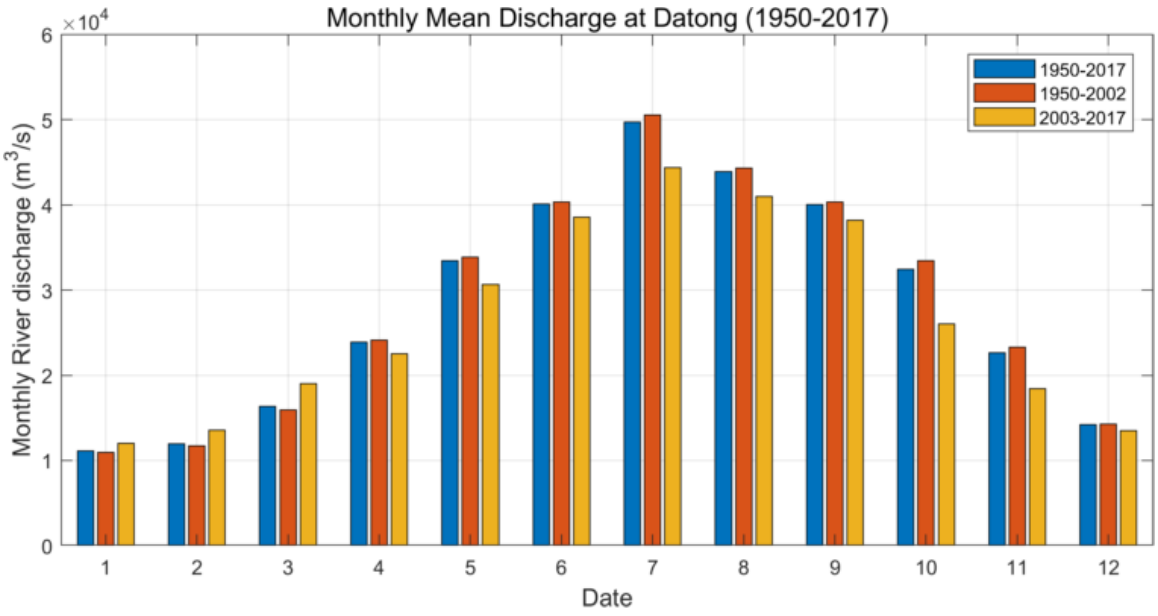

Fig.2.4 Monthly mean discharge at Datong (long term: 1950-2017; before the TGD: 1950-2002; after the TGD: 2003-2017)

2.2.2 Tide and currents

Tide

Semi-diurnal (e.g. M_2) and diurnal (e.g. K_1 & O_1) tides affect the Yangtze estuary (Zhang, 1995; Chen, 1998). The M_2 tide comes from the southeast and enters the estuary in the direction of 305°. The K_1 and O_1 tides come from the north as a standing wave with its amplitude increasing towards the south.

The tidal form numbers, i.e. the amplitude ratio between diurnal tides (H_{K1+O1}) and semi-diurnal tides (H_{M2+S2}), at all tidal stations (Figure 2.5) are in the range of 0.2-0.3, so less than 0.5. Therefore, we can conclude that the semi-diurnal tides dominate in the estuary. The super harmonic tides (e.g. M_4) are negligible outside the river mouth. From the river mouth to upstream the M_4 tide increases to about 0.2 m.

The tidal information at those stations, from outside the mouth to the upstream part of the estuary, is given in Table 2.2, showing that the tidal range is about 2.5 m at the seaside of the river mouth, e.g. at LHS (Luhuashan). Around the mouth bar, at NPJ (Niupijiao) and ZJ(Zhongjun), it increases to 2.6-2.7 m. Further upstream the range decreases to 2.0 m at XLJ(Xiuliujing) and 1.55 m at JY(Jiangyin), which is about 240 km from the river mouth. The tidal range approaches zero at Datong, 640 km from the mouth. The tidal range is higher in the north part of the estuary than in the south. The falling period (period of water level falling) is longer than the rising period and this asymmetry increases in upstream direction.

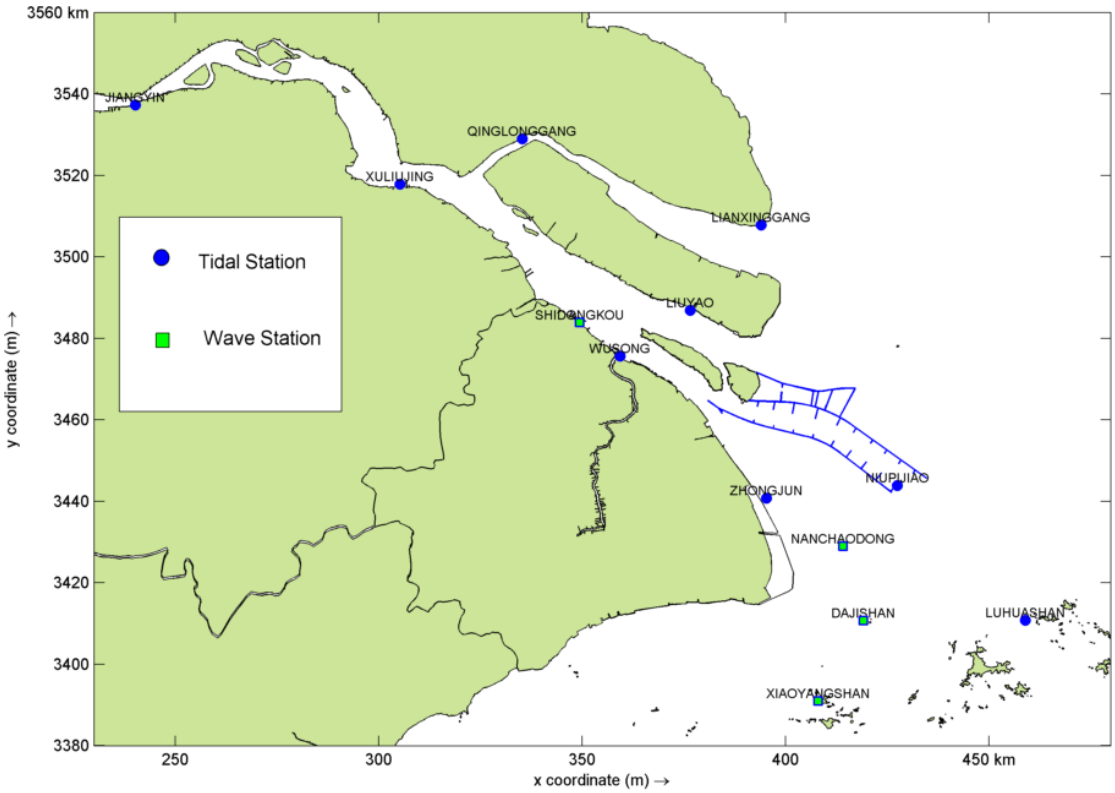

Fig.2.5 The locations of gauge stations for water levels and waves
Abbreviation: LHS-Luhuashan; NPJ-Niupijiao; ZJ-Zhongjun; LY -Liuyao; WS - Wusong; LXG-Lianxinggang; QLG-Qinglonggang; XLJ- Xuliujing; JY-Jiangyin

Table 2.2 Tidal characteristics at stations along the Yangtze Estuary

Stations	LHS	NPJ	ZJ	LY	WS	LXG	QLG	XLJ	JY
H_{M2}	1.17	1.27	1.21	1.06	1.01	1.35	1.01	0.88	0.72
H_{S2}	0.53	0.59	0.54	0.47	0.43	0.63	0.39	0.37	0.30
H_{K1}	0.28	0.27	0.26	0.24	0.23	0.24	0.19	0.21	0.18
H_{O1}	0.18	0.15	0.16	0.15	0.15	0.13	0.13	0.15	0.13
H_{M4}	0.03	0.04	0.13	0.18	0.16	0.13	0.27	0.17	0.21
H_{K1+O1}/H_{M2+S2}	0.27	0.23	0.24	0.26	0.26	0.19	0.22	0.29	0.30
H_{M4}/H_{M2}	0.03	0.03	0.11	0.17	0.16	0.10	0.27	0.20	0.29
Mean range	2.46	2.72	2.63	2.35	2.23	2.96	2.52	2.00	1.55
T_{rising}	6:00	6:02	5:13	4:45	4:57	5:32	3:26	4:30	3:57
$T_{falling}$	6:25	6:23	7:12	7:40	7:28	6:53	8:59	7:55	8:28
$T_{falling}$- T_{rising}	0:25	0:21	1:59	2:55	2:31	1:21	5:33	3:25	4:31

LHS: Luhuashan; NPJ: Niupijiao; ZJ: Zhongjun; LY: Liuyao; WS: Wusong; LXG: Lianxinggang; QLG: Qinglonggang; XLJ: Xuliujing; JY: Jiangyin
H_{M2}, H_{S2}, H_{K1}, H_{O1}, H_{M4}: amplitudes of M_2, S_2, K_1, O_1 and M_4 tides in m; Mean range: mean tidal range in m; $T_{rising/falling}$: period of water rising/falling

Current

Based on the analysis of current measurements in the 1980's and 1990's, Xu et al. (1995) and Chen (1998) conclude that semi-diurnal tidal currents are dominant in the Yangtze Estuary. It shows the collinear character of the tidal currents in the channels within the estuary, and the rotational character in the shoal area outside the mouth. Recent tidal currents observations at stations (Figure 2.6) show the same characteristics. Hourly current data at these stations were measured during spring tide in Aug. 21-22, 2005. The depth-averaged current vectors over a tidal period (12h25min) are shown in Figure 2.6, together with residual flux. The currents show a clearly rotational character east of the mouth bar, whereas within the estuary they are mainly collinear.

The maximum depth-averaged velocities at the stations are listed in Table 2.3. Landward currents are defined as flood currents and vice versa. At most stations the maximum ebb velocity is larger than the maximum flood velocity, except in the upper part of NC (NC1 and NC2), where the maximum flood currents are slightly larger than the maximum ebb currents. The maximum ebb velocity is about 2.64 m/s measured at the lower reach of NP. The maximum flood current is about 2.16 m/s occurring in NC.

We also observe that the mean ebb velocity is larger than the mean flood velocity at all observation points. This is explained by the enhancement of ebb current by river discharge and corresponding reduction of the flood current. The magnitude of the mean ebb current in NC is the largest among the three main outlets. The mean flood currents in the SP are the largest, indicating a large import of sea water through this channel.

The residual flux calculated based on the time series of the observed current velocity and the water depth are shown in Figure 2.6 (right panel) and Table 2.3. From the figure and the table, we can observe that the residual flux is generally directed seawards, with a magnitude of about 1.2-8.6 m^2/s. In the middle of each outlets, the residual flux is in NE~ENE direction.

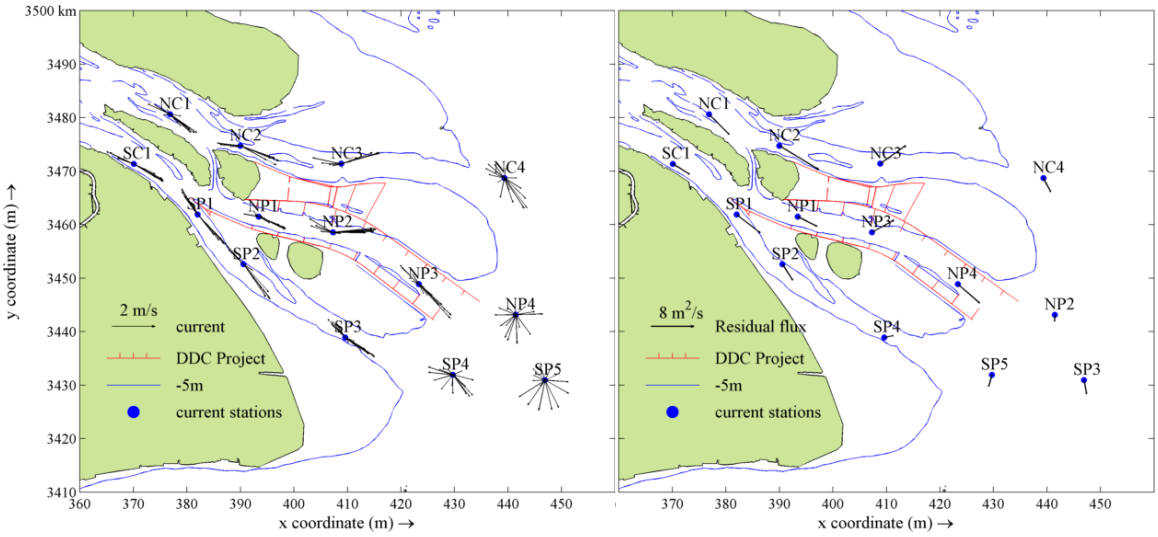

Fig.2.6 Current velocity vectors (left) and residual flux (right) at observation points in August 21-22, 2005(spring tide)

Table 2.3 Depth averaged current velocity and residual flux in the Yangtze Estuary during spring tide (Aug. 21-22, 2005)

Locations	Max. depth averaged velocity				Mean depth averaged velocity				Residual flux	
	Flood		Ebb		Flood		Ebb			
	M	D	M	D	M	D	M	D	M	D
NC1	1.61	293.5	1.60	125.9	0.82	295.8	1.15	126.9	5.35	135.2
NC2	2.16	285.8	2.13	111.5	0.98	274.1	1.46	111.1	8.58	121.2
NC3	1.81	276.1	2.28	73.8	0.99	287.0	1.54	78.2	5.81	54.4
NC4	1.07	296.5	1.75	142.7	0.79	274.2	1.05	117.3	2.90	151.8
SC1	1.79	303.5	1.90	125.6	0.93	297.4	1.35	119.2	3.65	121.4
NP1	1.44	286.8	1.73	114.1	0.73	289.9	1.05	106.2	4.02	117.1
NP2	1.48	313.4	2.64	136.0	0.98	315.4	1.41	127.7	4.71	61.1
NP3	1.71	246.2	1.58	60.1	0.94	268.2	1.03	102.0	5.37	131.2
NP4	2.10	293.8	2.22	81.9	1.06	298.1	1.40	90.5	1.21	183.3
SP1	1.81	328.7	2.06	139.2	1.06	327.0	1.44	132.5	5.53	131.2
SP2	1.71	322.1	2.19	144.7	1.02	293.5	1.44	141.0	3.48	147.3
SP3	1.75	276.4	1.48	129.8	0.94	263.2	1.04	116.9	1.69	78.6
SP4	1.45	237.2	1.46	123.5	0.97	262.6	1.12	100.9	2.23	196.5
SP5	1.91	315.1	2.06	124.4	1.06	321.3	1.04	115.0	2.60	170.3

M: magnitude of velocity (m/s) and flux (m^2/s); D: direction of velocity in degree.

2.2.3 Wind and waves

As the Yangtze Estuary is exposed to the sea in eastward direction, wind and waves from N~E~S can influence the estuary. Wave data are available at three stations in front of the mouth bar as shown in Figure 2.5. The Xiaoyangshan station is surrounded by the islands. Hence, the measured data at this station poorly represent the wind and wave characteristics of offshore wave and wind of the Yangtze Estuary. Therefore, the measurement data at Nancaodong (also called Yinshuichuan) and Dajishan (outside of the estuary) are used to study wind and wave characteristics in the estuary and at the seaward edge of the estuary, respectively.

The recent data are not available at these two stations. The wind and wave data measured four times (8:00, 11:00, 14:00 and 17:00) per day at Nancaodong in 1977 and at Dajishan in 1982 were analyzed. Here the measured wave height is the $H_{1/10}$ wave height. The statistical analysis of wave height and wind speed grades in each direction is applied to the measured wind and wave data. Table 2.4 and 2.5 show the statistical analysis results of wind speed and wave height at Nancaodong station with wind and wave roses shown in Figure 2.7. The statistical analysis results of the measurement at Dajishan are shown in Table 2.6 & 2.7 and in Figure 2.8.

Figure 2.7 and Table 2.4 clearly show that wind occurrence varies between 5 and10% in most directions, except for westerly winds (less than 2% in SW~W~WNW) at Nancaodong in 1977. The occurrence of wind from north (NNW~N~NNE) was relatively high. The strongest wind at this station was from NE or NW, with a magnitude of 18 m/s. The dominant and the strongest wave directions differed from

those of wind at Nancaodong in 1977, as is shown in Figure 2.7. Waves from the east had the largest occurrence: 19.3%. The occurrence of waves from ENE and ESE accounted for about 10.3% and 11.9%. The wave with the largest height (2.5 m) in 1977 came from ENE. The difference in direction distribution between waves and wind at this station is mainly due to the sheltering effect of JDS (Jiuduansha Shoal) and NS (Nanhui Spit) against waves from northerly and southerly directions.

From Figure 2.8 and Table 2.6 we can find the dominant wind direction at Dajishan in 1982 was NNE with occurrence of 17.8%. The strongest wind was from N with a speed of 23 m/s. The dominant wave direction at Dajishan in 1982 was from NE, with occurrence of 17.7%. The largest waves came from N with a magnitude of 4.2 m.

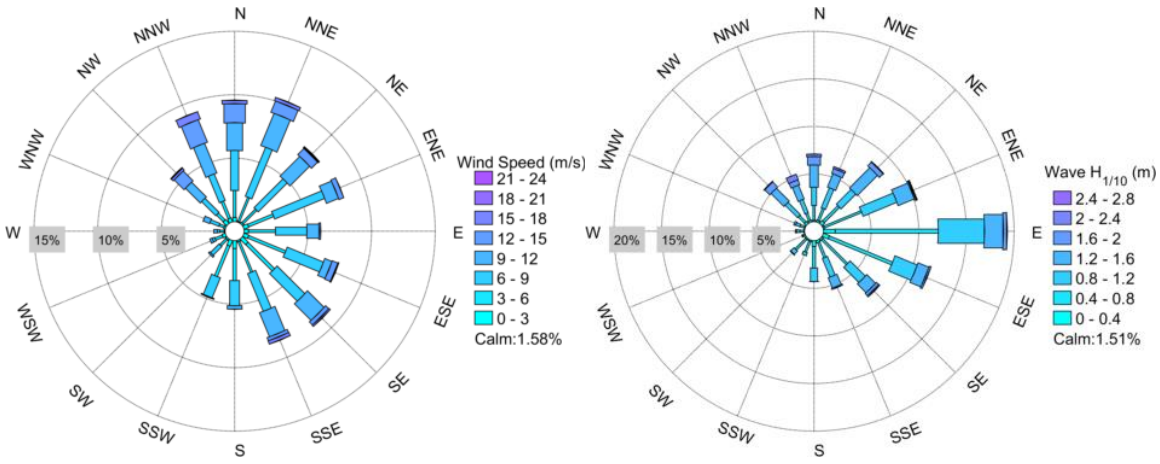

Fig.2.7 Wind rose (Left) and wave rose (Right) at Nancaodong based on wave heights four times (8:00, 11:00, 14:00 and 17:00) per day in 1977

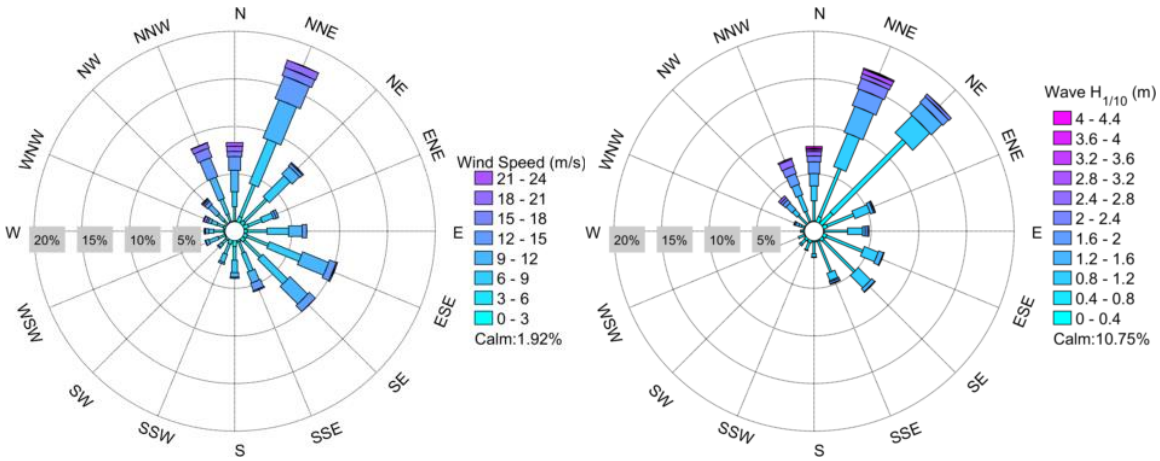

Fig.2.8 Wind rose (Left) and wave rose (Right) at Dajishan based on wave heights four times (8:00, 11:00, 14:00 and 17:00) per day in 1982

Chen (1998) analyzes the wave data at Nancaodong and Gaoqiao stations and points out that waves in the estuary are of the mixed type, with wind wave accounting of 67% and swell mixed with wind wave for the remaining 33%. The occurrences of waves from N and NNE account for about 10%. The waves from NNW, SE and SSE account for 8% each. Based on the analysis of 10 years of wave observation data at stations in

the Yangtze Estuary, Chen (1998) concludes that wave comes predominantly from the north in winter and from the south in summer, which is consistent with the wind direction. Northerly and southerly winds and waves are stronger than those from other directions, which can be explained from the northerly storm winds in winter and southerly typhoon winds in summer. The wave height decreases in landward direction. The recorded largest wave height is about 6.1 m at Nancaodong (17:00, Aug. 29, 1970), and 3.2 m at Gaoqiao (14:00 Sep. 10, 1977). The long-term mean wave height ($H_{1/10}$) is about 1.0 m at Nancaodong and 0.2 m at Gaoqiao. Chen (1998) also proposes the average annual wind speed to be about 7.1 m/s based on the 24-year data at Nancaodong station.

Table 2.4 Wind speed statistical analysis results at Nancaodong (1977)

Speed / Direction	0~3	3~6	6~9	9~12	12~15	15~18	18~21	P (%)	Mean* (m/s)	Max (m/s)
N	0.34	2.12	3.15	2.19	1.51	0.27	0	9.59	8.0	15
NNE	0.07	2.05	4.18	2.74	0.96	0.27	0	10.27	8.0	16
NE	0.14	1.51	3.22	2.19	0.68	0.07	0.07	7.88	7.9	18
ENE	0.41	2.12	4.25	1.03	0.41	0	0	8.22	6.5	14
E	0.34	2.12	2.47	0.96	0.14	0	0	6.03	6.1	13
ESE	0.41	3.15	3.08	0.62	0.48	0.07	0	7.81	6.1	16
SE	0.62	2.95	3.08	1.85	0.34	0.14	0	8.97	6.5	17
SSE	0.14	2.60	3.22	2.05	0.27	0.27	0	8.56	7.0	16
S	0.62	2.53	1.99	0.27	0	0	0	5.41	5.1	10
SSW	0.48	2.60	1.71	0.07	0	0	0	4.86	4.8	10
SW	0.14	0.68	0.96	0.14	0	0	0	1.92	5.5	9
WSW	0.27	0.62	0.21	0.21	0	0	0	1.30	5.0	11
W	0.07	0.34	0.21	0.27	0	0	0	0.89	6.5	10
WNW	0.14	0.41	0.75	0.55	0	0	0	1.85	6.9	11
NW	0.41	0.75	1.58	1.64	1.10	0.21	0.07	5.75	8.6	18
NNW	0.34	1.44	2.26	2.53	1.92	0.62	0	9.11	9.0	17
P(%)	4.93	28.01	36.30	19.32	7.81	1.92	0.14	98.42	-	-
Calm(%)	-	-	-	-	-	-	-	1.58	-	-

*the mean of wind speed not accounting for calms and missing values

Table 2.5 Wave height ($H_{1/10}$) statistical results at Nancaodong (1977)

Height / Direction	0~ 0.4	0.4~ 0.8	0.8~ 1.2	1.2~ 1.6	1.6~ 2.0	2.0~ 2.4	2.4~ 2.8	P (%)	Mean* (m)	Max (m)
N	0.14	1.58	1.92	2.33	0.89	0.27	0	7.12	1.12	2.1
NNE	0.21	1.37	2.26	1.51	0.55	0.21	0	6.10	1.04	2.1
NE	0.41	2.26	2.19	3.01	0.55	0.07	0	8.49	1.02	2.0
ENE	0.14	4.25	3.84	1.85	0.14	0.07	0.07	10.34	0.84	2.5
E	1.23	10.82	4.86	1.99	0.41	0	0	19.32	0.72	1.6
ESE	0.68	7.19	2.53	1.23	0.21	0	0	11.85	0.71	1.6
SE	0.21	3.70	2.26	1.30	0.34	0.14	0	7.95	0.85	2.2
SSE	0.27	1.71	2.12	1.16	0.14	0	0	5.41	0.89	1.8
S	0.62	2.26	1.44	0	0	0	0	4.32	0.60	1.1
SSW	0.14	1.23	0.34	0	0	0	0	1.71	0.57	1.1
SW	0.14	1.58	0.48	0.07	0	0	0	2.26	0.58	1.4
WSW	0	0.21	0.07	0.07	0	0	0	0.34	0.80	1.2
W	0.07	0.41	0.34	0.14	0	0	0	0.96	0.74	1.3
WNW	0.07	0.48	0.48	0.21	0	0	0	1.23	0.78	1.5
NW	0.27	0.96	1.85	1.92	0.75	0.07	0	5.82	1.09	2.1
NNW	0.21	0.82	1.51	1.58	0.55	0.62	0	5.27	1.20	2.2
P(%)	4.79	40.82	28.49	18.36	4.52	1.44	0.07	98.49	-	-
Calm(%)	-	-	-	-	-	-	-	1.51	-	-

*the mean of wave height not accounting for calms and missing values

Table 2.6 Wind speed statistical analysis results at Dajishan (1982)

Speed / Direction	0~3	3~6	6~9	9~12	12~15	15~18	18~21	21~24	P (%)	Mean* (m/s)	Max (m/s)
N	0.07	1.51	1.58	2.26	1.44	0.55	0.55	0.41	8.36	10.5	23
NNE	0.62	3.63	5.00	4.32	2.53	0.89	0.82	0	17.81	8.8	20
NE	0.41	3.29	3.08	1.10	0.34	0.14	0	0	8.36	6.3	16
ENE	0.55	1.51	1.23	0.27	0.27	0	0	0	3.84	5.7	14
E	0.34	2.05	2.26	1.44	0.48	0	0	0	6.58	6.7	14
ESE	0.41	2.40	3.63	2.95	0.75	0.14	0	0	10.27	7.6	16
SE	0.41	2.40	3.70	2.60	0.89	0	0	0	10	7.3	14
SSE	0.21	1.23	2.05	1.23	0.82	0.14	0	0	5.68	7.8	15
S	0.62	1.44	1.30	0.48	0.14	0	0	0	3.97	5.4	12
SSW	0.41	1.16	0.89	0.21	0	0	0	0	2.67	4.9	10
SW	0.21	0.62	0.41	0.14	0	0	0	0	1.37	5.3	10
WSW	0.07	0.75	1.03	0.34	0.07	0	0	0	2.26	6.3	13
W	0.14	1.03	0.55	0.34	0.07	0.07	0	0	2.19	6.1	15
WNW	0.21	0.75	0.62	0.34	0.21	0.27	0.07	0	2.47	7.8	20
NW	0	0.55	0.89	1.23	0.41	0.21	0.14	0.07	3.49	9.8	21
NNW	0.07	0.82	1.71	2.40	2.12	1.03	0.55	0.07	8.77	10.8	21
P(%)	4.73	25.14	29.93	21.64	10.55	3.42	2.12	0.55	98.08	-	-
Calm(%)	-	-	-	-	-	-	-		1.92	-	-

*the mean of wind speed not accounting for calms and missing values

Table 2.7 Wave height ($H_{1/10}$) statistical analysis results at Dajishan (1982)

Height / Direction	0~ 0.4	0.4~ 0.8	0.8~ 1.2	1.2~ 1.6	1.6~ 2.0	2.0~ 2.4	2.4~ 2.8	2.8~ 3.2	>3.2	P (%)	Mean* (m)	Max (m)
N	0.07	2.12	1.58	1.30	1.23	0.62	0.48	0.21	0.14	7.95	1.38	4.2
NNE	0.62	5.48	3.77	2.95	1.85	1.16	0.48	0.48	0.14	16.92	1.15	3.4
NE	1.64	10.75	2.53	1.58	0.82	0.34	0	0	0	17.67	0.72	2.3
ENE	0.48	3.01	1.71	0.34	0.14	0.07	0	0	0	5.75	0.70	2.1
E	0.07	2.47	1.58	0.27	0.27	0.14	0	0	0	4.79	0.84	2.0
ESE	0.41	4.11	1.58	0.55	0	0.07	0	0	0	6.71	0.68	2.1
SE	0.34	4.66	1.85	0.41	0.07	0	0	0	0	7.33	0.66	1.6
SSE	0.14	3.49	0.82	0.14	0.21	0.07	0	0	0	4.86	0.70	2.0
S	0.14	1.23	0.34	0.07	0	0	0	0	0	1.78	0.61	1.2
SSW	0.27	0.82	0.07	0	0	0	0	0	0	1.16	0.45	0.9
SW	0.27	0.55	0.21	0	0	0	0	0	0	1.03	0.50	0.8
WSW	0.07	0.68	0	0	0	0	0	0	0	0.75	0.45	0.6
W	0.14	0.21	0.07	0	0	0	0	0	0	0.41	0.55	0.8
WNW	0.07	0.34	0.27	0.34	0.14	0.07	0	0	0	1.23	1.07	2.3
NW	0	1.30	0.68	0.89	0.41	0.27	0.27	0	0	3.84	1.18	2.5
NNW	0.07	1.16	1.78	1.16	1.16	0.82	0.75	0.14	0	7.05	1.41	2.8
P(%)	4.79	42.40	18.84	10.00	6.30	3.63	1.99	0.82	0.27	89.25	-	-
Calm(%)	-	-	-	-	-	-	-	-		10.75	-	-

*the mean of wave height not accounting for calms and missing values

2.2.4 Salinity

Hu et al. (1995) obtain salinity distributions in the Yangtze Estuary and its adjacent coastal area based on observations from 1975 to 1991. They point out the salinity distribution in the Yangtze Estuary shows obviously seasonal variation, i.e. more stratification in wet season and well-mixing in dry season. Kong et al., (2004) describe the characteristics of the temporal and spatial variation of salinity in the Yangtze Estuary by analyzed the measured hydrodynamic and salinity in February and July 2003, representing dry and wet seasons, respectively. They point out that the order of salinity distribution, from high to low, is NB, SP, NP and NC. They also find that the saltwater flows backwards from the NB to the SB in dry season. Zhu et al. (2018) investigated the salt intrusion based on 3D modelling of the Yangtze Estuary by applying ECOM-si

model package. They point out that the northerly wind produces southward currents along the Subei coast as well as the landward Ekman transport, which enhances the saltwater intrusion in the NC and NB and weakens the saltwater intrusion in the NP and SP. The Three Gorges Dam (TGD) increases river discharge in winter, which weakens saltwater intrusion, and is favorable for reducing the burden of freshwater supplement in the highly populated estuarine region.

Figure 2.9 shows the salinity distributions around the river mouth in August (wet season) and February (dry season). The spatial distribution of salinity as shown in Figure 2.9 can be split into horizontal and vertical distribution patterns. The horizontal salinity gradient is larger at the river mouth than in the adjacent coastal sea. In the wet season a strong stratification can be observed around the river mouth. The freshwater front extends from the river mouth in NE direction at the water surface and in SE direction at the bottom. In the dry season, the stratification around the river mouth is much weaker. The freshwater plume at the water surface is not clearly distinguishable in this season.

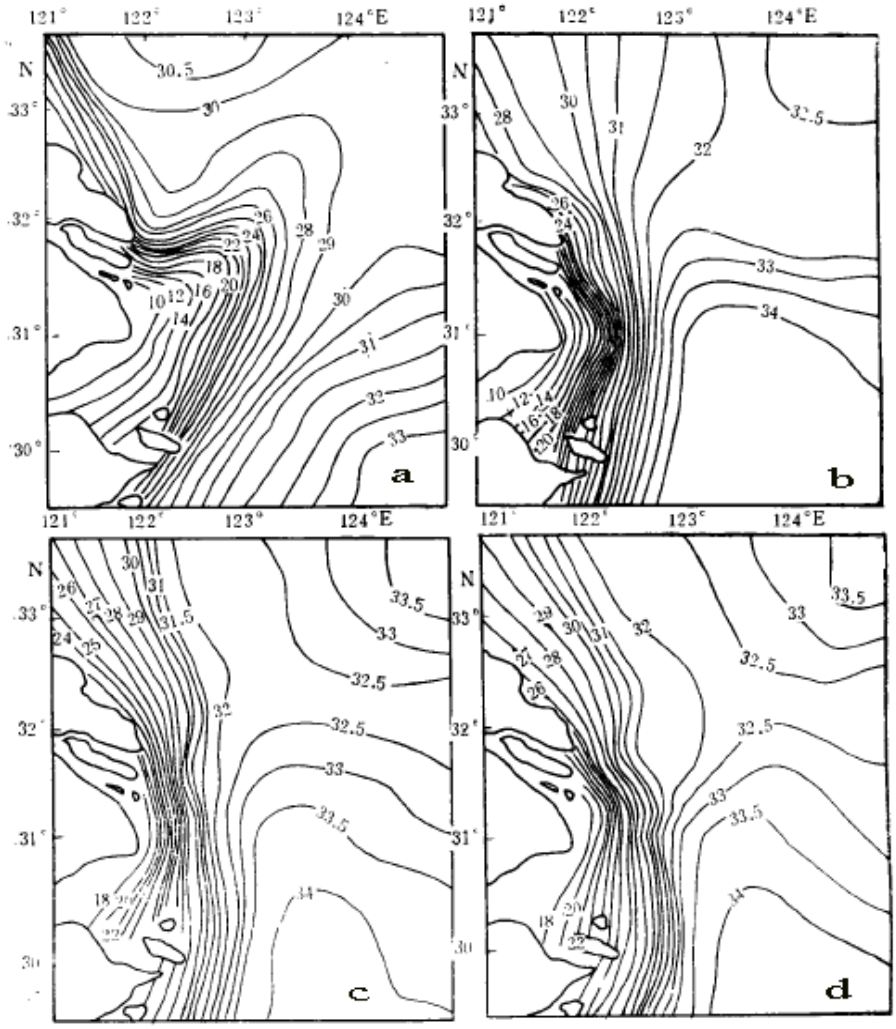

Fig.2.9 Salinity distribution around the Yangtze Estuary (Hu et al., 1995)
(a, b: salinity distributions at surface and bottom layers in summer/wet season; c, d: salinity distributions at surface and bottom layers in winter/dry season)

Like in most estuaries, mixing is a combination of internally generated and boundary generated turbulence, the relative magnitudes of which vary in space and time (Dyer, 1997). The result of this can often be seen in the form of salinity profiles in highly stratified and in partially mixed estuaries. Chen (1998) also states that mixing in the Yangtze Estuary varies in space and time. Highly stratified, partially mixed and well mixed salinity profiles can exist at the same time at different location, or at one location at different points in time. In general, the estuary is mainly of the partially mixed type. Chen (1998) points out that the 12 m depth contour separates two types of mixing: west of it the vertical salinity gradient is moderate and we have a partially mixed system; east of it the system is highly stratified. In the shallow areas, with water depth less than 5 m, the well mixed type is found.

2.3 Sediment

2.3.1 Sediment load

Sediment load from Datong

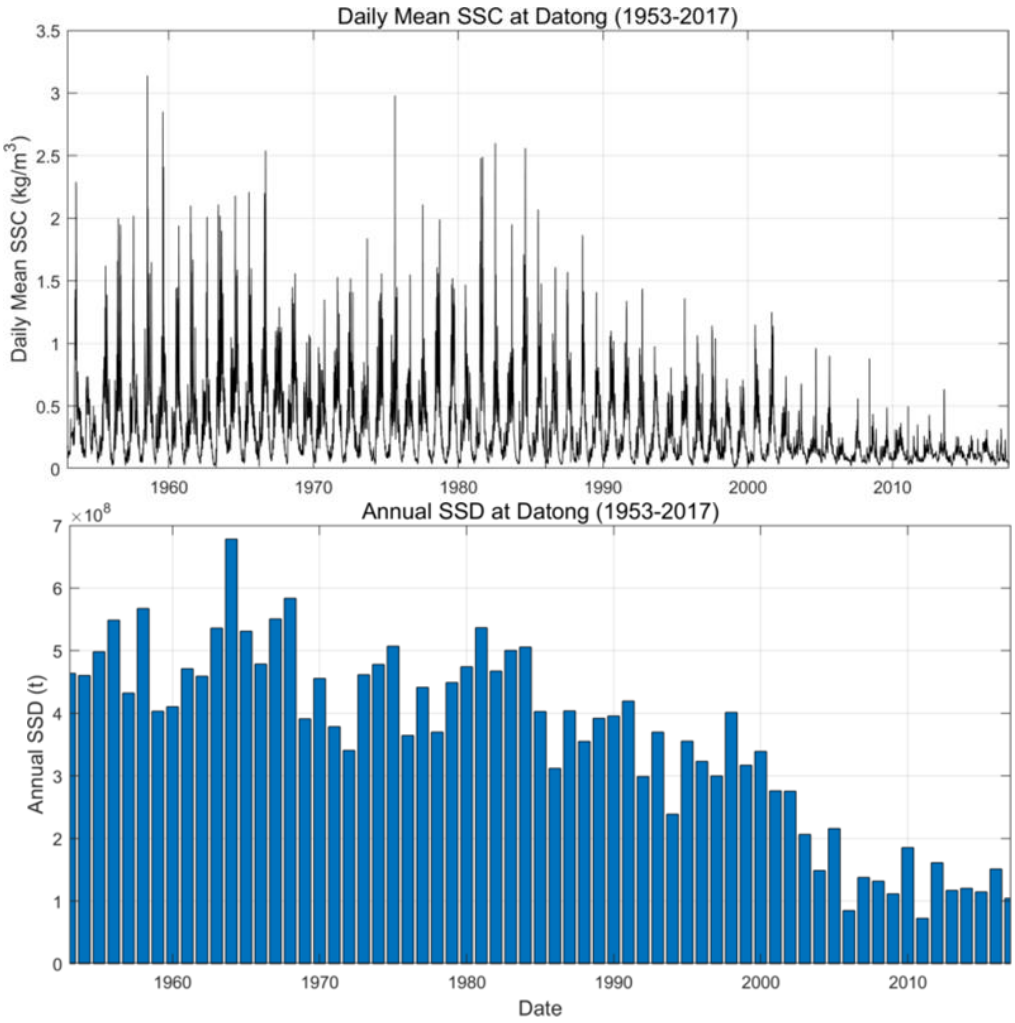

Fig.2.10 Top: Daily mean suspended sediment concentration at Datong; Bottom: Annual suspended sediment load at Datong

The river basin is the main sediment source for the Yangtze Estuary. Figure 2.10 shows the daily mean suspended sediment concentration (SSC) at Datong from 1953~2017. The long-term annual mean suspended sediment discharge (SSD) is about 414 mt/a (million tons per year) before 2000 (Changjiang Sediment Bulletin, 2001). A clear decreasing trend of the sediment load can be found after 1990. The average SSD at Datong was about 430 mt/a before 1990, with a mean concentration of about 0.5 kg/m^3. In the 1990's the SSD dropped to about 342 mt/a, which is about 80% of the previous years. In the last decade, the SSD kept on decreasing, with the average of about 163 mt/a being only 38% of that before 1990. In 2011, the SSD reached the historic low of 71 mt.

The fluvial sediment deposited around the mouth bar and the subaqueous delta can be re-suspended. During flood, some of this material may be imported back into to the estuary. The import of sediment from sea though the North Branch has been confirmed by radioactive tracer measurements (Dai et al, 2011). Therefore, marine deposits can also be a source of sediment in the estuary.

Temporal Sediment load distribution from Datong

The suspended sediment load varies with the river runoff: the larger the water discharges the higher the suspended sediment load. Figure 2.11 shows the long-term mean monthly sediment load over a year. The sediment load in wet season (May ~October) accounts for 87.5% of annual value. The highest sediment load, in July, amounts to 23.4% of the total annual load, whereas the lowest sediment load, in January and February, is about 0.7%.

It also can be observed from Figure 2.11 that the reduction in SSD after 2003, when the TGD was constructed. Although this might suggest the reduction in SSD due to this dam, the timeseries of SSD in Figure 2.10 show that the decrease is much more gradual since 1990. Therefore, the decrease of SSD is rather due to the combination of all dams in the upstream and "water & soil conservation project" in the river basin (Zhang and Liao, 2008).

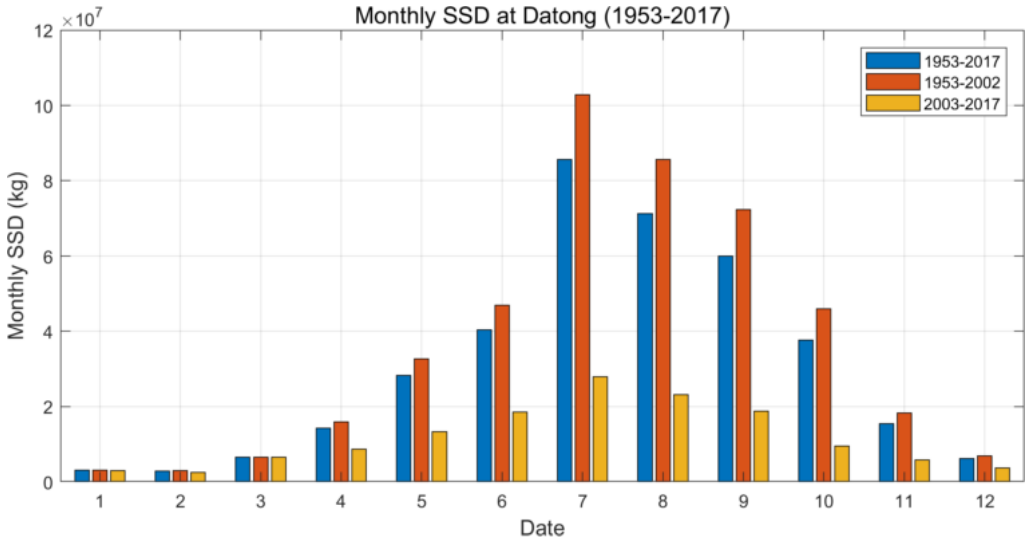

Fig.2.11 Monthly suspended sediment load at Datong (1953-2017)

The mean SSC is about 0.5 kg/m^3 (1953~2000) at Datong. The SSC is higher in the wet season, with a magnitude close to 1.0 kg/m^3. In the dry season the SSC is lower, about 0.1 kg/m^3. In the last decade the mean SSC has decreased by about 50%, and the suspended sediment load has decreased accordingly (Yang et al., 2006).

2.3.2 Suspended sediment concentration in the estuary

Spatial distribution of sediment concentration

The longitudinal distribution of the SSC exhibits a low-high-low variation from upstream via the mouth bar area to the sea (Dai et al., 2013). Figure 2.12 shows the locations of the SSC stations in the Yangtze Estuary with data available in 1999, 2000 and 2006. The time series of SSC at those stations are shown in Figure 2.13 together with the monthly mean value. We can observe from Figure 2.13 that the seasonal variation of the SSC varies with the locations. The SSC variation within a year in the reach from Datong to Xuliujing is similar to that at Datong, i.e. high in the wet season and low in the dry season. The SSC variation in the reach along the outlets near the mouth bar is opposite to this: higher in the dry season and lower in the wet season, mainly due to the more severe wind and wave climate in winter, which is in accordance with the dry season in the Yangtze Estuary (Dai et al.2013). Figure 2.13a and b also demonstrate the recent decrease in sediment load, as the SSC in 2006 is lower than in 1999 and 2000. At the inner side of the mouth bar (represented by Hengsha station) the decrease of SSC is also visible (Figure 2.13e and f), but at the front of the mouth bar (Sheshan, Niupijiao and Nancaodong) it is not. This can be explained by the local sediment availability from the shoals and flats in the mouth bar area (Dai et al., 2013) and the locally present stirring mechanisms (e.g. estuarine circulation, wind, waves).

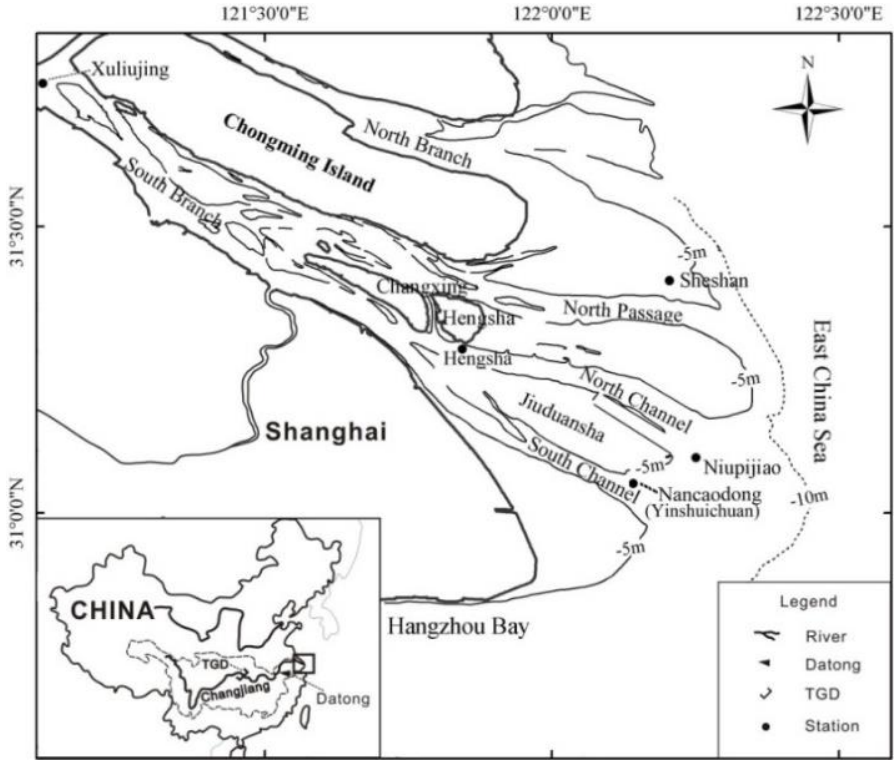

Fig.2.12 The locations of the sediment concentration stations (Dai et al. 2013)

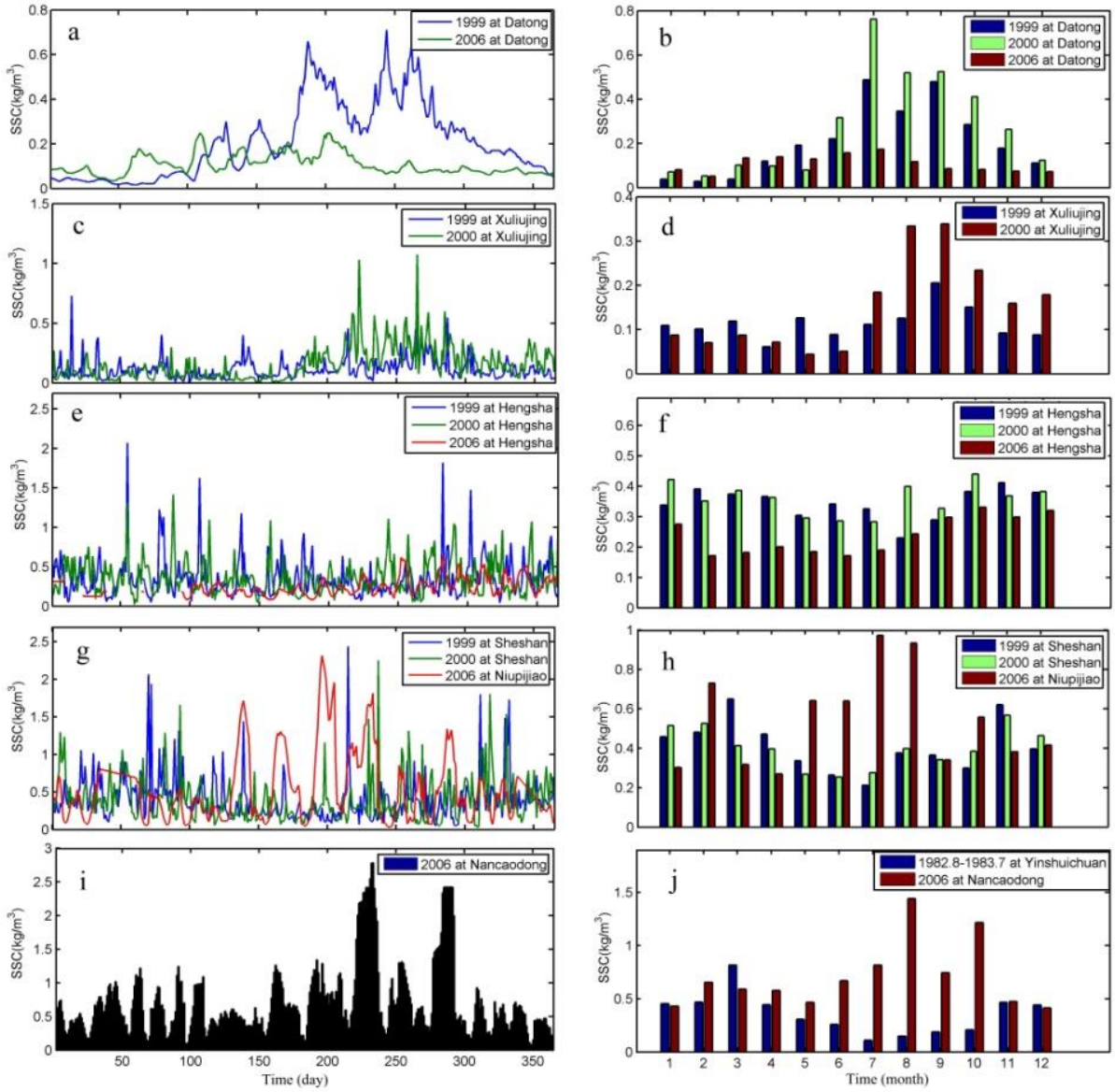

Fig.2.13 The SSC time series and the monthly mean at stations in the Yangtze Estuary (Dai et al., 2013)

One of the important features of the horizontal distribution of SSC are the relatively high values in the mouth bar area. This can be explained by the existence of the Estuary Turbidity Maximum (ETM) around the mouth bar area. Figure 2.14 shows the distribution of the ETM zone in the Yangtze Estuary (Shen et al., 1992). It can be observed that the location of the ETM zone coincides with the mouth bar.

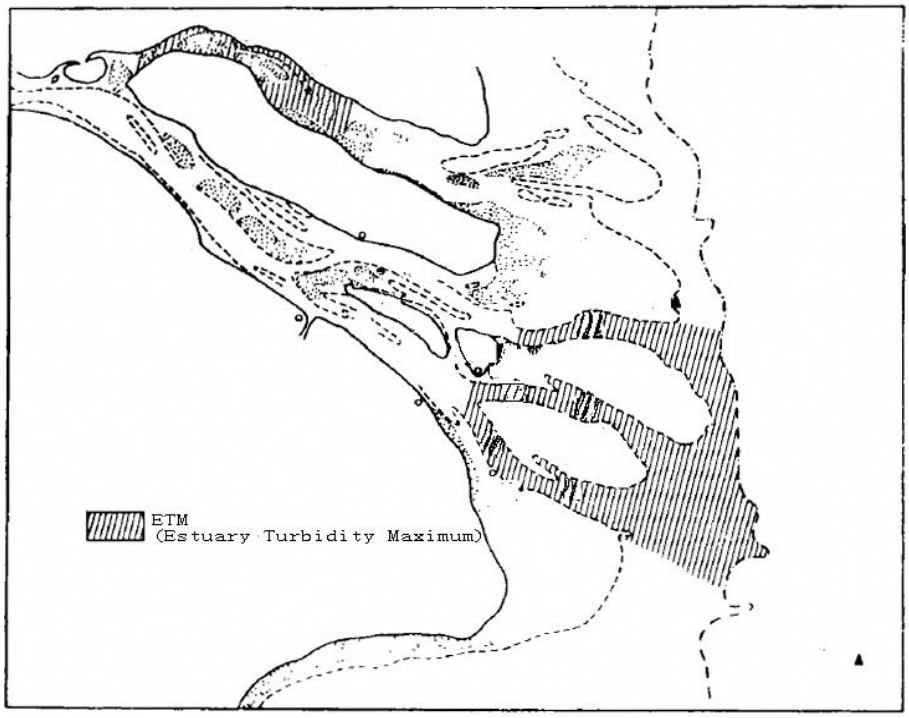

Fig.2.14 Distribution of ETM in the Yangtze Estuary (Shen et al., 1992)

2.3.3 Sediment diameter and composition

Bed material

Yun (2004) describes the longitudinal distribution of sediment diameter based on the measurements at the surface layer of the river bed in 1965 and 1992. He points out that the sediment at the bed upstream of the mouth bar mainly consists of fine sand with a mean diameter larger than 100 μm. Around the mouth bar the sediment at the bed becomes finer, with a mean diameter smaller than 30 μm, except for the mouth of NC, middle NP and the shoreface of the shoals. At the subaqueous delta the mean grain diameter at the bed is about 8 μm. The fraction of the fines (clay and silt range) increases in the longitudinal direction along the estuary.

Analysis of bed material samples from the surface layer (top 5 cm) shows a large variation of sediment composition in time (spring- neap, dry-wet) and in space (channel and shoal, upper and lower reach). Figure 2.15 shows the sample locations for the bed sediment samples taken in the dry season (February, 2003). In Figure 2.16 the mean grain diameter is plotted against the depth and the distance along the estuary from Jiangyin. The mean diameter in this figure ranges 6 to 250 μm. The distribution of the sediment diameter shows longitudinal (downstream) and lateral (cross-stream) variations. In downstream direction the sediment becomes finer from land to sea, in cross-stream direction the sediment is finer on top of the shoals (small water depth) than that in the deeper parts of the channel. The diameter at the wave-exposed shoal face (e.g. D30, D44) are large even with small water depth.

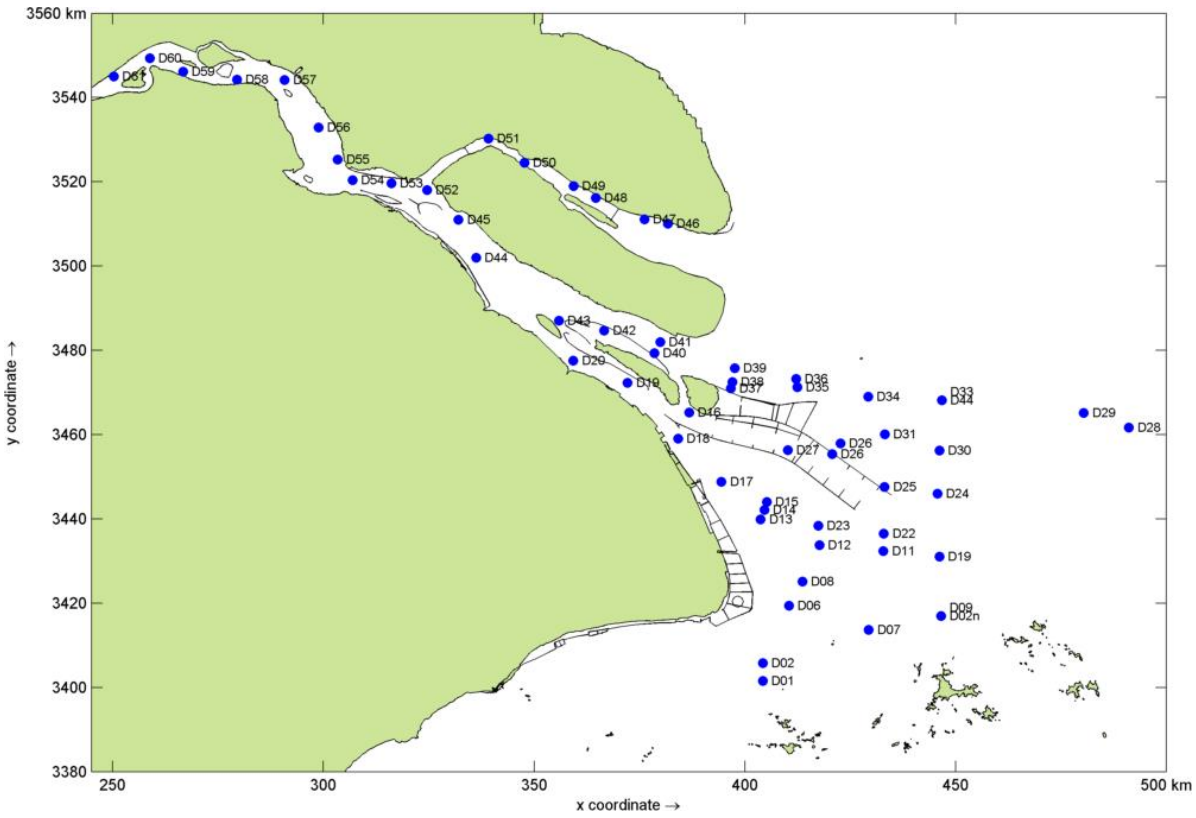

Fig.2.15 Location for sediment samples taken at the top layer of the bed in Feb. 2003

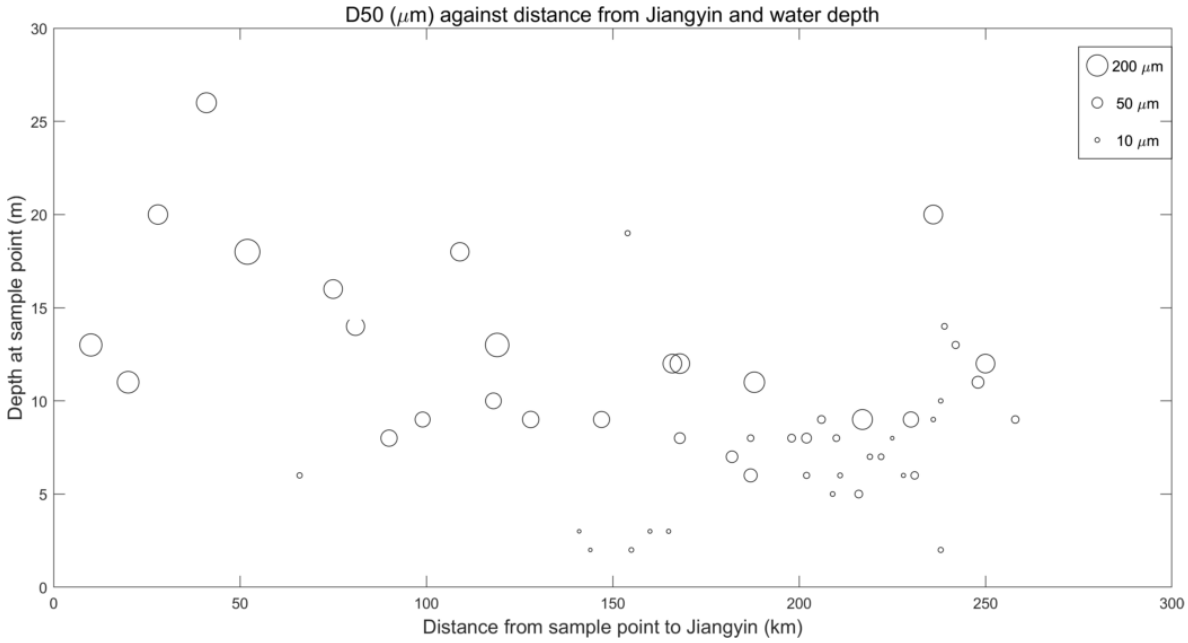

Fig.2.16 Mean sediment diameter in the top layer of the bed against the distance from sample point to Jiangyin (X-axis) and the water depth (Y-axis) in Feb. 2003

Some sediment samples were taken at the top layer of the bed at the locations (Figure 2.17) in August 2005. The clay, silt and sand fractions of each sample are also shown in Figure 2.18. The longitudinal distribution of the fines is similar to the one described by Yun (2004). There is a transition point around the bifurcation of SP and NP. Seawards of this point, silt and clay fractions are clearly dominant, whereas at the landward side the sand fraction (>64μm) is more dominant.

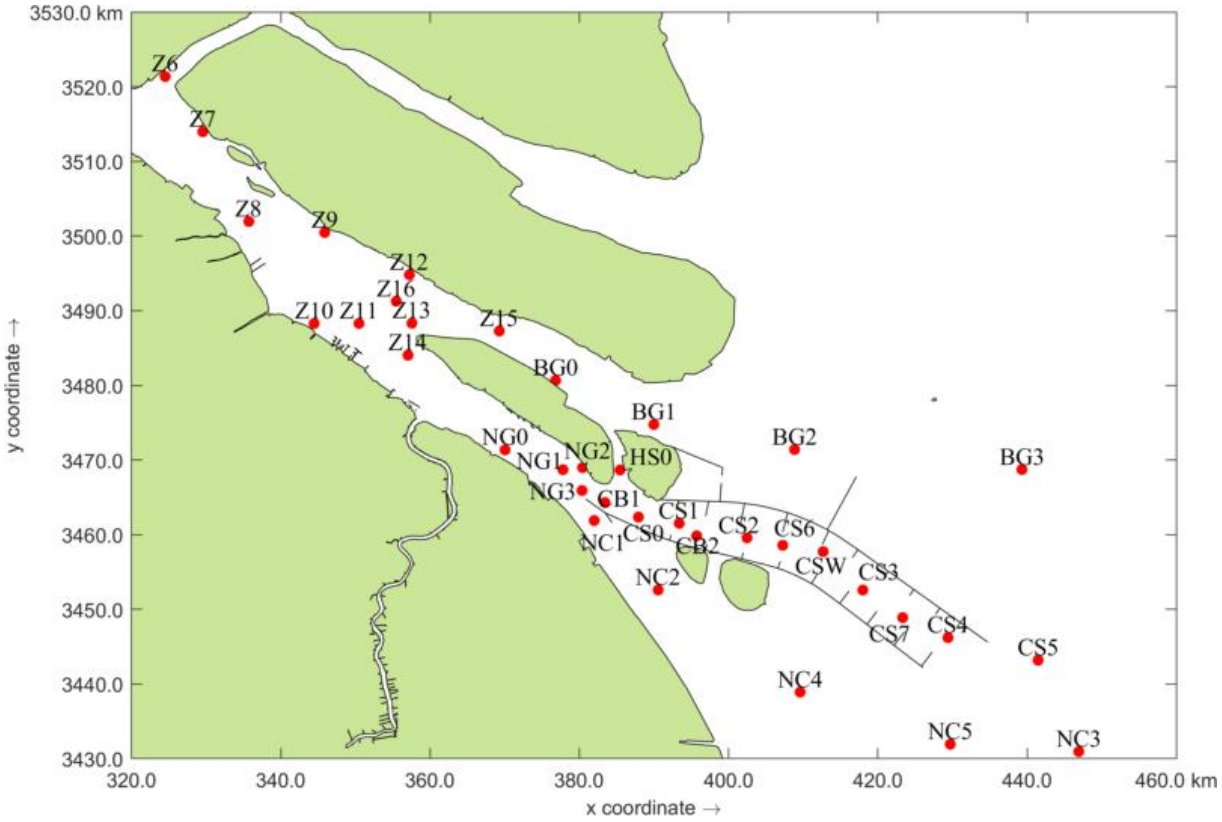

Fig.2.17 Locations of bed sediment samples in the Yangtze Estuary in August 2005

Bed sediment samples of 5 cm thick surface layer along the reach from Datong to Jiangyin were also taken in October, 2006 (see Figure 2.19 for locations). The cumulative frequency of the different grain sizes of these samples is shown in Figure 2.20. The grain size in the upper reach of the estuary ranges from 10 to 280 μm. The sediment is finer at the top of shoals in the reach, which is indicated by the red lines in Figure 2.20. The cumulative frequency of grain size from the samples of August, 2005 (see Figure 2.17 for locations) is shown in Figure 2.21. The mean diameter of the bed material in the reach from Xuliujing to the sea is about 10-120 μm. Hence, we can conclude that the sediment at the bed in the estuary becomes finer in the seaward direction.

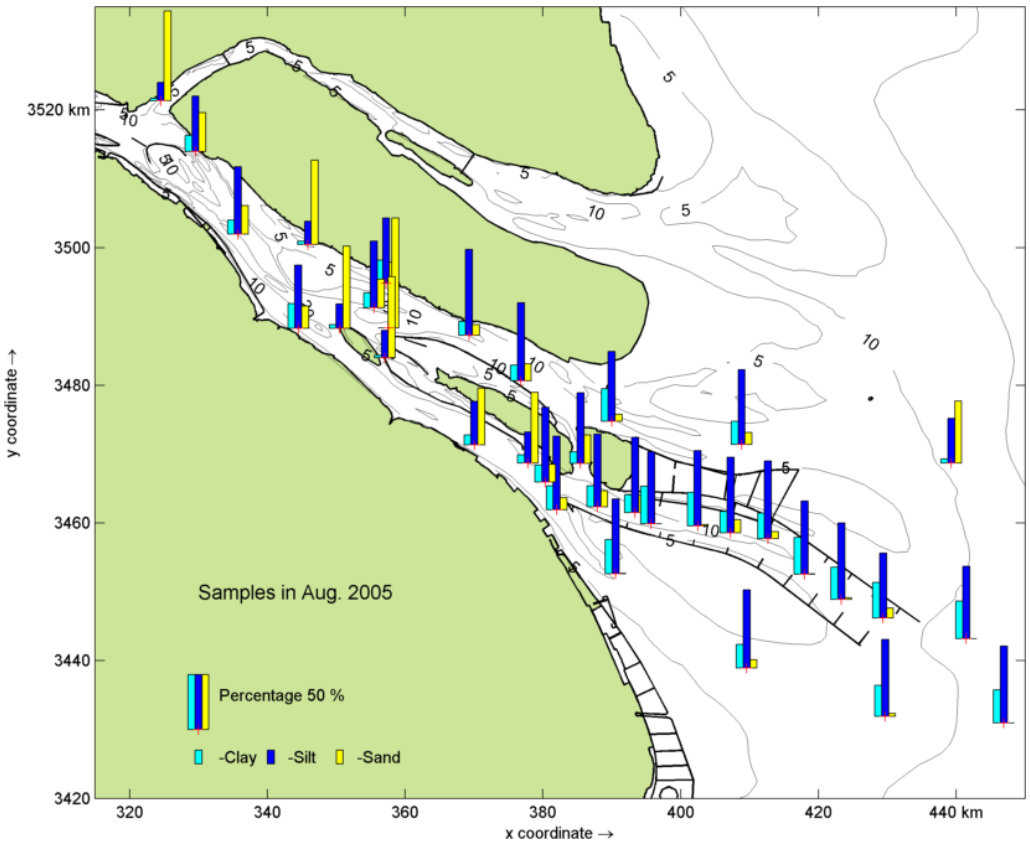

Fig.2.18 Clay, silt and sand composition in sediment sample at top layer of the bed in the Yangtze Estuary in Aug. 2005 (clay: <4μm; silt: 4-64μm; sand: 64-2000μm)

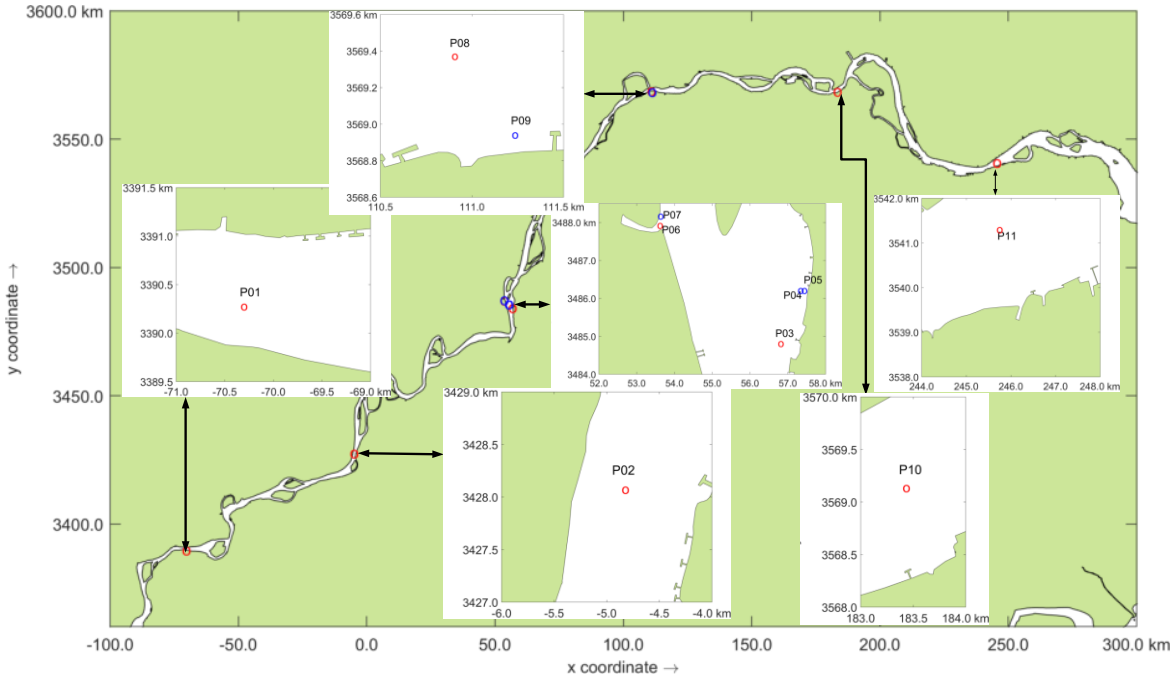

Fig.2.19 Locations of bed sediment samples from Datong to Jiangyin in Oct. 2006

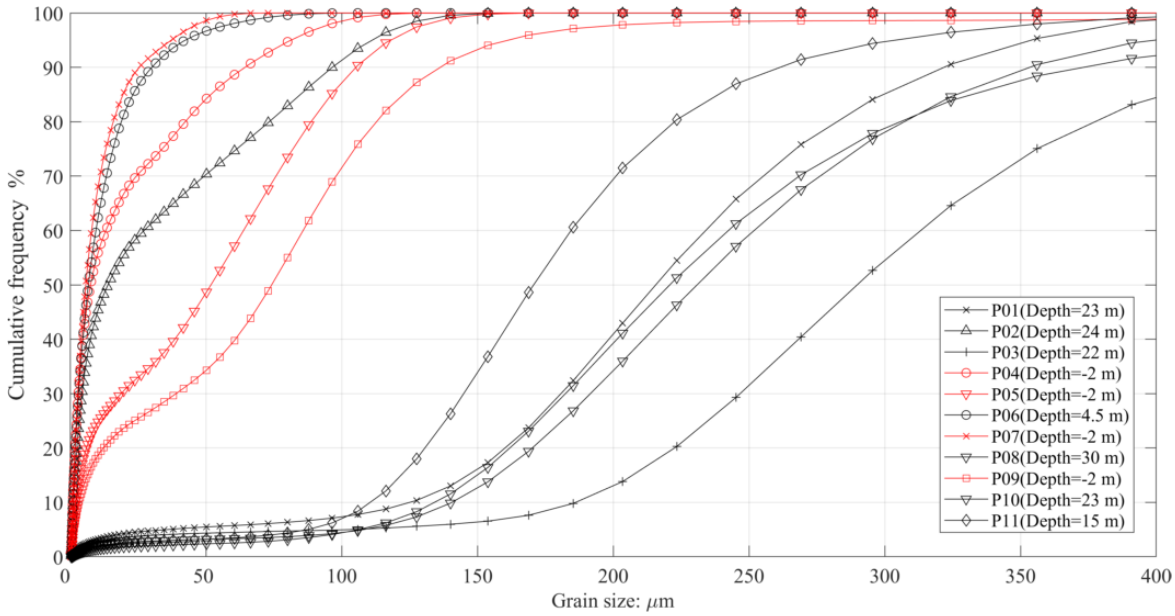

Fig.2.20 Cumulative frequency of grain size in different bed material samples (From Datong to Jiangyin in Oct. 2006)

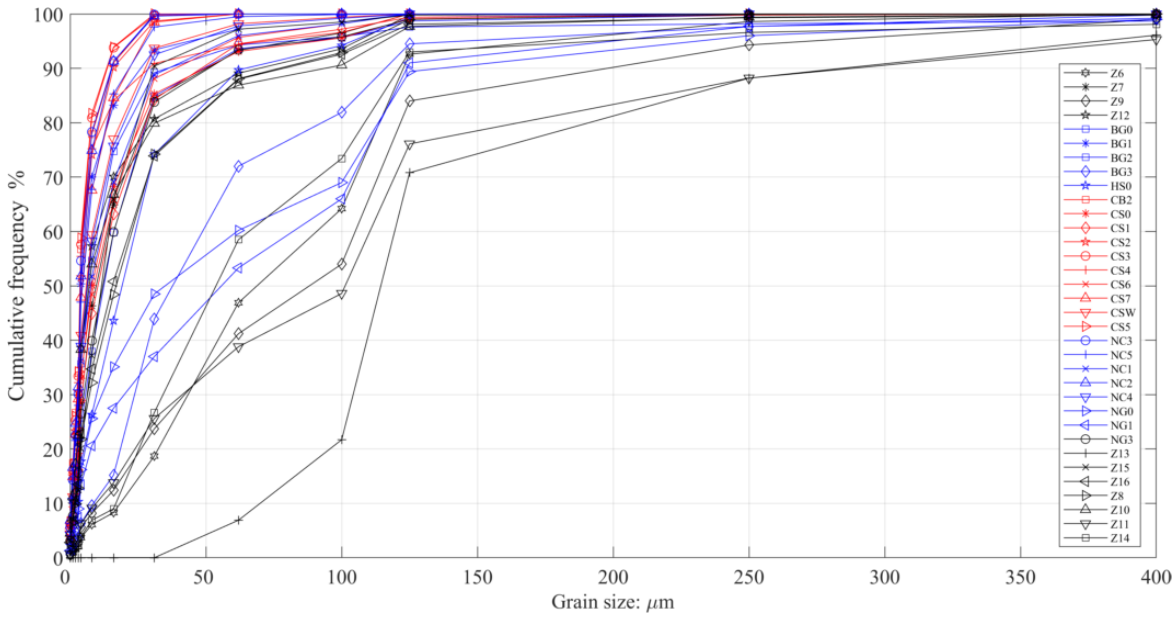

Fig.2.21 Cumulative frequency of grain size in different bed material samples (From Xuliujing to sea in Aug. 2005)

Liu et al. (2010) describe the spatial distribution of the sediment in the Yangtze estuary based on 2 cm thick surface layer of the bottom samples taken from the inner estuary in February, 2003 and from the outer estuary in July, 2006 (Figure 2.22). The large content of silt and clay at the bed of the mouth bar area can be observed from this figure.

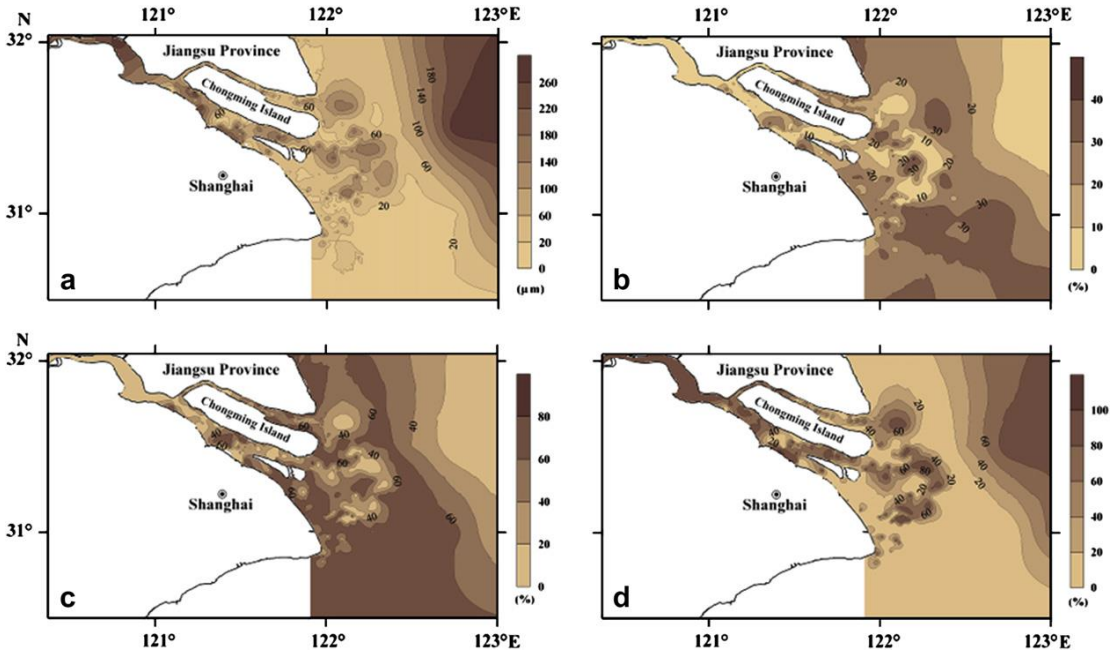

Fig.2.22 Spatial distribution of mean diameter (a), contents of clay (b), silt (c) and sand (d) in sea-bottom sediment (Liu et al., 2010)

Suspended sediment

According to the sediment Bulletins of China (Changjiang Sediment Bulletin, 2001-2017), the mean diameter of the suspended sediment is about 17μm at Datong with the range in 8~42 μm (1953~2000). The mean diameter has decreased to about 10 μm in 2006-2017.

The grain size measurements of suspended sediment at some locations in the reach from Datong to Jiangyin in Oct. 2006 and in the reach from Xuliujing to the sea in August, 2005 are also available to gain more insight of the suspended sediment in the estuary. The locations of suspended sediment sample in the reach from Datong to Jiangyin is shown in Figure 2.23, with the locations of suspended sediment sample in August 2005 shown in Figure 2.17. Figures 2.24 and 2.25 show the grain size distribution of the suspended sediment at different locations. Clearly, the suspended sediment in the upper reach of the estuary mainly consists of clay and silt fractions. The mean diameter of the suspended sediment is about 5-8 μm. In the reach from Xuliujing to the sea, the grains size of the suspended sediment shows a much larger range than that in the upper reach. The mean diameter varies in the range 5-30 μm. The sand fraction is mainly found in the layers near bottom.

The mean diameter of the suspended sediment and bed material along the estuary is summarized in Table 2.8. In conclusion, suspended sediment in the Yangtze Estuary is mainly fine-grained sediment typically in the silt and clay range, with a small content of fine sand. The bed material in the Yangtze Estuary mainly consists of fine sand and silt. The suspended load in the reach from Datong to Jiangyin does not appear in the bed, as has little exchange between the suspend sediment and bed. This reveals that the suspended sediment in the upstream of the Yangtze Estuary acts as wash load. Further downstream, this wash load is deposited and is re-suspended, thus becomes part of the

morphological processes around the mouth bar area, as agrees with the description of longitudinal characteristics of suspended sediment by Yun (2004).

Table 2.8 Mean diameter of sediment in the Yangtze Estuary

Reach	Suspension d_{50} (μm)	Bed material d_{50} (μm)
Datong ~Jiangyin	5-8	10-280
Xuliujing~ Sea	5-30	10-120

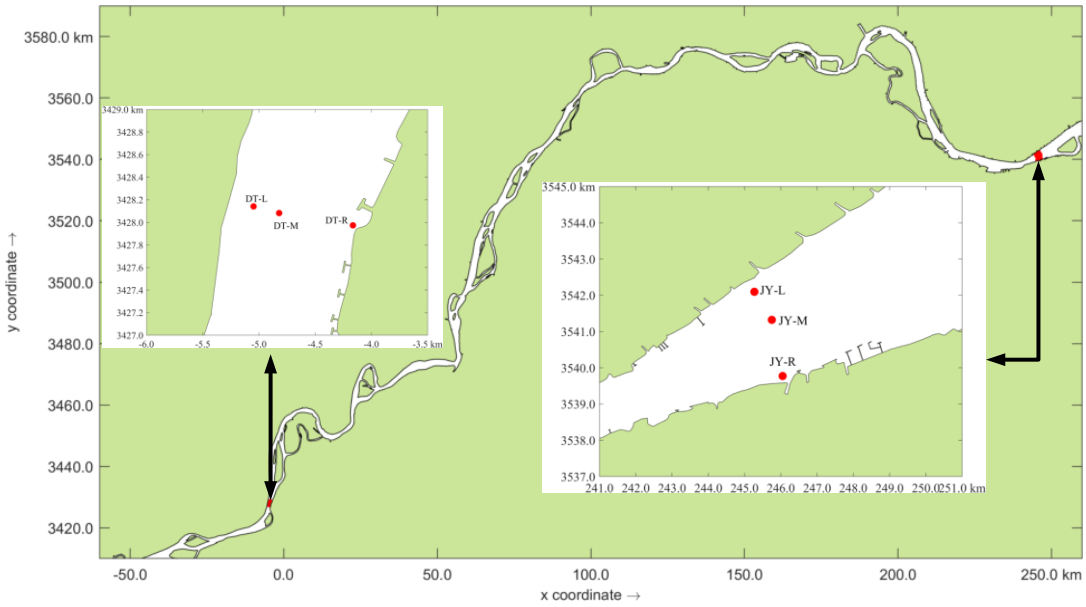

Fig.2.23 Locations of Suspended sediment samples from Datong to Jiangyin in October 2006

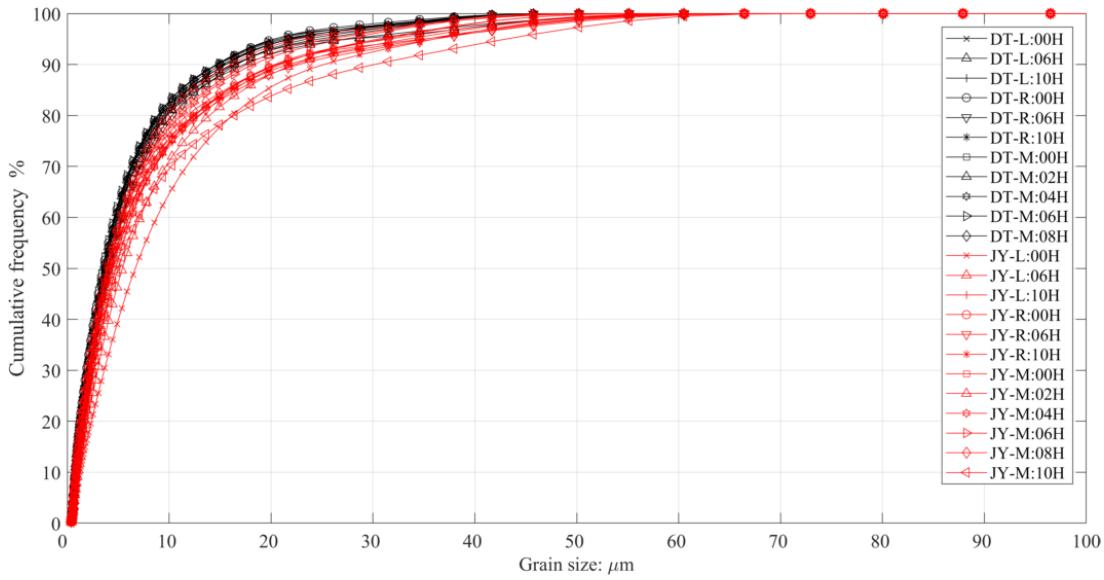

Fig.2.24 Cumulative frequency of grain size in different suspended sediment samples (From Datong to Jiang in Oct. 2006)

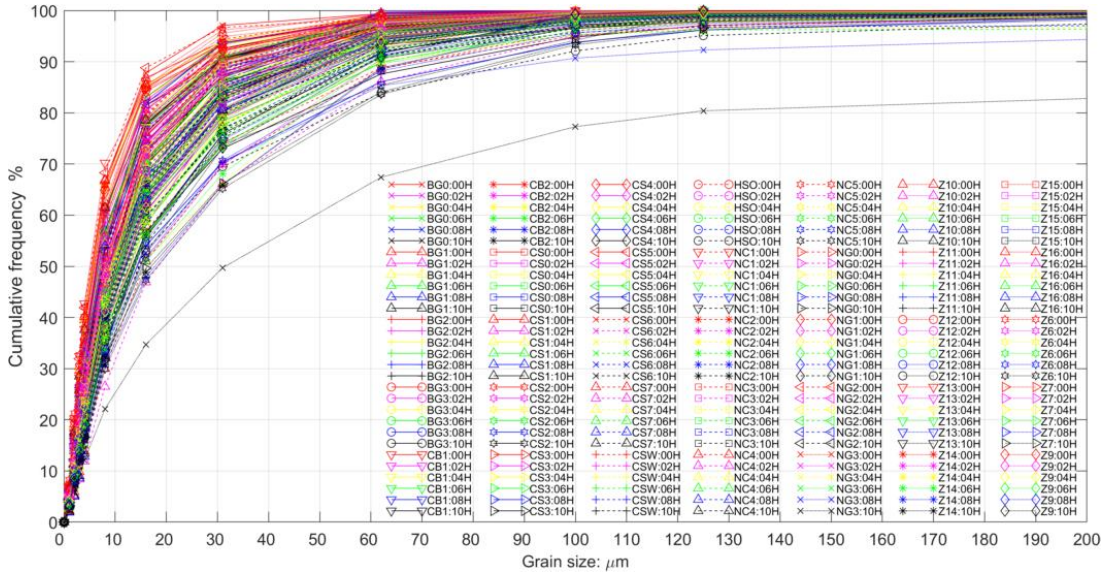

Fig.2.25 Cumulative frequency of grain size in different suspended sediment samples (From Xuliujing to sea in Aug. 2005)

2.3.4 Sediment transport

The sediment transport and the sediment budget of the Yangtze Estuary has been studied by Lin (1984), Milliman et al. (1985), Su and Wang (1989), Eisma (1998) and Dai et al. (2013), Zhao et al. (2018). However, these studies are based on the limited measurements in the estuary or within certain part of it. To our knowledge, a systematic study of the overall sediment budget is still lacking. The main problem behind this is that the Yangtze Estuary is such a huge and complex system, hydrodynamically as well as sedimentologically (Milliman et al., 1985).

Shen et al. (2001) analyze bathymetry differences based on navigation charts from the last 150 years. They indicate that about 80% of the sediment from the river ultimately reaches the river mouth. About 30% is deposited in the subaqueous delta east of the river mouth, 40% is deposited in the Hangzhou Bay, and the remaining 10% is transported further to south. This sediment budget has raised much discussion, because navigation charts are primarily meant to enable safe navigation, not to accurately map out the bathymetry. Yang et al. (2003) analyze the bathymetric data of the Yangtze sub-aqueous delta surveyed from 1958 to 1997 together with the river sediment data of the same period. They propose a concept of the critical threshold of river sediment discharge that separates delta progradation from recession.

Recently, Wang et al. (2015) investigate the human impact on morphodynamic thresholds in estuarine systems, such as the Scheldt Estuary and the Wadden Sea basins in the Netherlands and the Yangtze Estuary in China, at various spatial scales, and identify mechanisms responsible for their change. They define the mega-scale development of the Yangtze Estuary thresholds in the fluvial sediment input into three aspects: the development of the sub-aqueous delta, the development of the tidal flats and the tidal amplification (via apparent hydraulic drag influenced by turbidity). Zhao et al. (2018) analyze the bathymetry data measured in the area from Xuliujing to sea in

the period 1958 and 2016. They conclude that the estuary exhibits an overall deposition trend in the last half century. The up-part of the SB (South Brach) was net eroded whereas the mouth bar area is net deposited.

2.4 Morphological development

Figure 2.26 sketches the layout of the Yangtze Estuary in ancient times (solid lines) compared with the present situation (dash line). Chen (1957), Chen et al. (1959, 1979) and Yun (2004) describe the estuary development over the last 2000 years from morphological point of view. They conclude that the sedimentation process of fluvial sediment dominates in this period. The south bank of the estuary extends towards sea. At the same time the shoals and island in the north of the estuary connected with the north bank and formed new land. Thus, the river mouth was narrowed and pushed seawards. The river courses were formed and channels were deepened.

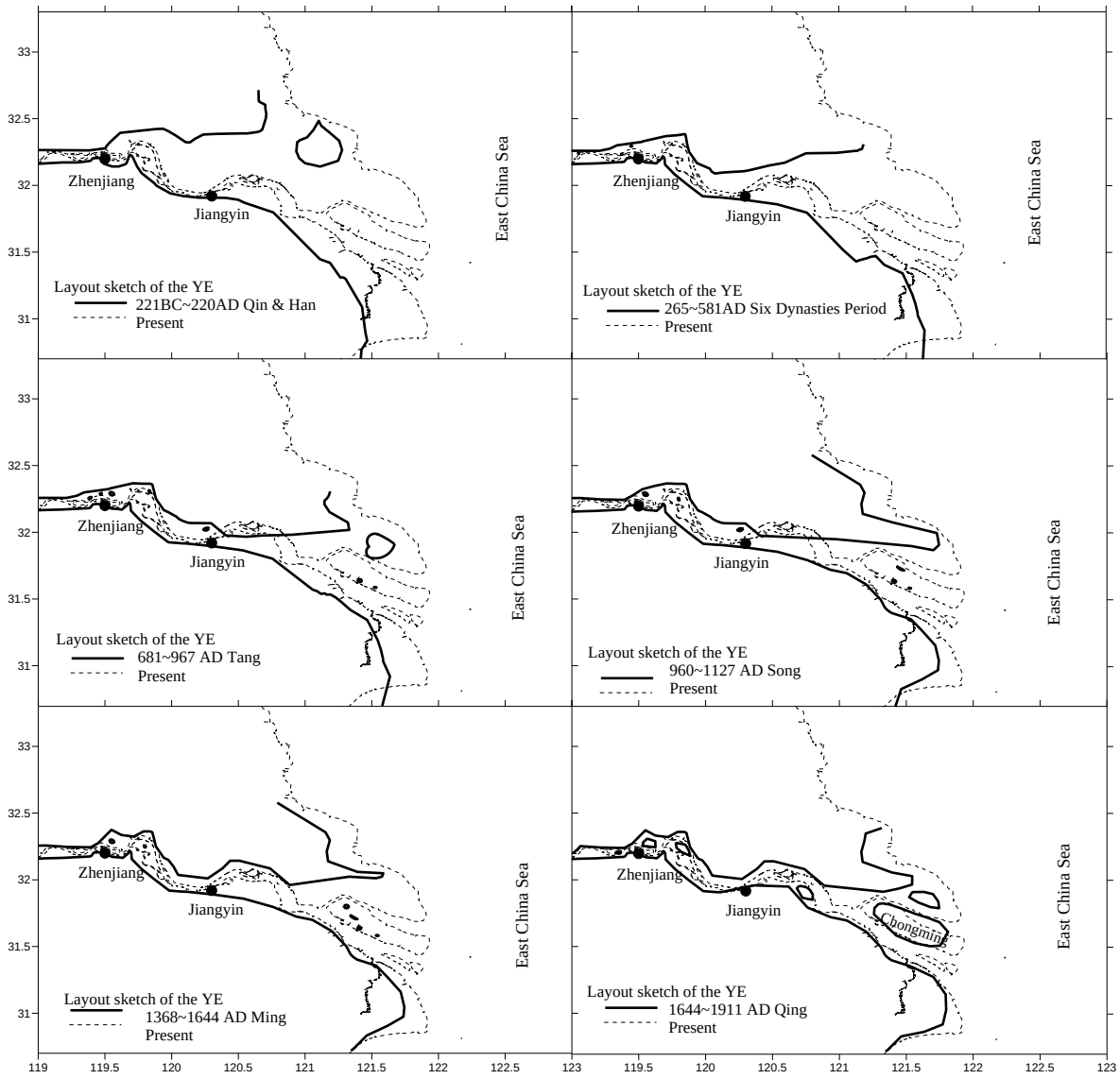

Fig.2.26 Coastline evolution of the Yangtze Estuary over time

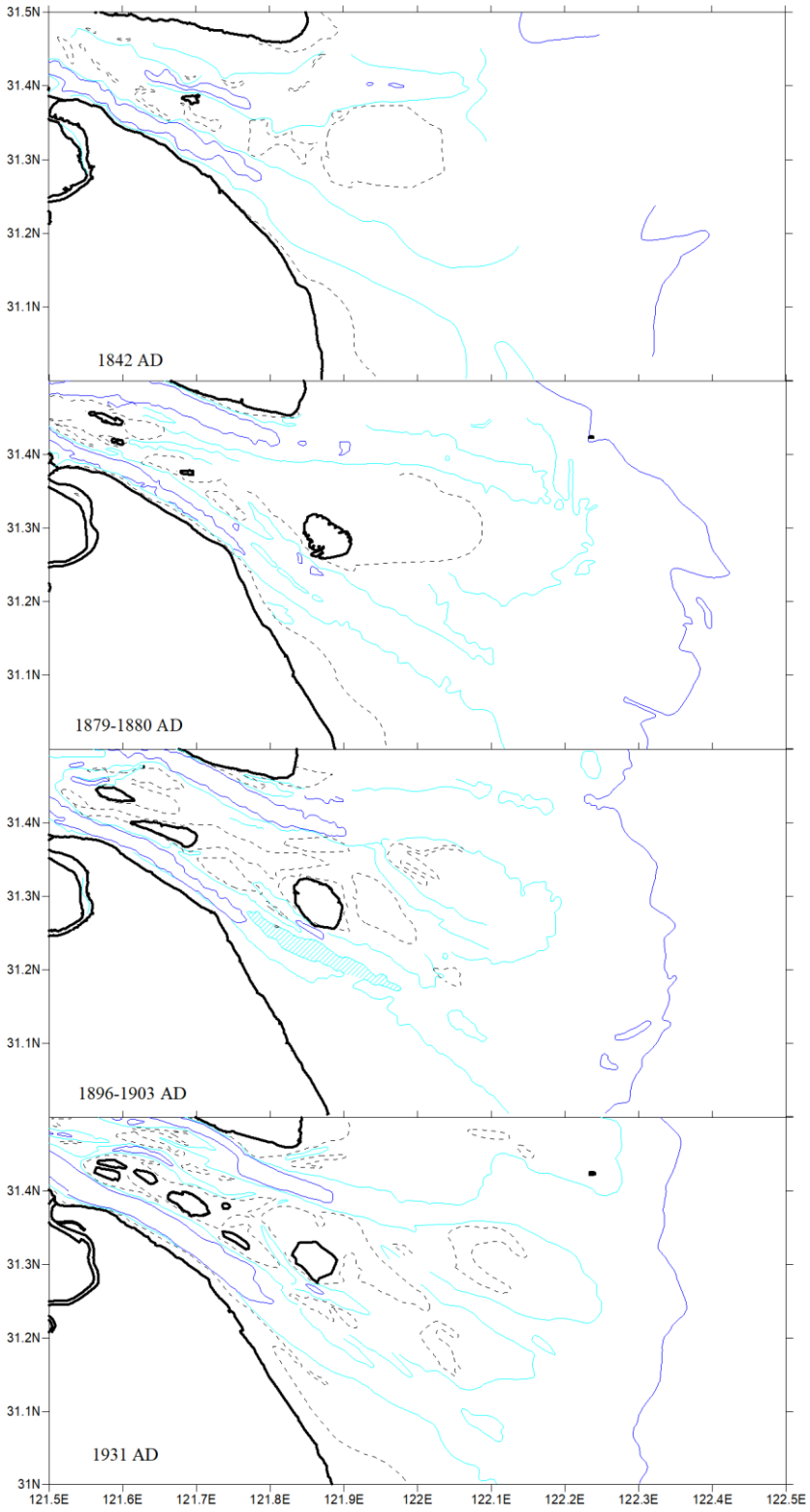

Fig.2.27a Layout and bathymetry around the mouth bar of the Yangtze Estuary (from top to bottom:1842, 1879-1880, 1896-1903 and 1931; black thick solid line: coastline; black dashed line: -2m contour; cyan solid line: -5m contour; blue solid line: -10m contour)

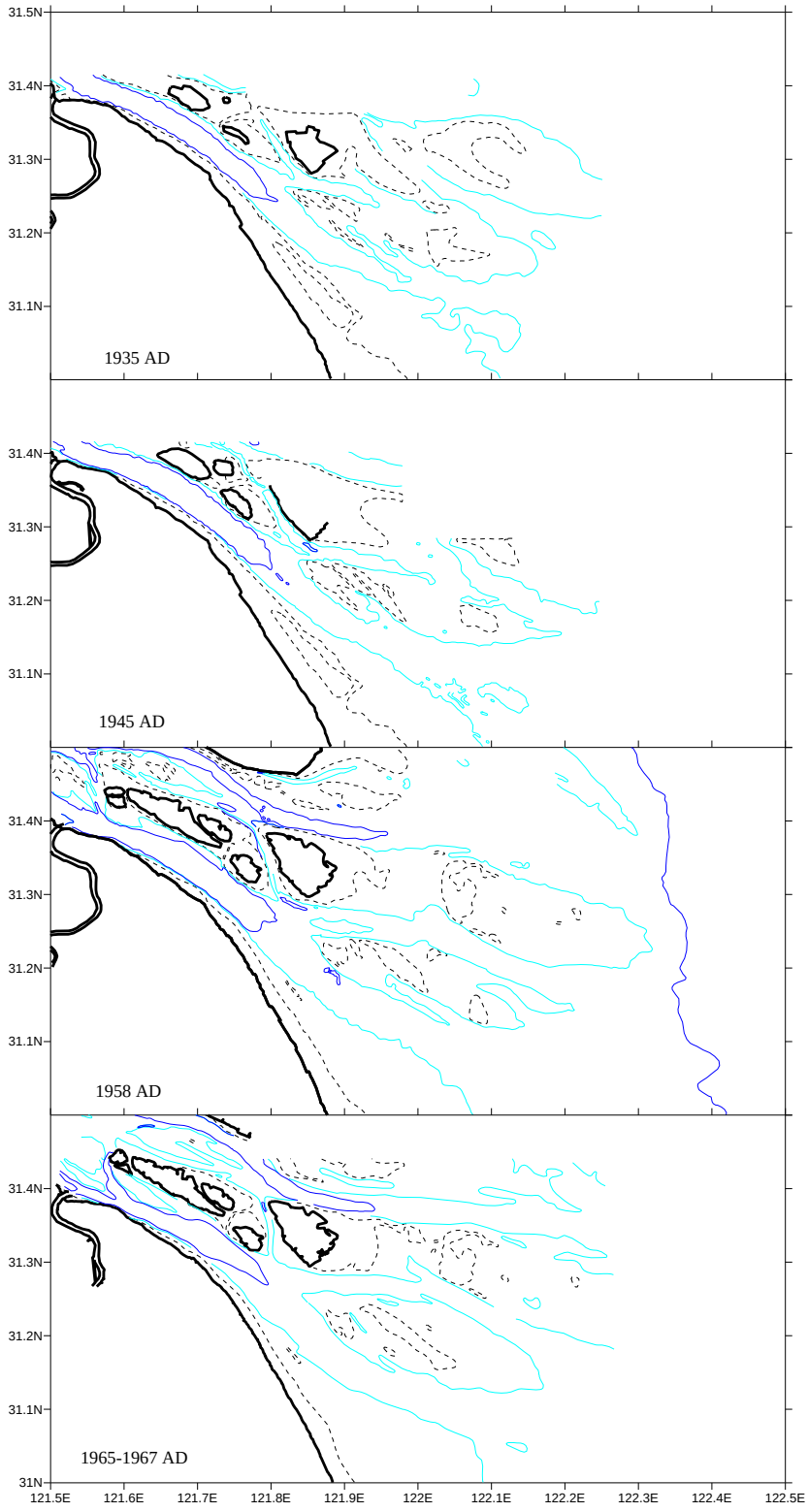

Fig.2.27b Layout and bathymetry around the mouth bar of the Yangtze Estuary (from top to bottom :1931, 1935, 1945 and 1965-67; black thick solid line: coastline; black dashed line: -2m contour; cyan solid line: -5m contour; blue solid line: -10m contour)

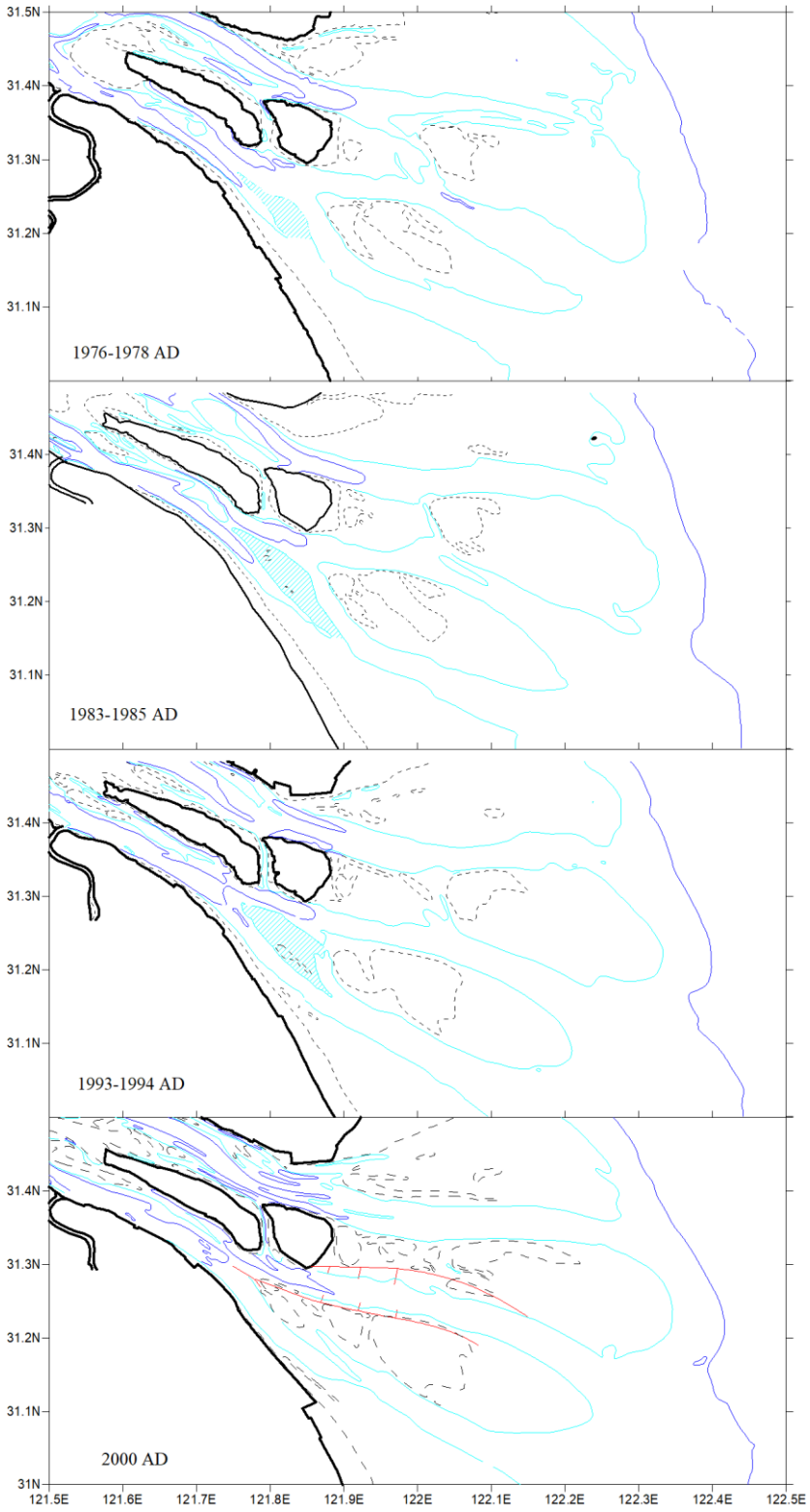

Fig.2.27c Layout and bathymetry around the mouth bar of the Yangtze Estuary (from top to bottom: 1976-1978, 1983-1985, 1993-1994 and 2000; black thick solid line: coastline; black dashed line: -2m contour; cyan solid line: -5m contour; blue solid line: -10m contour; red line: DDC project)

Figure 2.27 shows the bathymetry around the mouth bar of the Yangtze Estuary every one or two decades since 1842. It demonstrates the evolution of channels and shoals around the mouth bar. The mouth bar, the shallow area between the upper reach and the sea already existed at the time of the first bathymetry data in 1842. The channel-shoal pattern around the mouth bar varied and new islands (Changxing and Hengsha) and shoals (Jiuduansha) established. As a consequence, the two-tier bifurcation of the South Branch formed (Yun, 2004). Yang et al. (2006) summarize the expansion rates of shoals (wet lands) in the mouth bar area in the last 50 years. They conclude that the shoals were relatively stable and kept on expanding until the 1990's. Recession of the shoals is observed since the 1990's and is attributed to the large reduction of the sediment input from upstream (Yang et al., 2006).

Wu et al. (2002) calculate the volume change in the mouth bar area (shown in Figure 2.28) based on navigation charts since 1842. They derived the volume of the area below MSL (Mean Sea Level: about 2 m above chart datum at the river mouth) at different points in time and obtained the amount of the erosion/sedimentation (Table 2.9). They conclude that deposition in general dominated in the mouth bar from 1842 to 1997, mainly at seaward faces of Hengsha, Jiuduansha and Chongming Island. Erosion occurred in the NP, the upper section of the NC and a minor part of the SP.

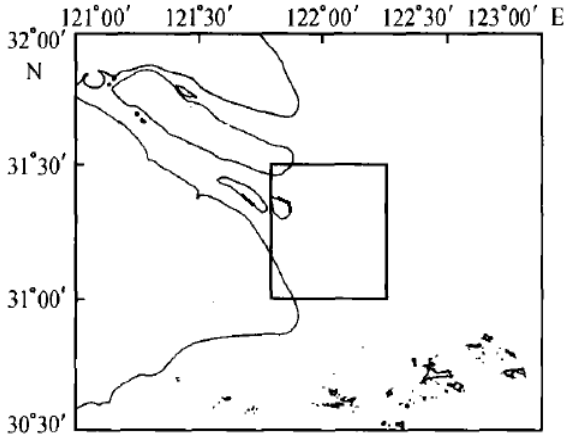

Fig.2.28 Area (rectangle) for erosion and sedimentation calculation (Wu et al., 2002)

Table 2.9 Erosion and sedimentation in the study area of the mouth bar of the Yangtze Estuary (Wu et al., 2002)

Period	Deposition (Million tons)	Annual deposition (Million tons/a)	Thickness of Deposition (m)	Deposition rate (cm/a)
1842-1880	2620	68.9	0.93	2.45
1842-1908	163	5.8	0.04	0.21
1908-1927	196	10.3	0.07	0.36
1927-1965	-181	-4.8	-0.06	-0.17
1965-1980	797	53.1	0.28	1.88
1980-1990	1298	129.8	0.47	4.65
1990-1995	163	32.7	0.06	1.18
1995-1997	-335	-167.4	-0.12	-6.19
1842-1997	3801	24.6	1.68	1.10

'-'indicates the occurrence of erosion.

2.5 Transport processes in the Yangtze Estuary

2.5.1 General overview of literature on transport process in estuaries

In general, fine suspended sediment concentrations in shallow basins (like estuaries, tidal inlets and lagoons) are much larger than those in the surrounding environment, i.e. river reaches and adjacent seas. This phenomenon is due to the following two mechanisms:

- The trapping of sediment within the system due to the balance between the landward transport (e.g. flood tide, gravitational circulation) and the seaward transport (e.g. river discharge, ebb tide);
- Some very fine sediment (clay fraction) remaining in suspension.

In the literature explanations are given of the high turbidity in these systems, for instance for the Wadden Sea (Postma, 1967; Groen, 1967; Dronkers, 1984), the Severn Estuary (Dyer, 1997), and the Yangtze Estuary (Shen, 2001). The relevant sediment transport processes and mechanisms discussed by these researchers are:

1. River flow

In most estuarine systems a net throughflow of water exists due to river discharge. Some of the rivers are regulated by upstream damming, which generally leads to a decrease of the sediment transport in the estuary. The influence of rivers with a large runoff and/or an abundant sediment load, however, cannot be ignored. For the Yangtze Estuary, the TGD now regulates the river discharge regime, with more discharge than before in the dry season and less in the wet season. One of the other interferences is the water conservation and soil protection project (Zhang and Liao, 2008) in the river basin, which strongly decrease the sediment yield from the river basin. The large decrease of sediment load at Datong since 1990s' is directly related to this project.

2. Tidal asymmetry

Van Straaten and Kuenen (1957), Postma (1967), Groen (1967), Dronkers (1984) Wang et al. (2002) and Guo et al. (2014) extensively discussed the net sediment transport due to tidal asymmetries. They conclude that, apart from velocity and ebb-flood duration asymmetries (important for coarse sediment), the asymmetry of slack water periods can be important for fine sediment transport. Also, the integration of the water motion over a tidal period yields a residual mass flux, known as Stokes' drift (Dyer, 1997), if the horizontal and vertical tide are not 90° out of phase. Geometry and structure can also induce horizontal asymmetry in estuaries with large intertidal areas (Wang et al., 2002).

3. Gravitational circulation

Fresh water from upstream flowing into coastal systems leads to horizontal density gradients. Such gradients generate a circulation in the system (called gravitational or estuarine circulation) with a net landward current near the bed. According to the vertical sediment concentration profile the concentration tends to be higher near the bed than that in the upper part of the water column. Thus, the gravitational circulation generates a net landward sediment transport.

The density of sea water depends on both salinity and temperature. In estuaries, the salinity range is large due to the mixing of fresh and saline waters, whereas the temperature range is generally small. This means that the influence of temperature gradients on density is negligible. We will therefore regard density currents induced by salinity gradients as the main contribution to the gravitational circulation.

4. Waves

Waves introduce extra turbulence and bed shear, thus stirring sediment from the bed and keeping it in suspension. Note that even small waves may already have a significant effect when they reach shallow water. This may be one of the explanations why the exposed parts of intertidal flats in estuaries are often more sandy than that in no-exposed area (e.g. Yun, 2004). Landward transport mechanisms (e.g. gravitational circulation, tidal asymmetry) in conjunction with the wave stirring effects lead to import of marine sediment or trapping fluvial sediment in the system.

5. Other transport process

Besides the mechanisms mentioned above, some others influence the sediment transport in estuaries, lagoons and tidal inlets. The temperature increases in summer will lower the fluid viscosity, hence augments the flocculation and the settling velocity of fine-grained sediment (Lin et al., 1995). The consolidation mechanism is also an important factor influencing the erodibility of the sediment (Teisson et al., 1993; Sanford, 2008; Van Kessel et al., 2011) the sediment transport with large range Biological processes are also seasonal and may influence sedimentation/erosion.

6. Human activities

The human activities can also strongly influence sediment transport phenomena and morphological changes in estuaries. Sometimes they directly change the bathymetry, e.g. by dredging or land reclamation. In other cases, they change the environmental conditions (e.g. regulating the flow regime by dams, or changing reflection properties of banks, or removing sediment trapping vegetation). In response to these alterations, sediment transport patterns and estuarine morphology will change, sometimes with a significant time lag. Local engineering works in the Yangtze Estuary, such as the DDC project, the large fresh water reservoirs and the reclamation works on the shoals, inevitably influence the sediment transport and the morphology in the estuary.

2.5.2 Transport mechanisms for the mouth bar area of the Yangtze Estuary

Various mechanisms which may influence the sediment transport have been discussed above. This gives guidance to the investigation of the sediment transport and the morphological change in estuaries. When considering the Yangtze Estuary, and especially the mouth bar area, the following processes/mechanisms for trapping sediment in the estuary in addition to tides need to be investigated.

- River runoff: this is so large that it obviously cannot be neglected. The associated sediment load is the main sediment supply to the estuary. Therefore, the fluvial processes should be taken into account.

- Estuarine circulation: the high turbidity level in the Yangtze Estuary reveals that there is a landward sediment transport mechanism that balances the net seaward transport by the river runoff. The salinity-induced gravitational circulation should therefore be considered.
- As fine cohesive sediment is predominantly present in the suspended sediment, fine sediment behavior (e.g. flocculation) is important to the sediment transport in the estuary.
- The yearly mean wave height ($H_{1/10}$) is in the order of 1 m in the estuary (Chen, 1998) if calms are ignored. Waves with significant height less than 1 m can have a substantial effect, especially in shallow areas. For longitudinal sediment trapping, an important formation mechanism of the mouth bar, the influence of waves will be therefore investigated.
- Engineering works in the estuary or in the river basin can modify the sediment transport in the estuary. Here, the influences of TGD and local DDC project on the sediment transport in the Yangtze Estuary are also taken into account.

The mentioned mechanism for sediment transport will be assessed and the formation of the mouth bar will be discussed in the following chapters.

3. Process-based model for the Yangtze Estuary[1]

3.1 Introduction

Although the morphological evolution of the Yangtze Estuary (Figure 3.1) has recently been the subject of a number of studies, which give access to extensive database and valuable information, its quantitative prediction rests mainly on extrapolation of measured data (Wang, 1986; Yu and Lou, 2004; Fan et al., 2006; Wang et al., 2007; Guo et al., 2014; Wei et al., 2017; Zhao et al., 2018) and empirical input/output relationships (Ding and Shi, 2000; Yang et al., 2001, 2006). The development of the Yangtze Estuary, however, is affected by human activities in the estuary as well as in the river basin. The river discharge into the Yangtze Estuary has changed due to engineering works in the river Basin. Massive dam building in the reservoir, including the completion of the TGD in 2003, has led to a significant reduction of the SSD into the Yangtze Estuary (Yang et al., 2005). These changes, together with the large-scale engineering works in the estuary itself and changing environmental conditions such as climate change and accelerated sea level rise, inevitably influence the morphological development of the estuary. Taking the effects of these changes and interferences into account is far beyond the possibilities offered by extrapolation of measurements and the application of empirical relationships. It is therefore critical to gain insight into the hydrodynamic and sediment transport processes associated with the system's response to the changes and interferences, in order to be able to predict this response and design adequate countermeasures.

As computer power grows, sophisticated morphodynamic models based on a detailed description of hydrodynamic and sediment transport processes are becoming increasingly valuable tools for coastal engineering and management. This type of models has benefited from a wide variety of practical applications worldwide (Gelfenbaum et al., 2003; Grunnet et al., 2004; Tonnon et al., 2007; Kuang et al., 2013; van der Wegen et al., 2016; Chu et al., 2018). The aim of this study is to gain insight into the processes relevant to the morphological evolution of the Yangtze Estuary, so as to understand the system's response to engineering works and environmental changes. We use a process-based hydrodynamic model for the Yangtze Estuary as the basic step to a morphodynamic study.

The process-based model for the Yangtze Estuary is set up based on the Delft3D modeling system, which fully integrates the effects of waves, currents and sediment transport on morphological developments in coastal, fluvial and estuarine waters (Roelvink and van Banning, 1994; Lesser et al., 2004; Hu et al., 2009; van der Wegen 2010; Gong et al., 2012; Kuang et al, 2013). The modeling system consists of a few

[1] This chapter is based on the conference papers 'Process-based Modeling for the Yangtze Estuary' by A. Chu, Z.B. Wang and H.J.de Vriend, presented at Coastal Dynamics 2009, and 'A Process-based Approach to Sediment Transport in the Yangtze Estuary', by A. Chu, Z.B. Wang, H.J.de Vriend and M.J.F Stive, presented at ICCE 2010.

modules, such as flow, wave and morphodynamic change, which can be coupled at time step level. A detailed description of those modules is reported by van Rijn (2000) and Lesser et al. (2004).

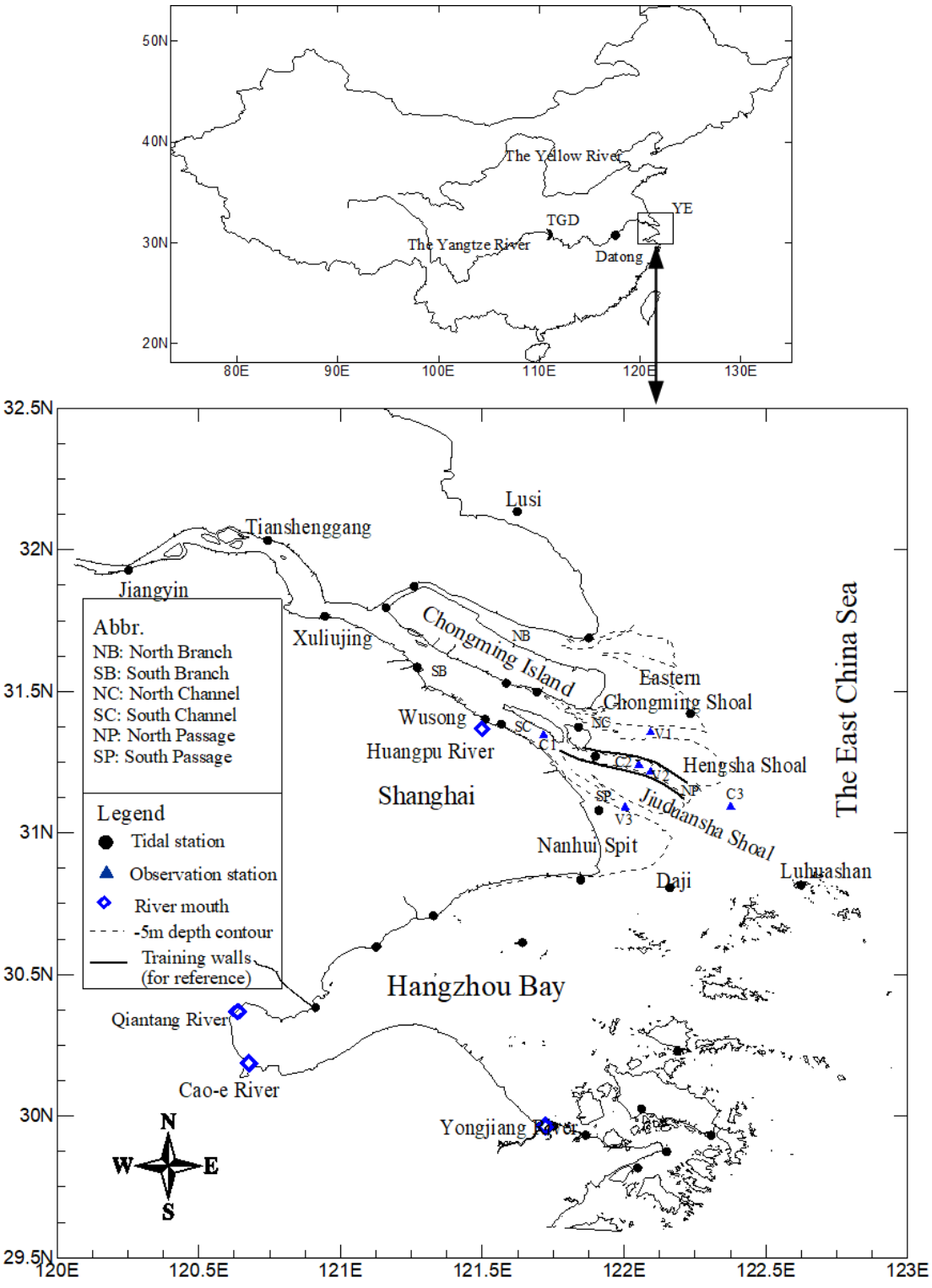

Fig.3.1 The study area and the layout of the Yangtze Estuary

3.2 Model set-up

3.2.1 Study area and model domain

Figure 3.2 shows the flow model domain, which covers the entire tidal region of the Yangtze River and its estuary, Hangzhou Bay and a part of the adjacent East China Sea. Instead of taking Jiangyin as the upstream river boundary, as was done in most previous models (Wu et al., 2006; Hu et al., 2009), the upper limit of the present model is taken at Datong, the tidal limit in wet season. One of the advantages of this set-up is that the upstream boundary is free from tidal effects. Another advantage is that long series of measured discharges and SSC are available at Datong gauging station, which can be directly provide as the boundary conditions. The same consideration is also applied to the Qiantang River, with the grid extending up to Lucipu, the lowest discharge observation station along this river. The adjacent water bodies, Hangzhou Bay and part of the East China Sea, are important for exchanging water, sediment and other substance from the Yangtze Estuary. Especially the interchange between the Yangtze Estuary and Hangzhou Bay cannot be neglected (Du 2007; Huang, 2007).

The flow model domain extends over some 800 km long in longitudinal direction and some 400 km in lateral direction. For computational efficiency, domain decomposition (Deltares, 2014) is applied. The model is separated into three domains, with internal boundaries at Xuliujing and Haining cross sections, as indicated by the different colors in Figure 3.2. All grids are boundary-fitted and orthogonal curvilinear. The river grid, from Datong to Xuliujing, has 1,056 grid points along the river and 30 in the transverse direction. It covers an approximately 500 km long river reach with grid resolution varying from 100 m to 1.5 km. The Xuliujing cross-section is normally considered as the boundary for salt intrusion. Therefore, the model upstream of this location is 2D depth-averaged. The estuary grid covers the 300 × 300 km area from Xuliujing to the seaward boundary (Figure 3.2). This grid consists of 200×200 grid points with a high resolution near the river outlets and coarser towards the open sea boundary. The grid size ranges from 200 m to 6 km. Simulations can be made with a single layer (2D depth-averaged) or multiple layers (3D) in the vertical. The k-ε turbulence closure is applied in the 3D simulation, with 12 σ-layers accounting for 3, 5, 8, 10, 12, 12, 12, 12, 10, 8, 5, and 3% of total water depth. The finer resolution near the water surface and the bed is meant to better approximate the salinity structure and sediment concentration structure. As there is no detailed bathymetry data available for the Qiantang River, data on the cross-sectional area are used to construct the bathymetry. As this part is far away from the area of interest, the influence on the results there is likely to be negligible.

This estuary grid is also used for wind wave simulations. Waves are computed along with flow model in order to investigate the wave influence on the sediment transport. The islands within the model domain are regarded as obstacles for wave propagation.

The DDC project is also taken into account and represented by local weir (Deltares, 2014) structure in the Yangtze Estuary model.

The bathymetry of the Yangtze Estuary model is shown in Figure 3.3. The bathymetry data is based on navigation charts of 2002. The depths at the grid points are obtained by triangular interpolation. The initial water depth was smoothed in order to get rid of small-scare perturbations, and to prevent unrealistically high sediment transport rates due to bathymetry artifacts.

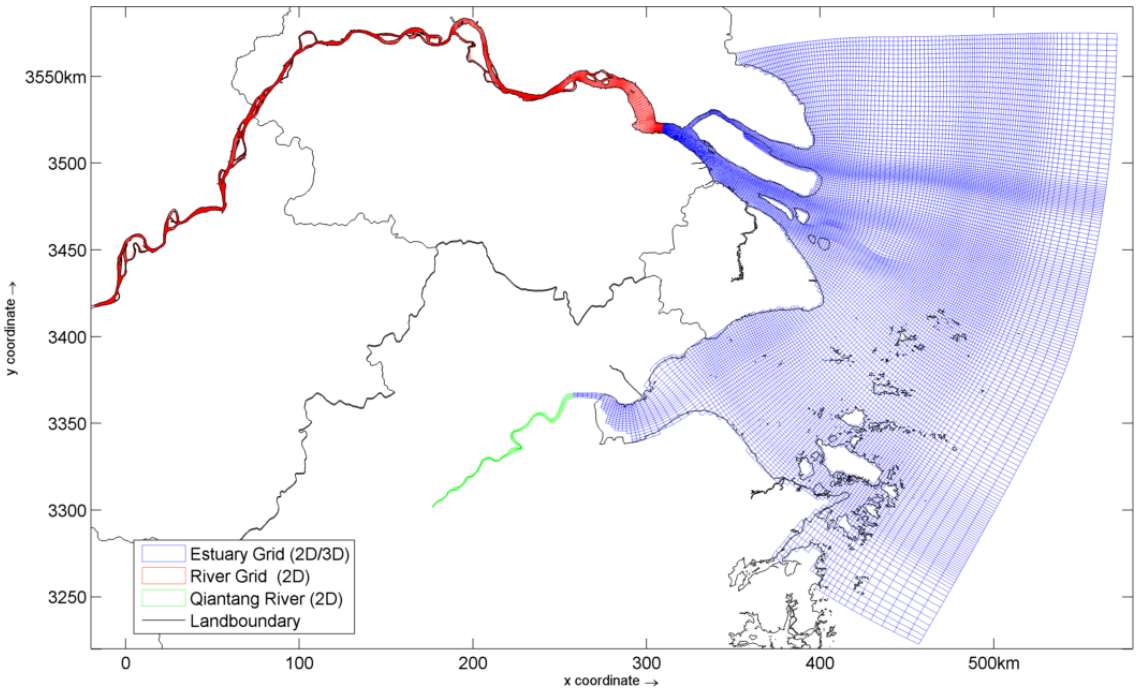

Fig.3.2 Grids of the Yangtze Estuary model (Red grid: Datong to Xuliujing; Blue grid: Xuliujing to Sea; Green grid: Lucipu to Haining)

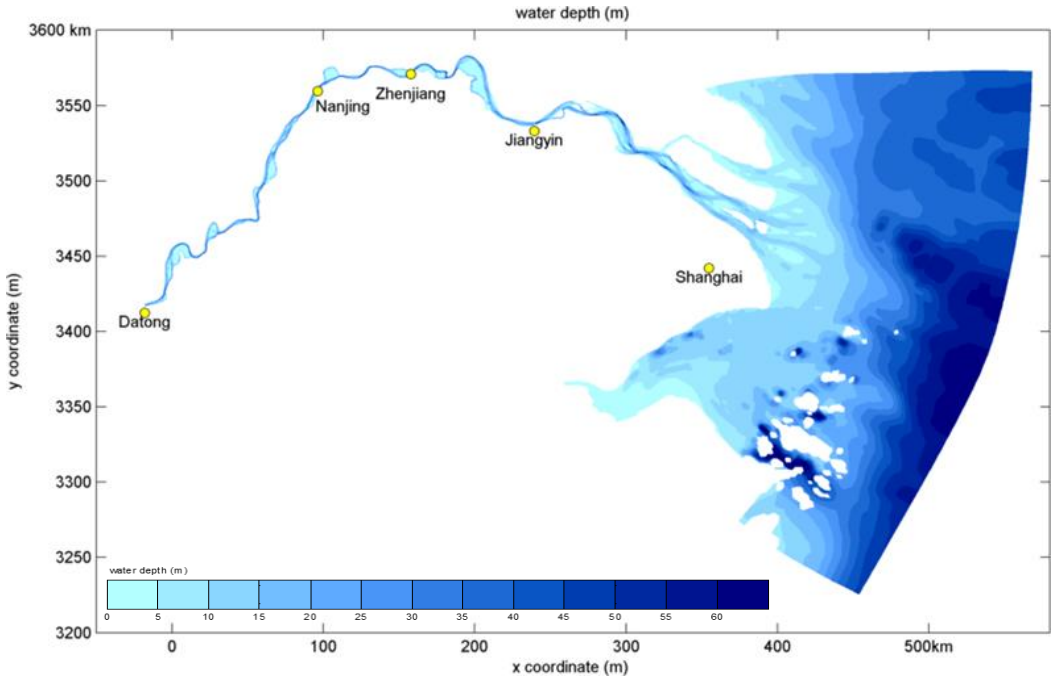

Fig.3.3 The bathymetry in the Yangtze Estuary Model domain (Water depth around the mouth bar is based on measurements in 2002)

3.2.2 Forcing conditions

- River discharge

Classified according to Dronkers (2005) the Yangtze Estuary is an estuary with fluvial deposits shaped by tide. Fluvial sediment supply is the main sediment input to the estuary. As mentioned above, the upstream boundary of the present Yangtze Estuary model is set at the tidal limit, Datong, where a long time series of measured data is available since 1950's. By specifying the monthly or daily observed total discharge with the associated sediment concentration, the fluvial input can be defined. Daily values are used for model calibration and validation purposes, longer-term mean values are used for the simulation to investigate mechanisms contributing to sediment transport in the estuary (Chapter 4).

Besides the Yangtze River, there are four other major rivers (Figure 3.1) debouching in the model domain: the Qiantang River, the Huangpu River, the Cao-e River and the Yongjiang River. Table 3.1 shows the average discharges of the major rivers in the domain. Although the Qiantang River has only 5% of discharge of the Yangtze River, it still has a considerable size and strong tidal currents, including the famous tidal bore. Here the measured discharges and concentrations at Lucipu are specified as the upstream boundary conditions. A weakly reflective boundary condition proposed in earlier study (Wang, 1994) has been applied. According to Table 3.1 and Figure 3.1, neither the discharges of the other three rivers are comparable to that of the Yangtze River, nor the spatial magnitudes of these rivers can practically be resolved in the model. Thus, these three rivers are indicated as freshwater sources in the model with average discharges (Wang, 1994).

Table 3.1 River discharge in the domain (Partly from Wang, 1994)

River	Discharge(m^3/s)
Yangtze River	28400
Qiangtang River	1500
Huangpu River	330
Cao-e River	144
Yongjiang River	111

- Tides

The tide is one of the main driving forces shaping the morphology of the Yangtze Estuary. To represent the tidal forces, the astronomic tidal constituents are specified at the open sea boundary. Zhang (1995) and Zhang (2005) point out that the semi-diurnal tides dominate in the estuary with the amplitude of M_2 tides larger than 1.2 m around the mouth. Harmonic analysis of water levels at stations in the estuary shows the primary tides of S_2, N_2, K_2, K_1, P_1 and O_1 are also significant, with amplitudes larger than 0.10 m. Therefore, these tides together with M_2 tide are specified at the open sea boundary. Model detail for tidal forces to drive the morphodynamic model of the estuary will be investigated in Chapter 5.

- Wind and waves

Swell due to typhoons, as well as locally generated wind waves, are important forces for the morphological development of the Yangtze Estuary, especially for the event-driven changes (Hu et al., 2009). In the present morphodynamic simulations we focus on long-term (years or decades) trends, at time scales much longer than a typical wave period. Hence only tidal and fluvial forces are considered in the first instance. The wave contribution to the sediment transport in the Yangtze Estuary will be analyzed separately later on (see Chapter 4).

Wind does not only generate waves, but also contributes to the residual transport of substance. The contribution of wind-driven currents to the sediment transport will be analyzed later on (see Chapter 4).

3.2.3 Relevant processes and mechanisms

- Salinity and density flow

The study area, the mouth bar, is exactly in the zone of interaction between saline water and fresh water, where the salinity distribution has a complex and time-varying structure. Salinity differences induce density gradients in horizontal and vertical directions, which in their turn lead to gravitational circulation transport. Although the current velocity is small near the bed, the near-bed sediment transport can be large, due to the higher concentration near bed. This mechanism can contribute considerably to the net sediment transport and the bed level change.

In addition, salinity is also important to fine cohesive sediment processes in the Yangtze Estuary (Liu, 1997). The dominant suspended sediment fraction is in the clay and fine silt range, with grain diameters less than 30 μm. The salinity influences the behavior of fine-grained sediment through physical and chemical effects. The ensuing flocculation will enhance the settling velocity of sediment around the mouth bar. Therefore, 3D simulations for salinity and density currents are included in the morphodynamic simulation.

- Sediment

The fine cohesive sediment in the Yangtze Estuary is predominantly in suspension (Yun, 2004; see Chapter 2). In addition, analysis of sediment samples from the top layer (5 cm) of the bed along the estuary shows that there are coarse particles available at the bed (Chapter 2). Therefore, 3 fractions of sediment are used in the model to represent the clay & fine silt, coarse silt and fine sand, respectively. When the fine-grained cohesive sediment is included, the sediment concertation, especially the high concertation, have many effects on flow and sediment transport, e.g. sediment-induced buoyancy effect and a two-layer fluid system due to fluid-mud (Winterwerp, 2001). The high concertation of the fine-grained cohesive sediment occurs in limited area, while flocculation mechanism presents in the entire estuary (Guo et al., 2011). Therefore, not all the effects of the high concertation on flow and sediment transport are included in this study, except its turbulence damping effect compensated by the relatively small bed roughness. The flocculation will be taken into account for the clay and silt fraction. The suspended sediment transport is modeled with an advection/diffusion equation. For the

sediment transport of coarse silt and fine sand the van Rijn 2004 formation is used (van Rijn, 2007a, 2007b; van Rijn et al., 2007).

3.2.4 Boundary conditions

- Flow boundary

The hydrodynamic model is driven by the astronomic tides mentioned above at the open sea boundary and observed discharges at the boundaries near Datong and Lucipu.

The main tidal constituents are prescribed together with the mean water level, but the information on either of these is limited. Since most part of the downstream boundary is in the open sea, however, the mean water level will be close to MSL (mean sea level), i.e. about 0.20 m above HH85 datum (Huanghai 1985 Datum, HH85 hereinafter). It is noted that the MSL decreases in the seaward direction in the estuary. It is high in the estuary, e.g. 0.64 m at Wusong, and low at the river mouth, e.g. 0.42 m at Luchaogang. The MSL at the open sea area is about 0.20 m with slight variations along the model boundaries, which is adjusted during the calibration to avoid unrealistic circulations.

The ideal way to obtain a consistent open sea boundary is deriving it from a larger ambient model. At present some information available stems from the China Sea Model (Zhang, 1995; Zhang, 2005), which gives the propagation maps of the M_2 and K_1 tides. An estimation of the M_2 and K_1 tides at the open sea boundary can be determined by digitizing those co-tidal maps. Besides M_2 and K_1 tides, however, other tidal constituents (S_2, N_2, K_2, K_1, P_1 and O_1) are also important in the Yangtze Estuary. To determine those tidal constituents at the open sea boundary, linear regression with one free parameter (Fang and Yang 1987; Wang, 1994; Zhang, 2005) has been used to obtain the relationship of tidal constants (amplitude and phase lag) between every two constituents. The relationships obtained from the regression analysis are shown in Figure 3.4 and Table 3.2. The first guess of tidal constituents along the open sea boundary is determined based on the model result of the China Sea Model (Zhang, 2005). These constituents are further modified during the calibration procedure to obtain a good agreement between the observed and calculated tidal constituents within the model domain.

Table 3.2 Relationship in amplitude and phase lag between two tides

Amplitude (m)	R^2	Phase lag (degree)	R^2
A_{S2}=0.33 A_{M2} +0.09	0.93	P_{S2}=0.98 P_{M2} +53	1.00
A_{N2}=0.17 A_{M2}	0.97	P_{N2}=1.01 P_{M2} -19	1.00
A_{K2}=0.29 H_{S2} -0.01	0.95	P_{K2}=0.98 P_{S2} + 1	1.00
A_{P1}=0.28 A_{K1}	0.87	P_{P1}=1.03 P_{K1} - 4	0.94
A_{O1}=0.58 A_{K1} +0.03	0.73	P_{O1}=1.06 P_{K1} - 62	0.94

Although some other harmonic constituents, e.g. M_4, MS_4, can be important to the residual sediment transport, these overtides mainly result from the interaction of the principal tides within the model domain (Wang et al., 1999) and can be neglected at the open sea boundary (Zhang, 2005). Different reference levels have been used for the

measured data of bathymetry and water level. All those data including bathymetry and water level have therefore been transferred to the same reference level, HH85.

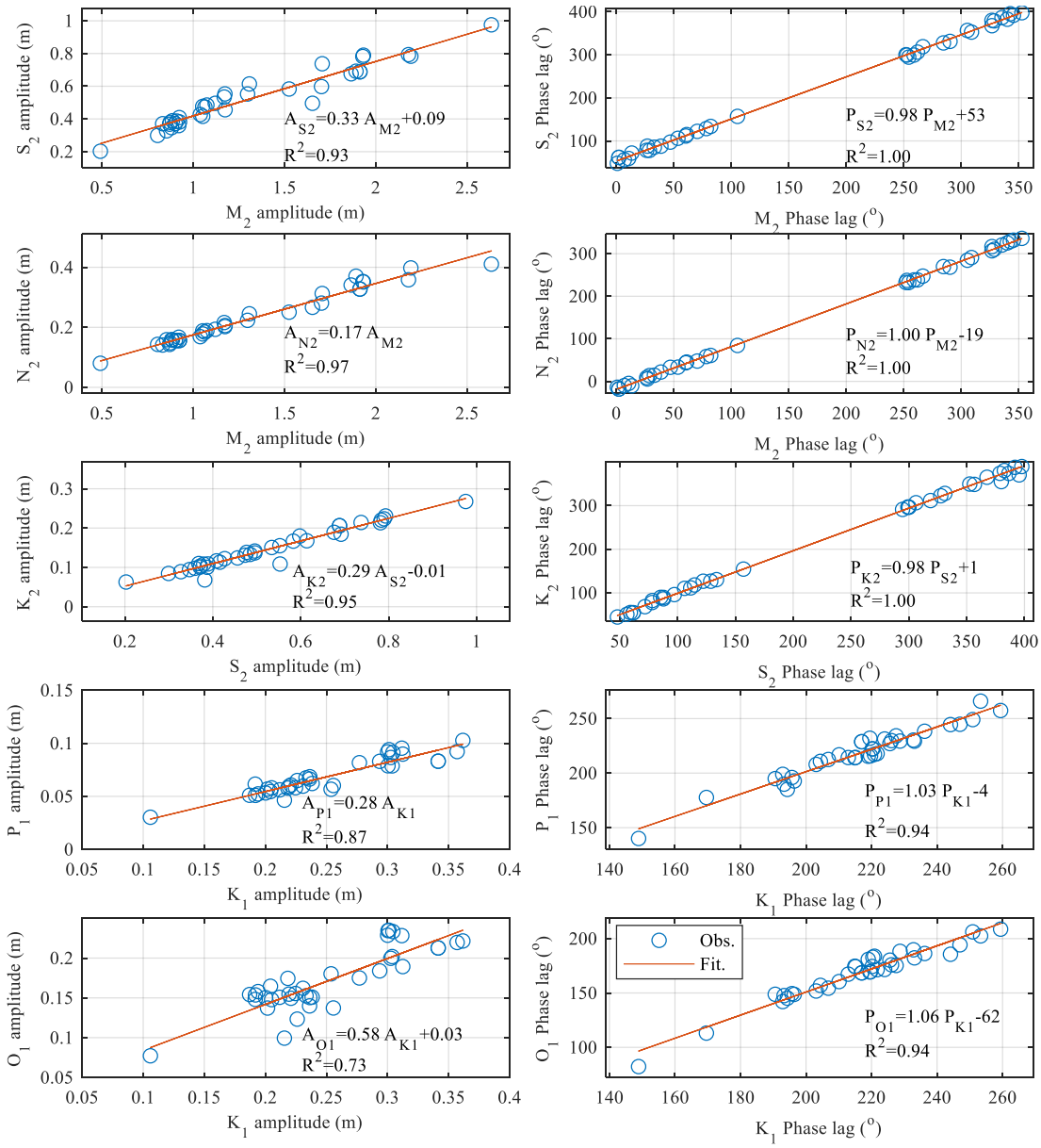

Fig.3.4 The relationship between every two tidal constituents

Table 3.3 Monthly mean discharge and suspended sediment concentration at Lucipu

Month	1	2	3	4	5	6	7	8	9	10	11	12
Discharge*	487	719	953	1399	1592	1992	920	725	671	563	526	520
SSC**	0.034	0.11	0.072	0.24	0.28	0.29	0.13	0.15	0.23	0.069	0.014	0.03

*Discharge: in m^3/s (Chen, 1998);

**SSC: suspended sediment concentration in kg/m^3 (Han et al., 2003)

The monthly mean discharge at Lucipu is provided as upper boundary condition of the Qiantang River (Table 3.3). The other three rivers, Huangpu, Cao'e and Yongjiang, are much less important with much smaller discharge and scale. Hence, they are

represented as water sources with long-term mean discharge of 330, 144 and 111 m^3/s, respectively (Wang, 1994; Chen, 1998; Han et al., 2003).

- Transport boundary

Sediment and salt are included in the model as substances transported by the water motion. The transport boundaries for salinity and sediment concentration should therefore be specified.

The salinity at the open sea boundary is derived based on the long-term average mean value (Marine Atlas of East China Sea, 1992). The runoff of the rivers at the upstream model boundaries is fresh, which means no salt input.

The fluvial sediment is the main source of material for the morphological development of the estuary (Lin, 1985). The main sediment fraction coming from upstream is the fine cohesive one. The measured sediment concentration at Datong is used as the boundary condition for this fine fraction. The measured sediment concentration at Lucipu (Table 3.2) is taken as a boundary condition for the sediment input from the Qiantang River. The sediment input from the other three rivers is regarded as minor as compared with the Yangtze River. A fine cohesive sediment concentration about 0.02 kg/m^3 is assumed to represent the sediment input from these rivers. A fine cohesive sediment concentration of about 0.02 kg/m^3 is also imposed at the open sea boundary (Gao 2008; Hu et al., 2009). For the coarse silt and sand fractions, equilibrium boundary conditions are applied. The specified salinity and sediment concentration are used for the inflow boundary condition with no concentration gradient assumed for the outflow situation.

The sediment transport is influenced by the sediment availability from the bed. Analysis of surface layer (top 5 cm) of bed material shows a large variation of sediment composition in time (spring- neap, dry wet) and in space (channel and shoal, upper and lower reach), as mentioned in Chapter 2. The Partheniades-Krone approach (Partheniades, 1962,1965; Krone, 1962, 1963) is applied to model the flux of cohesive fines to and from the bed. The bed boundary conditions for the other fractions are calculated with the van Rijn 2004 formulae (van Rijn, 2007a, 2007b; van Rijn et al., 2007).

3.2.5 Physical parameters

- Bottom friction for flow model

The most important physical parameter of the Yangtze Estuary model is the bed friction coefficient, which determines the bed shear stress and consequently the spatial distribution of the velocity field. The Manning coefficient is chosen to represent the bottom roughness. The previous researches (Yi and Ye, 1983; Wang 1994; Dou, 1997 and Luo 2003) show that a suitable range of this coefficient in the estuary is 0.010~ 0.012 $s/m^{1/3}$. Therefore, the value of $0.01 s/m^{1/3}$ is firstly applied to the model. Calibration against water level observations ultimately led to a value of $0.011 s/m^{1/3}$ in the estuarine part (blue grid in Figure 3.2) and 0.019 $s/m^{1/3}$ in the riverine part.

- Bottom friction for wave model

The bottom friction model for SWAN-model of the Yangtze Estuary is the empirical model of JONSWAP (Hasselmann et al., 1973). They proposed to use bottom friction coefficient of 0.038 m^2s^{-3} for swell conditions. Bouws and Komen (1983) used a bottom friction coefficient of 0.067 m^2s^{-3} for fully-developed wave conditions in shallow water without current influence. Previous researches of wave modeling based on SWAN in the East China Sea (Xu and Zhang, 2004; Chu et al., 2005) propose to use larger bottom friction coefficient (about 0.1-0.15 m^2s^{-3}), because of the dissipative muddy bed. Therefore, a bottom coefficient of 0.15 m^2s^{-3} is applied in the simulation of the Yangtze Estuary wave model.

- Horizontal diffusivity

For the transport of salt and suspended sediment the diffusivity is also an important parameter. Especially in 2DH simulations, its modeling can be complicated, as a number of dispersion effects (basically advection) are mimicked as diffusion.

Saline water meets freshwater around the river mouth, which results in various mixing types. Gravitational circulation and stratification-induced dispersion play a role in suspended sediment transport. These effects can only be simulated properly in three dimensions. However, 3D simulation in the present type of large-scale model implies high demands on computer power. Hence 2D depth-averaged (2DH) models are still needed as tools for primary calibrations and quick access computations. In such models the stratification-induced dispersive transport must be represented by enhanced diffusion, i.e. large eddy diffusivity coefficient.

Therefore, the value of 250-400m^2/s for horizontal diffusivity is implemented for 2DH simulation with salinity (Wang, 1994). For the 3D simulation the mixing of salt and fresh water is purely driven by the density difference with the background of horizontal diffusivity in the order of 1 m^2/s.

- Sediment parameters

Settling velocity

In the present model study three fractions are used to represent the different types of sediment involved. The settling velocities of coarse silt and fine sand can be calculated following the van Rijn 2004 approach (van Rijn, 2007a, 2007b). The setting velocity for the mud fraction, however, should be given as input. The settling velocity of mud fraction may vary with time and with the location in the model, along with the influencing factors (Liu, 1997). One of those factors is the salinity, which may enhance flocculation, hence larger settling velocities. To determine the settling velocity of the mud fraction two methods can be used. One is the settling velocity formula as a function of the sediment diameter. The other is to derive the settling velocity based on the observed suspended sediment concentration profiles.

Settling velocity of a single particle

As the fine cohesive sediment (< 30 μm, Chapter 2) dominates in the suspended particulate matter in the Yangtze Estuary, we can use Stoke's law for the settling velocity (van Rijn, 1993):

$$\omega_s = \frac{(s-1)gd^2}{18v} \tag{3.1}$$

in which:

ω_s = settling velocity in still water
d = grain diameter
s = specific gravity (=2.65)
v = kinematic viscosity
g = acceleration of gravity

In addition to Stoke's law, the following empirical formula (Zhang, 1997) is also widely used for the settling velocity in the Yangtze River:

$$\omega_s = \sqrt{(13.95\frac{v}{d})^2 + 1.09\frac{\gamma_s-\gamma}{\gamma}gd} - 13.95\frac{v}{d} \tag{3.2}$$

in which:

ω_s = settling velocity in still water
d = diameter of the sediment
γ_s = volume weight of sediment
γ = volume weight of water
g = acceleration of gravity
υ = kinematic viscosity

The kinematic viscosity of water can be approximated by (van Rijn, 1993):

$$\upsilon = [1.14 - 0.031(T-15) + 0.00068(T-15)^2] \times 10^{-6} \tag{3.3}$$

in which T is the temperature.

According the measurement at Datong, the mean diameter (d_{50}) of the suspended sediment is about 10~30 μm (Yun, 2004). The Changjiang Sediment Bulletins (2001~2017) also give the mean diameter of the suspended load at Datong, as shown in Table 3.4. The mean diameter of the suspended sediment entering the Yangtze Estuary will therefore be in the order of 10 μm.

Table 3.4 Mean diameter of suspended sediment at Datong

Year	2001	2002	2003	2004	2005	2006	2007	2008	2009
d_{50}(μm)	8	12	10	8	8	8	13	12	10
Year	2010	2011	2012	2013	2014	2015	2016	2017	Mean
d_{50}(μm)	13	9	11	9	12	11	14	16	11

Based on Eq. (3.1) and (3.2) and assuming water temperature of about 15°C, we find settling velocities of about 0.08 mm/s and 0.06 mm/s, respectively.

Settling velocity of suspended sediment in the field

Tang (2007) determined the settling velocity from Eq. (3.2) based on the observed floc size: about 0.8 mm/s and 0.45 mm/s in the wet season (summer) and the dry season (winter), respectively. Shi et al. (2004) analyzed the measured concentration and current velocity in the Yangtze Estuary in 1978 and 1990. They propose that the settling velocity is about 2-4 mm/s based on regression analysis assuming a Rouse profile (Rouse, 1938) of sediment concentration distribution in vertical. The measured data in 2003 is used to obtain the settling velocity by using the similar method of Shi et al. (2004). The Rouse profile (Rouse, 1938; van Rijn, 1993) of the concentration C at height z above the bed is given by

$$\mathrm{C} = \mathrm{C_a}\left(\frac{\mathrm{a}}{\mathrm{h}-\mathrm{a}}\frac{\mathrm{h}}{\mathrm{z}}\right)^{\omega_s/\beta\kappa u_*} \tag{3.4}$$

in which:

a = the height above the bed of the reference level
C_a = the sediment concentration at the reference level
ω_s = settling velocity in still water
h = water depth
κ = von Karman constant (=0.4)
u_* = bed friction velocity
β = a constant, usually taken equal to 1 (Dyer, 1986).

Current velocities and sediment concentrations were recorded at 6 different heights above the bed (1.0h, 0.8h, 0.6h, 0.4h, 0.2h and 0. 0h, here h and 0.0h referring about 0.5 m above the bed and 0.5 m below the water surface). Using the measured values at 0.8h and 0.2h, the ratio ω_s/β in the exponent of Eq. (3.4) can be calculated from (van Rijn, 1993)

$$\frac{\omega_s}{\beta} = 0.6644\mathrm{u_*}\ln\frac{\mathrm{C_{08}}}{\mathrm{C_{02}}} \tag{3.5}$$

in which, C_{08} and C_{02} are the concentrations at 0.8h and 0.2h above the bed. The friction velocity is proportional to the depth-averaged velocity and the bed roughness:

$$\mathrm{u_*} = \frac{\sqrt{\mathrm{g}}}{\mathrm{C}}\bar{\mathrm{u}} = \frac{\mathrm{n}\sqrt{\mathrm{g}}}{\mathrm{h}^{1/6}}\bar{\mathrm{u}} \tag{3.6}$$

in which:

C = Chézy coefficient
n = Manning coefficient
$\bar{u}$ = depth averaged velocity

Current velocity and concentration measurements at heights above the bed (h, 0.8h, 0.6h, 0.4h, 0.2h and 0h) are available at the stations shown in Figure 3.5 during a spring-neap cycle in February, 2003. These stations are located in regions with different characteristics (e.g. salinity, bed form). Therefore, two groups of stations are considered, representing the two regions: stations D0301, D0309 and D0310 represent the upstream region of large roughness without salinity effects, stations D0306, D0307, D0312 and D0315 the region of small roughness with salinity effects.

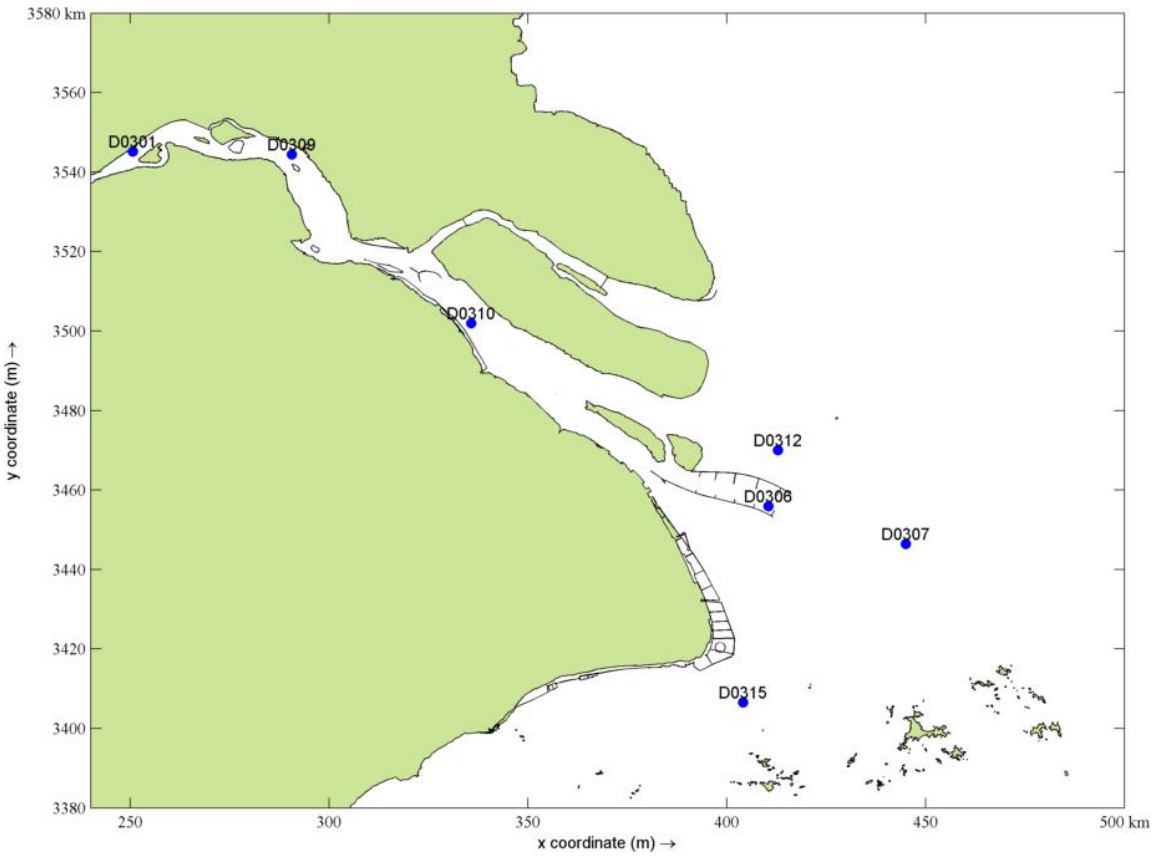

Fig.3.5 Stations for calculating sediment setting velocity in the Yangtze Estuary in2003

By applying Eq. (3.5) and (3.6) we can calculate ω_s/β, yielding settling velocities. The value of the settling velocity determined from the measurement data in 2003 is shown in Figure 3.6. The range and the mean of the settling velocity are listed in Table 3.5. The following observations are made from these results:

1) The settling velocity calculated based on measured concentration profiles is in the order of 10^0 mm/s, which is substantially larger than that of single particles based on Eq (3.1) and (3.2). The explanation of this higher settling velocity can be flocculation of fine cohesive sediment. The flocculation process is enhanced by electrolytic effects where fresh water meets saline water. Earlier research on flocculation (Guan et al., 1992) shows that it happens near the salinity front in the Yangtze Estuary, at salinities between 0.08 and 1.0 ppt. Lin et al. (1995) claim that the flocculation peak is found at salinities between 0.10 and 20 ppt. Although salinity at the stations of group 1 is low (in the order of 0.2 ppt), flocculation may occur there and it is not yet fully activated (Guo et al., 2011). This explains why at these stations the mean settling velocity calculated from the measured concentration profiles is much larger than the calculated value based on the sediment diameter.
2) The settling velocity at stations of group 2 is larger than in those of group 1, no matter how the friction velocity and the roughness height are determined. At these stations the salinity levels are high (above 5 ppt) and the flocculation process is fully activated. This explains why the settling velocity in the mouth bar area is a few times higher than in the upper reach of the Yangtze Estuary.

Table 3.5 Settling velocity calculated based on measurements

Groups	Roughness	Salinity (ppt)	Settling velocity (mm/s)	
		Range	Range	Mean
Group 1	n=0.019	0~0.4	0~6	1
Group 2	n=0.011	2~28	0~12	2.5

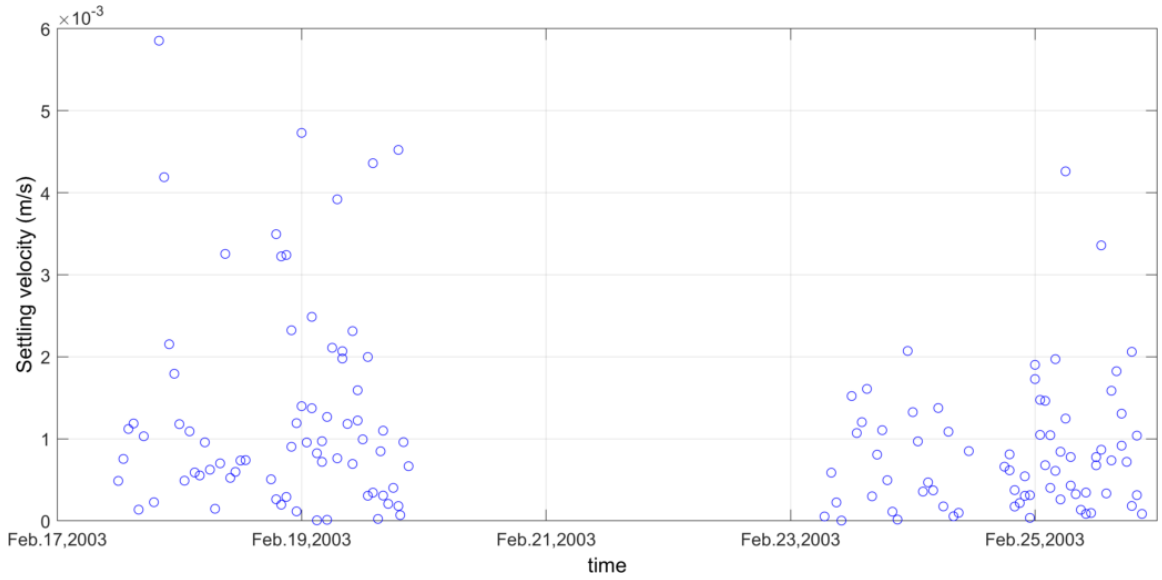

Fig.3.6a Settling velocity calculated using data at D0301, D0309 and D0310 (Roughness: n=0.019, Manning coefficient)

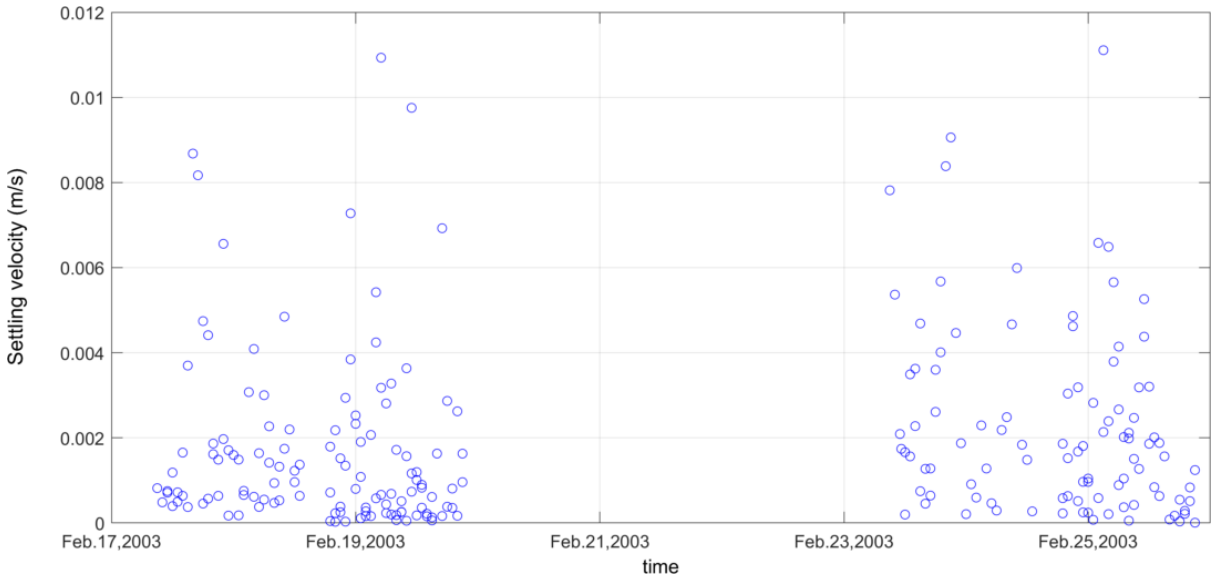

Fig.3.6b Settling velocity calculated using data at D0306, D0307, D0312 and D0315 (Roughness: n=0.011, Manning coefficient)

In brief, based on Eq. (3.1) or (3.2), the settling velocity for suspended sediment in the Yangtze Estuary is in the order of 10^{-2} mm/s for individual particles and 10^{-1} mm/s for flocs. The calculated settling velocity based on measured current velocity and

concentration in the estuary is in the order of 10^0 mm/s. Shi et al. (2004), however, point out that calculating settling velocities from concentration profiles assuming a Rouse profile tends to yield too high values. Therefore, we use 0.25 mm/s as a settling velocity of flocs in fresh water and 0.5 mm/s in saline water with salinity larger than 5 ppt.

Parameters for erosion and deposition fluxes

The transport of suspended sediment is calculated by solving the advection-diffusion equation for suspended sediment, coupled online with the hydrodynamics. Important sub-models concern the erosion and deposition fluxes at the bed. To calculate these quantities different formulations should be applied for the different types of sediment. For the coarser sediment (coarse silt and fine sand), Van Rijn's 2004 transport formula (van Rijn 2007a, 2007b; van Rijn et al., 2007) is used. For the fine cohesive sediment (mud) the Partheniades-Krone formulation (Partheniades, 1962,1965; Krone, 1962, 1963) is used to calculate the exchange fluxes between bed and flow. The cohesive sediment erosion and deposition fluxes can be represented as (Deltares, 2014)

$$E = M\, S(\tau_{c,b}, \tau_{cr,e}) \tag{3.7}$$

$$D = \omega_s c_b S(\tau_{c,b}, \tau_{cr,d}) \tag{3.8}$$

$$c_b = c(z=\Delta z_b/2,t) \tag{3.9}$$

in which:

E	= erosion flux (kg/m^2/s)
M	= user-specified erosion parameter (kg/m^2/s)
$S(\tau_{c,b}, \tau_{cr,e})$	= erosion step function
D	= deposition flux (kg/m^2/s)
ω_s	= (hindered) settling velocity (m/s)
c_b	= average near-bed sediment concentration
$S(\tau_{c,b}, \tau_{cr,d})$	= deposition step function
$\tau_{c,b}$	= mean bed shear stress due to current (N/m^2)
$\tau_{cr,e}$	= critical shear stress for erosion (N/m^2)
$\tau_{cr,d}$	= critical shear stress for deposition (N/m^2)

The critical erosion shear stress for fine cohesive sediment can be influenced by cohesive particle-particle interaction effects ($\varphi_{cohesive}$), by packing effects ($\varphi_{packing}$) and by biological and organic material effects (φ_{bo}), represented by (van Rijn 2007a)

$$\tau_{cr,e} = \varphi_{bo}\, \varphi_{packing}\, \varphi_{cohesive}\, \tau_{cr,o} \quad \text{for particles } <62\mu m \tag{3.10}$$

where $\tau_{cr,o}$ is the critical shear stress for erosion of cohesive particles, which varies between 0.18 and 0.7 N/m^2 (Li, 2006; van Rijn 2007a).

The critical shear stress for deposition is usually taken smaller than the critical shear stress for erosion (Cao and Wang, 1993; Li, 2006). This implies that erosion and deposition cannot occur simultaneously and that the suspended sediment concentration

during erosion has no upper limit. Hu et al. (2009) use practically the same values of these two critical shear stresses to simulate sediment transport in the Yangtze Estuary. Winterwerp and Kesteren (2004) propose an infinitely large critical shear stress for deposition, such that erosion and deposition can occur simultaneously. After the calibration against a series of observed sediment concentration data in the model domain, values of 0.2 N/m^2 and 0.1N/m^2 are applied for the critical shear stress for erosion and deposition with a value of 2×10^{-5} $kg/m^2/s$ for the erosion parameter M in the present study.

3.3 Model calibration and validation results

3.3.1 General

In this study model calibration focuses on the proper representation of flow and transport processes around the mouth bar of the Yangtze Estuary. The calibration of the Yangtze Estuary Model has been carried out in different steps. First, the tidal wave model in 2DH is calibrated against the measured water levels in order to get proper representation of the tidal propagation in the estuary. Second, the calibration for current and transport (salinity and sediment concentration) is carried out. Then the wind wave model of the Yangtze Estuary is calibrated briefly, as to study the wave effect on sediment flux later on (chapter 4). Finally, the calibrated model is validated against measurement data at locations different from calibration data set in another period.

3.3.2 Flow model

- Water levels

To calibrate the tidal propagation model, uncertainties, such as open boundary conditions, bathymetry, Manning coefficient and horizontal eddy viscosity, are considered.

First the sensitivity to the open boundary condition is investigated. Here the tidal constituents are used for comparison between simulation and observation. Every time a six months simulation is carried out. A tidal analysis is applied for the computed water levels at stations where the observed water levels (at least one year) are available. The tidal constituents from the tidal analysis on simulated and observed water levels are compared with each other. Based on the comparison modifications are made the open sea boundary.

The bathymetry and the Manning coefficient are also adjusted to obtain good agreement between simulation and observation. The bathymetry data are from navigation maps with different reference datum. Those bathymetry data have been transferred to the same reference datum, so as to the water levels. Some minor local modification is allowed for the bathymetry during the calibration. The Manning coefficient is an important physical parameter that influences the mean water level in the upstream part of the model, as well as the propagation and damping of the tidal wave. The Manning coefficient, together with the horizontal eddy viscosity, is modified during the calibration to adjust the upstream water level to the observed data. The above procedure

has been repeated in order to get the proper tidal propagation along the estuary.

The computed water levels for the stations in the Yangtze Estuary are harmonically analyzed by T-tide (Pawlowicz et al., 2002) in the Open Earth Tool box (oss.deltres.nl). The harmonic analysis is also applied to the observed (or predicted) water levels at each station to obtain the tidal constituents. The stations, the locations of which are shown in Figure 3.7a, can be considered as representative for the overall pattern of tidal propagation along the estuary. Water levels at each station from January 1 to July 15, 2004 were simulated with the 2DH model driven by the measured river discharges and the tidal constituents mentioned above. The results were analyzed to obtain the '*computed*' tidal constants of the major tidal components. The '*measured*' tidal constants were obtained from tidal analysis of measured water levels at each station during the same time period. At some stations the water level data in 2004 are not available. In those cases, the measured water levels in other years are analyzed, assuming little variation of the tidal constants within a few years.

Figures 3.7b~3.7h show the constituents resulting from the tidal analyses. Besides the values of amplitudes and phase lags, the tidal constituents are also represented by arrows, of which the magnitude indicates the amplitude and the directions the phase lag. The constituents of the observed water levels are represented by black arrows and numbers, those of the simulated water levels in blue. The observation data at stations marked with '*' in Figure 3.7a are not available. Therefore, tide table data at these stations are used. The differences between the two types of constituents are also shown in the figures by red arrows. Figures 3.7b~3.7h show that the black arrows coincide with the blue ones, and that red ones are hardly visible. This means that the amplitudes of the main constituents based on the computed and measured vertical tides are almost equal and the phase differences are small. In general, the present model gives a good representation of the vertical tide throughout the estuary.

The water level data at stations around the mouth bar are selected to verify the model result. With the same parameter settings of the calibrated model, the model is applied to validate the observed water levels in Aug. 2005. Figures 3.8 shows the simulated and measured water level time series at stations (see Figure 3.7a for locations) around the mouth bar area. These figures confirm the good agreement between the modeled and observed water levels.

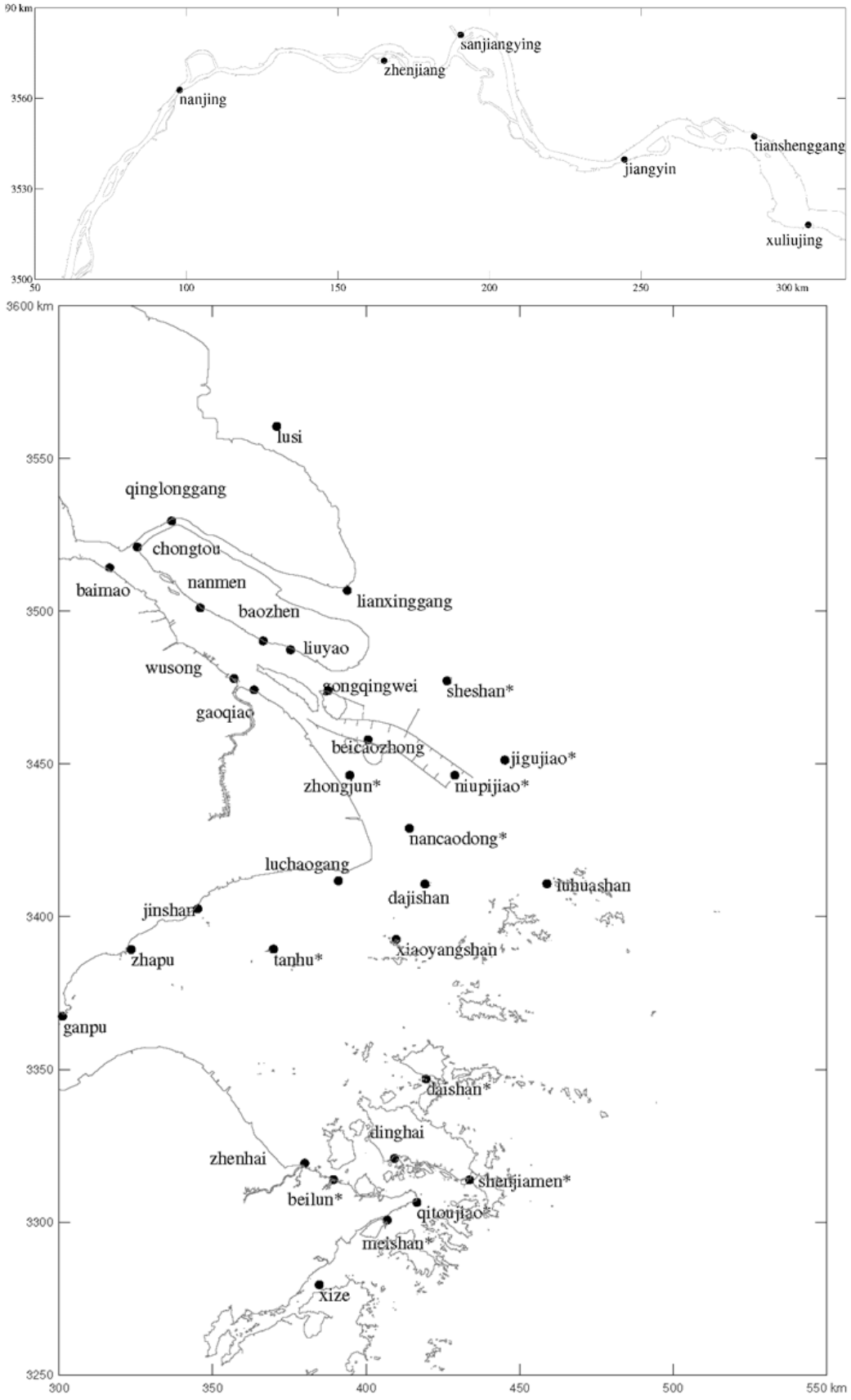

Fig.3.7a Tidal stations in the domain area for tidal analysis (station with "*" indicates the tidal table data available)

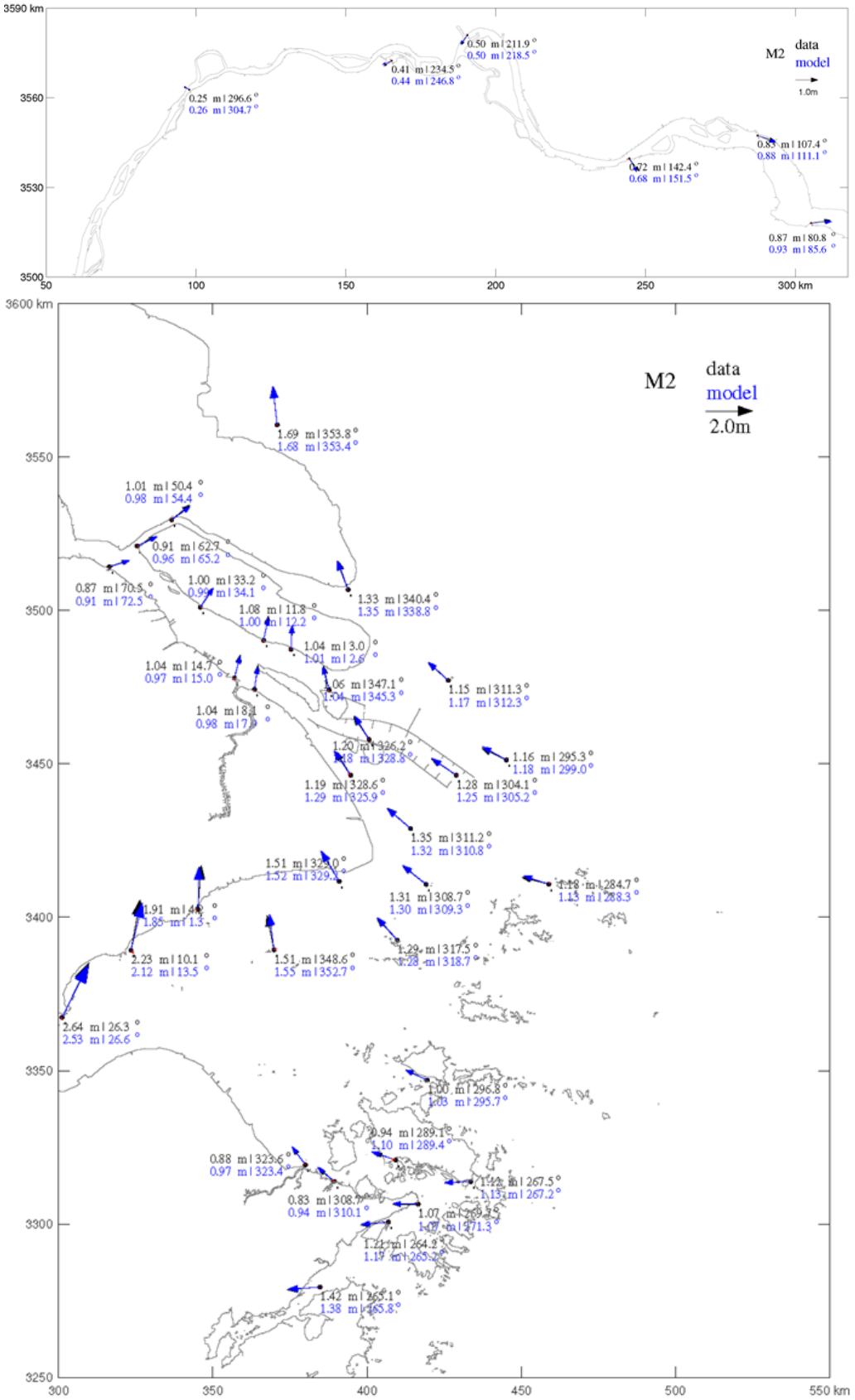

Fig.3.7b Comparison of M_2 tidal constituent (black: tidal analysis result based on observed/predicted water level; blue: tidal analysis result based on simulated water levels; red: difference between observed and simulated tidal constituent)

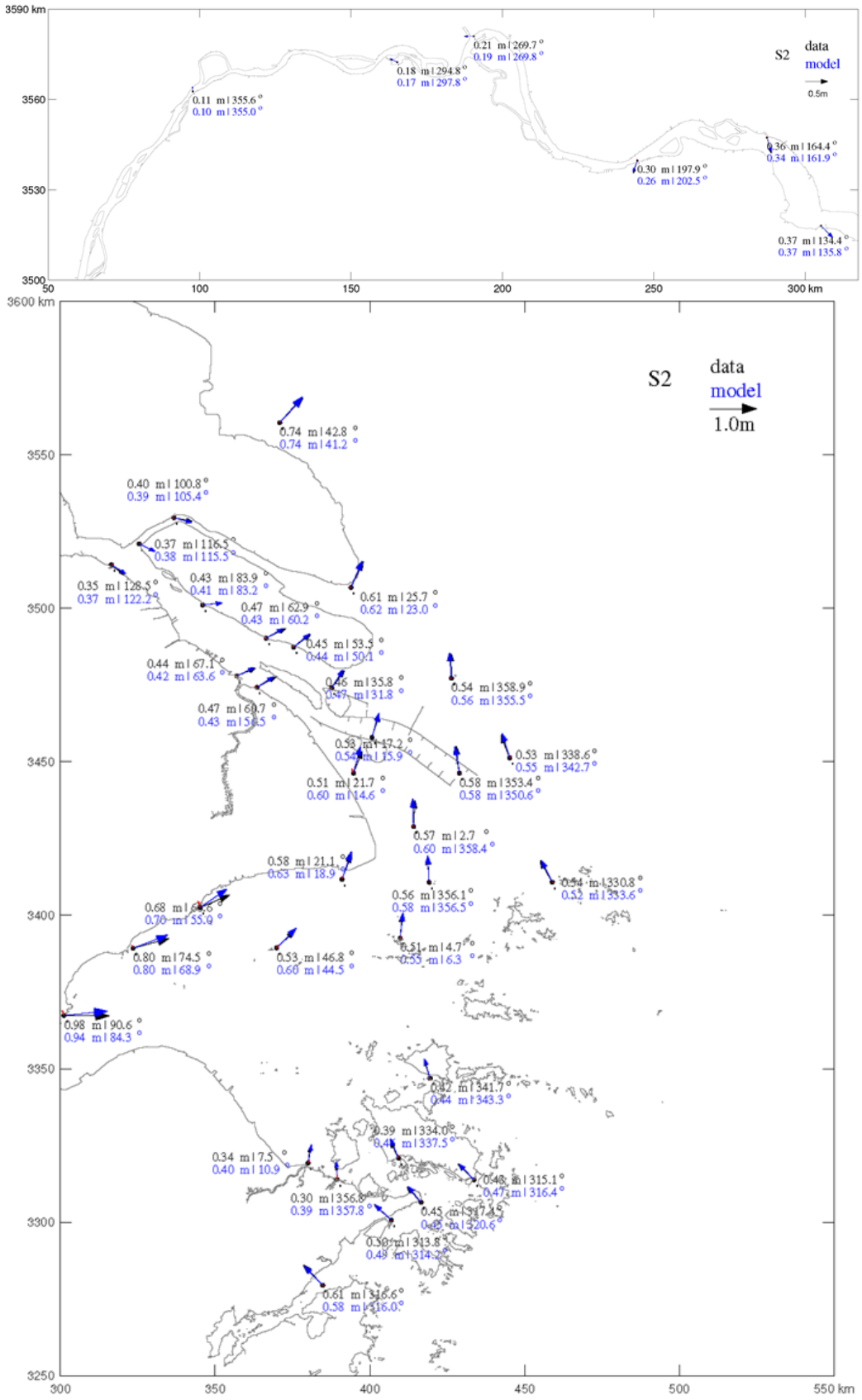

Fig.3.7c Comparison of S_2 tidal constituent (black: tidal analysis result based on observed/predicted water level; blue: tidal analysis result based on simulated water levels; red: difference between observed and simulated tidal constituent)

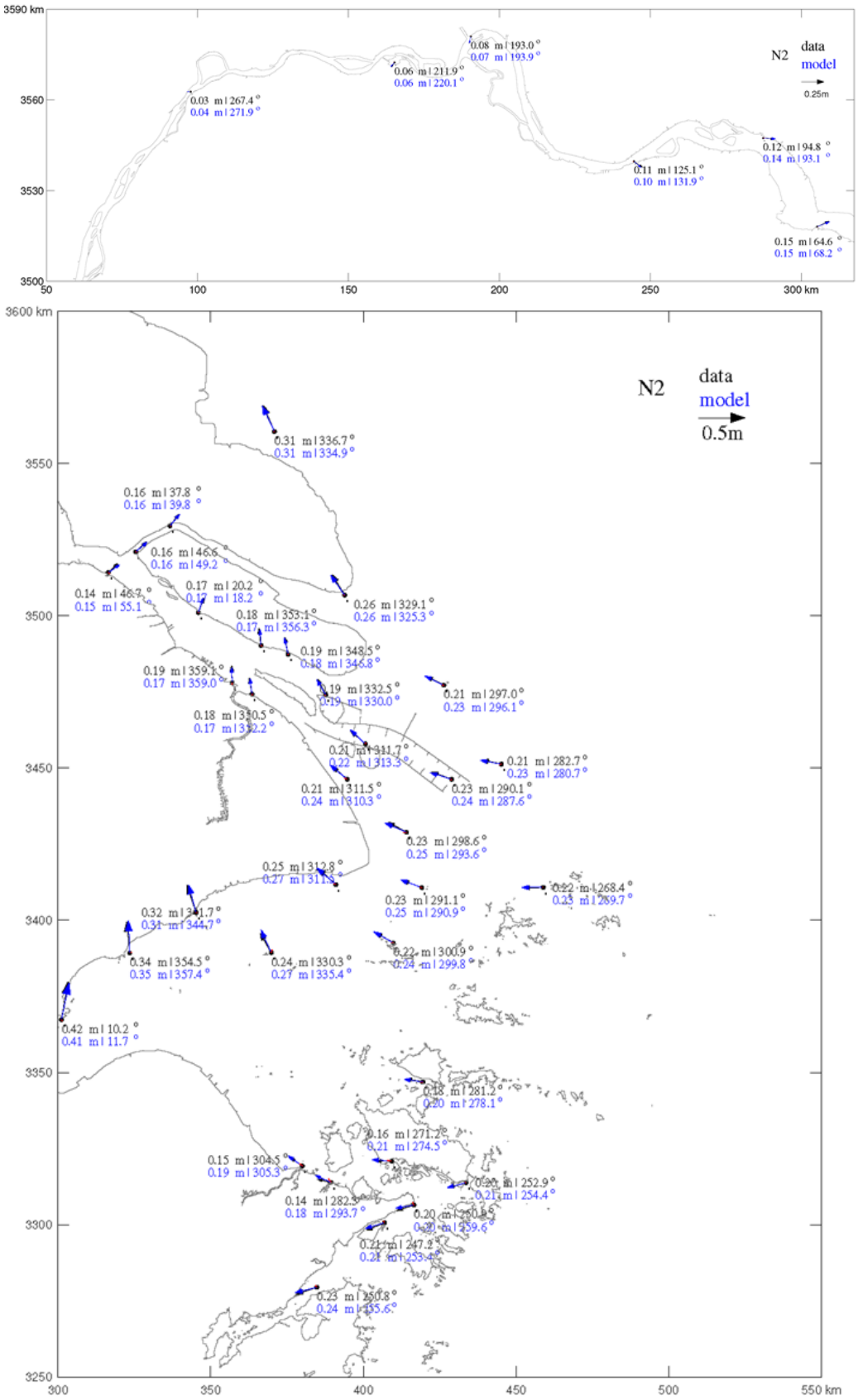

Fig.3.7d Comparison of N_2 tidal constituent (black: tidal analysis result based on observed/predicted water level; blue: tidal analysis result based on simulated water levels; red: difference between observed and simulated tidal constituent)

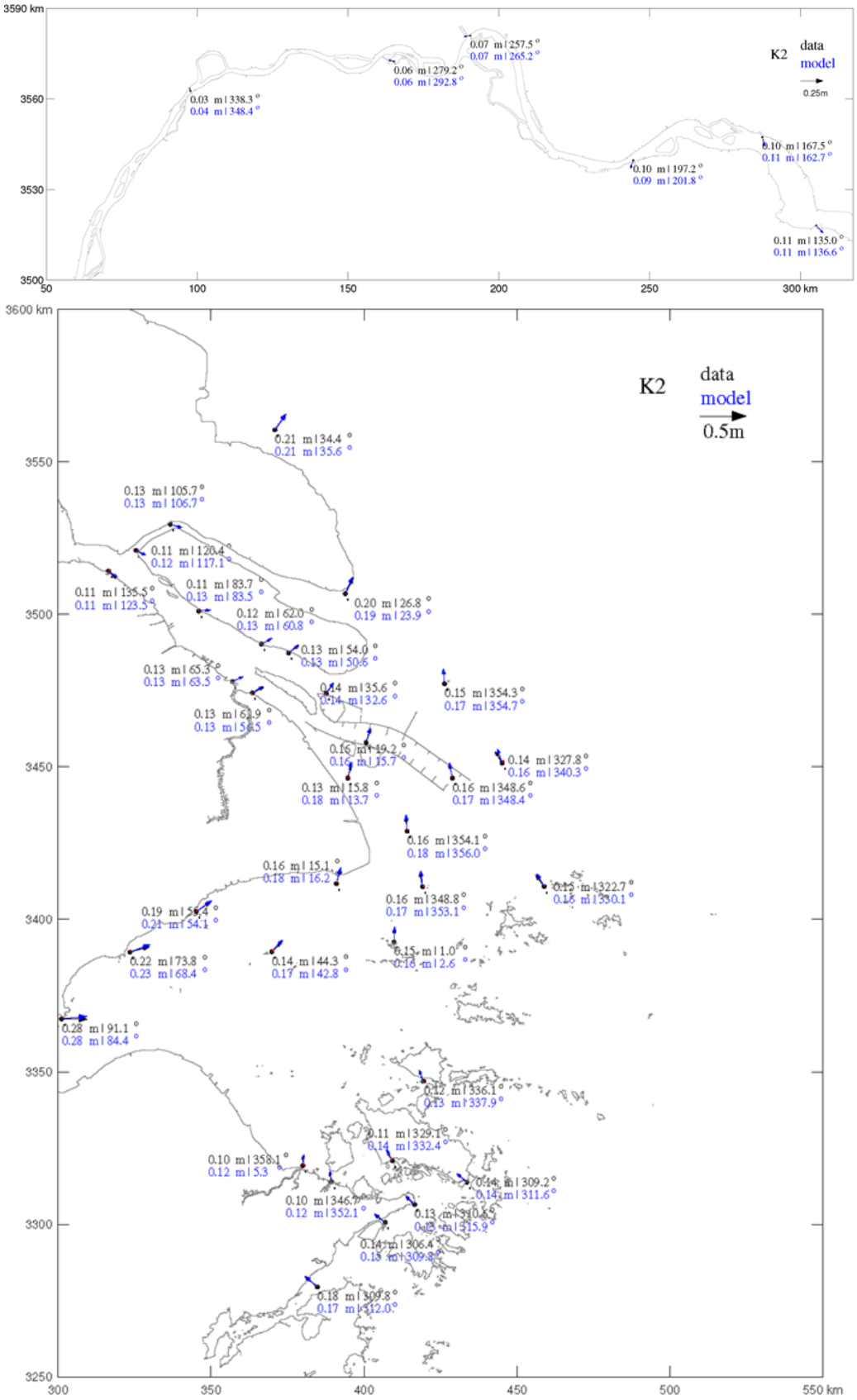

Fig.3.7e Comparison of K_2 tidal constituent (black: tidal analysis result based on observed/predicted water level; blue: tidal analysis result based on simulated water levels; red: difference between observed and simulated tidal constituent)

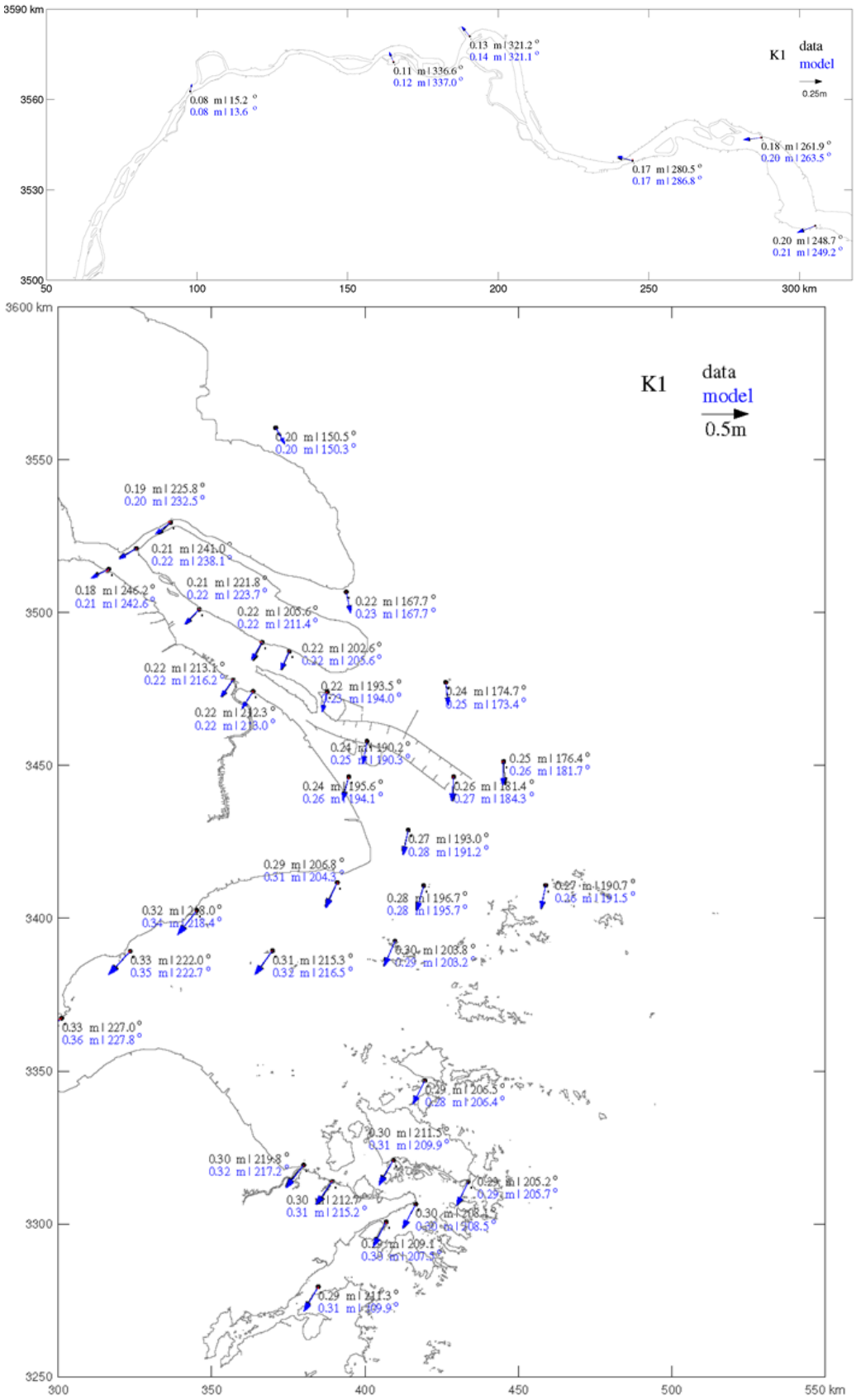

Fig.3.7f Comparison of K_1 tidal constituent (black: tidal analysis result based on observed/predicted water level; blue: tidal analysis result based on simulated water levels; red: difference between observed and simulated tidal constituent)

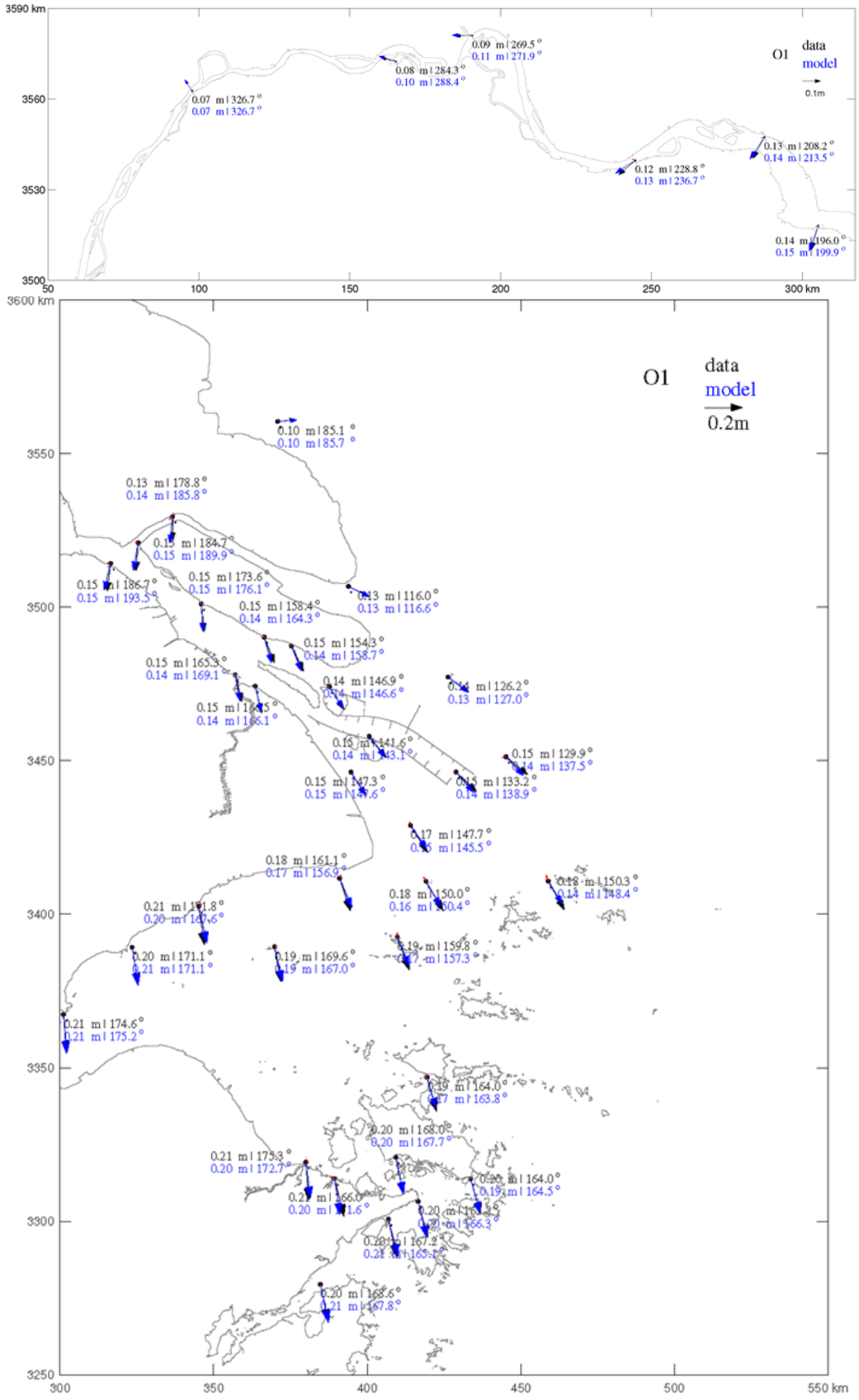

Fig.3.7g Comparison of O_1 tidal constituent (black: tidal analysis result based on observed/predicted water level; blue: tidal analysis result based on simulated water levels; red: difference between observed and simulated tidal constituent)

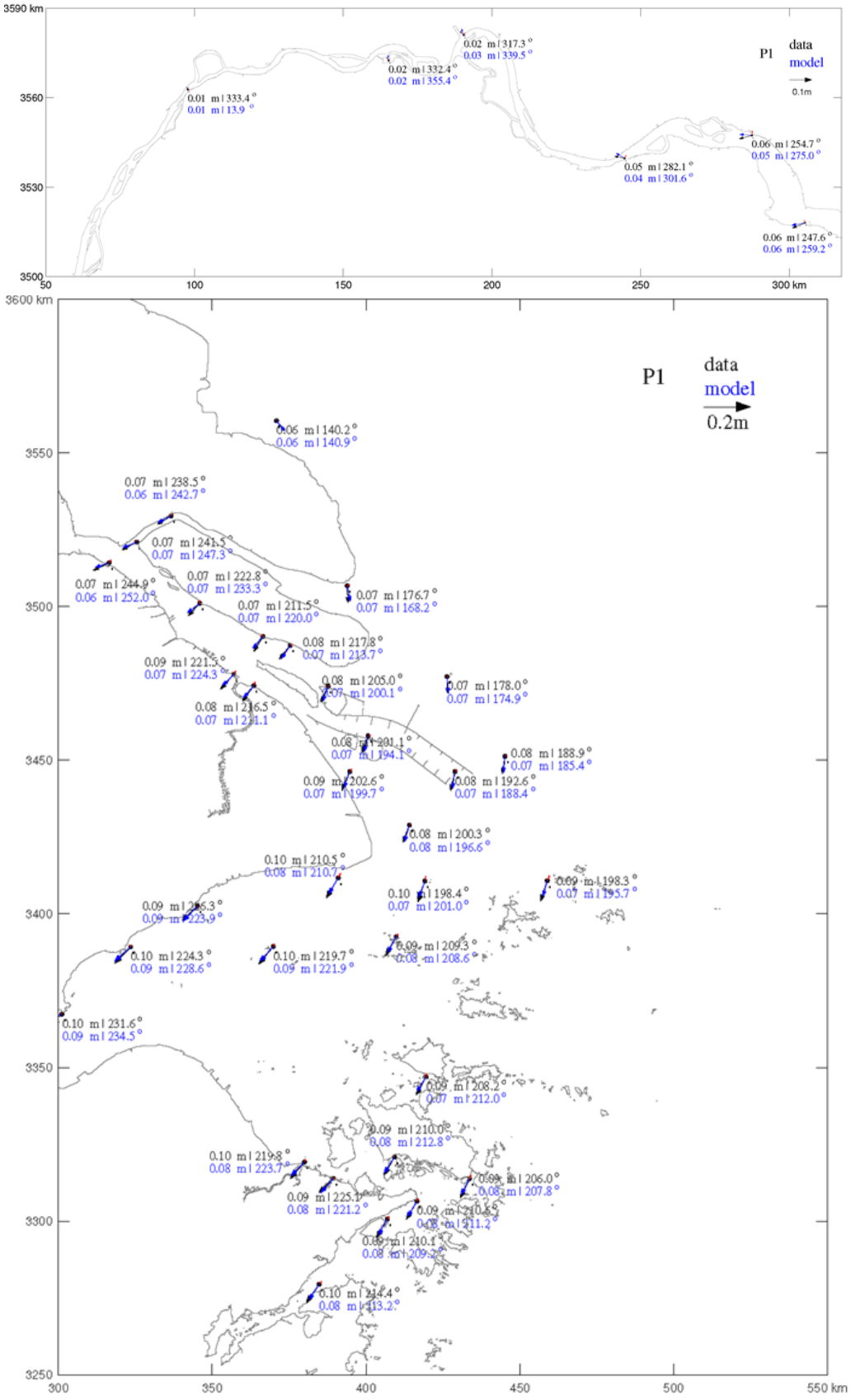

Fig.3.7h Comparison of P_1 tidal constituent (black: tidal analysis result based on observed/predicted water level; blue: tidal analysis result based on simulated water levels; red: difference between observed and simulated tidal constituent)

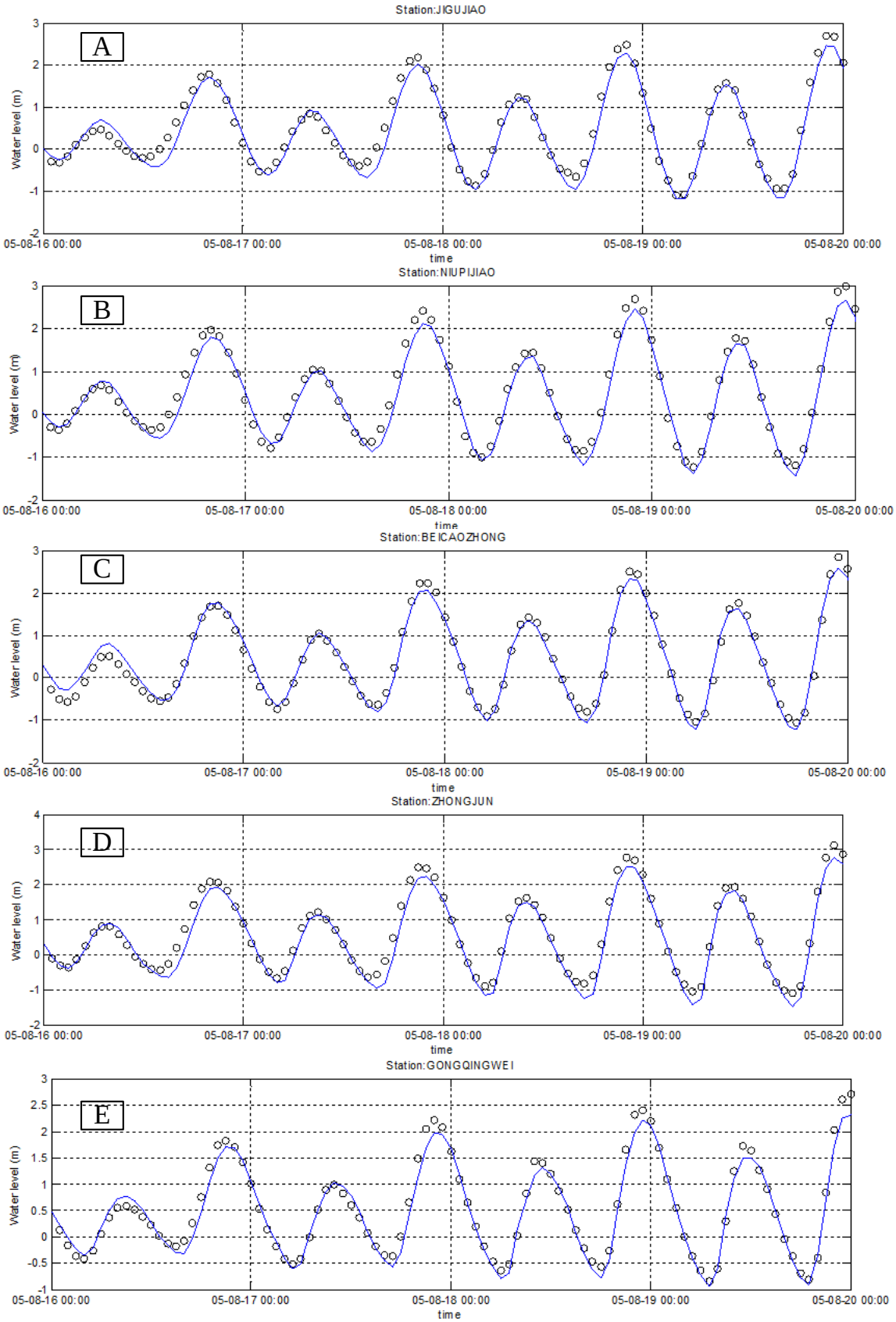

Fig.3.8 Water level comparison between the observation (symbol 'o') and computation (line) at stations (From Top to Bottom: A- Jigujiao; B-Niupijiao; C-Beicaozhong; D-Zhongjun; E- Gongqingwei)

- Currents

Long-term series of currents velocities for model calibration and validation are absent. The calibration for current therefore focuses on the area along the main channels of the outlets crossing the mouth bar. Flow measurement data in Feb. 2003 (dry season) are used for calibration. As shown in Figure 3.1, the stations are located around the mouth bar area, so that they yield a representative picture of the current field in the area of interest. Station C1 is in the SC, C2 represents the middle of the NP, and C3 can be regarded as the seaward end of the NP.

Figure 3.9 shows the comparison of the depth-averaged current velocity and direction between observation and 2DH model results. Although the agreement is less than that for the water levels, the agreement between measurements and model is satisfactory.

The stations considered are located in the interaction zone between saline and fresh water, so the velocity profile can be strongly influenced by density currents. Therefore, the calibration is extended to the vertical profile of the velocity through 3D simulation. The comparison of calculated and measured current velocity and direction profiles at these stations over a typical tidal day (say 25 hours) is shown in Figures 3.10a~3.10c. We can find that the calculated velocity profiles are similar to measured ones. The currents in the channels (stations C1 and C2) are mainly collinear, with a peak velocity of more than 2 m/s. At the seaward end of the NP (station C3) the current is rotational, with smaller velocities than those in the channels. The agreement between the calculated and the measured current fields is also satisfactory.

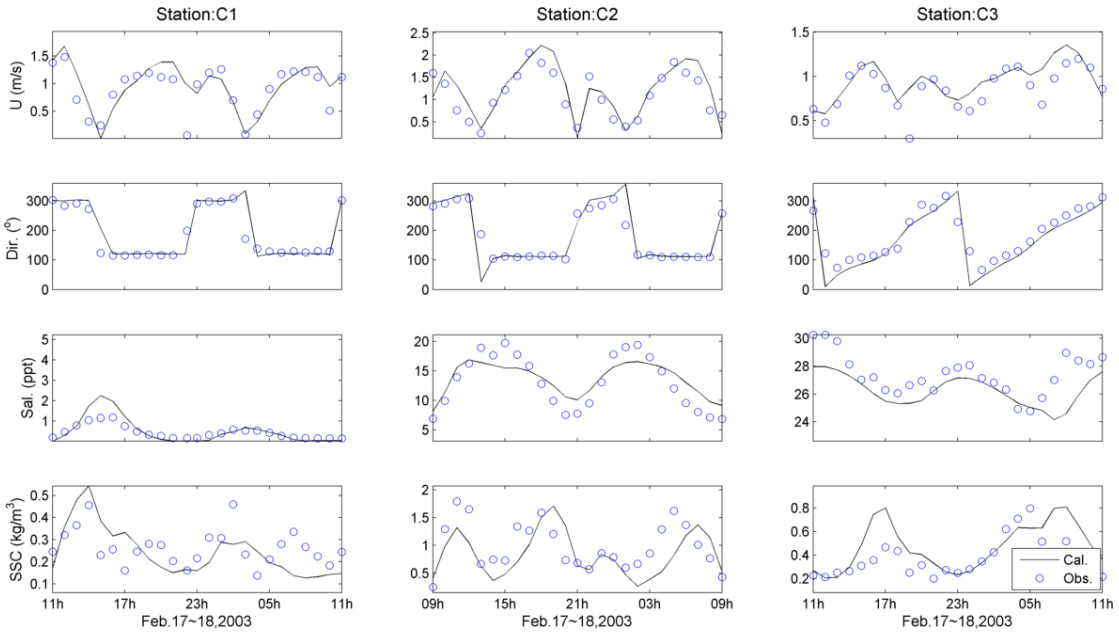

Fig.3.9 Comparison of depth averaged results between measurement (symbol) and calculation (line) at stations C1, C2 and C3 (From top to bottom: depth averaged current speed, current direction, salinity and suspended sediment concentration)

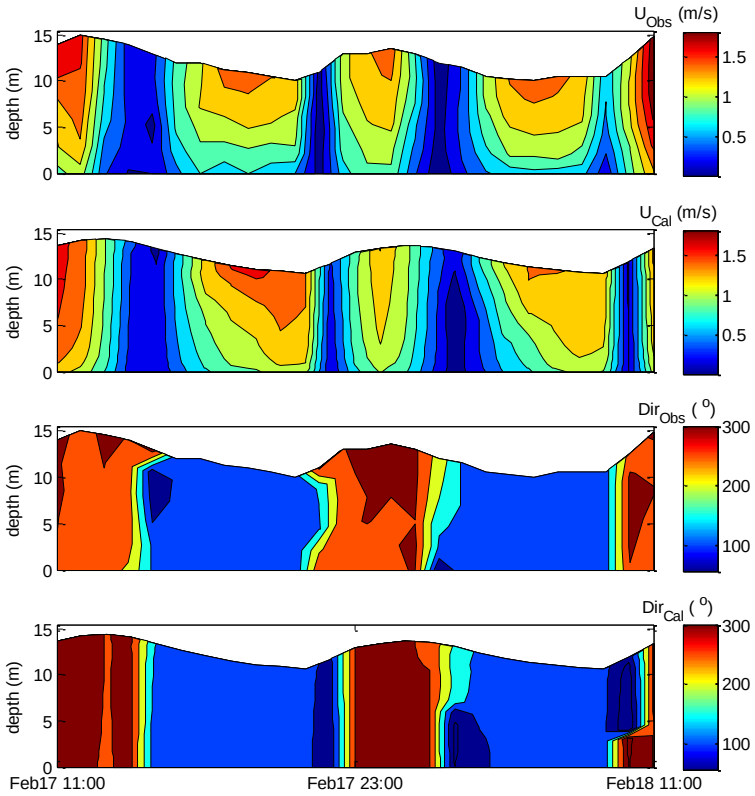

Fig.3.10a Comparison of current speed and direction between observation and calculation in the middle of the SC (C1) of the Yangtze Estuary in 2003

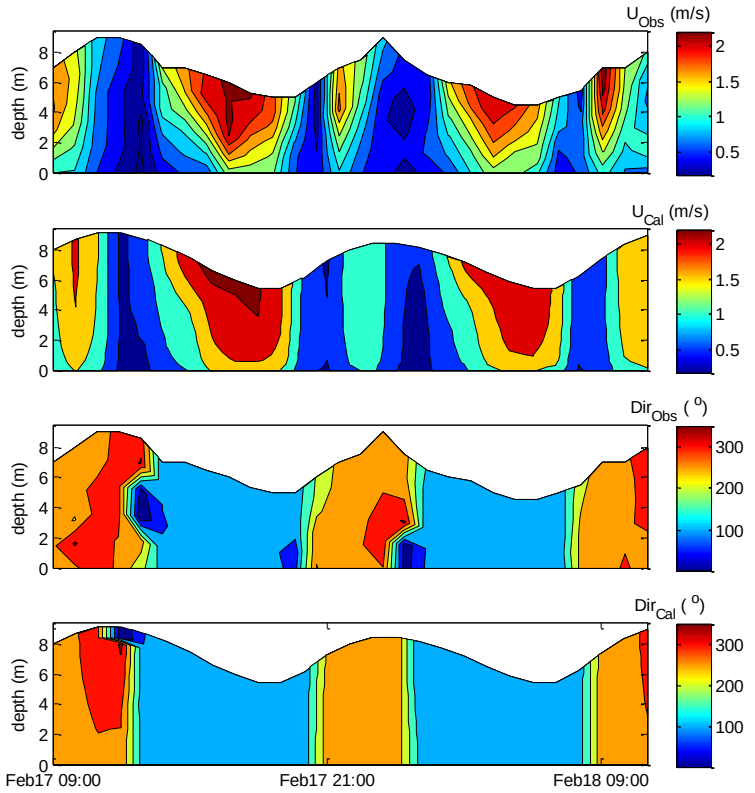

Fig.3.10b Comparison of current speed and direction between observation and calculation in the middle of the NP (C2) of the Yangtze Estuary in 2003

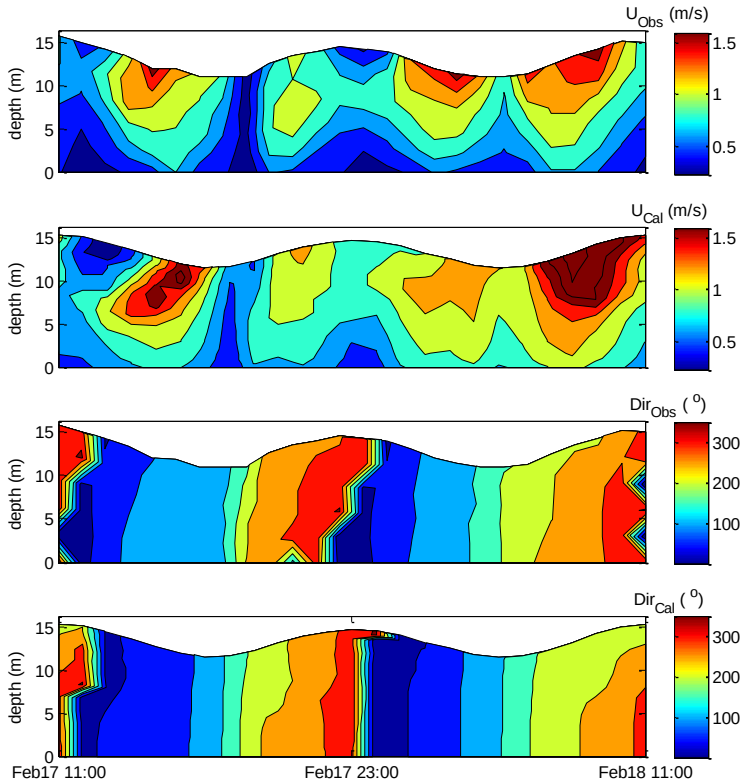

Fig.3.10c Comparison of current speed and direction between observation and calculation at the seaward end of the NP (C3) of the Yangtze Estuary in 2003

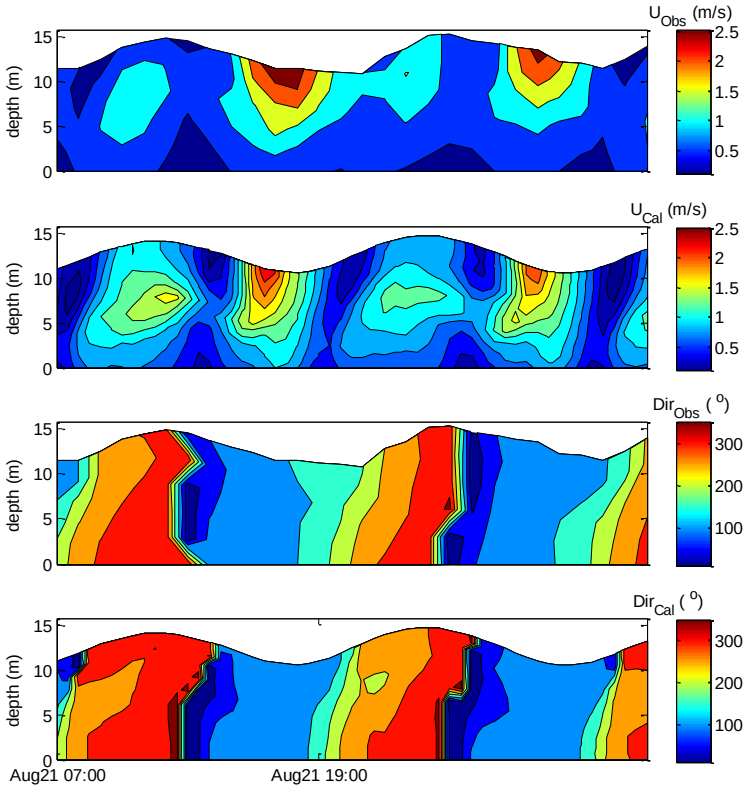

Fig.3.11a Comparison of current speed and direction between observation and calculation in the middle of the NC (V1) of the Yangtze Estuary in Aug.2005

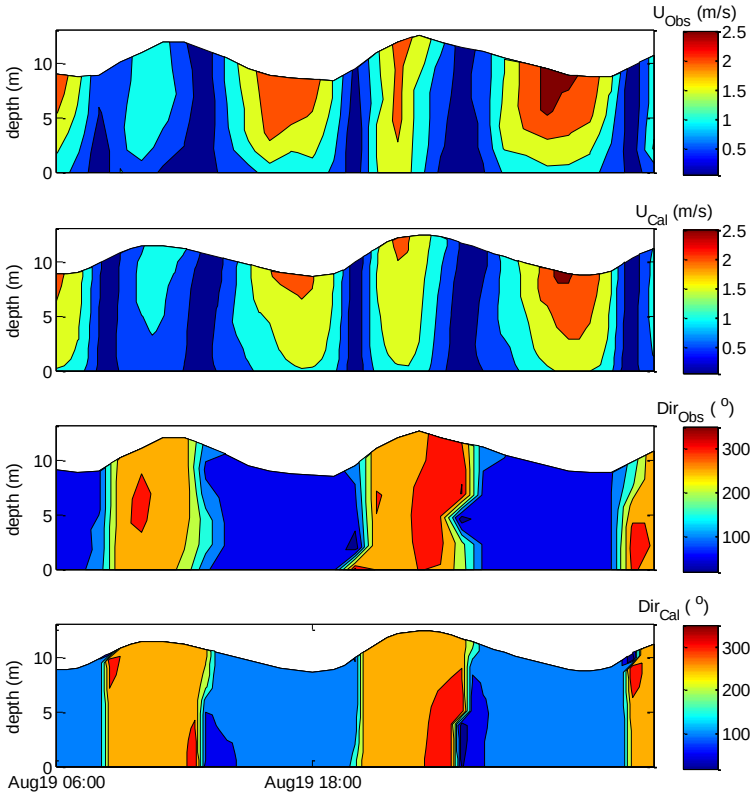

Fig.3.11b Comparison of current speed and direction between observation and calculation in the middle of the NP (V2) of the Yangtze Estuary in Aug.2005

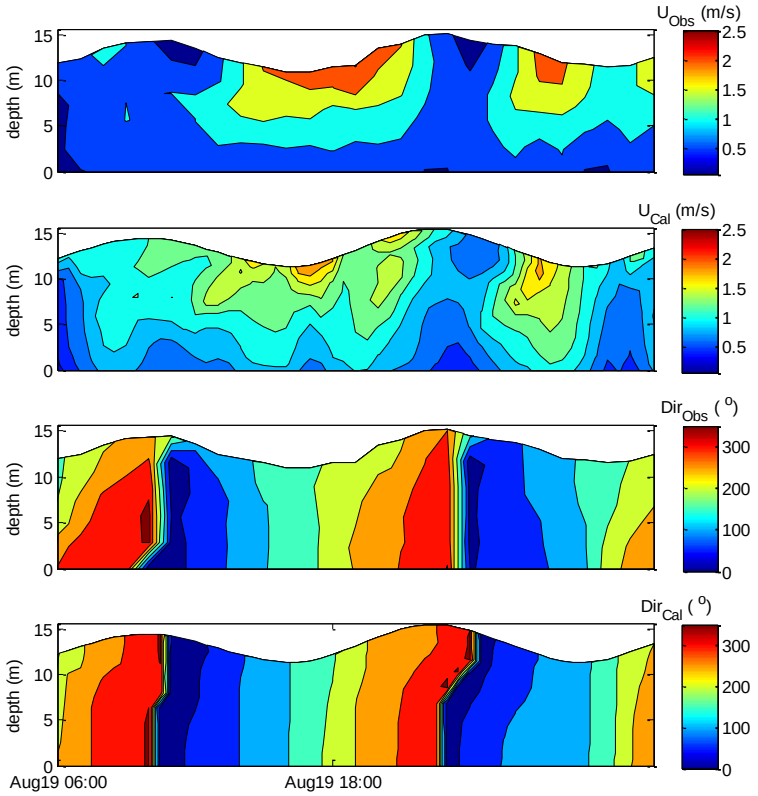

Fig.3.11c Comparison of current speed and direction between observation and calculation in the middle of the SP (V3) of the Yangtze Estuary in Aug.2005

Data for the verification of the model are collected in Aug., 2005. They represent the situation in the wet season. For the verification procedure we mainly focus on the vertical profile of the flow velocity. Therefore, Figures 3.11a~3.11c show the observed and calculated current magnitude and direction at verification stations (V1, V2 and V3, see Figure 3.1 for locations) in the middle of the three main outlets. Good agreement is found between the observed and calculated results.

In conclusion, both calibration and validation results show that the model results agree well with the observations for current around the mouth bar area. The present model gives thus a good representation of the flow conditions around the mouth bar area in the Yangtze Estuary.

3.3.3 Transport model

The type of salinity structure around the mouth bar area varies in space and time, and so does the sediment concentration distribution. The large seasonal variation of freshwater discharge associated with sediment load from the Yangtze River may lead to different distribution patterns of salinity and sediment concentration around the mouth. Therefore, the observation data of salinity and sediment concentration in Feb., 2003 are used for calibration, as they represent the situation in the dry season. The data measured in Aug., 2005 are used for validation, to check the model performance in the wet season.

Figure 3.9 compares, apart from current velocities and directions, the measured and calculated depth-averaged salinity and SSC. Although the current velocities and directions show good agreement, the salinity and SSC results exhibit some differences, possibly caused by processes not included in the model, such as density currents, wind and waves.

Both for the salinity and for the SSC the vertical structure is important. Hence, we will focus their calibration on the 3D results. Figures 3.12a~3.12c show the salinity and SSC profiles measured and calculated at selected stations for calibration in Feb., 2003. At most stations there is good agreement, but there are still some discrepancies. The present model underestimates the salinity in NP, possibly due to aspects not included in the model, such as wind, waves and human activities, or due to an insufficient spatial resolution to represent details of the bathymetry.

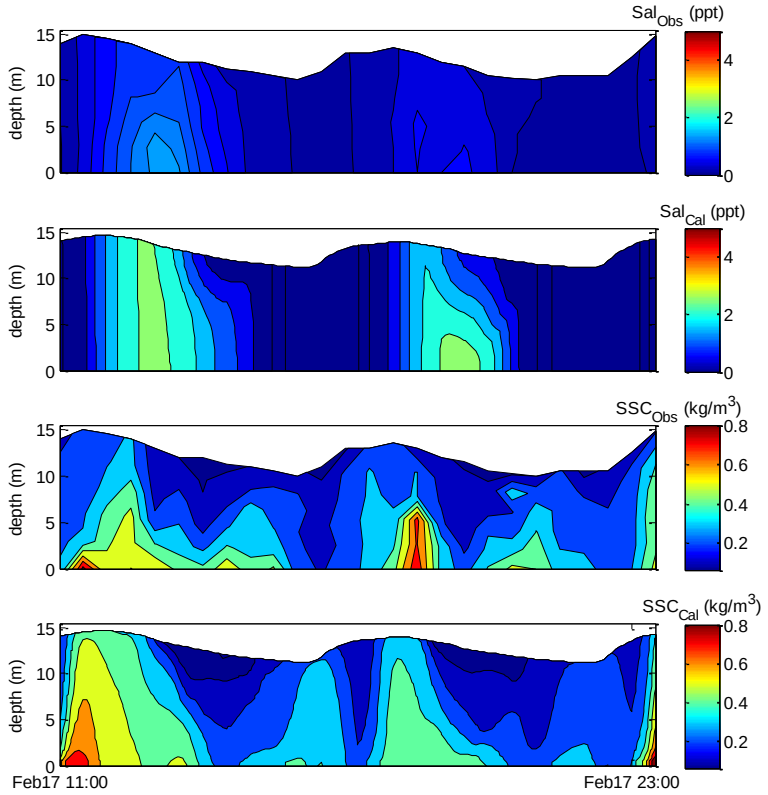

Fig.3.12a Comparison of Salinity and SSC between observation and calculation in the middle of the SC (C1) of the Yangtze Estuary in Feb. 2003

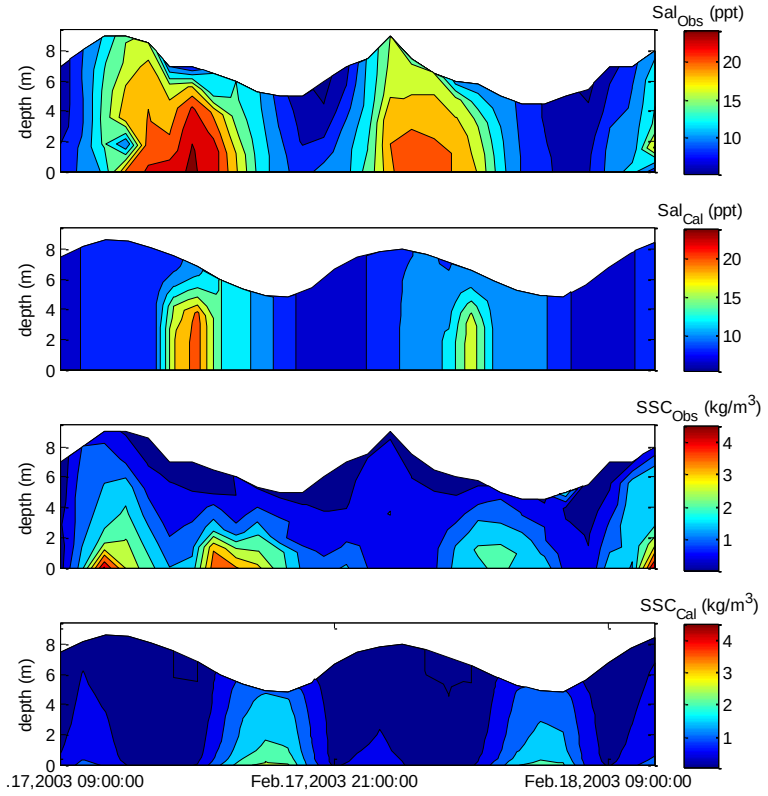

Fig.3.12b Comparison of Salinity and SSC between observation and calculation in the middle of the NP (C2) of the Yangtze Estuary in Feb. 2003

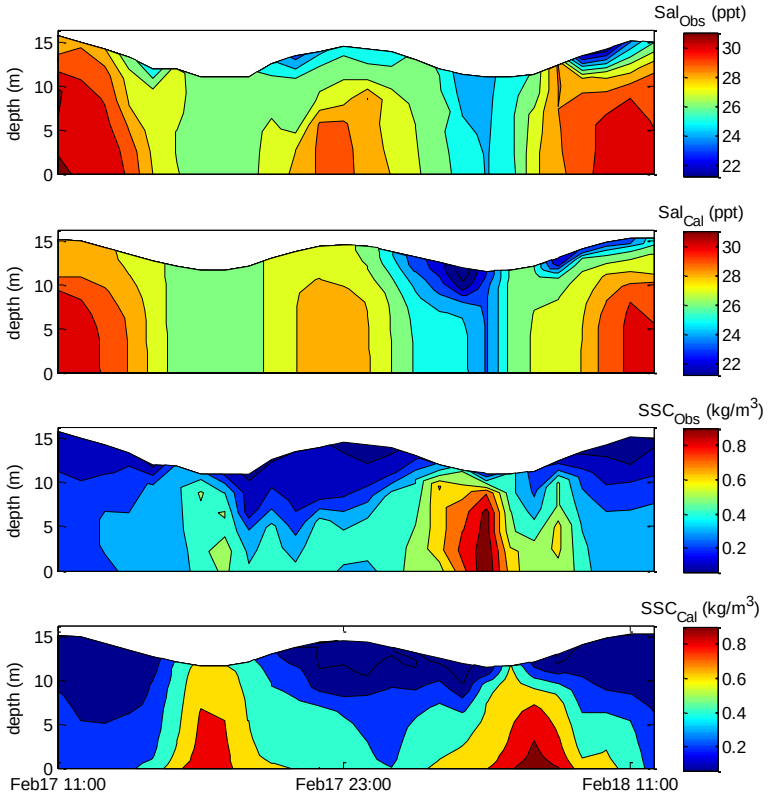

Fig.3.12c Comparison of Salinity and SSC between observation and calculation at the seaward end of the NP (C3) of the Yangtze Estuary in Feb. 2003

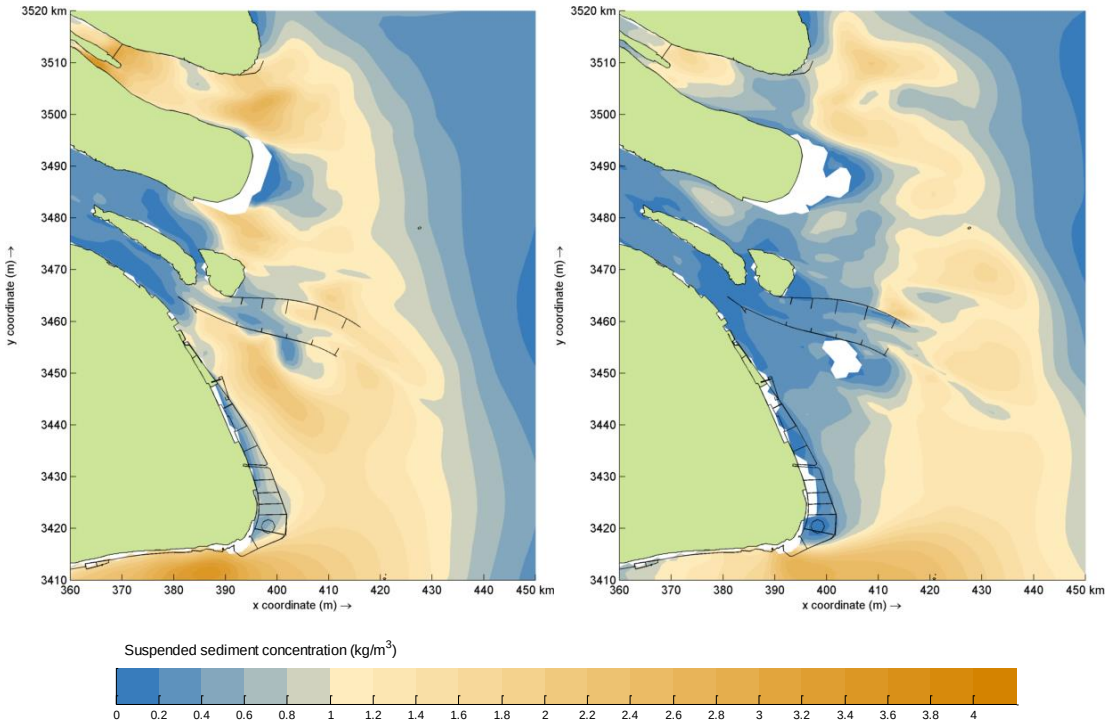

Fig.3.13 Mud concentration distribution around the mouth bar in the Yangtze Estuary during maximum flood (left) and ebb (right) in February 2003

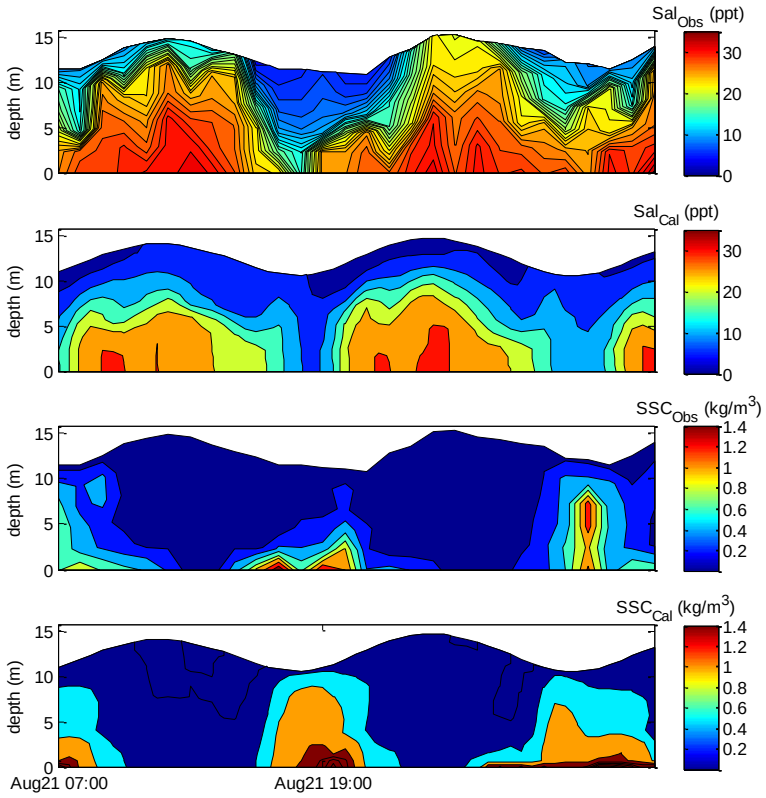

Fig.3.14a Comparison of Salinity and SSC between observation and calculation at the middle of NC (V1) of the Yangtze Estuary in Aug. 2005

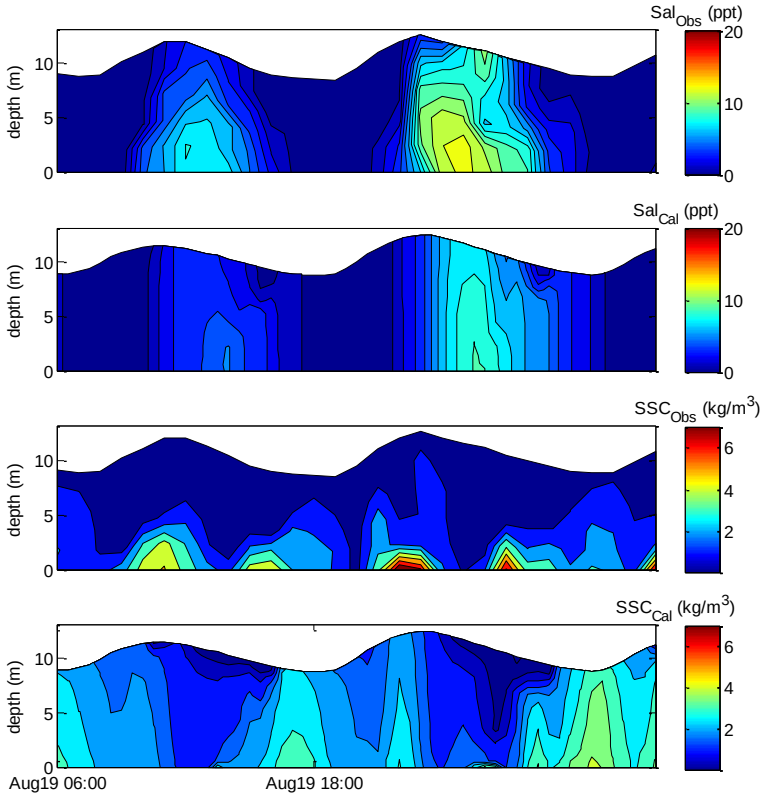

Fig.3.14b Comparison of Salinity and SSC between observation and calculation at the middle of NP (V2) of the Yangtze Estuary in Aug. 2005

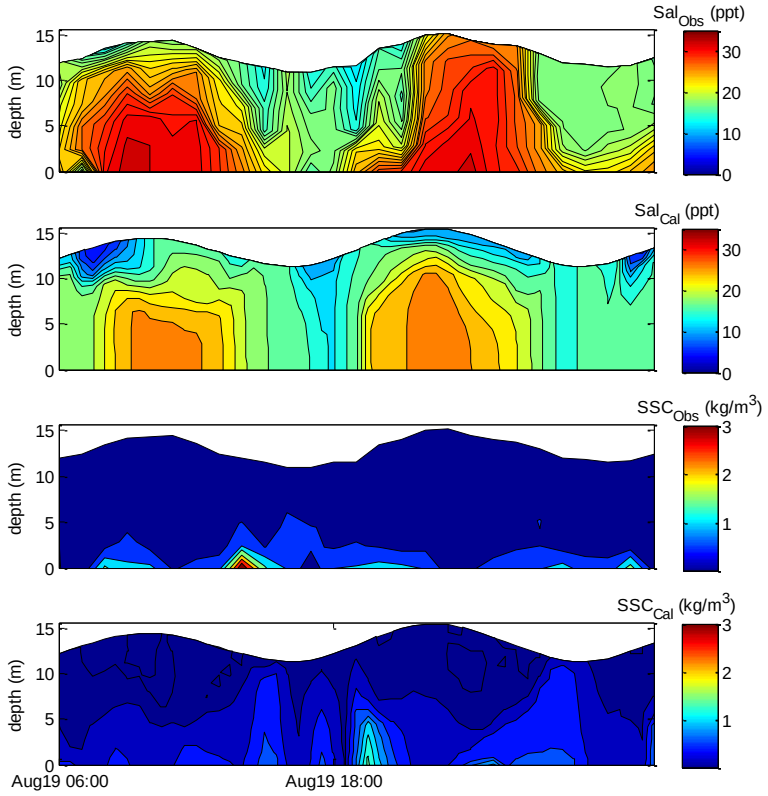

Fig.3.14c Comparison of Salinity and SSC between observation and calculation at the middle of SP (V3) of the Yangtze Estuary in Aug. 2005

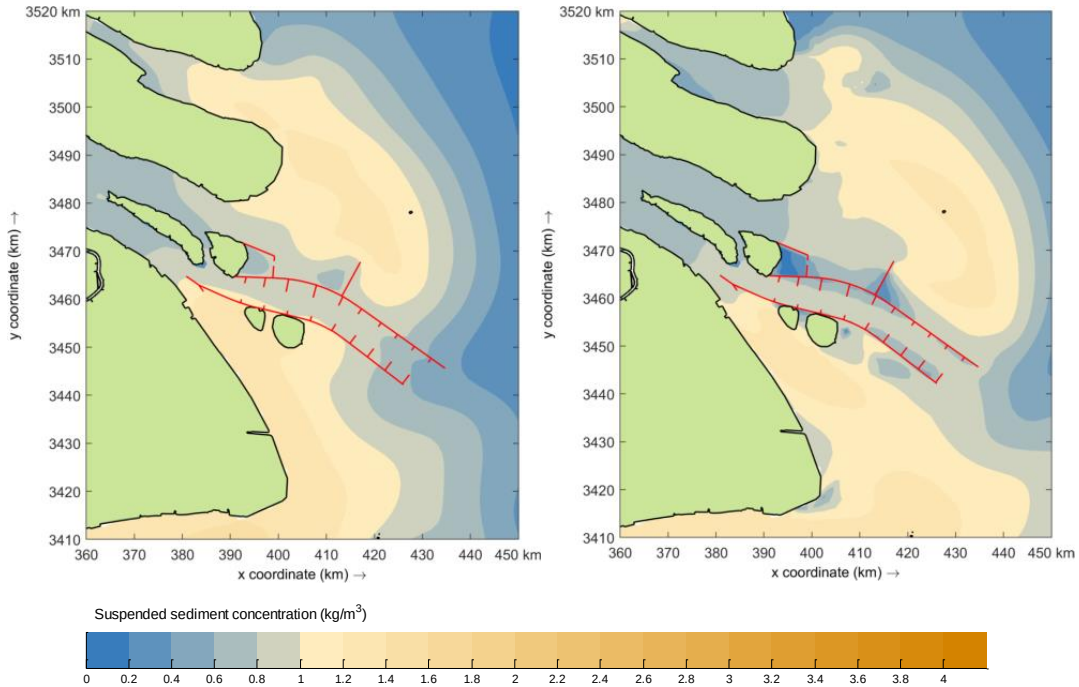

Fig.3.15 Mud concentration distribution around the mouth bar in the Yangtze Estuary during maximum flood (left) and ebb (right) during spring tide in August, 2005

Besides the calibration of salinity and SSC at instrumented stations, the overall distribution pattern of the concentration fields is also examined. The main feature of the SSC distribution in the Yangtze Estuary is the existence of the ETM. Figure 3.13 shows the simulated SSC (mud fraction) distribution in the estuary at maximum flood and maximum ebb, respectively. The location of the simulated ETM zone is consistent with the mouth bar, which agrees well with the reported results (Shen et al., 1992; also see Figure 2.14).

The validation of salinity and SSC against observation in Aug., 2005 is shown in Figures 3.14a ~3.14c. From these figures we can find that the observed salinity is well represented by the model. However, the observed near bed large concentration (~ a few kg/m^3) is not reproduced by the model. Possible reasons for the discrepancies between simulation and observation are factors influencing the sediment transport processes (Guo et al., 2011), especially in the Yangtze Estuary where the fluid mud, wave, wind and human activities interact, leading to a complication of the sediment transport. In general, the simulated SSC show a similar trend to the observed data, although the accuracy of SSC is not as high as that of the velocity. The location of the simulated ETM zone of the verification case is shown in Figure 3.15, as agrees well with the reported results

In conclusion, the calibration and validation of salinity and SSC show that the present model captures the vertical and horizontal salinity and SSC distributions fairly well, be it with some local exceptions.

3.3.4 Wind wave model

As pointed out by Chen (1998), wind waves are dominant in the Yangtze Estuary, with rare events of pure swell. Therefore, the wave model based on SWAN is set up to simulate locally generated wind waves. The grid of the flow model is also used for the wave model. At the open sea boundary, the wave condition is calculated by using Bretschneider formula (Bretschneider, 1963) based on the wind condition. Depth-induced breaking, bottom friction, wind growth, white-capping, refraction and frequency shift are taken into account in the model. The major calibration parameter for the wind wave model for the Yangtze Estuary is the friction parameter. This parameter has been modified to get good agreement between the observed and computed wave data.

Wind and wave in the study area show an obviously seasonal characteristic, i.e. wind and wave come from the south in summer and from the north in winter (Chen, 1998). This seasonal variation has been taken into account in the calibration and validation procedure. The measured data in winter are used for calibration. The calibrated model is further validated against the measurements under summer conditions.

The wind observations at Xiaoyangshan (see Figure 3.7a for location) at every hour from Feb. 15 to Feb. 28, 2003 are applied to compute the wave field. Figure 3.16 shows the simulated wave field at 14:00 on Feb. 21, 2003. The spatial distribution pattern of the wave height in the Yangtze Estuary is as expected, with an overall landward

decrease (Chen, 1998) and sheltering effects of islands and shoals. The simulated wave height is calibrated against the observations at Xiaoyangshan. Here the originally observed wave height is $H_{1/10}$, which is approximately the average wave height of the 10 highest waves in an observed wave train. An empirical relationship (Shao, 1994) is used to translate this into an observed significant wave height. Figure 3.17 shows that the simulated significant wave height and direction agree well with the observed ones, despite a slight overestimation of the wave height. This is probably due to the existence of islands close to the monitoring points, the effect of which cannot be fully incorporated in a spectral wave model. Therefore, the Xiaoyangshan station is probably not the best station for wave observations to compare with the model. However, it is the only station with recent wave data available.

The calibrated model is used to simulate the wave field in Jun., 1982. The wind observation at Dajishan at 8:00, 11:00, 14:00 and 17:00 on each day in Jun., 1982 was used as input to the model. The simulated wave height and direction are plotted against the observations at Dajishan in Figure 3.18. The simulated wave height variation is similar to the measured one, although there are some discrepancies. The observed wave direction is well represented by the simulation.

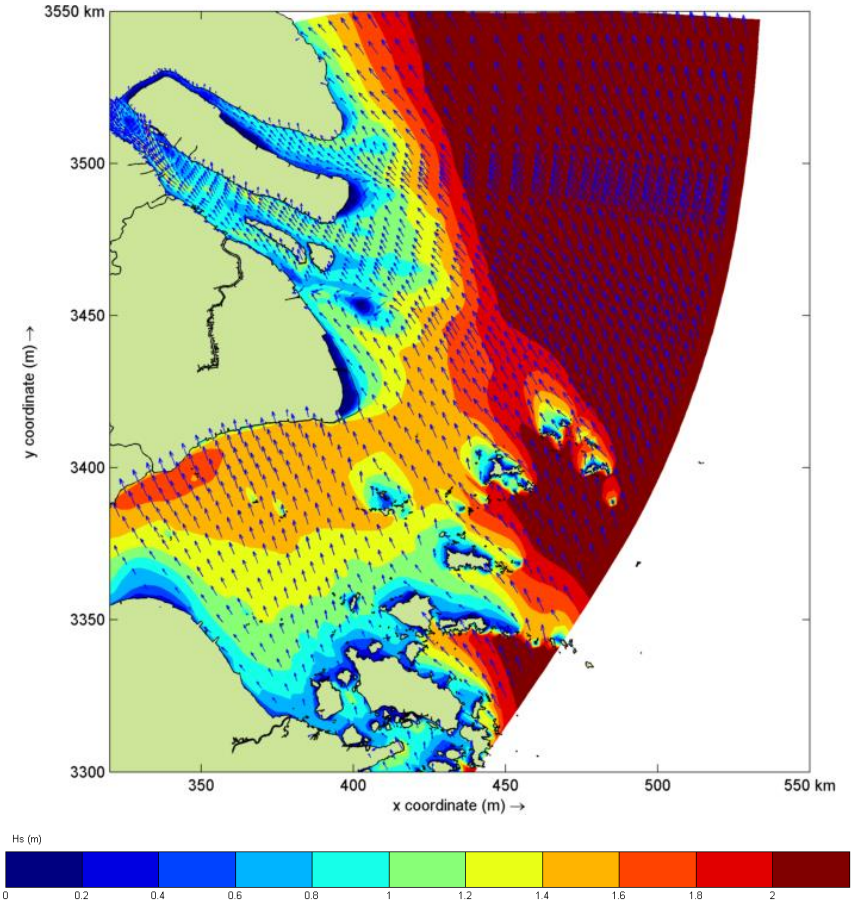

Fig.3.16 Simulated wave height (Hs) at 14:00 on Feb. 21, 2003 (Wind speed: 14m/s, SSE; Blue arrow: the wave direction)

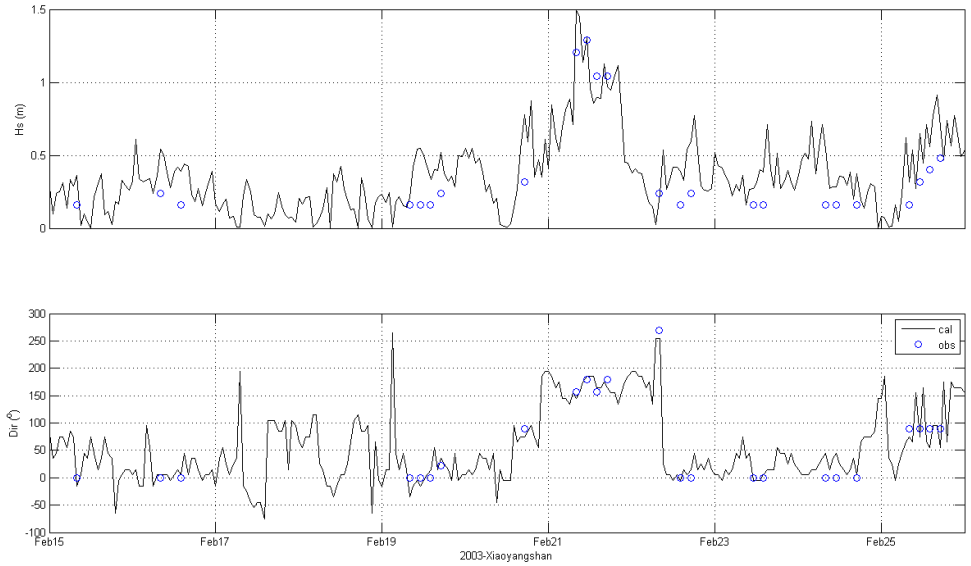

Fig.3.17 Comparison of wave height (Hs: top) and direction (bottom) time series at Xiaoyangshan between the observation and simulation (Feb. 15- Feb. 25, 2003)

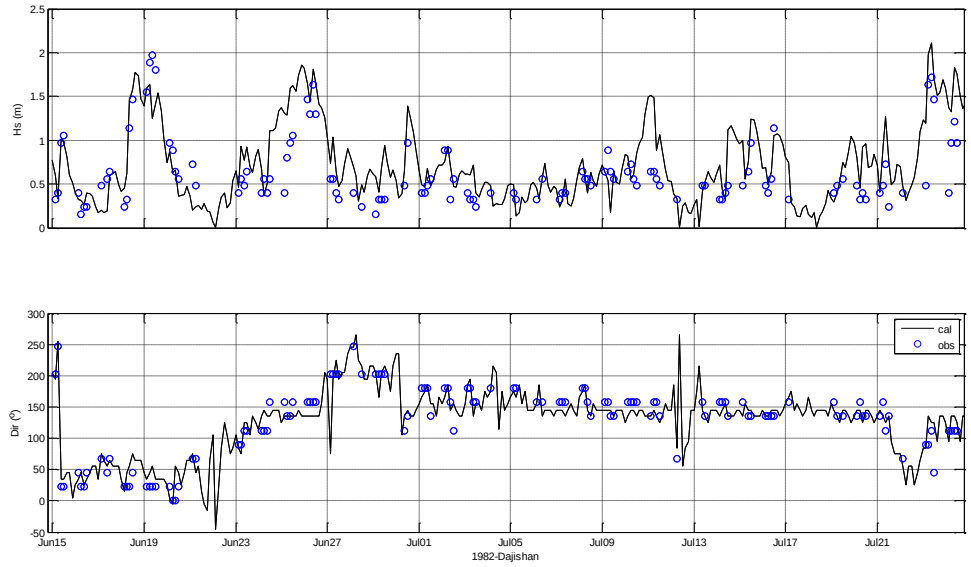

Fig.3.18 Comparison of wave height (Hs: top) and direction (bottom) time series at Dajishan between the observation and simulation (Jun. 15- Jul.25, 1982)

The validation case concerns observations at Nancaodong station (formerly called Yinshuichuan) from Jun. 15 to Jul. 15, 1977. The observed wind data of this station at 8:00, 11:00, 14:00 and 17:00 on each day in this period are used to drive the model. The comparison shown in Figure 3.19 does not lead to an essentially different conclusion on the validity of the model: acceptable, with discrepancies in the wave height and good agreement of the wave direction.

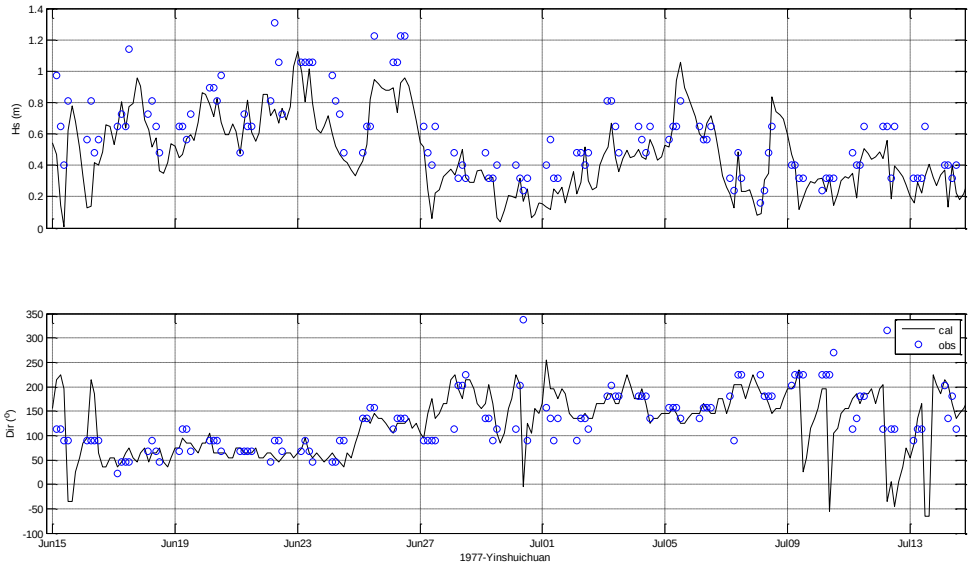

Fig.3.19 Comparison of wave height (Hs: top) and direction (bottom) time series at Nancaodong between the observation and simulation (Jun. 15- Jul. 15, 1977)

3.4 Concluding discussions

In the present model Manning coefficients are used of about 0.011s/m$^{1/3}$ in the estuary and 0.019 s/m$^{1/3}$ in the upper reach. This implies that the bottom of the estuary is 'smooth'. This can partly be the result of turbulence damping due to the high sediment and salt concentrations near bed, resulting in a decrease of apparent bottom roughness (Winterwerp, 2001; Lely, 2007). This turbulence damping also reduces the turbulent mixing of substance, with large concentration and density gradients in the vertical. The change in turbulence intensity due to the stratification of the water column will furthermore yield a velocity profile different from that in clear water.

The salinity-stratification induces significant local effects on the transport of suspended matter. Some effects of the gravitational circulation might be mimicked by an enhanced large horizontal diffusivity in a 2DH model, but an accurate representation requires a 3D model.

The sediments within the system are in the clay, silt and fine sand ranges. The interaction of different fractions is important (van Ledden, 2003). More details of sediment transport can be obtained if we include more sediment fractions, but if too many sediment fractions are included the computational effort will become unacceptable. Therefore, 3 factions of mud (clay and fine silt), silt (coarse silt) 40μm and sand (fine sand) 200μm are used as a compromise.

The calibration and validation results show that the model properly represents the hydrodynamics in the estuary. The salt and sediment transport are also captured reasonably well. Therefore, the model is considered suitable to investigate the mechanisms of sediment transport in the Yangtze Estuary.

4. Sediment Transport in the Mouth Bar Area of the Yangtze Estuary: Process-based Model Approach[2]

4.1 Introduction

To set-up a morphodynamic model for the Yangtze Estuary, it is essential to identify the processes playing a significant role in sediment transport patterns. In Chapter 2, literature survey and data analysis already suggest the relevant processes. In this Chapter a series of sediment transport simulations is performed in order to test the influence of the various processes and mechanisms. The results from these simulations are compared to each other to gain insight into the physics behind the sediment transport pattern change around the mouth bar and the dominant processes and mechanisms.

4.2 Method

For the large scale-evolution of an estuary with the morphological time scale of decades and centuries, the morphological change within a few years may be considered as "initial". The feedback of morphological changes on hydrodynamics and sediment transport can be negligible. ISE (Initial Sedimentation and Erosion) models definitely deserve their place in coastal morphological modeling as a diagnostic tool for process analysis and orientation (De Vriend et al., 1993b). Therefore, the calibrated and validated Yangtze Estuary model is used to simulate the initial sedimentation and erosion around the mouth bar area. The model results are used to assess the processes/mechanisms related to sediment transport in the mouth bar area of the Yangtze Estuary. It is important to understand the dominant processes/mechanisms for sediment trapping in the mouth bar area, since this is essential to understanding the short-term and long-term behavior of the mouth bar of the Yangtze Estuary.

To account for the sediment trapping in the mouth bar of the Yangtze Estuary, the mouth bar is defined as one unit as shown in Figure 4.1. The location of the mouth bar in the Yangtze Estuary is defined as the shallow part in the river mouth (see Chapter 1). Therefore, two cross-sections representing the upstream and downstream boundaries of the mouth bar are selected as shown in Figure 4.1. The sediment that fluxes at these boundaries will be determined to establish the sediment budget of the mouth bar area. The net sediment import at a boundary is defined as the sediment flux entering the mouth bar area minus the flux leaving it.

In order to identify the contributions of various processes/mechanisms to the sediment trapping in the mouth bar area, numerical experiments have been set up with different combinations of driving forces.

[2] Part of this chapter is based on conference papers 'Modeling processes controlling sediment transport at the mouth bar of the Yangtze Estuary' by Ao Chu, Z.B. Wang, H.J. de Vriend and J. Tai, present at 2013 IAHR World Congress and 'Influence of the Three Gorges Dam on Sediment Budget at Mouth Bar of the Yangtze Estuary' by Ao Chu, J. Tai and S. Gu, presented at PACOMS, 2014.

Influence of river input variation

Simulation of one year with long term monthly mean discharge as river input is carried out to study the influence of discharge variation on the sediment transport at the mouth bar. To determine the monthly mean discharge from the river a time series of discharge data from 1950 to 2017 at Datong is used. This data set can be separated to two parts, before and after construction of the TGD, i.e. 1950-2002 and 2003-2017, respectively. The TGD started to impound water in 2003, which eventually regulates the discharge. As shown in Table 4.1, the monthly mean discharge after construction of the TGD is more homogenous than before. As a consequence, there is less discharge in the flood season and more in the dry season. Therefore, the monthly mean discharge from 1950 to 2002 at Datong is regarded as representative of the natural condition. The monthly mean discharge from 2003 to 2017 is regarded as being regulated by the TGD. In addition, a large decrease of sediment load from upstream to the estuary has been observed (see Chapter 2), especially after the TGD constructed. Thus, a different suspended sediment concentration (see Table 4.1) is specified together with the discharge to represent the sediment load into the estuary.

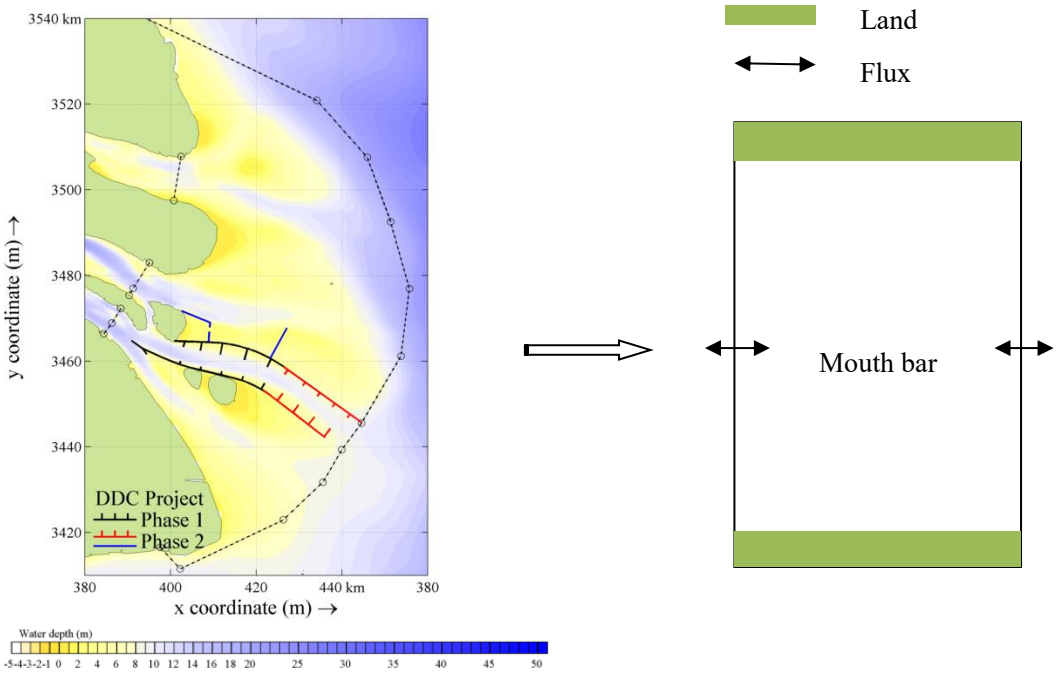

Fig.4.1 The cross-sections (red dash lines) to control the sediment fluxes into the mouth bar of the Yangtze Estuary (left); sketch for the mouth bar into a unit (right)

Table 4.1 Monthly mean discharge (Q:m^3/s) and SSC (kg/m^3) at Datong

Period	Q / SSC	Month 1	2	3	4	5	6	7	8	9	10	11	12
1950-2002	Q	11000	11700	16000	24100	33900	40300	50500	44300	40300	33400	23300	14300
1953-2002	SSC	0.104	0.101	0.149	0.246	0.350	0.430	0.742	0.706	0.689	0.518	0.305	0.179
2003-2017	Q	13600	14100	19400	24000	31900	40600	47100	40700	34800	26000	19700	15200
2003-2017	SSC	0.082	0.068	0.122	0.136	0.167	0.177	0.222	0.230	0.207	0.139	0.118	0.096

Normal condition without wind and wave

The contribution of various combination of processes/mechanisms on sediment transport around the mouth bar is further studied by applying a constant discharge of 30000 m^3/s (slightly larger than the long-term mean value) from upstream with sediment concentration of about 0.5 kg/m^3. Table 4.2a lists the overview of forcing processes and mechanisms. Case C04 includes most forcing processes and mechanisms, except the wind and wave forces, and is regarded as the reference simulation. In addition to the reference simulation a few experimental model runs were defined. Case C03 differs from the reference simulation by excluding flocculation. Therefore, the difference between the results of these two cases can be regarded as the contribution of flocculation. Case C02 excludes salinity and flocculation. An estimation of the contribution of the gravitational circulation can be obtained by analyzing the difference between C03 and C02. Case C01 is a 2DH simulation with all settings the same as in case C02.

Each experiment was run for 15 days (spring neap cycle) after a 15-day spin−up period starting from the average condition of a spring-neap tidal cycle. The cumulative sediment fluxes through the predefined cross-sections were calculated and used to evaluate the erosion/sedimentation within the area between the two cross-sections.

The presence of the mouth bar can also influence the sediment trapping in this area. Therefore, the flat bed with water depth of about 7.0 m below MSL is applied to the area east to the upstream control section to represent the 'no mouth bar′ situation. The value 7.0 m is determined based on the average water depth in this area. The situations with presence and absence of mouth bar are both simulated with different combinations of processes/mechanisms listed in Table 4.2a. The simulations with name start with 'C' represent the situation with mouth bar and those with 'N′ the situation without.

Table 4.2a Combination of processes/mechanisms for Yangtze Estuary model (normal conditions, with and without the mouth bar)

	2D/3D	Forces				Salinity	Flocculation	Transport mechanisms
		Discharge	Tide	Wind	Wave			
C01	2D	+	+	-	-	-	-	MF, TA
C02	3D	+	+	-	-	-	-	MF, TA, P.GC
C03	3D	+	+	-	-	+	-	MF, TA, GC
C04	3D	+	+	-	-	+	+	MF, TA, GC, FL
N01	2D	+	+	-	-	-	-	MF, TA
N02	3D	+	+	-	-	-	-	MF, TA,P.GC
N03	3D	+	+	-	-	+	-	MF, TA, GC
N04	3D	+	+	-	-	+	+	MF, TA, GC, FL

C**/N**: simulation in/excluding the mouth bar; MF: transport due to mean flow; TA: transport due to tidal asymmetry; P.GC: part of gravitational circulation resulted from the discrepancy of velocity and concentration in vertical; GC: gravitational circulation including the P.GC and the density flow contribution; FL: flocculation of fine sediment.

The DDC project (training dikes and groins) is also included in the model, as the DDC project can largely influence the sediment transport pattern around the Yangtze Estuary. The simulation period is taken in 2003 with the first phase of the DDC project implemented. The training dikes and the groins in that situation are schematized as local weirs in the model (Deltares, 2014).

Influence of wind and wave

Table 4.2b Combination of processes/mechanisms for Yangtze Estuary model (with influence of wind and wave in Summer and Winter)

	3D	Forces				Salinity	Flocculation	Transport mechanisms
		Discharge	Tide	Wind	Wave			
C05	+	+	+	+	-	+	+	C04, wind (Sum.)
C06	+	+	+	+	+	+	+	C04, wind, wave (Sum.)
C07	+	+	+	+	-	+	+	C04, wind (Win.)
C08	+	+	+	+	+	+	+	C04, wind, wave (Win.)

Sum.: Summer, wind from ESE, 7m/s; Win.: winter, wind from WNW, 7m/s.

To account for the wind and wave influence on the sediment transport around the mouth bar area, wind and wave forces are superimposed on C04. Analysis of observed wind/wave data (1980-1990) at stations in the Yangtze Estuary (Chen 1998) reveals different wind/wave characteristics in winter and summer. It shows that the dominant wind comes from WNW direction in the winter half-year (from November to April of next year) with average magnitudes around 7 m/s. In the summer half-year (May ~ October), the wind comes from ESE with comparable magnitude. Consequently, cases C05 and C07 represents the wind forces in summer and winter time with the same setup as C04. Chen (1998) points out that waves in this region are mainly wind wave (as opposed to swell). This means that wind and waves always come from the same direction and can be combined in the same run (C06 and C08). Table 4.2b shows how wind and wave effects are combined in the various runs.

Influence of DDC project

The above-mentioned scenarios are designed for the model set up in 2003, which means the second phase of the DDC project in the Yangtze Estuary has not been completed yet. In order to investigate the influence of the different phases of the DDC project on the sediment transport, C09 and C10 (shown in Table 4.2c) are designed to represent two situations without DDC structures and with all structures constructed. The dredging activity of the DDC project would not be included at the present study.

Table 4.2c Combination of processes/mechanisms for Yangtze Estuary model (with influence of the construction of the DDC project)

	3D	Forces				Salinity	Flocculation	Transport mechanisms
		Discharge	Tide	Wind	Wave			
C09	+	+	+	-	-	+	+	C04, No DDC
C10	+	+	+	-	-	+	+	C04, Complete DDC

4.3 Model results and discussion

4.3.1 Influence of discharge variation

Two simulations with monthly mean discharge before and after construction of the TGD are carried out to study the sediment transport in the mouth bar area with varied discharge from upstream. The model results are also compared with the observations as an extra validation of the transport model. The cumulative sediment flux through two control sections around the mouth bar is shown in Table 4.3a. Figure 4.2a shows the sediment trapped in the mouth bar of the Yangtze Estuary in each month within a year under natural condition.

Similarly, the sediment budget in the mouth bar under the influence of the TGD can also be calculated. The results are shown in Table 4.3b and Figure 4.2b.

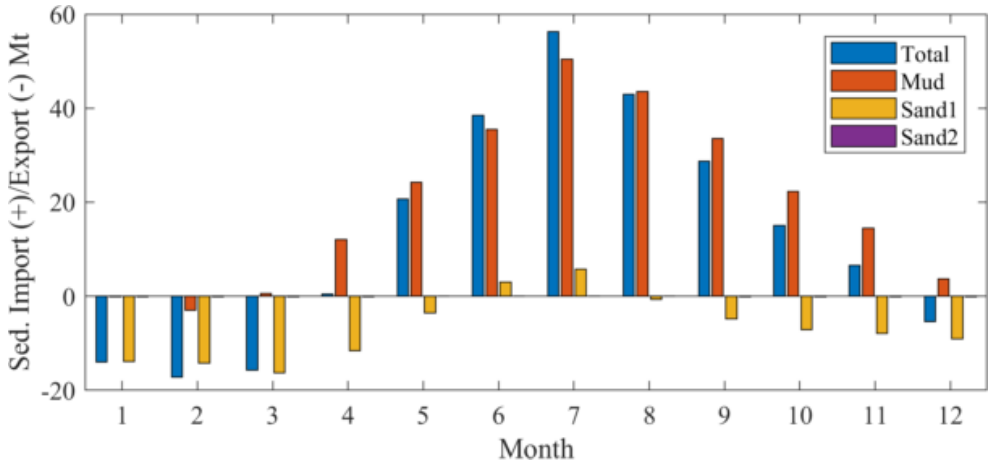

Fig.4.2a Sediment import to (+) and export from (-) the mouth bar area of Yangtze Estuary (before TGD: monthly mean discharge at Datong, 1950-2002; Mt: Million tons)

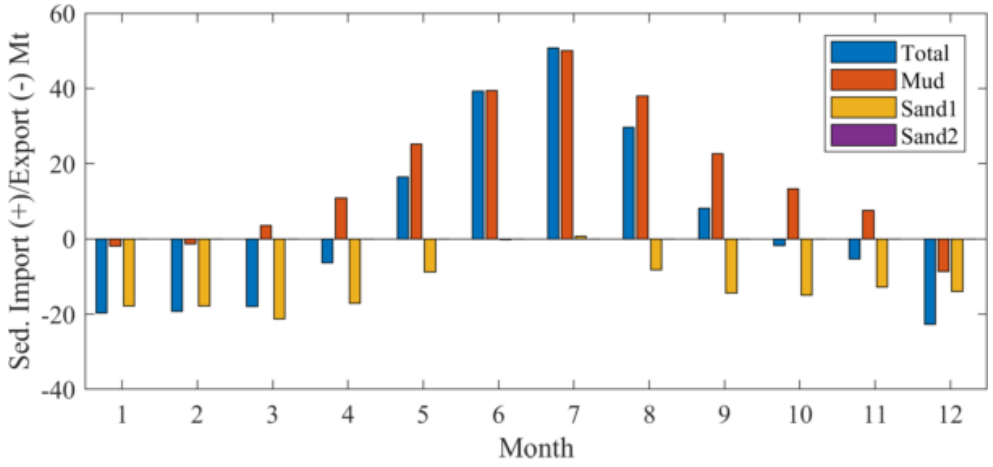

Fig.4.2b Sediment import to (+) and export from (-) the mouth bar area of Yangtze Estuary (after TGD: monthly mean discharge at Datong, 2003-2017; Mt: Million tons)

Table 4.3a Sediment import to (+) and export from (-) the mouth bar of Yangtze Estuary (before TGD: monthly mean Q at Datong 1950-2002; Mt: Million tons)

Simulation	Fraction	Fluxes (Mt)		Net	ISE	$Q(m^3/s)/SSC(kg/m^3)$ at Datong
		West	East			
Jan.	Mud	8.23	-8.30	-0.07	E	11000/0.104
	Sand1	-11.63	-2.18	-13.81	E	
	Sand2	-0.05	-0.02	-0.06	E	
	Total	-3.44	-10.50	-13.94	E	
Feb.	Mud	6.59	-9.53	-2.95	E	11700/0.101
	Sand1	-11.23	-2.94	-14.17	E	
	Sand2	-0.05	-0.03	-0.08	E	
	Total	-4.70	-12.50	-17.20	E	
Mar.	Mud	11.55	-10.98	0.58	S	16000/0.149
	Sand1	-11.58	-4.65	-16.23	E	
	Sand2	-0.06	-0.05	-0.10	E	
	Total	-0.08	-15.67	-15.75	E	
Apr.	Mud	23.99	-11.90	12.09	S	24100/0.246
	Sand1	-6.73	-4.84	-11.57	E	
	Sand2	-0.04	-0.04	-0.08	E	
	Total	17.23	-16.78	0.44	S	
May.	Mud	40.32	-16.05	24.28	S	33900/0.350
	Sand1	-0.56	-2.96	-3.51	E	
	Sand2	0.00	-0.03	-0.03	E	
	Total	39.76	-19.03	20.73	S	
Jun.	Mud	52.11	-16.62	35.49	S	40300/0.430
	Sand1	4.07	-1.11	2.96	S	
	Sand2	0.03	-0.02	0.01	S	
	Total	56.21	-17.75	38.46	S	
Jul.	Mud	85.23	-34.81	50.42	S	50500/0.742
	Sand1	9.38	-3.57	5.82	S	
	Sand2	0.06	-0.02	0.04	S	
	Total	94.66	-38.40	56.27	S	
Aug.	Mud	83.07	-39.50	43.57	S	44300/0.706
	Sand1	6.39	-6.99	-0.61	E	
	Sand2	0.04	-0.05	-0.01	E	
	Total	89.50	-46.53	42.97	S	
Sep.	Mud	68.25	-34.65	33.60	S	40300/0.689
	Sand1	2.67	-7.45	-4.78	E	
	Sand2	0.02	-0.06	-0.04	E	
	Total	70.93	-42.16	28.77	S	
Oct.	Mud	48.57	-26.32	22.25	S	33400/0.518
	Sand1	-1.02	-6.08	-7.10	E	
	Sand2	-0.01	-0.04	-0.05	E	
	Total	47.54	-32.44	15.10	S	
Nov.	Mud	24.62	-10.11	14.50	S	23300/0.305
	Sand1	-5.08	-2.82	-7.90	E	
	Sand2	-0.02	-0.02	-0.05	E	
	Total	19.52	-12.96	6.56	S	
Dec.	Mud	11.99	-8.30	3.69	S	14300/0.179
	Sand1	-7.93	-1.07	-9.00	E	
	Sand2	-0.03	-0.01	-0.04	E	
	Total	4.03	-9.38	-5.35	E	
Total	Mud	464.52	-227.07	237.44	S	28700/-
	Sand1	-33.24	-46.66	-79.90	E	
	Sand2	-0.12	-0.38	-0.50	E	
	Total	431.16	-274.11	157.05	S	

'West' and 'East': the west and east cross-sections of the mouth bar (see Fig.4.1);

Table 4.3b Sediment import (+) and export (-) of the mouth bar in the Yangtze Estuary (after TGD: monthly mean discharge at Datong, 2003-2017; Mt: Million tons)

Simulation	Fraction	Fluxes (Mt)		Net	ISE	Q(m3/s)/SSC(kg/m3）at Datong
		West	East			
Jan.	Mud	6.15	-8.01	-1.86	E	13600/0.082
	Sand1	-15.68	-2.13	-17.82	E	
	Sand2	-0.05	-0.02	-0.07	E	
	Total	-9.59	-10.16	-19.75	E	
Feb.	Mud	7.92	-9.32	-1.39	E	14100/0.068
	Sand1	-14.56	-3.27	-17.83	E	
	Sand2	-0.06	-0.03	-0.09	E	
	Total	-6.69	-12.62	-19.31	E	
Mar.	Mud	13.64	-10.11	3.53	S	19400/0.122
	Sand1	-15.93	-5.41	-21.33	E	
	Sand2	-0.07	-0.05	-0.11	E	
	Total	-2.36	-15.56	-17.92	E	
Apr.	Mud	21.90	-11.08	10.83	S	24000/0.136
	Sand1	-12.43	-4.69	-17.12	E	
	Sand2	-0.05	-0.05	-0.10	E	
	Total	9.42	-15.81	-6.39	E	
May.	Mud	36.68	-11.43	25.25	S	31900/0.167
	Sand1	-7.03	-1.78	-8.81	E	
	Sand2	-0.02	-0.03	-0.05	E	
	Total	29.63	-13.24	16.39	S	
Jun.	Mud	55.32	-15.93	39.39	S	40600/0.177
	Sand1	-0.84	0.71	-0.13	E	
	Sand2	0.01	-0.02	-0.01	E	
	Total	54.48	-15.23	39.25	S	
Jul.	Mud	79.61	-29.56	50.05	S	47100/0.222
	Sand1	1.75	-1.07	0.68	S	
	Sand2	0.03	-0.03	0.00	S	
	Total	81.39	-30.66	50.73	S	
Aug.	Mud	71.18	-33.20	37.98	S	40700/0.230
	Sand1	-3.02	-5.21	-8.23	E	
	Sand2	0.01	-0.05	-0.05	E	
	Total	68.17	-38.47	29.70	S	
Sep.	Mud	50.36	-27.67	22.68	S	34800/0.207
	Sand1	-7.50	-6.94	-14.44	E	
	Sand2	-0.02	-0.07	-0.09	E	
	Total	42.84	-34.68	8.16	S	
Oct.	Mud	31.11	-17.83	13.29	S	26000/01.39
	Sand1	-10.66	-4.33	-14.99	E	
	Sand2	-0.03	-0.05	-0.09	E	
	Total	20.42	-22.21	-1.79	E	
Nov.	Mud	14.19	-6.70	7.49	S	19700/0.118
	Sand1	-11.55	-1.20	-12.76	E	
	Sand2	-0.04	-0.03	-0.07	E	
	Total	2.60	-7.93	-5.33	E	
Dec.	Mud	-2.78	-5.88	-8.66	S	15200/0.096
	Sand1	-15.20	1.20	-14.00	E	
	Sand2	-0.05	-0.02	-0.07	E	
	Total	-18.03	-4.69	-22.73	E	
Total	Mud	385.3	-186.7	198.6	S	27300/-
	Sand1	-112.7	-34.1	-146.8	E	
	Sand2	-0.3	-0.4	-0.8	E	
	Total	272.3	-221.3	51.0	S	

'West' and 'East': the west and east cross-sections of the mouth bar (see Fig.4.1);

Figure 4.3 shows the cumulative sedimentation and erosion around the mouth bar area in periods of 1990-2003 and 2003-2007. Although the area in Figure 4.3 does not cover the entire area predefined by two cross-sections, the result shown in this figure can give some reference for the simulation results of annually sediment budget in the mouth bar area. The sediment volume change in the measured area (Figure 4.3) is calculated and given in Table 4.4. We can clearly find the amount of sediment trapped in the mouth bar area after 2003 is much smaller than that before.

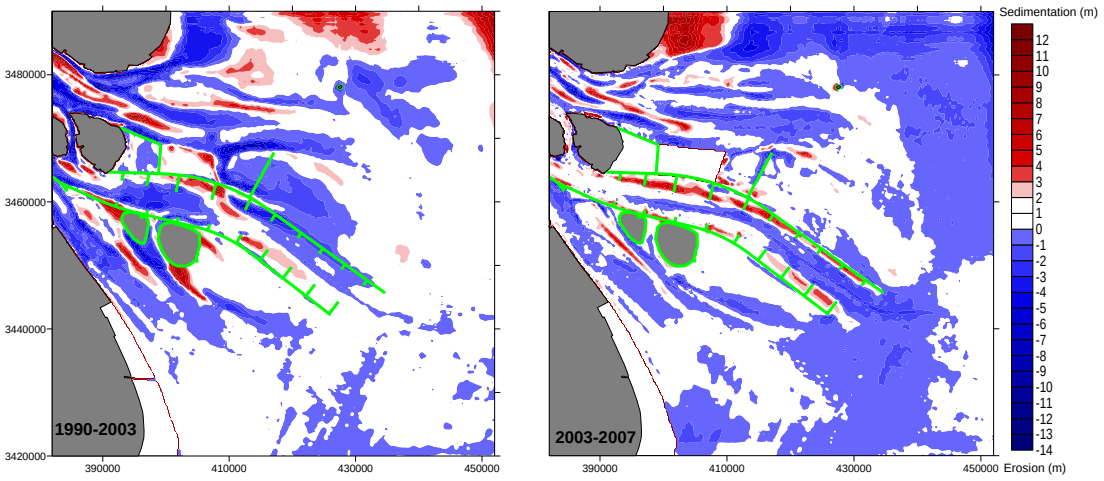

Fig.4.3 Observed sedimentation and erosion around the mouth bar in periods of 1990-2003 (left) and 2003-2007 (right)

Table 4.4 Measured sediment volume change around the mouth bar area (see Fig.4.3)

Period	Import/export (million m^3)	Annual budget (million m^3)
1990-2003	+1113	79.5
2003-2007	+90.8	18.2

From Table 4.3 and Figure 4.2, we can conclude,

1. The amount of sediment trapped in the mouth bar area changes with the discharge from upstream. The trend is sedimentation in the wet season and erosion in the dry season. Before the TGD was constructed, deposition happens at the mouth bar from May to November with erosion in the other months of the year. After construction of the TGD, sedimentation occurs from May to September with erosion in the other months of the year. This agrees well with observations along the access channel in the NP (Tan et al., 2009).
2. The magnitude of sedimentation after construction of the TGD is much smaller than that before. The maximum sediment trapped in the mouth bar accounts of 56 million tons in July before construction of the TGD. After construction of the TGD, the maximum net deposition in the mouth bar is about 51 million tons. In a normal year the total volume of sediment trapped in the mouth bar area is about 157 million tons, which is much larger than the 51 million tons after construction of the TGD. This decrease tendency agrees well with the measured annual sediment volume change before and after 2003 (see Table 4.4). If 1.6 t/m^3 is assumed to be the density of

sediment deposition in the Yangtze Estuary (Wu et al., 2006), the measured annual deposition in the observed area in the period 1990-2003 is about 127 million tons, and about 29 million tons in the period 2003-2007. It should be careful that the dredging of the access channels in the study area are not included in the observed data, neither for the Yangtze Estuary model. Since the area with measured bathymetry covers about 89% of the mouth bar area as defined by two control sections, the annual sediment budgets before and after 2003 are approximated as 139 and 46 million tons, respectively. The magnitudes of the simulated sediment budget are comparable with the observations.

4.3.2 Normal condition without wind and wave

The spring-neap tidal cycle of 15 days is selected for all simulations listed in Table 4.2a. Figure 4.4 gives the tidal water level at Niupijiao during a spring-neap cycle. The simulations were carried out for the same period of this cycle. The simulation starts shortly after neap tide. The cycle is not entirely closed, in that there is a slight discrepancy between the water levels at the beginning and at the end, but this will not lead to a large error in the mean sediment transport.

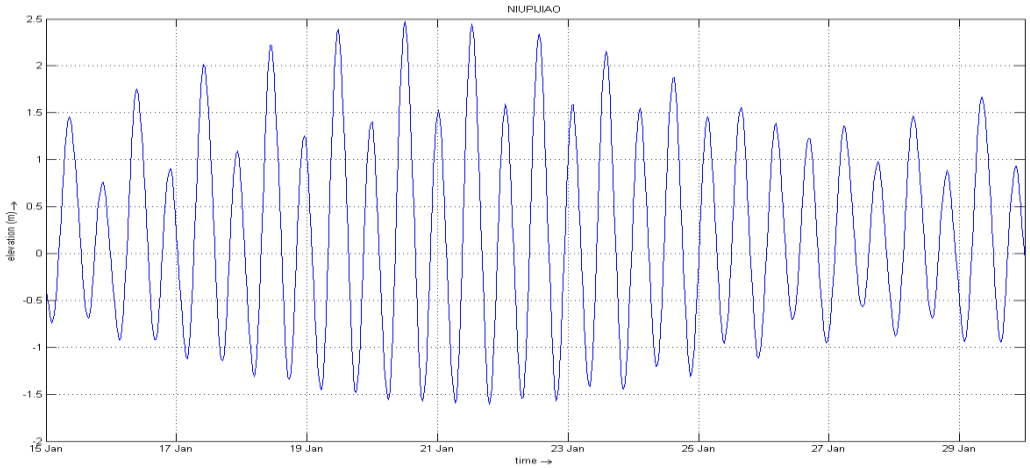

Fig.4.4 Simulated water level at Niupijiao

Eight different numerical experiments have been carried out with different transport mechanisms considered. First, flow and transport patterns are presented in order to assess the contributions of different process and mechanisms to the total sediment transport. Then we focus on the sediment balance in the mouth bar area as derived from the transport fluxes through the control sections. The import to or export from the mouth bar area can be determined and the processes/mechanisms in favor of mouth bar formation can be obtained.

Figure 4.5 shows the sediment transport patterns for each sediment fraction. Figure 4.5a shows the mud (clay and fine silt range) transport under different scenarios. The sand1 (coarse silt, d_{50} = 40 μm) transport pattern is shown in Figure 4.5b. The sand2 (fine sand, d_{50} = 200 μm) transport rate is much smaller than those of the other two fractions. Therefore, the transport pattern of sand2 is not shown here. From these figures, the

following observations are made:
- The transport magnitudes of the mud fraction are larger than those of the sand fraction, which means mud dominates in the estuary.
-The NC is the major outlet of the sediment to sea, followed by the NP and the SP.
-The transport patterns for various combinations of mechanisms are quite different; seawards of the Hengsha Shoal a large eddy can be observed in case C02, whereas it is not visible in cases C03 and C04; another eddy occurs at the seaward end of Jiuduansha Shoal in cases C03 and C04.

The net sediment transport over 15 days through the control sections is shown in Figure 4.6a and 4.6b, for the simulations with and without the mouth bar, respectively. The difference of fluxes through the two control sections is the amount of sediment deposited/eroded in/from the mouth bar area. As three sediment fractions have been included in the model, sediment fluxes of the individual fraction and the sum of all fractions are computed. This yields the sediment budgets shown in Table 4.5 and 4.6, with and without mouth bar, respectively.

Table 4.5 Sediment budget (Mt: million tons) of the mouth bar area in the Yangtze Estuary (with mouth bar, normal discharge over 15 days)

Simulation	Fraction	Fluxes (Mt)		Net	ISE	Xuliujing	Transport mechanisms
		West	East				
C01	Mud	20.53	-46.01	-25.49	E	18.74	MF+
	Sand1	-3.13	-3.33	-6.46	E	6.44	TA
	Sand2	0.00	-0.01	-0.01	E	0.01	
	Total	17.4	-49.4	-32.0	E	25.2	
C02	Mud	20.49	-39.21	-18.72	E	18.68	MF +
	Sand1	-3.47	-3.06	-6.54	E	7.70	TA +
	Sand2	0.00	-0.02	-0.02	E	0.02	P.GC
	Total	17.0	-42.3	-25.3	E	26.4	
C03	Mud	20.23	-8.61	11.62	S	18.78	MF +
	Sand1	-3.54	-2.13	-5.67	E	7.73	TA +
	Sand2	0.00	-0.01	-0.01	E	0.02	GC
	Total	16.7	-10.7	5.9	S	26.5	
C04	Mud	20.10	-6.77	13.33	S	18.79	MF +
	Sand1	-0.79	-1.87	-2.66	E	7.71	TA +
	Sand2	0.00	-0.01	-0.01	E	0.02	GC +
	Total	19.3	-8.7	10.7	S	26.5	FL

'West' and 'East': the west and east cross-sections of the mouth bar (see Fig.4.1); 'Xuliujing': cross section at Xuliujing for reference; 'Net': the net sediment fluxes for the mouth bar; 'ISE': initial sedimentation/erosion; '+ /-': positive/negative indicating the import/export sediment of the control area; MF: transport due to mean flow; TA: transport due to tidal asymmetry; (P.)GC: transport due to (part of) gravitational circulation; FL: flocculation of fine cohesive sediment.

Table 4.6 Sediment budget (Mt: million tons) of the mouth bar area in the Yangtze Estuary (without mouth bar, normal discharge over 15 days)

Simulation	Fraction	Fluxes (Mt)		Net	ISE	Xuliujing	Transport mechanisms
		West	East				
N01	Mud	29.04	-52.39	-23.35	E	18.88	MF+
	Sand1	5.75	-10.08	-4.34	E	7.17	TA
	Sand2	0.03	-0.06	-0.03	E	0.01	
	Total	34.8	-62.5	-27.7	E	26.07	
N02	Mud	29.39	-42.12	-12.73	E	18.91	MF +
	Sand1	4.00	-8.33	-4.33	E	8.26	TA +
	Sand2	0.04	-0.05	-0.02	E	0.02	P.GC
	Total	33.4	-50.5	-17.1	E	27.19	
N03	Mud	29.39	8.61	38.00	S	19.00	MF +
	Sand1	5.32	-8.82	-3.50	E	8.28	TA +
	Sand2	0.05	-0.05	-0.01	E	0.02	GC
	Total	34.8	-0.3	34.5	S	27.30	
N04	Mud	29.71	9.48	39.19	S	19.00	MF +
	Sand1	8.86	-6.14	2.72	E	8.26	TA +
	Sand2	0.05	-0.05	0.00	E	0.02	GC +
	Total	38.6	3.3	41.9	S	27.28	

'West' and 'East': the west and east cross-sections of the mouth bar (see Fig.4.1); 'Xuliujing': cross section at Xuliujing for reference; 'Net': the net sediment fluxes for the mouth bar; 'ISE': initial sedimentation/erosion; '+ /-': positive/negative indicating the import/export sediment of the control area; MF: transport due to mean flow; TA: transport due to tidal asymmetry; (P.)GC: transport due to (part of) gravitational circulation; FL: flocculation of fine cohesive sediment.

The following observations are made from Figures 4.5 & 4.6 and Tables 4.5 & 4.6:

1. Figure 4.5 shows that the NC is the main outlet to discharge river sediment to the sea. The SC also exports sediment, about half of the amount through the NC. The NB mainly imports sediment. The modeled characteristics of the sediment transport paths agree to earlier reports (Shen et al., 2001, Yun 2004).
2. The sediment fluxes shown in Table 4.5 reveal that the mud fraction dominates the system, in agreement with the observations reported in literature (Chen, 1998; Yun, 2004). The mud flux through the Xuliujing cross-section is about 19 million ton over 15 days (a spring-neap tide) with the yearly amount in the order of 400-500 million ton, which is approximately the same magnitude as observed(Yun, 2004).
3. The presence of the mouth bar influences the sediment transport, see Table 4.5 and Table 4.6. The differences are mainly in the magnitude of the fluxes, whereas the sign (import/export) is the same in either case. This means that the excluding of the mouth bar will not lead to essential change of the sediment trapped feature in the Yangtze Estuary.
4. The results of simulation C01/N01 (2DH without salinity) and C02/N02 (3D without salinity) indicate sediment export from the mouth bar area. The results of the other two simulations (C03: 3D with salinity; C04: 3D with salinity and flocculation) show that the sediment is trapped in the mouth bar area. This indicates that the river discharge and tides are the main forces for the water movement in the estuary and introduce the transport due to mean flow and tidal asymmetry. However, their combination will not lead to the sediment deposition in the mouth bar area, unless the salinity process is included. This reveals that salinity is the prerequisite process for sediment trapped in the mouth bar area.

5. The mouth bar area is exporting the sand fractions in all combinations. The mud tends to be trapped in the mouth bar area when the gravitational circulation is included. Also, the sand export is less in that case.
6. The flocculation mechanism enhances the deposition in the mouth bar at the present situation. If we take the mud deposition in case C03 as a reference, the flocculation in case C04 is about 15% larger. In the situation without mouth bar, however, we see the opposite: the deposition in the mouth bar area in case N03 is larger than in case N04. This is due to a difference in horizontal sediment concentration gradients between these two cases.
7. The amount of mud trapped in the mouth bar area amounts to 60 and 70% of the river input (value at Xuliujing) in cases C03 and C04. This is larger than the value of 40-50% derived from the historical bathymetry data (Shen et al., 2001). It is noted that these bathymetric data have to be translated from volumes to tons, which is a quite uncertain calculation because of the density of the deposited mud. The total amounts of sediment trapped in the mouth bar are about 22% and 40% (C03 and C04) of the river input, which agrees well with the reported magnitudes (Shen et al., 2001).

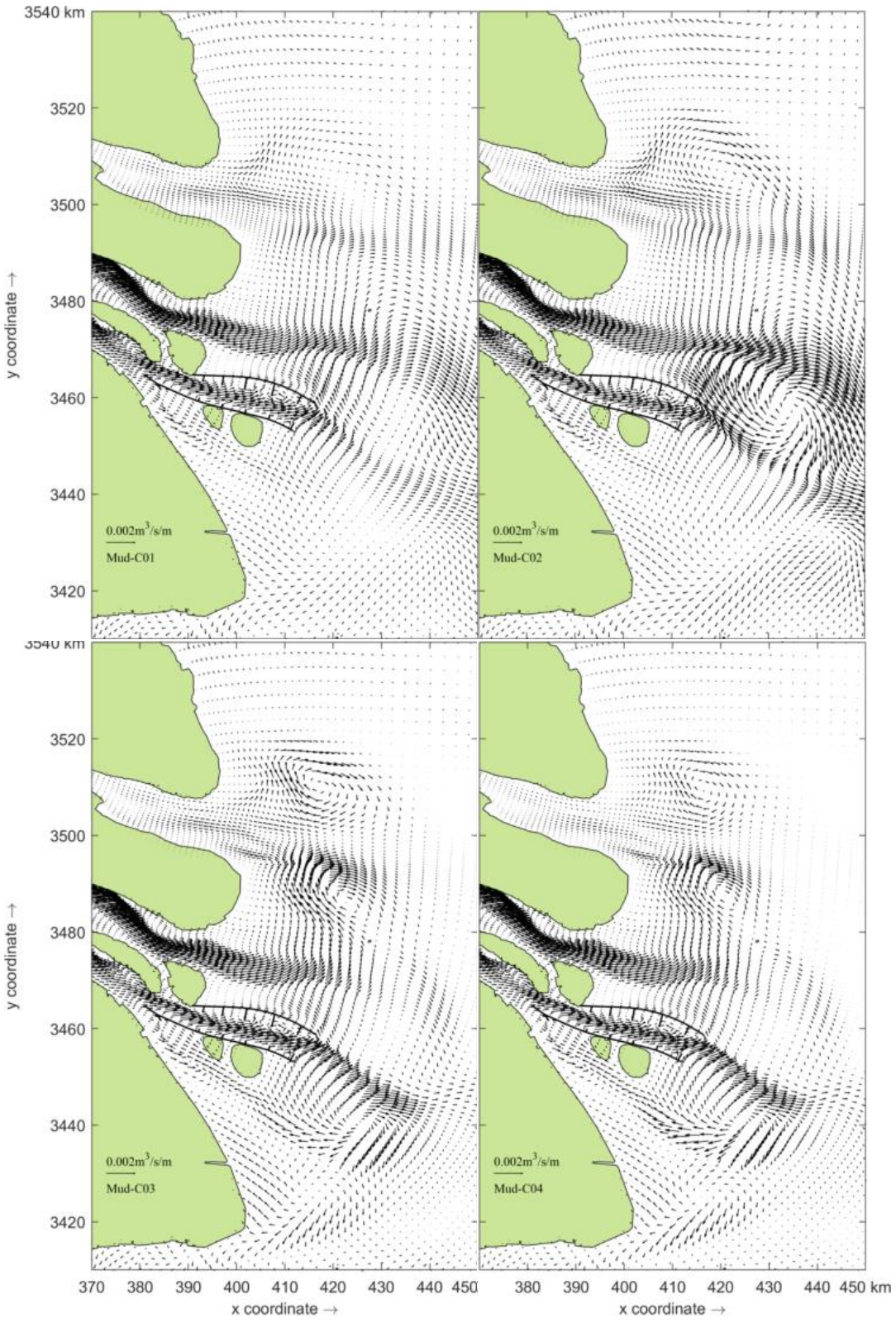

Fig.4.5a Transport pattern for mud around the mouth bar area with different transport mechanism involved (Top left: C01, 2DH without salinity; Top right: C02, 3D without salinity; Bottom left:C03, 3D with salinity; Bottom right: C04, 3D with salinity and flocculation; 15-day average)

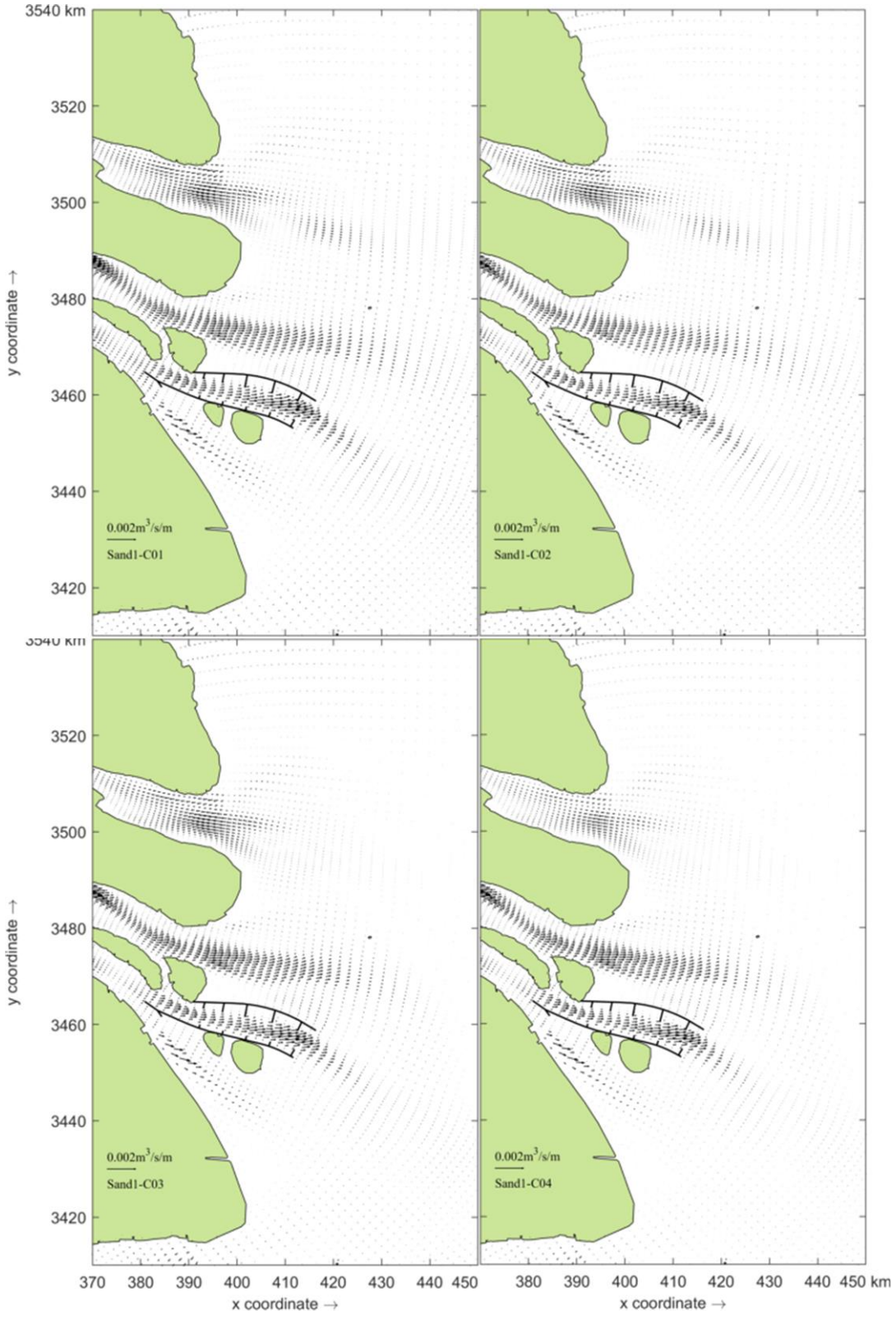

Fig.4.5b Transport pattern for sand1 around the mouth bar area with different transport mechanism involved (Top left: C01, 2DH without salinity; Top right: C02, 3D without salinity; Bottom left:C03, 3D with salinity; Bottom right: C04, 3D with salinity and flocculation; 15-day average)

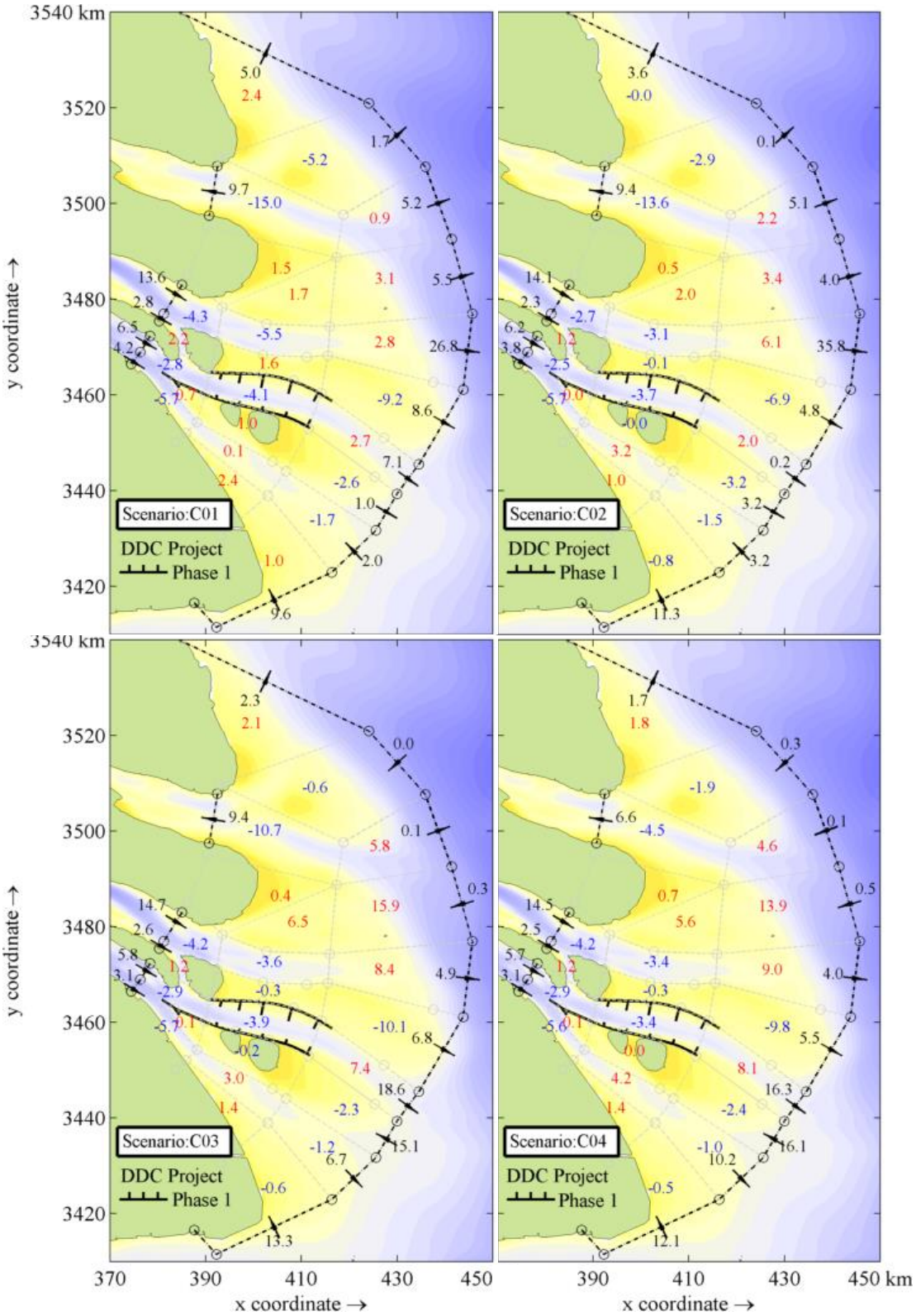

Fig.4.6a Sediment fluxes (arrows in unit of million tons) through cross-sections over 15 days with mouth bar (Black numbers: fluxes; Red: deposition in polygons; Blue: erosion in polygons; Top left: C01, 2DH without salinity; Top right: C02, 3D without salinity; Bottom left:C03, 3D with salinity; Bottom right: C04, 3D with salinity and flocculation)

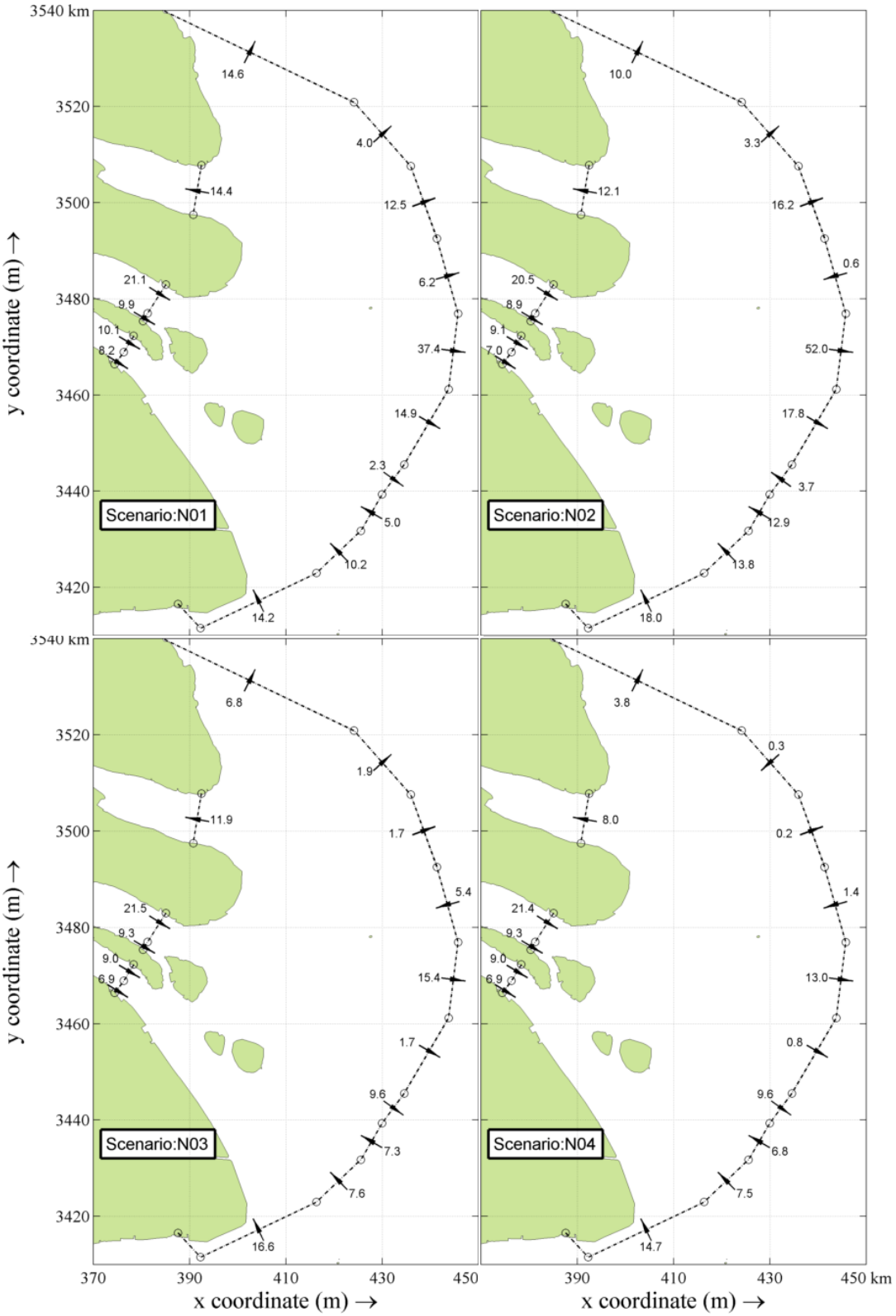

Fig.4.6b Sediment fluxes (arrows in unit of million tons) through cross-sections over 15 days without mouth bar (Black numbers: fluxes; Top left: N01, 2DH without salinity; Top right: N02, 3D without salinity; Bottom left: N03, 3D with salinity; Bottom right: N04, 3D with salinity and flocculation)

4.3.3 Influence of wind-wave and the DDC project

Figure 4.7 shows the 15-day cumulative sediment transport through the various segments of the control sections if wind and wave effects are included in the model. The mean situations of wind speed in winter and summer are represented. The results for the sediment budget in the mouth bar area with wind and waves included are presented in Table 4.7. From Table 4.7 and Figure 4.7 we can conclude that the characteristics of the sediment budget are similar to those in case C04. Wind and waves slightly enhance the amount of sediment trapped in the mouth bar area, but by less than 6-23%.

The 15-day cumulative sediment transport for scenarios of C09 and C10, without DDC and with completed DDC structures, are shown in Figure 8 and Table 4.7, too. It can be found that the influence of the structures on the sediment transport is limited in the region near the DDC project. The characteristics of the sediment trapped in the mouth bar area is the same as C04. The amount sediment trapped in the mouth bar area under each condition of two different phases (C09 and C10) of the DDC project differs from that of case C04 less than 15%.

Table 4.7 Sediment budget (million tons) of the mouth bar in the Yangtze Estuary (With mouth bar, with wind or wave, normal discharge over 15 days)

Simulation	Fraction	Fluxes (mt)		Net	ISE	Xuliujing	Transport mechanisms
		West	East				
C05	Mud	20.37	-5.41	14.97	S	18.90	MF +TA
	Sand1	-0.71	-2.25	-2.96	E	7.53	GC +FL
	Sand2	0.00	-0.02	-0.01	E	0.02	Wind+Wave/ESE
	Total	19.7	-7.7	12.0	S	26.4	
C06	Mud	21.44	-7.19	14.25	S	18.72	MF +TA
	Sand1	-0.02	-2.81	-2.84	E	7.56	GC +FL
	Sand2	0.01	-0.03	-0.02	E	0.02	Wind /ESE
	Total	21.4	-10.0	11.4	S	26.3	
C07	Mud	19.99	-4.84	15.15	S	18.63	MF +TA
	Sand1	-0.89	-1.02	-1.91	E	7.87	GC +FL
	Sand2	0.00	-0.01	-0.01	E	0.02	Wind /WNW
	Total	19.1	-5.9	13.2	S	26.5	
C08	Mud	20.82	-6.60	14.22	S	18.52	MF +TA
	Sand1	-1.05	-0.83	-1.88	E	8.03	GC +FL
	Sand2	0.00	-0.01	-0.01	E	0.02	Wind+Wave/WNW
	Total	19.8	-7.4	12.3	S	26.6	
C09	Mud	20.08	-7.61	12.47	S	18.80	C04 without DDC
	Sand1	-0.87	-2.05	-2.93	E	7.80	
	Sand2	0.00	-0.01	-0.01	E	0.02	
	Total	19.2	-9.7	9.5	S	26.6	
C10	Mud	19.70	-3.77	15.93	S	18.74	C04+complete
	Sand1	-0.96	-2.69	-3.65	E	7.72	DDC
	Sand2	0.00	-0.01	-0.01	E	0.02	
	Total	18.7	-6.5	12.3	S	26.5	

'West' and 'East': the west and east control sections of the mouth bar area (see Fig.4.1); 'Xuliujing': cross section at Xuliujing for reference; 'Net': the net sediment fluxes for the mouth bar; 'ISE': initial sedimentation/erosion; '+ /-': positive/negative indicating the import/export sediment of the control area; MF: transport due to mean flow; TA: transport due to tidal asymmetry; (P.)GC: transport due to (part of) gravitational circulation; FL: flocculation of fine cohesive sediment; wind speed: 7m/s.

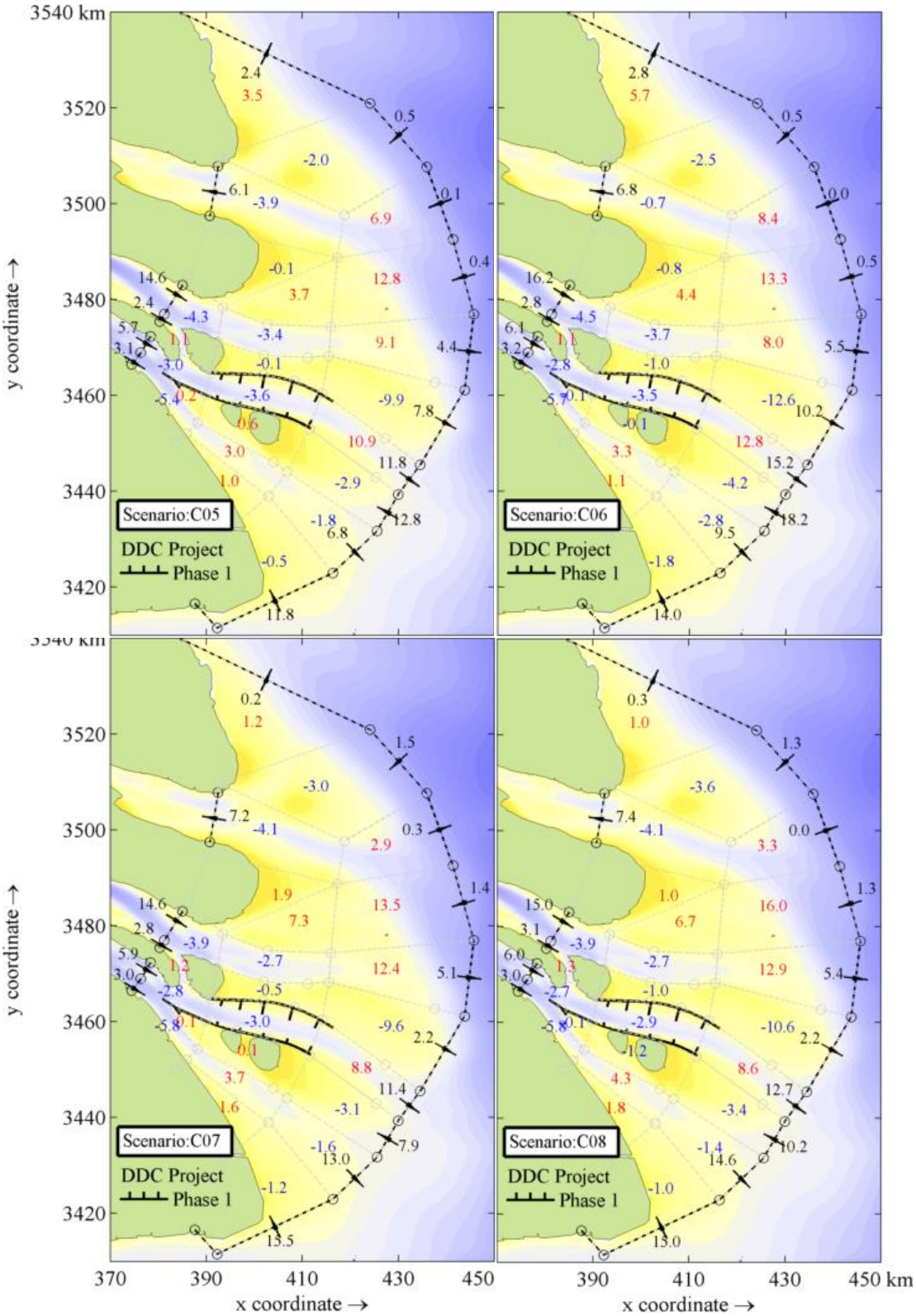

Fig.4.7 Sediment fluxes (arrows in unit of million tons) through cross-sections over 15 days with mouth bar (Black numbers: fluxes; Red: deposition in polygons; Blue: erosion in polygons; Top left: C05=C04+Wind/ESE; Top right: C06= C04+Wind+Wave/ESE; Bottom left: C07=C04+Wind/WNW; Bottom right: C0=C04+Wind+Wave/WNW)

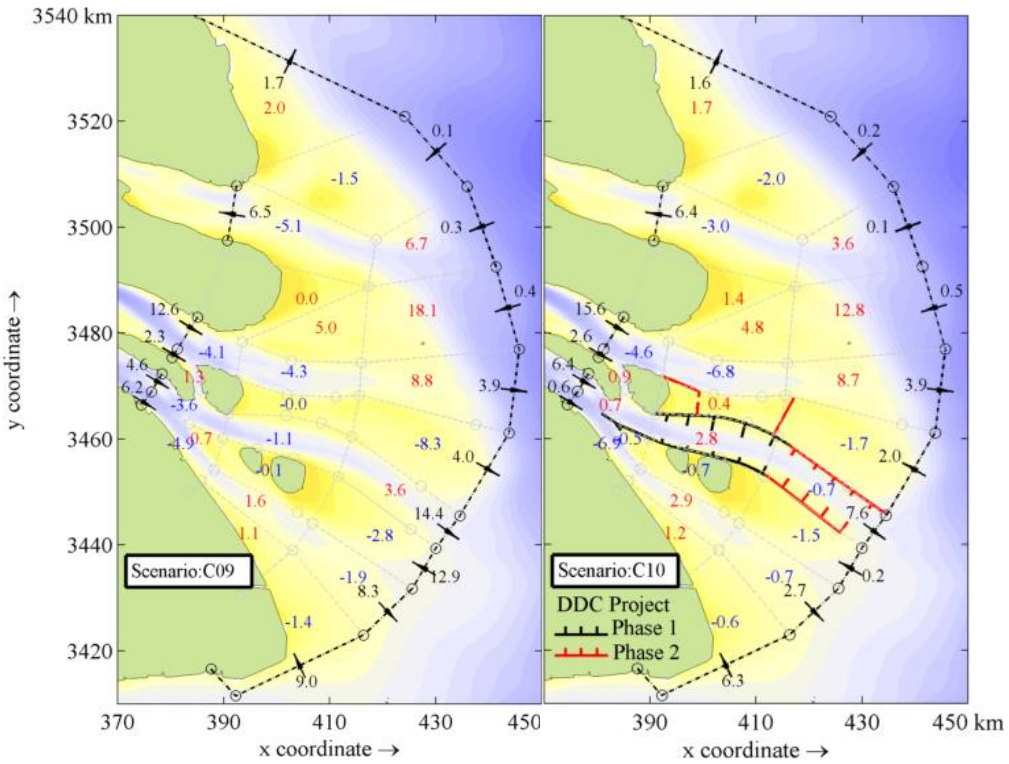

Fig.4.8 Sediment fluxes (arrows in unit of million tons) through cross-sections over 15 days with mouth bar (Black numbers: fluxes; Red: deposition in polygons; Blue: erosion in polygons; Left: C09=C04 without structures of the DDC project; Right: C10=C04+complete structures of the DDC Project)

4.4 Conclusion and Remarks

The process-based ISE-model of the Yangtze Estuary is applied to study the sediment transport patterns caused by various combinations of processes/mechanisms around the mouth bar area. In order to investigate the influence of mouth bar on the sediment transport, an idealized bathymetry without the mouth bar is applied in an additional series of simulations. Three sediment fractions are used in the model. A river discharge of 30,000 m^3/s is used, which is slightly larger than the long-term mean value of 28,400 m^3/s. A mean suspended sediment concentration of 0.5 kg/m^3 is used to represent the sediment input from the river. The sediment budget of the mouth bar area is obtained from the difference between the incoming and outgoing sediment fluxes through two control sections.

The following conclusions can be drawn:

1. The amount of sediment trapped in the mouth bar area varies largely with the river discharge. In general, a higher river discharge gives more deposition in the mouth bar area, leading to a net sedimentation in the wet season and a net erosion in the dry season, with net deposition annually. A decreasing trend in the annual net deposition has recently become visible. The deposition rate at present is down to 1/3 of the magnitude in the past.

2. River discharge and tides are the primary drivers of the water motion in the estuary. Mean flow and tidal asymmetry cause sediment transport, but their combination alone will not lead to the formation of a mouth bar, or rather sedimentation in the mouth bar area.
3. The sediment transport due to the gravitational circulation (obtained by including salinity processes in the model) is a necessary condition for the sediment trapped in the mouth bar area. This means that salinity and its inducing density currents are a prerequisite for mouth bar formation in the Yangtze Estuary.
4. Flocculation of fine cohesive sediment will enhance deposition in the mouth bar area.
5. Wind and waves may influence the sediment flux through the control sections, without changing the overall characteristics of the sediment budget. They will enhance the sediment trapped in the mouth bar area by less than 6-23%.
6. The DDC structures in different phases would not change the feature of sediment trapped in the mouth bar area. The influence of no structures or full structures included in the model on the sediment budget in the mouth bar area is less than 15% in comparison with case C04.

The above conclusions are based on a process-based ISE model applied over a spring-neap tidal cycle and with a mean river discharge. Clearly, this approach has its limitations. Computation time, however, restricts the possibility of fully three-dimensional simulations over a sufficiently long period (e.g. seasons, years or decades). This is also one of the reasons to use an ISE-model instead of a medium-term morphodynamic model. Logically, an ISE-model does not describe the morphological evolution of the mouth bar.

The observed river discharge and SSC are used to represent upstream boundary conditions to calculate the sediment flux under different scenarios. The tidal condition is represented by the full spring-neap tidal cycle with a series of tidal components, instead of the simplified tidal conditions. The selection of such tidal condition is based on the result of analytical expression of long-term net sediment transport in estuaries (Chapter 5).

By considering mean conditions, the effects of extreme events (floods, droughts, storms) is not included. The same goes for other processes, such as biological ones, which can contribute to the sediment transport in the mouth bar area. Also, the assumption of a well-mixed bed composition differs from the real situation. Finally, the schematization of the bathymetry without the mouth bar introduces a mismatch between bathymetry and external forces. Given the fair agreement with observations, these influences are likely to be small with respect to the dominant processes and therefore the conclusions are not expected to change essentially if these effects are taken into account.

5. Analysis on Residual Coarse Sediment Transport in Estuaries[3]

5.1 Introduction

Natural morphological development is the result of a dynamic interaction between water motion, sediment transport and bed topography. In most estuarine environments tide is the most important forcing factor and residual sediment transport determines morphological development. Therefore, mechanisms and processes influencing residual sediment transport play a key role in development and understanding of how an estuary responds to changing natural forces and human interference.

Tidal asymmetry is one of important factors influencing residual sediment transport, hence morphological development in estuaries and tidal basins (Aubrey, 1986; Dronkers, 1986). In last few decades a large number of investigations have been carried out on tidal asymmetry and its effect on these phenomena. Boon and Byrne (1981), Speer and Aubrey (1985), Friedrichs and Aubrey (1988, 1994), Dronkers (1986), Van der Spek (1997) and Lanzoni and Seminara (1998, 2002) investigate influence of basin morphology on asymmetry of vertical and horizontal tides. They conclude that shallow basins with little tidal flats tend to be flood-dominant, whereas basins with deep channels and much inter-tidal storage area tend to be ebb-dominant. The contribution of tidal asymmetry to residual transport has been investigated for fine sediment (Postma, 1967; Groen, 1967; Dronkers 1986, Ridderinkhof, 1997; Schuttelaas and De Swart, 2000) and for coarse sediment (Aubrey, 1986; Van de Kreeke and Robaczewska, 1993; Van de Kreeke and Dunsbergen, 2000; Elias, 2006). Aubrey (1986) connects morphology and tidal asymmetry by the net sediment transport due to the tidal asymmetry, i.e. for coarse sediment there is a net import due to flood-dominance and for fine sediment ebb-dominance yields a net export. Ranasinghe and Pattiaratchi (2000) and Woodworth et al. (2005) investigate the tidal asymmetry in diurnal tidal regions. Guo et al. (2014) study the role of river discharge and tidal asymmetry on morphodynamic in the Yangtze Estuary based on a 1D model. Song et al. (2011) propose a general formula to calculate tidal sediment transport.

Van de Kreeke and Robaczewska (1993) derive an analytical expression for residual coarse sediment transport. They conclude that tidally residual coarse sediment transport is only determined by interactions of M_0 & M_2, M_4 & M_2 and triad interaction of M_2, M_4 & M_6. Based on the result of a hydrodynamic model of the Ems Estuary they find that in order to produce the net sediment transport it does not make a significant difference whether the model is driven by M_0, M_2, M_4 and M_6 only, or by the full tidal signal. Therefore they claim that a periodic boundary condition based on constituents of M_0, M_2, M_4 and M_6 will be sufficient to drive practical morphodynamic models. Note that this conclusion pertains to transport of coarse sediment by astronomical tide, and that M_0 refers to the residual current, which is much smaller than the dominant M_2 tidal

[3] This chapter is based on the journal paper published in *Estuarine Coastal & Shelf Science*: Ao Chu, Zhengbing Wang and H.J. de Vreind (2015), Analysis on residual coarse sediment transport in estuaries, Estuarine Coastal & Shelf Science, 163, 194-205, http://dx.doi.org/10.1016/j.ecss.2015.06.003.

current. The approximate expression by Van de Kreeke and Robaczewska (1993) so far is applicable in situations with a relatively small residual current. In many estuarine environments, however, such as the Yangtze Estuary, the residual current is not only caused by tides but primarily by the river discharge. This means that the residual current cannot be assumed to be relatively small. Therefore, the present study considers the approximate expression by Van de Kreeke and Robaczewska (1993) in situations with and without a significant residual current. The approximate expression is re-derived with all higher-order terms included. The result is used to explain why the original expression underestimated residual sediment transport in cases with a significant residual current. The present analytical expression is furthermore used to check whether it is possible to determine the "representative tide" or "morphological tide" (De Vriend et al., 1993b; Latteux, 1995), i.e. the tide that produces the right net sediment transport.

5.2 Residual coarse sediment transport

5.2.1 The Van de Kreeke and Robaczewska (1993) approach

To determine the effect of tidal currents on transport of coarse sediment, first the transport rate is assumed to be a function of local depth-averaged velocity (Bagnold, 1966)

$$S \propto \|u\|^2 u \tag{5.1}$$

in which, S is sediment transport rate and u is local instantaneous current velocity. Coarse sediment here is defined as having a diameter such that $u_*/w<1$, where u_* is the shear velocity and w is the fall velocity (Van de Kreeke and Robaczewska 1993).

Assuming the tidal current velocity to be dominated by M_2 tidal constituent, the collinear current velocity signal ***u(t)*** considered by van de Kreeke and Robaczewska (1993) can be written as:

$$u(t) = u_{M0} + u_{M2}\cos(\omega_{M2}t) + \sum_i^N u_i \cos(\omega_i t - \varphi_i) \tag{5.2}$$

in which:

u_{M0} = Eulerian residual flow

u_{M2} = amplitude of M_2 tidal current constituent

u_i = amplitude of the other tidal current constituents

ω_{M2} = angular frequency of M_2

ω_i = angular frequency of the other tidal constituents

φ_i = phase of tidal constituent ***i*** relative to M_2

N = number of the other tidal constituents

Normalizing the expression for ***u(t)*** by the amplitude of M_2 results in

$$\frac{U(t)}{u_{M2}} = \varepsilon_{M0} + \cos\omega_{M2}t + \sum_i^N \varepsilon_i \cos(\omega_i t - \varphi_i) \quad (5.3)$$

where

$$\varepsilon_{M0} = \frac{u_{M0}}{u_{M2}}\ ,\ \varepsilon_i = \frac{u_i}{u_{M2}}$$

Therefore, the dimensionless residual coarse sediment transport can be expressed in the following

$$\frac{<S>}{fu_{M2}^3} = < [\varepsilon_{M0} + \cos\omega_{M2}t + \sum_i^N \varepsilon_i \cos(\omega_i t - \varphi_i)]^3 > \quad (5.4)$$

in which f is the coefficient and the angle brackets stand for the tidal averaging

$$< > = \frac{1}{T}\int_{t1-\frac{T}{2}}^{t1+\frac{T}{2}} dt \quad (5.5)$$

in which T is the period of M_2.

Pingree and Griffith (1979), Aubrey (1986) and Fry and Aubrey (1990) discuss the net bed-load transport and focus on the residual (tidally averaged) sediment transport as a result of tidal asymmetry caused by interaction of M_2 and M_4. Van de Kreeke & Robaczewska (1993) derive an analytical expression for residual bed load transport contributed by interactions of all tidal constituents considered, including the residual current. In their study firstly constituents M_0, M_2, M_4, M_6 and S_2 are used to represent the tidal current. By introducing $\omega_{S2}=\omega_{M2}+\Delta\sigma$ the velocity expression is

$$\frac{u(t)}{u_{M2}} = \varepsilon_{M0} + \cos(\omega_{M2}t) + \varepsilon_{M4}\cos(2\omega_{M2}t - \beta) + \varepsilon_{M6}\cos(3\omega_{M2}t - \gamma) + \varepsilon_{S2}\cos[(\omega_{M2} + \Delta\sigma)t - \alpha] \quad (5.6)$$

in which

ε_{M4} = $\frac{u_{M4}}{u_{M2}}$

ε_{M6} = $\frac{u_{M6}}{u_{M2}}$

ε_{S2} = $\frac{u_{S2}}{u_{M2}}$

α = the phase of S_2 relative to M_2

β = the phase of M_4 relative to M_2

γ = the phase of M_6 relative to M_2

$\Delta\sigma$ is the beat frequency of M_2 and S_2. Using Eq. (5.4) and substituting Eq. (5.6) for ***u(t)*** yields the following expression for the dimensionless residual coarse sediment transport.

$$\frac{<S>}{fu_{M2}^3} = < [\varepsilon_{M0} + \cos(\omega_{M2}t) + \varepsilon_{M4}\cos(2\omega_{M2}t - \beta) + \varepsilon_{M6}\cos(3\omega_{M2}t - \gamma) + \varepsilon_{s2}\cos((\omega_{M2} + \Delta\sigma)t - \alpha)]^3 > \quad (5.7)$$

When integrating over one M_2 tidal period, the variation of the sediment flux due to the beat frequency can be approximated as constant in time, for example,

$$\frac{\varepsilon_i}{T}\int_{t_1-\frac{T}{2}}^{t_1+\frac{T}{2}} \cos(\Delta\sigma t)F\,dt \approx \cos(\Delta\sigma t_1)\frac{\varepsilon_i}{T}\int_{t_1-\frac{T}{2}}^{t_1+\frac{T}{2}} F dt \quad (5.8)$$

in which, F is the arbitrary cosine function of M_2 angle frequency and $\Delta\sigma$ is the beat frequency of M_2 and other constituent.

Van de Kreeke & Robaczewska (1993) point out that when neglecting terms of $O(\varepsilon^3)$ the residual coarse sediment transport can be written as

$$\begin{aligned}
\frac{<S>}{fu_{M2}^3} = \quad & \frac{3}{2}\varepsilon_{M0} && M_0, M_2 \\
& + \frac{3}{4}\varepsilon_{M4}\cos(\beta) && M_4, M_2 \\
& + \frac{3}{2}\varepsilon_{M4}\varepsilon_{M6}\cos(\beta - \gamma) && M_4, M_6, M_2 \\
& + \frac{3}{2}\varepsilon_{M4}\varepsilon_{s2}\cos(\Delta\sigma t + \beta - \alpha) && M_4, S_2, M_2 \\
& + 3\varepsilon_{M0}\varepsilon_{s2}\cos(\Delta\sigma t - \alpha) && M_0, S_2, M_2
\end{aligned} \quad (5.9)$$

In this equation, each term is the result of interactions of two or more tidal constituents, as indicated to the right. The interactions of M_2 & M_0, M_2 & M_4 and triad interactions of M_2, M_4 and M_6 lead to a constant residual sediment flux. Interactions involving S_2 cause a sediment flux varying in time with the beat frequency $\Delta\sigma$ corresponding to a period of about 14.8 days. Van de Kreeke and Robaczewska (1993) also consider tidal constituents M_0, M_2, S_2, N_2, M_4, MS_4, M_6 and K_1 to represent the current. They conclude that, in addition to the terms at the right hand side of Eq.(5.9), interactions (M_2, MS_4) and (M_2, K_1) and triad interactions (M_2, M_0, N_2), (M_2, M_4, N_2), (M_2, M_6, MS_4), (M_2, S_2, MS_4) and (M_2, N_2, MS_4) contribute to the sediment flux. However, each of these fluxes fluctuates with its corresponding beat frequency and therefore does not contribute to the residual sediment transport. Consequently, the residual (a few months) coarse sediment flux is given by the first three terms in Eq. (5.9),

$$\begin{aligned}
\frac{<S>}{fu_{M2}^3} = \quad & \frac{3}{2}\varepsilon_{M0} && M_0, M_2 \\
& + \frac{3}{4}\varepsilon_{M4}\cos(\beta) && M_4, M_2 \\
& + \frac{3}{2}\varepsilon_{M4}\varepsilon_{M6}\cos(\beta - \gamma) && M_4, M_6, M_2
\end{aligned} \quad (5.10)$$

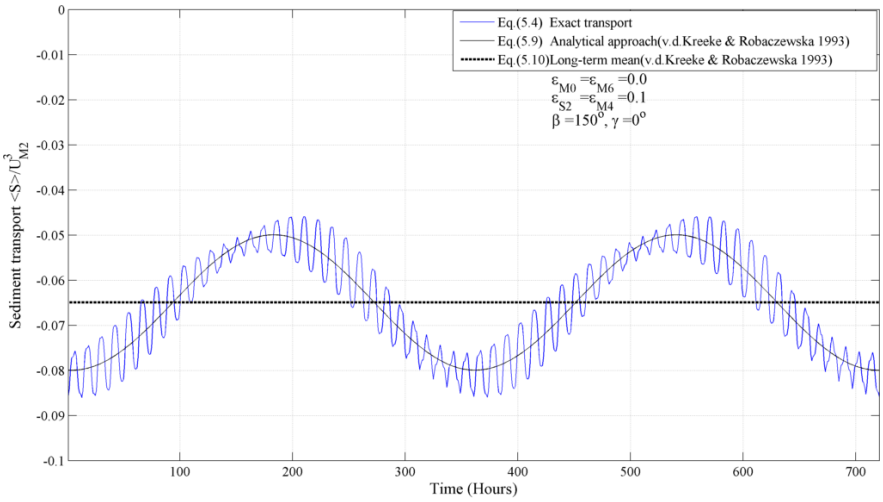

Fig.5.1 Comparison of numerically and analytically calculated residual sediment transport according to Van de Kreeke and Robaczewska (1993), with ε_{M0}=0.0.

Figure 5.1 shows the transport rates based on Eq. (5.4), (5.9) and (5.10), respectively. The residual current (M_0) is assumed to be zero, which is approximately true for the Dutch estuaries (Van de Kreeke & Robaczewska, 1993). This explains why in this case the analytical solution agrees rather well with the numerical one. Thus, the residual coarse sediment transport flux can be approximated by Eq. (5.10).

This conclusion, however, is not valid for situations with a significant residual current. The transport rate under the same conditions as shown in Figure 5.1, but now with a non-zero residual current, is calculated numerically using Eq. (5.4). Figure 5.2 compares the result with the analytical solution Eq. (5.9). Clearly, the result of the analytical expression (Eq.5.9) is smaller than the median of numerical calculation over entire computational period. Apparently, Eq. (5.9) does not include all relevant interactions with M_0. In the following sections we will investigate which interactions these are.

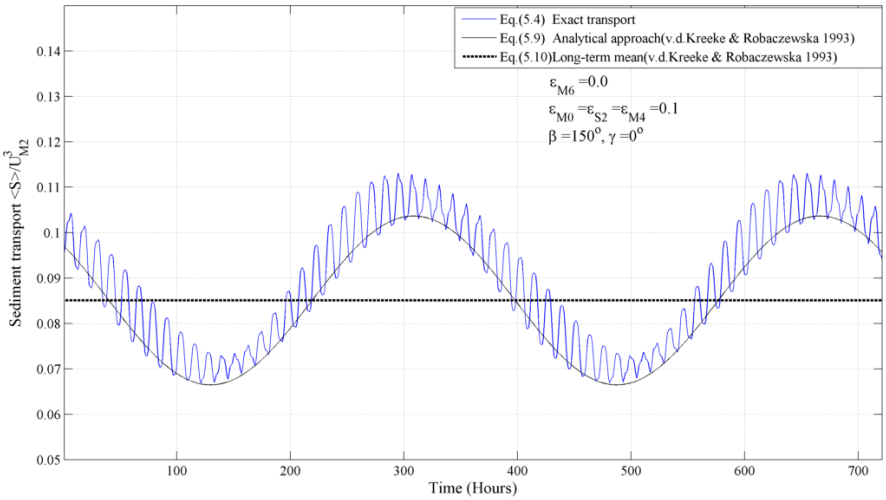

Fig.5.2 Comparison of numerically and analytically calculated residual sediment transport with ε_{M0}=0.1 (approach of Van de Kreeke and Robaczewska, 1993)

5.2.2 Present approach

In order to find an analytical solution for coarse sediment transport in estuaries with a significant M_0, the derivation proposed by Van de Kreeke & Robaczewska (1993) is repeated without ignoring M_0. In addition, the compound tidal constituent MN_4 and the principle lunar tide O_1 are also included. Table 5.1 lists the set of tidal current constituents used to approximate the tidal current.

Table 5.1 Tidal constituents set for velocity approximation

Constituent	Amplitude		Angular frequency	Phase
	Original	u_i/u_{M2}		
M_0	u_0	ε_{M0}	-	-
M_2	u_{M2}	1	σ	ϕ_{M2}
S_2	u_{S2}	ε_{s2}	$\sigma+\Delta\sigma_1$	$\alpha_1= \phi_{M2}- \phi_{S2}$
N_2	u_{N2}	ε_{N2}	$\sigma-\Delta\sigma_2$	$\alpha_2= \phi_{M2}- \phi_{N2}$
M_4	u_{M4}	ε_{M4}	2σ	$\beta= 2\phi_{M2}- \phi_{M4}$
MS_4	u_{S2}	ε_{MS4}	$2\sigma+\Delta\sigma_1$	$\alpha_3= \phi_{M2+} \phi_{S2}- \phi_{MS4}$
MN_4	u_{MN2}	ε_{MN4}	$2\sigma-\Delta\sigma_2$	$\alpha_4= \phi_{M2+} \phi_{N2}- \phi_{MN4}$
M_6	u_{M6}	ε_{M6}	3σ	$\gamma= 3\phi_{M2}- \phi_{M6}$
K_1	u_{K1}	ε_{k1}	$\sigma/2+\Delta\sigma_3$	$\alpha_5= \phi_{M2}/2- \phi_{K1}$
O_1	u_{O1}	ε_{O1}	$\sigma/2- \Delta\sigma_3$	$\alpha_6= \phi_{M2}/2- \phi_{O1}$

By maintaining terms of $O(\varepsilon^3)$, the analytical expression for residual coarse sediment flux becomes

$$\frac{< S >}{f u_{M_2}^3} =$$

$$
\begin{aligned}
& 3/2\ \varepsilon_{M0} && M_0, M_2 \\
& + 3/4\ \varepsilon_{M4} \cos(\beta) && M_4, M_2 \\
& + 3/4\ \varepsilon_{M4}\ \varepsilon_{M6} \cos(\beta - \gamma) && M_4, M_6, M_2 \\
& + 3/2\ \varepsilon_{S2}\ \varepsilon_{MS4} \cos(\alpha_1 - \alpha_3) && S_2, MS_4, M_2 \\
& + 3/2\ \varepsilon_{N2}\ \varepsilon_{MN4} \cos(\alpha_2 - \alpha_4) && N_2, MN_4, M_2 \\
& + 3/2\ \varepsilon_{K1}\ \varepsilon_{O1} \cos(\alpha_5 + \alpha_6) && K_1, O_1, M_2 \\
& + \varepsilon_{M0}^3 && M_0 \\
& + 3/2\ \varepsilon_{M0}\ \varepsilon_{S2}^2 && M_0, S_2 \\
& + 3/2\ \varepsilon_{M0}\ \varepsilon_{N2}^2 && M_0, N_2 \\
& + 3/2\ \varepsilon_{M0}\ \varepsilon_{M4}^2 && M_0, M_4 \\
& + 3/2\ \varepsilon_{M0}\ \varepsilon_{MS4}^2 && M_0, MS_4 \\
& + 3/2\ \varepsilon_{M0}\ \varepsilon_{MN4}^2 && M_0, MN_4 \\
& + 3/2\ \varepsilon_{M0}\ \varepsilon_{M6}^2 && M_0, M_6 \\
& + 3/2\ \varepsilon_{M0}\ \varepsilon_{K1}^2 && M_0, K_1 \\
& + 3/2\ \varepsilon_{M0}\ \varepsilon_{O1}^2 && M_0, O_1 \\
& + 3/4\ \varepsilon_{MS4} \cos(\alpha_3 - \sigma_1 t) && MS_4, M_2 \\
& + 3/4\ \varepsilon_{MN4} \cos(\alpha_4 + \sigma_2 t) && MN_4, M_2
\end{aligned}
$$

$+ 3\ \varepsilon_{M0}\ \varepsilon_{S2} \cos(\alpha_1 - \sigma_1 t)$ — S_2, M_0, M_2

$+ 3/2\ \varepsilon_{M4}\ \varepsilon_{S2} \cos(\alpha_1 - \beta - \sigma_1 t)$ — S_2, M_4, M_2

$+ 3/2\ \varepsilon_{MN4}\ \varepsilon_{S2} \cos(\alpha_1 - \alpha_4 - \sigma_1 t - \sigma_2 t)$ — S_2, MN_4, M_2

$+ 3\ \varepsilon_{M0}\ \varepsilon_{N2} \cos(\alpha_2 + \sigma_2 t)$ — N_2, M_0, M_2

$+ 3/2\ \varepsilon_{M4}\ \varepsilon_{N2} \cos(\alpha_2 - \beta + \sigma_2 t)$ — N_2, M_4, M_2

$+ 3/2\ \varepsilon_{N2}\ \varepsilon_{MS4} \cos(\alpha_2 - \alpha_3 + \sigma_1 t + \sigma_2 t)$ — N_2, MS_4, M_2

$+ 3/2\ \varepsilon_{M6}\ \varepsilon_{MS4} \cos(\alpha_3 - \gamma - \sigma_1 t)$ — M_6, MS_4, M_2

$+ 3/2\ \varepsilon_{M6}\ \varepsilon_{MN4} \cos(\alpha_4 - \gamma + \sigma_2 t)$ — M_6, MN_4, M_2

$+ 3/4\ \varepsilon_{K1}^2 \cos(2\alpha_5 - 2\sigma_3 t)$ — K_1, M_2

$+ 3/4\ \varepsilon_{O1}^2 \cos(2\alpha_6 + 2\sigma_3 t)$ — O_1, M_2

$+ 3\varepsilon_{M0}\ \varepsilon_{N2}\ \varepsilon_{S2} \cos(\alpha_1 - \alpha_2 - \sigma_1 t - \sigma_2 t)$ — M_0, S_2, N_2

$+ 3\ \varepsilon_{M0}\ \varepsilon_{M4}\ \varepsilon_{MS4} \cos(\alpha_3 - \beta - \sigma_1 t)$ — M_0, M_4, MS_4

$+ 3\ \varepsilon_{M0}\ \varepsilon_{M4}\ \varepsilon_{MN4} \cos(\alpha_4 - \beta + \sigma_2 t)$ — M_0, M_4, MN_4

$+ 3\ \varepsilon_{M0}\ \varepsilon_{MN4}\ \varepsilon_{MS4} \cos(\alpha_3 - \alpha_4 - \sigma_1 t - \sigma_2 t)$ — M_0, MS_4, MN_4

$+ 3\ \varepsilon_{M0}\ \varepsilon_{K1}\ \varepsilon_{O1} \cos(\alpha_5 - \alpha_6 - 2\sigma_3 t)$ — M_0, K_1, O_1

$+ 3/2\ \varepsilon_{M4}\ \varepsilon_{N2}\ \varepsilon_{S2} \cos(\alpha_1 + \alpha_2 - \beta - \sigma_1 t + \sigma_2 t)$ — S_2, N_2, M_4

$+ 3/2\ \varepsilon_{N2}\ \varepsilon_{S2}\ \varepsilon_{MS4} \cos(\alpha_1 + \alpha_2 - \alpha_3 + \sigma_2 t)$ — S_2, N_2, MS_4

$+ 3/2\ \varepsilon_{N2}\ \varepsilon_{MN4}\ \varepsilon_{S2} \cos(\alpha_1 + \alpha_2 - \alpha_4 - \sigma_1 t)$ — S_2, N_2, MN_4

$+ 3/2\ \varepsilon_{M4}\ \varepsilon_{M6}\ \varepsilon_{S2} \cos(\alpha_1 + \beta - \gamma - \sigma_1 t)$ — S_2, M_4, M_6

$+ 3/2\ \varepsilon_{M6}\ \varepsilon_{S2}\ \varepsilon_{MS4} \cos(\alpha_1 + \alpha_3 - \gamma - 2\sigma_1 t)$ — S_2, MS_4, M_6

$+ 3/2\ \varepsilon_{M6}\ \varepsilon_{MN4}\ \varepsilon_{S2} \cos(\alpha_1 + \alpha_4 - \gamma - \sigma_1 t + \sigma_2 t)$ — S_2, MN_4, M_6

$+ 3/4\ \varepsilon_{K1}^2\ \varepsilon_{S2} \cos(\alpha_1 - 2\alpha_5 - \sigma_1 t + 2\sigma_3 t)$ — S_2, K_1

$+ 3/2\ \varepsilon_{M4}\ \varepsilon_{M6}\ \varepsilon_{N2} \cos(\alpha_2 + \beta - \gamma + \sigma_2 t)$ — N_2, M_4, M_6

$+ 3/2\ \varepsilon_{M6}\ \varepsilon_{N2}\ \varepsilon_{MS4} \cos(\alpha_2 + \alpha_3 - \gamma - \sigma_1 t + \sigma_2 t)$ — N_2, MS_4, M_6

$+ 3/2\ \varepsilon_{M6}\ \varepsilon_{N2}\ \varepsilon_{MN4} \cos(\alpha_2 + \alpha_4 - \gamma + 2\sigma_2 t)$ — N_2, MN_4, M_6

$+ 3/4\ \varepsilon_{K1}^2\ \varepsilon_{N2} \cos(\alpha_2 - 2\alpha_5 + \sigma_2 t + 2\sigma_3 t)$ — N_2, K_1

$+ 3/4\ \varepsilon_{M4}\ \varepsilon_{S2}^2 \cos(2\alpha_1 - \beta - 2\sigma_1 t)$ — M_4, S_2

$+ 3/4\ \varepsilon_{M4}\ \varepsilon_{N2}^2 \cos(2\alpha_2 - \beta + 2\sigma_2 t)$ — M_4, N_2

$+ 3/4\ \varepsilon_{S2}^2\ \varepsilon_{MS4} \cos(2\alpha_1 - \alpha_3 - \sigma_1 t)$ — MS_4, S_2

$+ 3/4\ \varepsilon_{N2}^2\ \varepsilon_{MS4} \cos(2\alpha_2 - \alpha_3 + \sigma_1 t + 2\sigma_2 t)$ — MS_4, N_2

$+ 3/4\ \varepsilon_{MN4}\ \varepsilon_{S2}^2 \cos(2\alpha_1 - \alpha_4 - 2\sigma_1 t - \sigma_2 t)$ — MN_4, S_2

$+ 3/4\ \varepsilon_{N2}^2\ \varepsilon_{MN4} \cos(2\alpha_2 - \alpha_4 + \sigma_2 t)$ — MN_4, N_2

$+ 3/4\ \varepsilon_{O1}^2\ \varepsilon_{S2} \cos(\alpha_1 - 2\alpha_6 - \sigma_1 t - 2\sigma_3 t)$ — S_2, O_1

$+ 3/4\ \varepsilon_{N2}\ \varepsilon_{O1}^2 \cos(\alpha_2 - 2\alpha_6 + \sigma_2 t - 2\sigma_3 t)$ — N_2, O_1

$+ 3/2\ \varepsilon_{K1}\ \varepsilon_{O1}\ \varepsilon_{S2} \cos(\alpha_1 - \alpha_5 - \alpha_6 - \sigma_1 t)$ — K_1, O_1, S_2

$+ 3/2\ \varepsilon_{K1}\ \varepsilon_{N2}\ \varepsilon_{O1} \cos(\alpha_2 - \alpha_5 - \alpha_6 + \sigma_2 t)$ — K_1, O_1, N_2

(5.11)

As compared with Eq. (5.9), Eq. (5.11) contains many more terms, due to the inclusion of more constituents and third-order interactions. For the same situation as in Figure 5.2, i.e. ε_{M0}, ε_{S2} & ε_{M4} equal to 0.1 and ε_{M6}=0, the sediment flux is calculated with both approximations. They are compared with the numerical result in Figure 5.3. Clearly, the result of Eq. (5.11) agrees best with the numerical calculation result. In another word, the present approach is applicable for assessment of residual coarse sediment transport with residual current accounted.

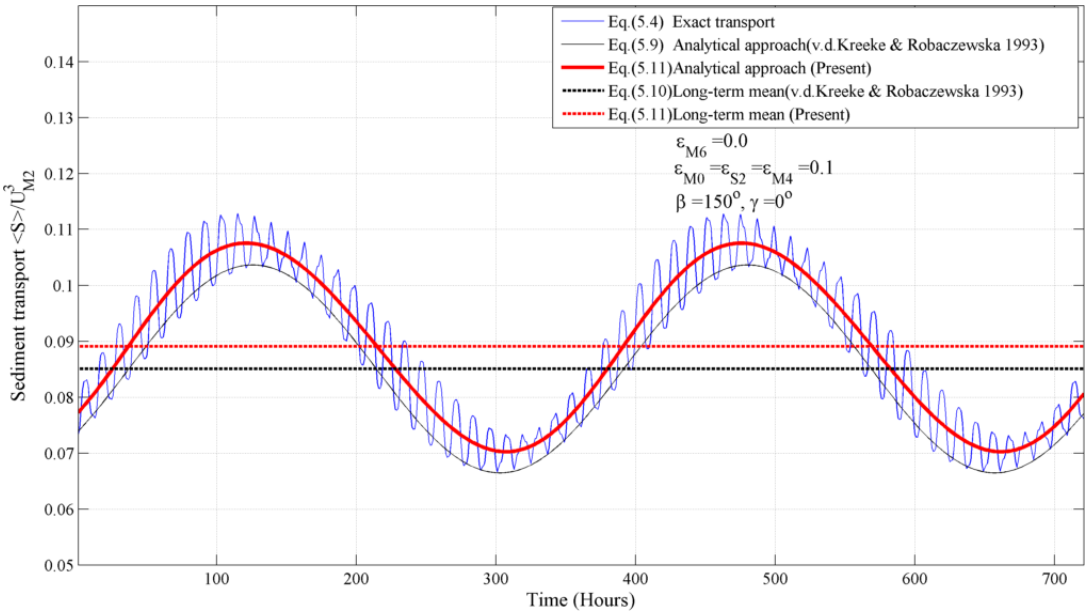

Fig.5.3 Comparison of numerically and analytically computed residual sediment flux with ε_0=0.1 (present approach and approach of Van de Kreeke and Robaczewska, 1993)

In Eq. (5.11) interactions of tidal constituents contributing to the coarse sediment transport can be distinguished into two groups: one has a net contribution to residual sediment flux and the other is fluctuation in time without contributing to residual flux.

Interactions with a net contribution

In addition to interactions of M_0 & M_2, M_2 & M_4 and triad interaction of M_2, M_4 & M_6, interaction of M_0 with any tidal current constituent, triad interactions of M_2, S_2 & MS_4 and M_2, N_2 & MN_4 also contribute to residual net sediment flux. Although the contribution of the latter interactions is of second order, they can be relative important depending on the phase angle of the compound constituent MS_4 (MN_4) relative to the phase angle of summation of M_2 and S_2 (N_2). Furthermore, the triad interaction of K_1, O_1 and M_2 has a net contribution, the importance of which depends on the phase angle of summation of K_1 and O_1 relative to M_2 phase.

Interactions leading to a time-fluctuating effect

Interactions of MS_4 & M_2 and MN_4 & M_2 yield the leading-order fluctuating terms, with beat frequencies of $\Delta\sigma_1$ and $\Delta\sigma_2$, respectively. These frequencies correspond to

periods of 14.8 and 27.6 days. All other interactions of tidal current constituents resulting in fluctuation of sediment flux in time are shown in Table 5.2 with their corresponding beat frequencies. As these interactions have no contribution to residual sediment flux, this net flux can be approximated by the first 15 terms in Eq. (5.11).

Table 5.2 Beat frequencies and interaction of tidal constituents

Beat frequency	Interaction of tidal current constituents
$\Delta\sigma_1$	$MS_4(M_2)$,S_2 (M_0,M_2; M_4,M_2;N_2,MN_4;M_4,M_6;MS_4),MS_4(M_6,M_2;M_0,M_4)
$\Delta\sigma_2$	$MN_4(M_2)$, N_2 (M_0,M_2; M_4,M_2;S_2,MS_4;M_4,M_6;MN_4), MN_4(M_6,M_2;M_0,M_4)
$2\Delta\sigma_3$	$K_1(M_2)$, $O_1(M_2)$, (M_0,K_1,O_1)
$\Delta\sigma_1+\Delta\sigma_2$	(S_2,MN_4;N_2,MS_4)M_2,(S_2,N_2;MS_4,MN_4)M_0
$\Delta\sigma_1-\Delta\sigma_2$	(S_2,N_2)M_4, (S_2,MN_4;N_2,MS_4)M_6
$2\Delta\sigma_1$	S_2(MS_4,M_6;M_4)
$2\Delta\sigma_2$	N_2(MN_4,M_6;M_4)
$2\Delta\sigma_1+\Delta\sigma_2$	$MN_4(S_2)$
$2\Delta\sigma_2+\Delta\sigma_1$	$MS_4(N_2)$
$\Delta\sigma_1-2\Delta\sigma_3$	$S_2(K_1)$
$\Delta\sigma_2+2\Delta\sigma_3$	$N_2(K_1)$
$\Delta\sigma_1+2\Delta\sigma_3$	S_2, O_1
$\Delta\sigma_2-2\Delta\sigma_3$	N_2, O_1

5.3 Application to the Yangtze Estuary

5.3.1 General condition of the Yangtze Estuary

Morphodynamic studies of estuaries usually require elaborate numerical sediment transport models. It is often cost-prohibitive to run such models for long enough periods of time to cover a wide range of real-life conditions. Instead, a periodic "representative tide" is often used and the residual sediment transport computed for this tide is taken as representative of the long term mean transport. For example, Gelfenbaum et al. (2003) select a morphological tide of 1.084 times of M_2 constituent at the offshore boundary in their study of the Grays harbour estuary. Lesser (2009) proposes an improved representative tide, which includes the residual effect of the triad interaction of O_1, K_1 and M_2. He uses an artificial diurnal tidal constituent C_1 to replace O_1 and K_1. This enables him to use a simple repeating double (24h50m28s) tide consisting of only M_2 and C_1 constituents. As we have shown above, however, many more tidal constituents will contribute to the long term mean when they interact with the M_0, and also the triad interaction of M_2, S_2 (N_2) and MS_4 (MN_4) will do so. As a consequence, a single morphological tide as normally used may not exist, especially in estuarine cases. Therefore, the method described by Latteux (1995) is used to establish plural morphological tides for different locations in the Yangtze Estuary.

The Yangtze Estuary is located halfway China's coastline (Figure 5.4). It has ample water and sediment supply from upstream and obvious tidal influence, creating an

estuary characterized by three major bifurcations and four outlets, with well-developed shoals, alternating channels, expanding sandbars and a vast submerged delta. The spatial-temporal dynamics of river runoff and tidal current dominate the morphological processes of the Yangtze Estuary.

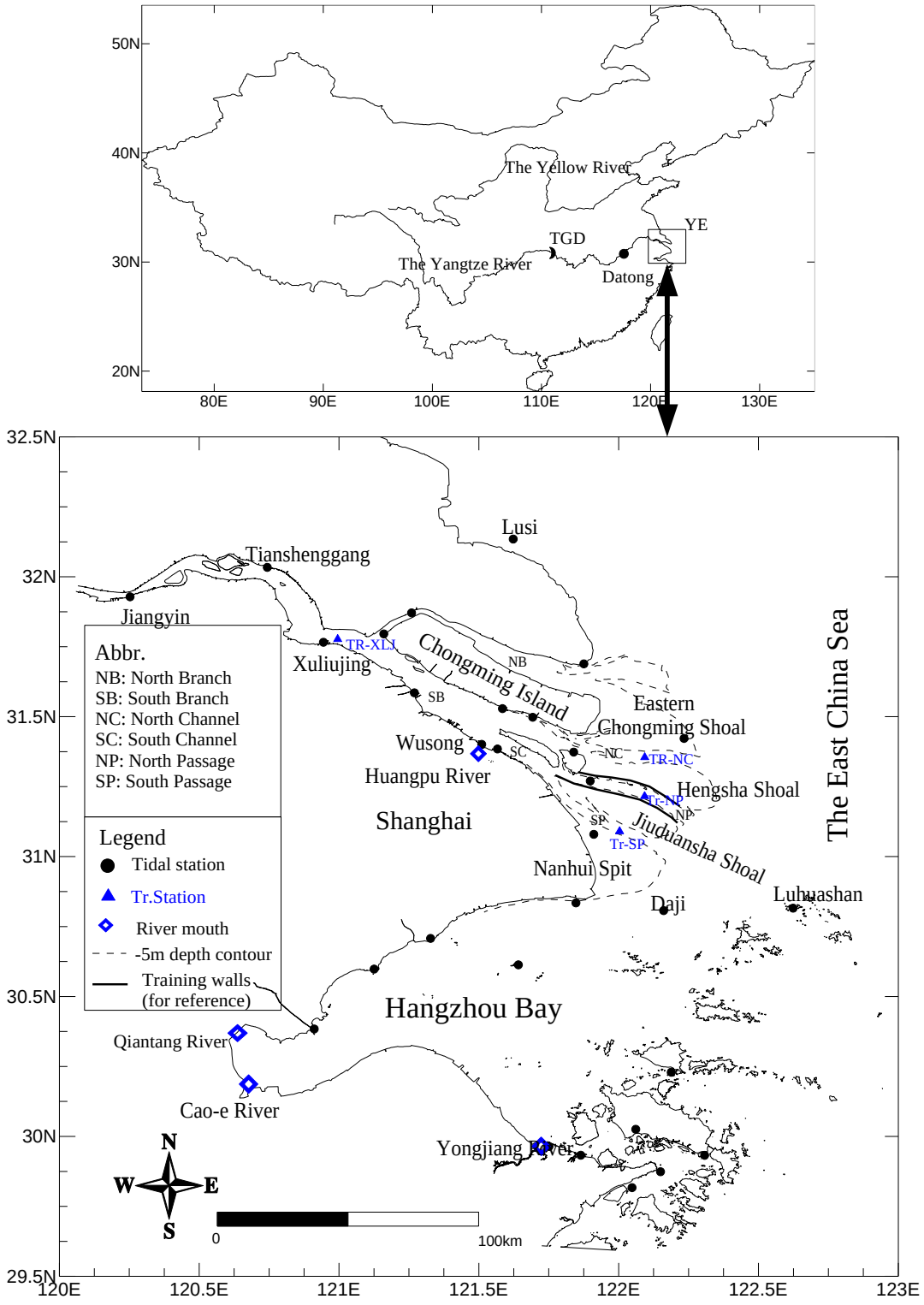

Fig.5.4. Study area and layout of the Yangtze Estuary

The part of the estuary of interest in this study is from the mouth to upstream, with its alternating shoals and channels. The bottom sediment in this area varies from clay to coarse sediment (Yun, 2004; Liu et al., 2009). Yun (2004) also analyzes the sediment samples collected from the bed along the main stream of the Yangtze Estuary in 1965 (May and June) and 1992 (May). He finds that the sediment in the area from Hengsha to upstream is coarser than that in downstream. The d_{50} is larger than 100μm in the area from Hengsha to upstream. From Hengsha to downstream the d_{50} is smaller than 30μm except the high hydrodynamics area, for example the North Channel. It has been concluded that suspended sediment acts as wash load in the upper part of the estuary and is hardly involved in bed level change until it reaches the mouth of the estuary. This indicates that the coarse sediment (bed-load) transport plays important role in the upper part of the estuary. The tide in the East China Sea off the estuary is semi-diurnal. The amplitude of M_2-constituent near the mouth is about 1.2 m. Maximum current velocities in the channels are between 1.5 and 2.5 m/s. The long-term average discharge from upstream is about 28400m^3/s with maximum of 92,600m^3/s and minimum of 4,620 m^3/s (Chu et al., 2013 Dai et al., 2014). The residual current caused by river discharge is about 0.3-0.5 m/s in the main channels around the mouth (Chen, 1998). The mixing of fresh water and saline water in the study area varies with alternating of river runoff and tidal current and results in a complex distribution of stratified, partially-mixed and well-mixed salinity patterns in the study area.

5.3.2 Process-based model of the Yangtze Estuary

The tidal current constituents in the Yangtze Estuary have been computed with a 2DH process-based model for the Yangtze Estuary (Chu et al., 2009, 2010). The model covers the entire tidal region of the Yangtze Estuary, the Hangzhou Bay and a large part of the adjacent East China Sea (see Figure 5.5 for grid). The upstream boundary is located at Datong, the tidal limit of the river, with the measured discharge as a boundary condition. At the open sea boundary, the water level according to the astronomic tidal constituents (M_2, S_2, N_2, K_2, K_1, O_1, P_1 and M_4) is imposed (for further detail referring Chu et al., 2009, 2010). The model results of the hydrodynamic model for the Yangtze Estuary are used in this study.

The model has been calibrated and validated against measurements of water levels and currents during spring and neap tides in dry and wet seasons (Chu et al., 2010). The computed amplitudes and phases of the tidal water level constituents (M_2, S_2, N_2, K_2, K_1, O_1, P_1 and M_4) were found to agree well with observations.

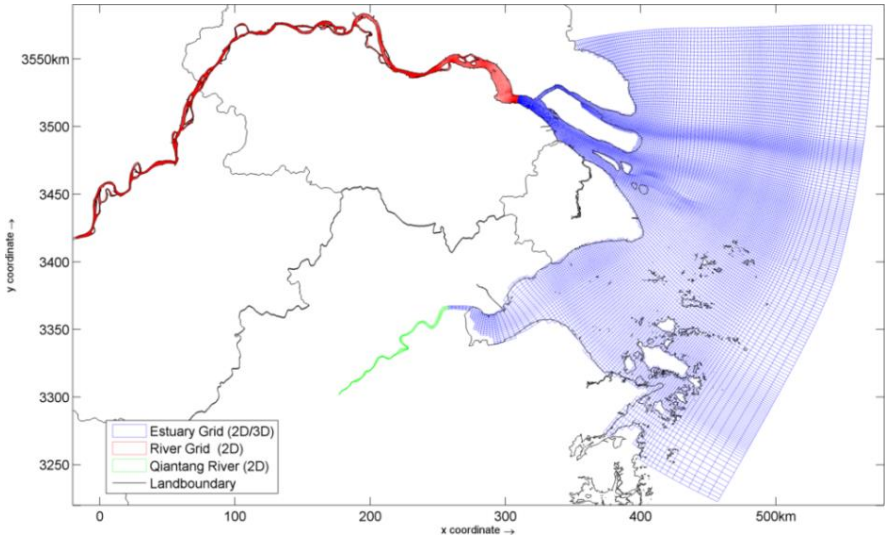

Fig.5.5 Grids of the Yangtze Estuary model (Red grid: Datong to Xuliujing; Blue grid: Xuliujing to Sea; Green grid: Lucipu to Haining)

5.3.3 Tidal current constituents

The tidal currents are computed with the model for two periods, February and August 2004. There are a few of observation data available in these two periods to verify the model performance. The discharges in these two months were about 19,300 and 41,100 m^3/s, which were 1/3 less and more than the long-term average discharge, representing the dry and wet seasons. Each case run starts one month before the desired period in order to get rid of start-up effects and the influence of the initial condition. In order to obtain the proper initial distribution of salinity in the model domain, the model is first used to simulate two years with the long term monthly-averaged river discharge from upstream. The hydrodynamics as well as the distributions of salinity under different discharges in the latter year can be used as the initial condition for the simulation starting with comparable discharges. It has been verified that this spin-up period is sufficient long to obtain the near-equilibrium state of the salinity distribution, independent on the initial condition (Chu et al., 2009).

Model results of duration more than 6 moths can be sufficient to precisely resolve all constituents considered. However, the residual current in such case the average of river discharge in this period, which cannot be regarded as representative for dry or wet seasons. Thus, the amplitudes and phases of tidal current constituents M_0, M_2, S_2, N_2, M_4, MS_4, MN_4 and K_1 are determined from the hydrodynamic model results of 30 days. Figure 5.6 shows the residual current field in dry and wet seasons, respectively. Clearly, there is a significant difference in M_0 in the main channels around the mouth bar. The amplitudes and phases of M_2, S_2, N_2, M_4, MS_4, MN_4 and K_1 in the dry season differ little from those in the wet season. The tidal ellipses of tidal current constituents M_2 and M_4 are shown in Figure 5.7. In general, three regions can be identified according to the principle directions of M_2 and M_4. At the mouth area, due to the occurrence of shoals, the principle directions of M_2 and M_4 in the channels are parallel to the orientations of the channels, having the character of revising tidal flow. At the shallow area of this

region, the ellipse reveals a rotation tidal current. In the seaward region, it is purely rotational current with the principle direction undistinguished. And in the upstream region, the principle directions are clearly determined by the orientation of the river. These features agree well with the description in the literature (Chen, 1998).

Table 5.3 lists the amplitudes and phases of tidal current constituents along the principal axis of M_2 tidal current constituent at four selected stations, viz. Tr-XLJ, Tr-NC, Tr-NP and Tr-SP (see Figure 5.4). Station Tr-XLJ is located in the middle of the Xuliujing cross-section and can be regarded as representative of the upper part of the estuary. The other three stations represent the middle parts of the North Channel, the North Passage and the South Passage, respectively. As expected, M_2 tidal current, with a magnitude of about 1m/s, is the strongest. S_2 current is about the half as strong. The magnitude of the residual current varies with the upstream discharge, i.e. large in the wet season and small in the dry season. The magnitude of M_0 around Xuliujing varies between 0.25 to 0.90 m/s. The residual currents in the middle of the outlets are in the range of 0.05 to 0.5 m/s. Obviously, the residual current is so strong that its contribution to the sediment transport cannot be ignored. The currents associated with the other tidal constituents, such as S_2, N_2, M_4, MS_4 and K_1, are smaller, but still relatively important, with magnitudes of 15-50% of the M_2 tide.

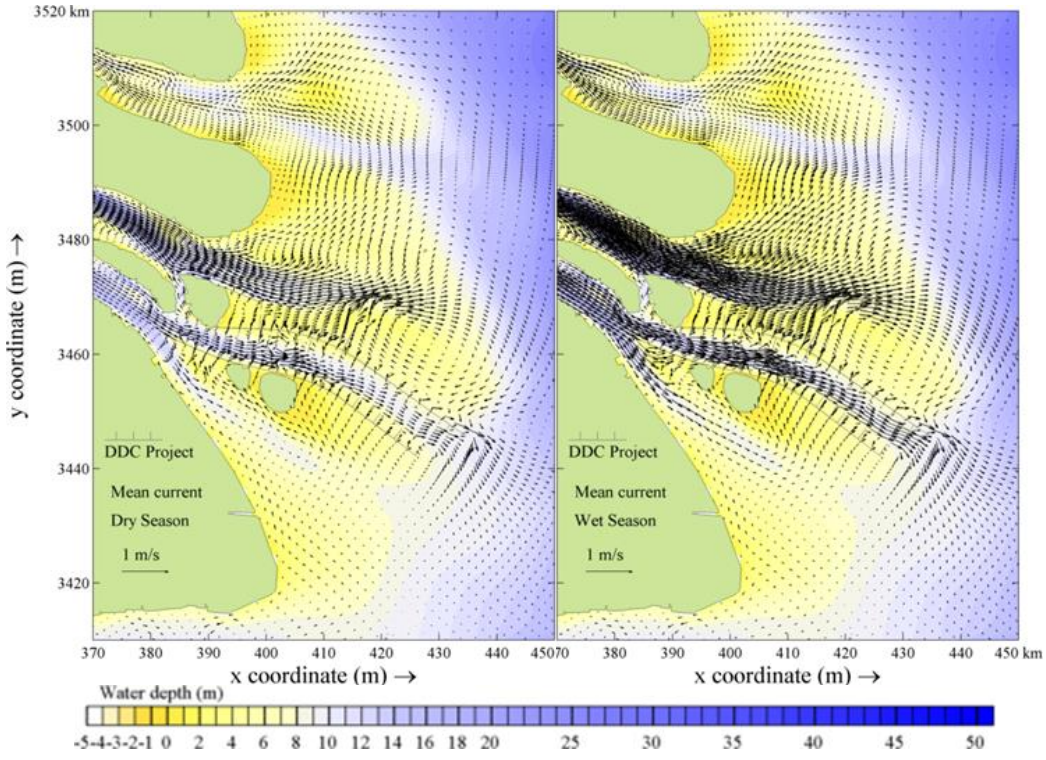

Fig.5.6 Residual current in Yangtze Estuary in a dry (Feb. 2004, left) and a wet (Aug. 2004, right) season, respectively (DDC: Deep Draft Channel project)

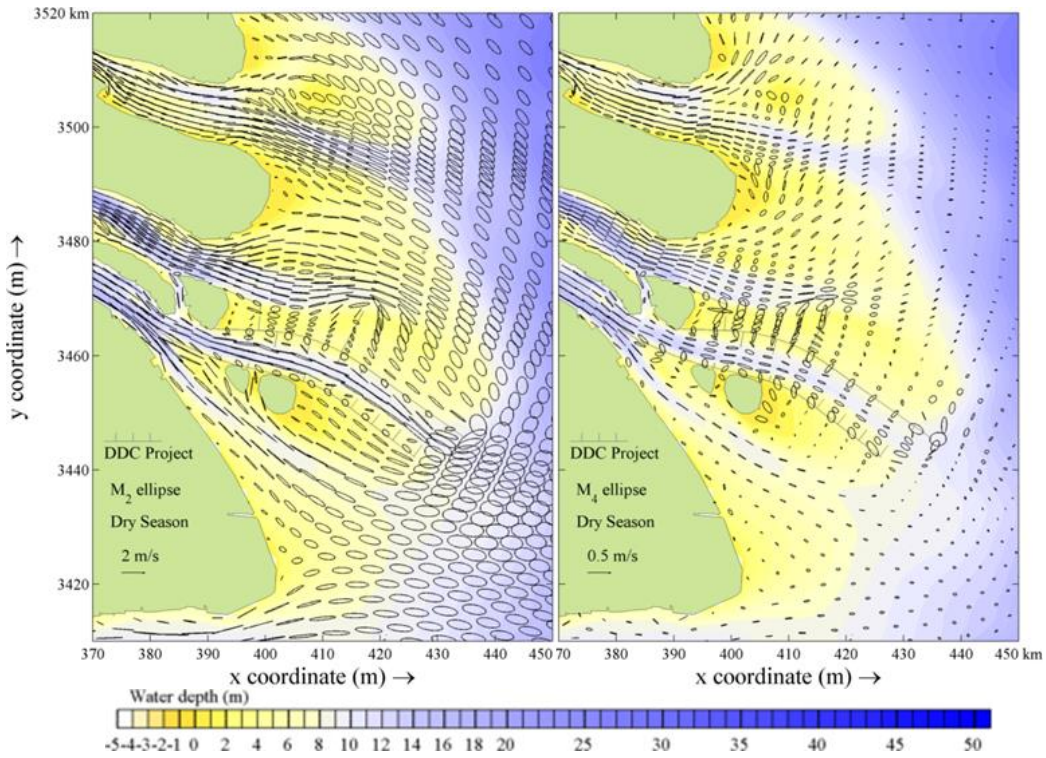

Fig.5.7 Tidal ellipses of M_2 (left) and M_4 (right) around the mouth bar of the Yangtze Estuary dry season (Feb. 2004)

Table 5.3 Amplitude (m/s) and phase difference (º) of tidal current constituents relative to M_2 at stations along the principal axis of M_2 in the Yangtze Estuary

Station	Constituents	M_0^*	M_0^{**}	M_2	$S_2(\alpha_1)$	$N_2(\alpha_2)$	$M_4(\beta)$	$MS_4(\alpha_3)$	$MN_4(\alpha_4)$	$M_6(\gamma)$	$K_1(\alpha_5)$
Tr-XLJ	Amplitude	0.25	0.88	1.10	0.53	0.24	0.31	0.31	0.14	0.06	0.21
	Phase	-	-	-	205	209	290	220	116	7	77
Tr-NC	Amplitude	0.35	0.52	1.14	0.63	0.31	0.23	0.23	0.13	0.04	0.17
	Phase	-	-	-	229	231	300	238	111	22	101
Tr-NP	Amplitude	0.13	0.29	1.03	0.55	0.26	0.09	0.11	0.05	0.03	0.17
	Phase	-	-	-	240	277	294	256	162	12	67
Tr-SP	Amplitude	0.06	0.11	1.05	0.58	0.27	0.11	0.14	0.05	0.03	0.14
	Phase	-	-	-	256	302	293	279	146	13	67

M_0^*: residual current in dry season; M_0^{**}: residual current in wet season.

5.3.4 Residual coarse sediment transport and representative tide

Based on the tidal current constituents listed in Table 5.3, the approximate residual coarse sediment transport in the upper part and in the middle of the main outlets of the estuary can be calculated from Eq. (5.11). Figure 5.8 shows the resulting 15-day residual transport rates at each station, together with the tidal currents in dry and wet seasons. It shows that the results of the analytical approach Eq. (5.11) agree well with the numerical computations Eq. (5.4) at these stations. Therefore, the residual transport can be approximated by Eq. (5.11).

A 15-day tidal record can be divided into 360 overlapping tidal cycles, each starting at a different hour. For each of these cycles the residual transport can be calculated. The cycle producing the same net transport rate as the long term computation can be taken as 'representative' of the whole period. These representative cycles are shown for each location in Figure 5.8.

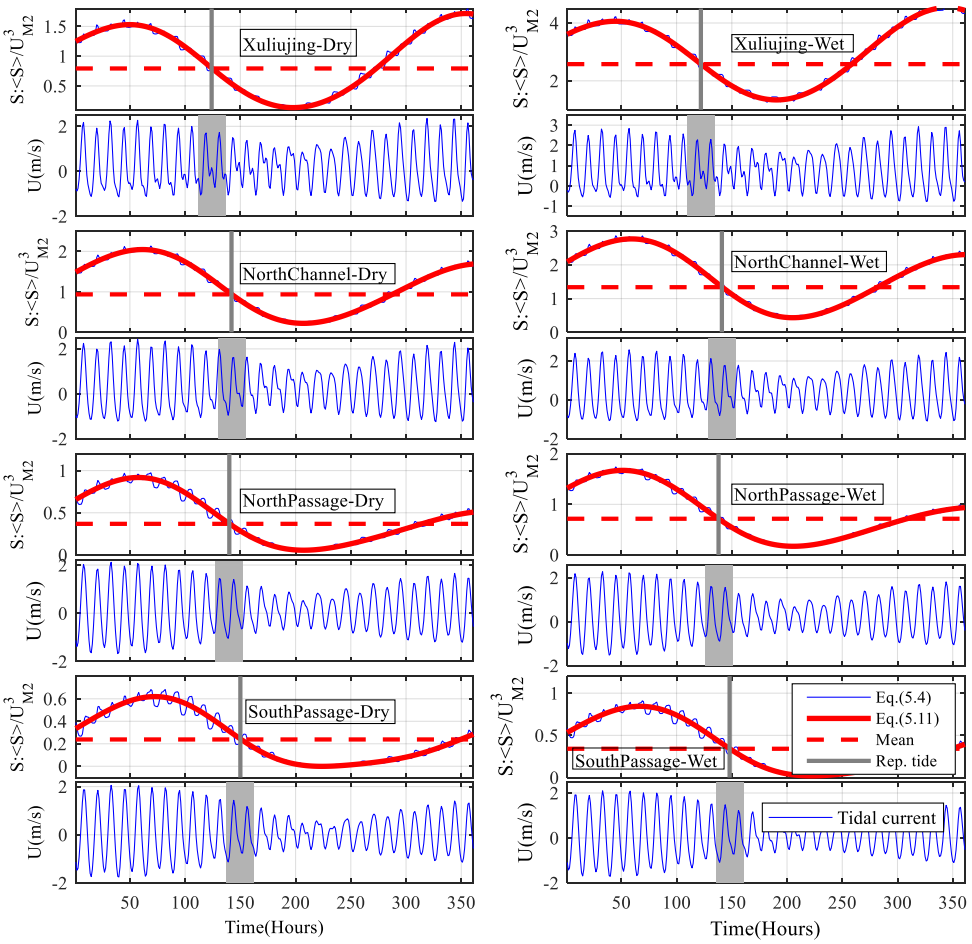

Fig.5.8 Approximated residual coarse sediment transport and tidal current at stations in the Yangtze Estuary in dry (left) season and wet (right) seasons (shadow indicates the tide producing the same sediment transport as the residual)

Table 5.4 shows the cycle number of the representative tide at each station. Apparently, the representative tide is not the same at every station, nor in every season. This means that a single tide cannot produce the residual sediment transport at every point in the model domain, let alone the right morphological evolution. It confirms the hypothesis that a single 'representative tide' to drive morphodynamic models of the Yangtze Estuary does not exist.

Table 5.4 Representative tide number (Hour) at each station in the Yangtze estuary

Seasons	Xuliujing	North Channel	North Passage	South Passage
Dry	124	142	140	150
Wet	122	141	138	148

5.4. Discussion

5.4.1 Choice of sediment transport formulations

In our analysis the sediment transport rate is assumed to be proportional to the third power (n=3) of the local instantaneous flow velocity. The quantitative description of sediment transport is still largely empirical (e.g. van Rijn, 1986, 2007). There is a variety of transport formulas and models, each with its own strong points and weaknesses. Van de Kreeke and Robaczewska (1993) point out those expressions with a different value of n have the same general form of the residual transport equation. They present the expression for n=5 and find that the residual current becomes relatively more important to the residual sediment transport. Meanwhile, in reality sediment transport can be influenced by many other factors (e.g. threshold of sediment motion, concentration gradient) the effects of which are worth investigating. In the case of suspended sediment transport several other mechanisms may yield a residual transport, even if the coarse-sediment residual is zero. The relaxation effect of the suspended sediment concentration is such a mechanism (Groen, 1967; Wang et al., 1999). Nevertheless, the present study gives the insight into the fundamental mechanism of coarse sediment transport in estuaries with a significant river discharge. The general conclusions from the analysis are valid independent of the sediment transport formula, even though the expression of residual transport rate does depend on the sediment transport formula. We also believe that at the scale of the Yangtze Estuary the conclusions apply even when suspended load is important and the sediment transport rate no longer depends exclusively on the local instantaneous flow velocity.

5.4.2 Character of the tide

In this study we discussed the residual coarse sediment transport by an M_2-dominated collinear tide. The triad interaction of M_2, K_1 and O_1 also contributes to the residual transport, due to the fact that the sum of the frequencies of O_1 and K_1 is exactly equal to that of M_2. The contribution of this triad interaction of M_2, K_1 and O_1 has been given by Lesser (2009), as well as in the present study, assuming the sediment transport rate to be proportional to U^3. Hoitink et al. (2003) point out that this interaction can be more important than the interaction of M_2 and M_4 if $2O_1K_1 > M_2M_4$. In the Yangtze Estuary the M_2 tide dominates and the triad interaction is negligible, as $2O_1K_1$ is much smaller than M2M4. In practice, the characteristics of the tide can largely influence the residual sediment transport. The importance of triad interaction (O_1, K_1, M_2) should be stressed because this triad interaction is different from others in terms of astronomical tidal constituents involved.

5.4.3 Tidal constituents as drivers of a morphodynamic model

The conclusion that a single representative tide to drive morphodynamic models does not exist has been verified for the Yangtze Estuary. In cases with a negligible river discharge, however, a representative tide consisting of M_0, M_2, M_4 and M_6 may still be

applicable. For small-scale models a representative tide may be determined following the procedure as applied above, but for large area models of estuaries with a significant river discharge the full set of tidal constituents is required. The importance of a tidal constituent is determined by its amplitude, which means that all significant constituents should be taken into account because of their interaction with M_0.

5.5 Conclusions

In this study a new analytical expression for residual coarse sediment transport is derived for M_2-dominated estuaries with a significant river discharge. Simplifying assumptions are the collinear tide current and a third-power relationship between the sediment transport rate and the local instantaneous flow velocity. The present approach is one step beyond the study of Van de Kreeke & Robaczewska (1993), as it takes into account the interaction between M_0 and the tidal constituents M_2, S_2, N_2, M_4, MS_4, MN_4, M_6, K_1 and O_1.

The interactions of M_2 & M_0, M_2 & M_4 and the triad interaction of M_2, M_4 & M_6 are known to yield a long term residual coarse sediment flux (Van de Kreeke & Robaczewska, 1993). The present analytical solution reveals that other interactions of tidal current constituents also contribute to the residual sediment flux, especially the interactions of all tidal constituents with M_0 and the triad interactions of (M_2, S_2 & MS_4), (M_2, N_2 & MN_4) and (M_2, K_1 & O_1).

The underestimation by the Van de Kreeke & Robaczewska (1993) model of the sediment flux in case of a significant residual current is due to the ignoring these interactions. The present analytical approach agrees well with numerical results with all constituents included.

This shows that a cyclic tide only with M_2 and its overtides is insufficient to drive practical morphodynamic models, except in cases without a significant net current. All relatively important tidal constituents should be taken into account in the tidal boundary condition of a morphodynamic model. When applying the present analytical approach to the sediment transport in the main channels of the Yangtze Estuary, a single representative tide producing the right transport field is shown not to exist. In other words, there is no single representative tide to drive morphodynamic models of this and similar estuaries.

6. Morphodynamic Modelling for the Yangtze Estuary – A Mor-Merge Approach with Multi-Discharge Levels[4]

6.1 Introduction

A fundamental problem in process-based morphological modelling in coastal and estuarine regions is that morphological evolution usually occurs at time scales several orders of magnitude larger than the time scale of hydrodynamically sediment transport. De Vriend et al. (1993b) discuss the potential of the separation of scales and distinguish three approaches to accelerating long-term morphodynamic modelling: input reduction, model reduction, and behavior-oriented modelling.

Approaches for model reduction are outlined by De Vriend et al. (1993a), Cayocca (2001), and Roelvink (2006), among others. These approaches propose increasing the effectiveness of morphological model acceleration by extrapolating the bed level change calculated for one tidal cycle to several tidal cycles before recalculating current, wave, and sediment transport fields. They introduce the "continuity correction" method, which can approximately update the flow fields without full hydrodynamic computation by assuming that the flow rate and flow pattern remain the same if the bed level change hardly alters the channel characteristics. After a few correction steps, the full hydrodynamics need to be recomputed with the updated bathymetry. Roelvink (2006) proposes the Rapid Assessment of Morphology (RAM) method, assuming the overall transport pattern to be invariant to small bed level changes. Later, Lesser (2009) presented the "online" method which computes sediment transport and morphological change simultaneously with hydrodynamic processes and combines the resulting bed level changes with a morphological acceleration factor (**MorFac**). The MorFac is a device used to assist in dealing with the difference in time-scales between hydrodynamic and morphological developments. It works by multiplying the sediment fluxes to and from the bed by a constant factor at hydrodynamic step, thereby effectively extending the morphological time step

These approaches for model reduction are designed for simulations over time spans much longer than those of individual storms and tidal cycles. Because it is practically impossible to run such long-term simulations with real-time boundary conditions, the reduction of model input is required. Such reduction techniques have been proposed by De Vriend et al. (1993b) and Latteux (1995). One or more morphologically representative tides are commonly used to represent tidal forcing. Similarly, wave forcing is reduced to representative wave conditions. Ideally, the representative input conditions (tide or wave) should produce the same residual sediment transport and morphological change patterns as the naturally varying forces in the entire study area

[4] This chapter is based on papers: "Parallel Morphodynamic Modelling for the Yangtze Estuary", published in Journal of Coastal Research by Ao Chu, Zhengbing Wang, H.J. de Vriend and J. Tai, 2018, DOI: 10.2112/SI85-129.1, and "Morphodynamic Modelling for the Yangtze Estuary – A Mor-Merge Approach with Multi-Discharge Levels", submitted to Estuarine Coastal & Shelf Science, by Ao Chu, Zhengbing Wang and H.J. de Vreind, (under review).

during the complete simulation period.

Commonly used input reduction techniques are summarized as follows.

Tide input reduction

The method proposed by Latteux (1995), Cayocca (2001), and Grunnet et al. (2004) is commonly used to select a "morphological tide". Based on this method, a transport computation over a complete tidal cycle (e.g. a spring-neap cycle) is first carried out for a number of representative points within the model area. Then an individual tidal cycle (e.g. 24 h 50 min) with the mean sediment transport pattern closest to the mean transport pattern of the full simulation is selected from these computations. An adjustment factor may be applied to match the sediment transport rate of an individual tide to that of the complete cycle. Based on this approach, Lesser (2009) claims that in the case of a semi-diurnal tide, an M_2 tide with 7–20% larger amplitude can be considered as the morphological tide. Lesser (2009) also suggests adding the artificial diurnal component (C_1) to take two diurnal components (K_1 and O_1) into account if the diurnal components are important in the morphological simulation. Dastgheib (2012) determines the morphological tide based on M_2, M_4, M_6, K_1, and O_1 for the Wadden Sea model.

An alternative approach to tidal input reduction is the "ensemble technique" (Bernades et al., 2006). First, the time series (17 days or 6 months) of tidal levels (the full tidal signal) is divided into a number of discrete classes by tidal range. Individual tides within each class are then averaged, yielding the "mean tide" of each tidal range class. Subsequently, the mean tides are assembled into a "consecutive tide", a time series of mean tides in ascending order of tidal range. Finally, a simulation is carried out using this "consecutive tide" with sediment transport and morphological changes updated during the simulation. The result at the end of this simulation is assumed to be the same as the result for the same time period of real tidal variation. A scaling factor, conceptually similar to the MorFac, can be applied to each mean tide in order to accelerate the simulation.

Wave (wind) input reduction

The reasoning behind selecting a representative wave condition is similar to that for selecting a representative tide, namely that the action of a limited set of wave conditions can produce the same mean sediment transport pattern as the full wave "climate". Steijn (1992) proposes a point-oriented method to determine wave conditions for each selected main wave direction sector. First, the nearshore wave climates at a number of selected points in the area of interest are determined by using a simple one-dimensional wave propagation model. Then the nearshore wave conditions are averaged across various main wave direction sectors for each selected point by using certain weighting factors. These factors reflect the relationship between sediment transport and wave characteristics (usually the wave height). These nearshore wave conditions are then further transformed to deep water wave conditions. Finally, the offshore wave conditions are compared and representative offshore wave conditions are selected for

the wave propagation model. Presently there are three widely applied methods for wave input reduction in coastal morphodynamic models: (1) the potential sediment transport method (Lesser, 2009; Dastgheib, 2012) assumes the morphological impact of a wave to be proportional to $H_s^{2.5}$, as this exponent roughly corresponds with the CERC formula for longshore transport. The wave records are divided into wave height classes based on significant wave height (H_s) and direction bins based on peak wave direction (D_p). The representative wave for each cluster of conditions is determined based on the potential sediment transport due to waves within those selected wave conditions. (2) the wave energy flux method (Dobrochnski, 2009; Dastgheib, 2012) uses the wave energy equation (with the function of H_s^2). Then the numbers of directional bins and wave height classes are chosen. Limited directional bins are determined, each with the same sum of wave energy fluxes. The wave height classes in each directional bin are determined by applying the same principle as for the direction bin to content equal energy flux in each class. Therefore, the sum of the energy fluxes is equal for all clusters of waves. The representative wave height in each cluster can be calculated using the wave energy flux equation. (3) the optimal method (Lesser, 2009; Dastgheib, 2012) selects an optimum subset of wave conditions that contribute most significantly to bottom change or residual sediment transport by performing an "elimination race algorithm". A loop is performed to discard wave classes by dropping the conditions contributing the least to the residual sediment transport or erosion/sedimentation. The weight of the dropped condition is transferred to the most closely correlated remaining condition in subsequent calculations of the average. Such a loop is iterated many times and the randomly assigned weight factors that most effectively minimize the RMS error are adopted. Therefore, selecting the "optimum" set of wave classes is simply a matter of deciding the level of RMS error offering a reasonable trade-off between computational effort and accuracy as determined by the Opti set of classes and weights.

To schematize wind input to a morphodynamic model, two situations should be considered. If the wind is highly correlated to the wave condition, and the major transport is induced by wave, the wind can be schematized based on correlation with the offshore wave conditions (e.g. Lesser, 2009; Dastgheib, 2012). If the wind is one of the main forces responsible for sediment transport in the study area and poorly correlated to the wave conditions, a method similar to the selection of a representative wave should be applied.

River discharge input reduction

In addition to tide and wave, river discharge is also an important factor driving sediment transport and morphological changes in estuaries. The application of morphological models to estuaries with significant river input has rarely been reported. Little is known regarding methods for the input reduction of river forcing (discharge and sediment load). Van Vuren (2005) evaluates four different discharge synthetization methods (classic probability distribution, multivariate distribution, bootstrap resampling, and nearest-neighbor resampling) on their capability of reproducing the historical discharge statistics of the Rhine, based on 100 years of daily discharge measurements at the

Niederrhein. Different discharge series based on these four methods are used to drive a 1D morphological model of the River Rhine and the impact of river discharge uncertainty on the morphological prediction is analyzed. Resampling methods are recommended to analyze the stochasticity of a morphodynamic river system induced by discharge variability. Hu et al. (2009) use the 5-year mean value of the monthly mean discharge to compose a discharge time series for one representative year. A morphological factor of 5 is used to accelerate the morphological simulation. Kuang et al. (2013) use the similar method to form one representative year with average discharges of four different seasons, i.e. dry, dry to wet, wet and wet to dry seasons. Recently, Guo et al. (2015) tested three methods for schematizing the river discharge of the Yangtze Estuary with a 1D model: a representative constant discharge, a non-compressed hydrograph, and a compressed hydrograph. The compressed hydrograph is defined as to squeeze the yearly hydrograph (the reference) to a shorter period. They conclude that a morphologically representative discharge is a suitable choice for schematizing river discharge if discharge is relatively small in comparison to the mean tidal discharge or varies within a small range. A compressed hydrograph with a morphological acceleration factor corresponding to the compressing coefficient can be imposed on the 1D model, but the magnitude of compression or acceleration is restricted. A non-compressed hydrograph of discharge is suitable for 1D modelling of estuary morphological development, but in 2D situations it may induce bed level changes that are far too exaggerated.

To summarize, in most coastal environments, sediment transport is governed by tidal currents, often in combination with waves, wind, and/or river discharge. Morphodynamic models for cases with negligible river discharge have been well established and applied. However, in many estuaries (e.g. the Yangtze), river runoff is an important driver of sediment transport. Morphological models considering both tidal and riverine drivers have not been well documented, although there are some 1D tests (Guo et al., 2014, 2015, 2016). In this study, we establish a morphodynamic model for the Yangtze Estuary that accounts for the estuary's considerable riverine input. The main focus of the study is on input reduction for the combination of tide and river discharge. Statistical analysis of the river discharge is applied to schematize the river input, yielding a manageable series of discharge levels representing the real-time river input.

In the present research the numerical model of the Yangtze Estuary is established based on the Delft3D modelling suite, which is developed by Deltares (www.deltares.nl). Available since 1985, it has become open source in 2010. The advised minimum requirements of hardware for the software are a configuration consisting of 1.5GHz processor, 2GB memory and 10GB disk space. Delft3D is supported on both Microsoft Windows and Redhat/Linux platform. Multi-program languages are used to develop the software, such as Fortran, C++, Perl and Python. Since it is open-source software, Delft3D is free to download via oss.deltares.nl (size of the source code: 1 GB).

6.2 Input schematization for the Yangtze Estuary

6.2.1 General condition of the Yangtze Estuary

The Yangtze Estuary is located halfway up China's coastline (see Figure 6.1). It has ample water and sediment supply from upstream and obvious tidal influence, creating an estuary characterized by three major bifurcations and four outlets, with well-developed shoals, alternating channels, extensive sandbars, and a vast submerged delta. The spatial-temporal dynamics of river runoff and tidal current dominate the morphological processes of the Yangtze Estuary.

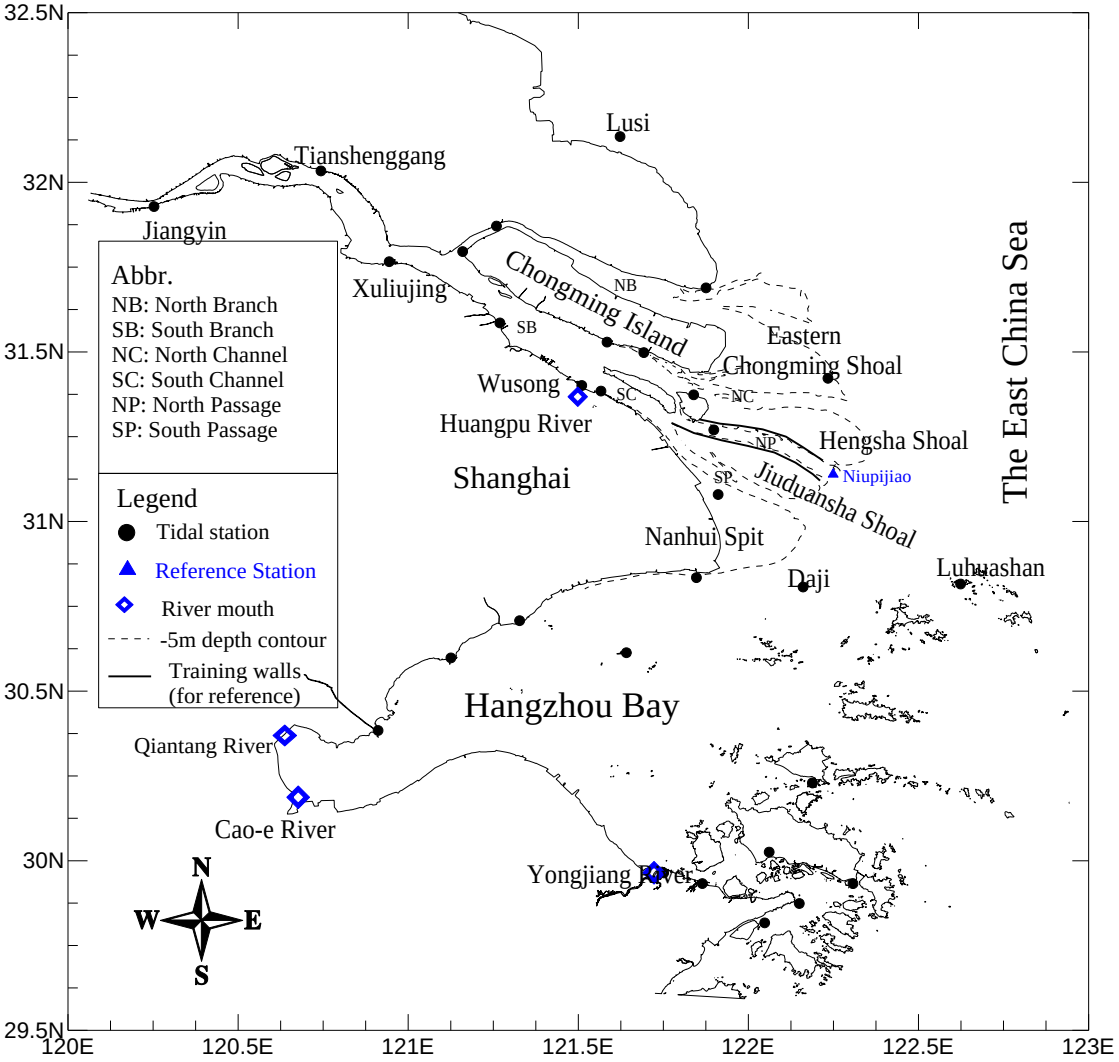

Fig.6.1 Study area and layout of the Yangtze Estuary

The part of the estuary considered in this study is at the river mouth, with its alternating shoals and channels. The sediment at the bed in this area varies from clay to coarse sediment (Yun, 2004; Liu et al., 2010). The tide in the East China Sea off the estuary is semi-diurnal. The amplitude of the M_2-constituent near the mouth is about 1.2 m. Maximum current velocities in the channels are between 1.5 and 2.5 m/s. The long-term average river discharge is about 28,400 m^3/s with a maximum of 92,600 m^3/s and

a minimum of 4,620 m^3/s (Chapter 2). The residual current caused by the river discharge is about 0.3 to 0.5 m/s in the main channels (Chen, 1998). Varying river discharge and tidal range in the study area result in a complex variation of the mixing patterns of fresh and saline water, forming stratified, partially-mixed and well-mixed salinity patterns.

6.2.2 Tide input reduction for the Yangtze Estuary model

Latteux (1995), Cayocca (2001), Grunnet et al. (2004), and Lesser (2009) use one or more representative 'morphological tides' to study coastal morphological changes in areas with negligible river discharge. In most estuaries, however, the river discharge is an essential element that cannot be ignored. For river morphological models, it has been shown that there is generally no single representative discharge for the morphological evolution (De Vries, 1973; Stevens et al., 1975; Baker, 1977). This theory has been derived for large scale 1D river models to produce the right water depth and longitudinal bed slope in the equilibrium state. Although to what extend the application of representative discharges of river morphology can be transfer to an estuary has never been investigated, it raises the question of how the combination of tides and river discharge can be schematized in estuarine morphological models.

Numerical experimentation has been carried out to determine the "morphological tide" of the study area based on the commonly adopted method (Latteux, 1995). The calibrated and validated process-based model of the Yangtze Estuary (Chapter 3) is used to simulate the sediment transport in this experiment. Figure 6.2 shows the model domain, which covers the entire tidal region of the Yangtze Estuary, Hangzhou Bay, and a large part of the adjacent East China Sea. The upstream boundary for the Yangtze Estuary is set at Datong, which is the tidal limit. Discharge and suspended sediment concentration (SSC) measurements are collected since the 1950s and can be used to determine the boundary conditions. The tidal constants M_2, S_2, K_2, N_2, K_1, O_1, and P_1 are provided for the open sea to represent tidal forcing for the model. The model of the Yangtze Estuary is 3D and simulates flow, salinity and sediment transport (Chapter 4). Three fractions, representing fine cohesive sediment in the clay and fine silt range (<32 µm), coarse silt (40 µm), and fine sand (200 µm), are included in the model. The transport of suspended sediment is calculated by solving the advection-diffusion equation, coupled online with the hydrodynamics. Important sub-models concerning the erosion and deposition fluxes at the bed are applied in the model. To calculate these quantities different formulations should be applied, because the two types of sediment behave differently. For the fine cohesive sediment, the Partheniades-Krone formulation (Partheniades, 1962,1965; Krone, 1962, 1963) is used to calculate the exchange fluxes with the bed. For the coarser non-cohesive sediment, Van Rijn's transport formula (van Rijn, 2007a, 2007b; van Rijn et al., 2007) is used. Bottom changes with MorFac of 1 are calculated in the estuary downstream of Xuliujing, starting from a 1:1:1 mixture of the three fractions at the bed. For more model details see Chapter3, 4 and 5.

Simulations over a spring-neap cycle of 14.8 days have been carried out using the process-based Yangtze Estuary model for two river discharges of 12,500 m^3/s and 55,000 m^3/s, chosen to represent the dry and wet seasons, respectively. These

simulations yielded the sediment transport rates over the spring-neap cycle.

Figure 6.3 shows the tidal levels and the depth-averaged SSC computed over a spring-neap cycle at Niupijiao station (see location in Figure 6.1) for the discharge of 55,000 m^3/s. Although the semi-diurnal tide dominates in the Yangtze Estuary, a large daily inequality can be observed in Figure 6.3. Therefore, every two tides (24 h 50 min) are defined as one tidal cycle (tidal day). In total, fourteen tidal days (see Figure 6.3) are included in the spring-neap cycle.

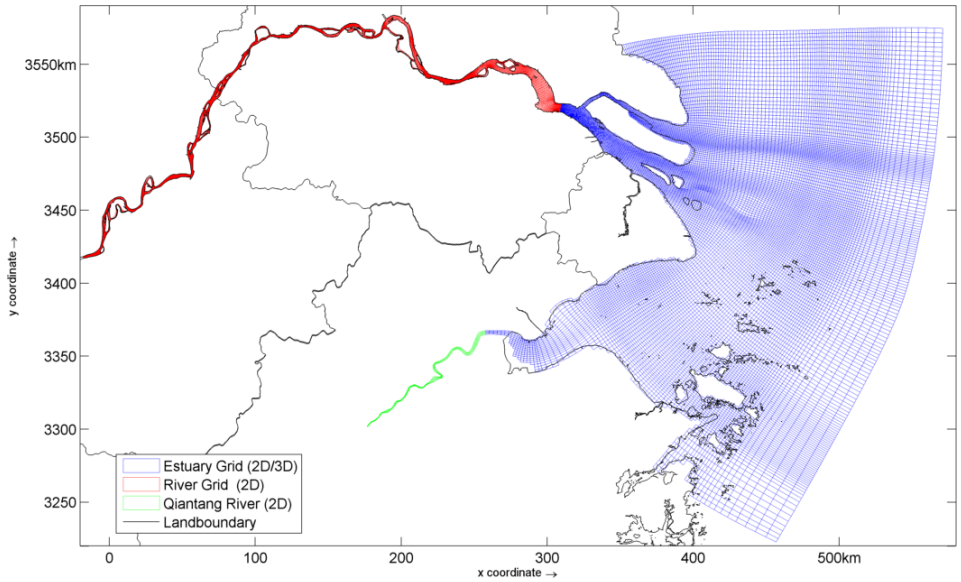

Fig.6.2 Model domain of the process-based Yangtze Estuary model

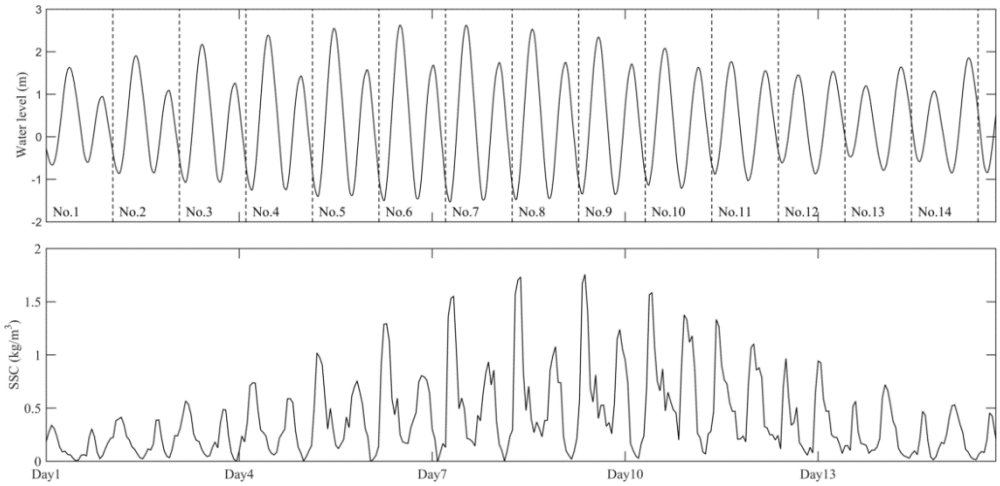

Fig.6.3 Water level (upper) and SSC near bed (lower) at Niupijiao during a spring-neap cycle with discharge of 55,000 m^3/s from upstream

The east and north components of the transport rate in the estuary domain over the spring-neap cycle have been compared with those during each individual tidal day in Figures 6.4 and 6.5 for the two seasons.

The correlation between simulated transport rates over an individual tidal day and the full spring-neap cycle is given in Table 6.1 for each season. It can be found that in the

dry season the correlation coefficient *R* is at its maximum (R^2= 0.93) around spring tide and at its minimum (R^2=0.52) around neap tide. Note that the value of *R* decreases as the tidal ranges become smaller. Thus, the correlation between the result for an individual tidal day and the full spring-neap cycle result becomes less significant as the tidal range decreases in the dry season. In the wet season all the values of *R* are close to 1. The result for the No. 4 tidal day is closest to that for the full spring-neap cycle.

Table 6.1 also shows that the range of tide No. 8 is comparable to that of tide No. 6, with values of 3.61 m vs. 3.64 m, respectively. The slope of the fit line for tide No. 8 in the dry season is 1.72, which is larger than the slope of 1.40 for tide No. 6. In the wet season, the slope of the fit line for tide No. 8 is also larger than that for tide No. 6: 1.12 vs. 1.08. This means that the transport rate during tide No. 8 is larger than that during tide No. 6. The same trend can be found for the other tide pairs, e.g. the slope of fit line for tide No. 9 is larger than that for tide No. 5, the slope of fit line for tide No. 10 is larger than that for tide No.4, in both dry and wet seasons. This indicates that the transport rate of an individual tide day after the spring tide is larger than that before the spring tide, even if their tidal ranges are comparable. This is mainly because the highest SSC occurs after the spring tide due to the relaxation effect (Galappatti and Vreugdenhil, 1986, Wang, 1992), see Figure 6.3.

Table 6.1 Relationship of the simulated transport rate over an individual tidal day with that over a full spring-neap cycle in dry and wet season

Tide	Q=12500 m^3/s			Q=55000 m^3/s		
No.	R^2	Slope	Range (m)	R^2	Slope	Range(m)
1	0.5184	0.28	1.92	0.9882	0.85	1.93
2	0.6359	0.41	2.35	0.9910	0.88	2.36
3	0.7309	0.59	2.77	0.9943	0.93	2.79
4	0.7942	0.83	3.15	0.9962	0.99	3.16
5	0.8445	1.12	3.45	0.9958	1.04	3.46
6	0.8893	1.40	3.64	0.9936	1.08	3.64
7	0.9199	1.62	3.70	0.9904	1.11	3.70
8	0.9282	1.72	3.61	0.9888	1.12	3.61
9	0.9153	1.66	3.39	0.9901	1.11	3.38
10	0.8721	1.45	3.04	0.9928	1.07	3.04
11	0.8058	1.13	2.62	0.9947	1.00	2.62
12	0.7187	0.79	2.23	0.9931	0.92	2.24
13	0.6711	0.56	2.03	0.9896	0.86	2.05
14	0.7340	0.50	2.17	0.9897	0.85	2.19

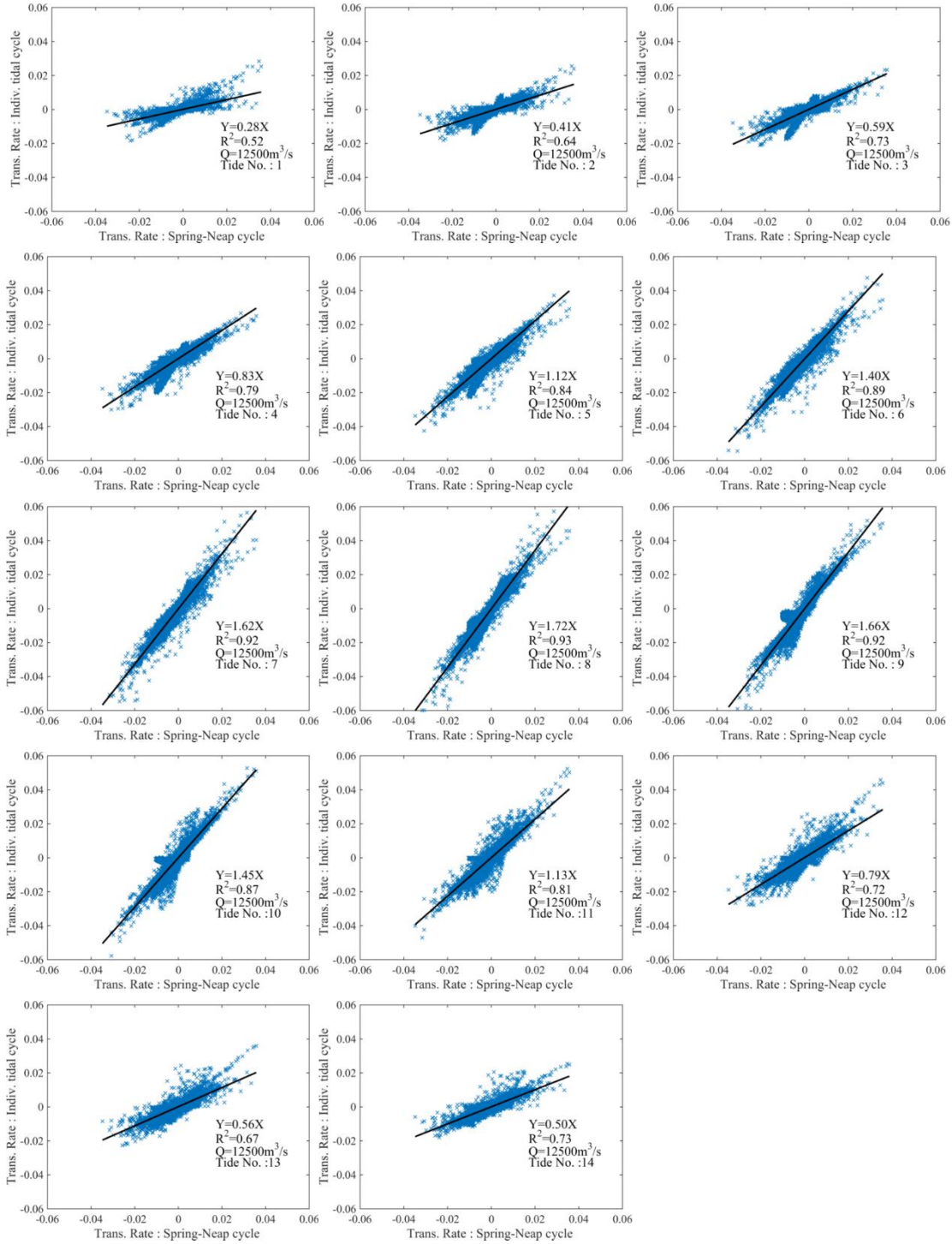

Fig.6.4 Transport rate (m^2/s) over the spring-neap cycle (X-axis) and over the individual tidal day (Y-Axis) with an upstream discharge of 12,500 m^3/s (Positive values indicate transport in the north or east direction)

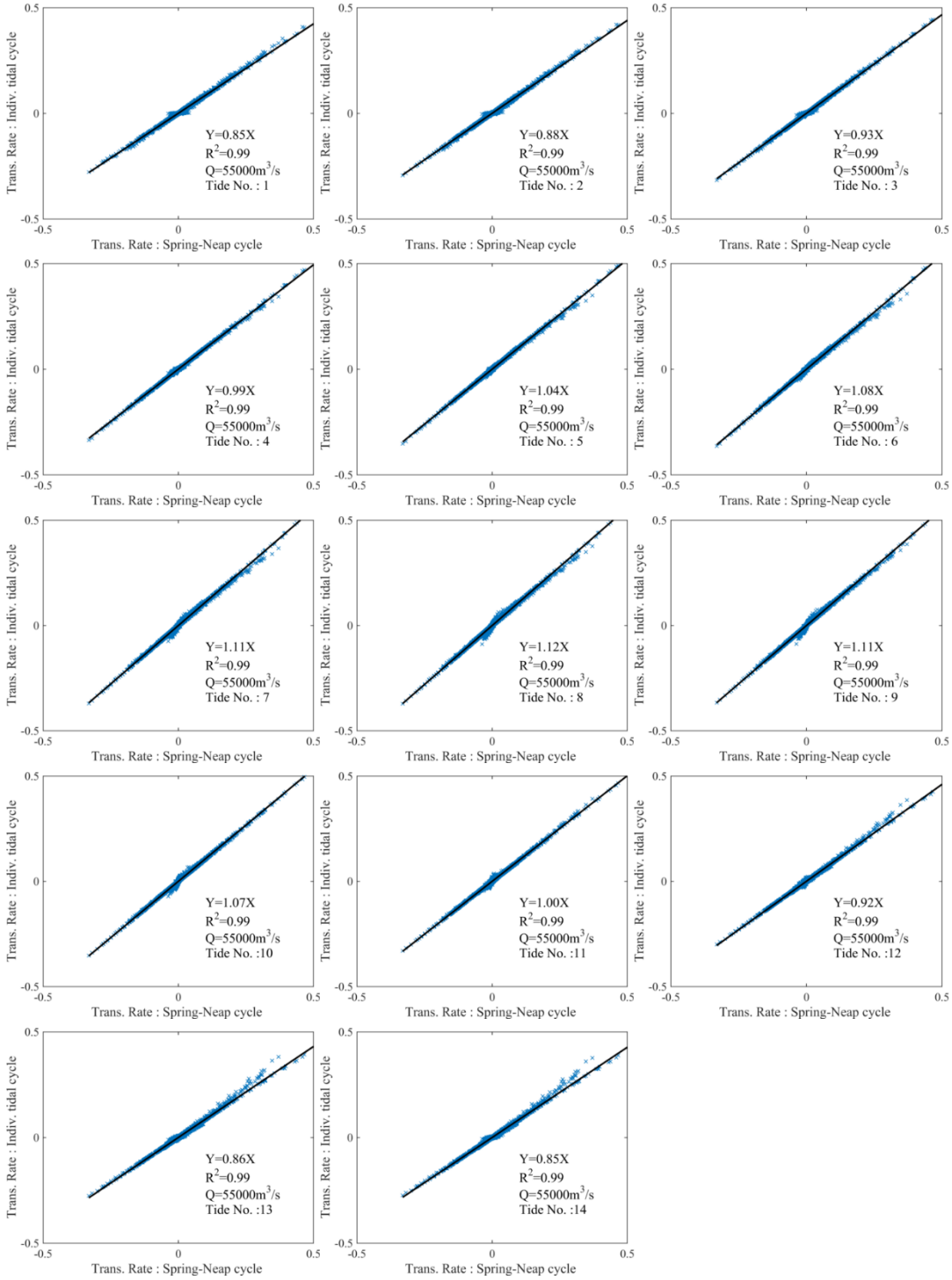

Fig.6.5 Transport rate (m^2/s) over the spring-neap cycle (X-axis) and over the individual tidal day (Y-Axis) with an upstream discharge of 55,000 m^3/s (Positive values indicate transport in the north or east direction)

In summary, we can conclude the following:

1. When the discharge from upstream is small, the spring tide (tide No. 7) seems to be the "morphological tide" with the transport rate significantly high (R^2=0.92) correlated to that of the spring-neap cycle.
2. In the case of a high river discharge, the selection of a "morphological tide" seems

irrelevant; the transport rate over any individual tidal day appears closely related to the result of the spring-neap tidal cycle.

3. The transport rate for individual tidal cycles with a comparable tidal range is larger for days after spring tide than that for days before spring tide.

Apparently, with the varying discharge of the Yangtze River using a simple "representative tide" for the morphological modelling of the estuary is not suitable. It may also be argued that the tidal constituent M_2 and its super harmonic tides can be used to develop a representative tide (e.g. Van der Wegen, 2010; Dastgheib 2012). However, it has been proven that no morphological tide can be defined to drive a practical morphodynamic model of the Yangtze Estuary (see Chapter 5).

In conclusion, the influence of the tidal forcing on the sediment transport in the Yangtze Estuary varies with the river discharge. The commonly used "morphological tide" method is not valid for estuaries with a large seasonal variation of the river input. Moreover, the transport rates before and after spring tides are asymmetric. Therefore, it is necessary to use the full spring-neap tidal cycle to determine tidal forcing in the Yangtze Estuary model.

6.2.3 River input reduction for the Yangtze Estuary model

Although river input reduction for estuarine morphodynamic models has not been well investigated, previous work, e.g. on the "ensemble technique" (Bernades et al., 2006), already provides some reference.

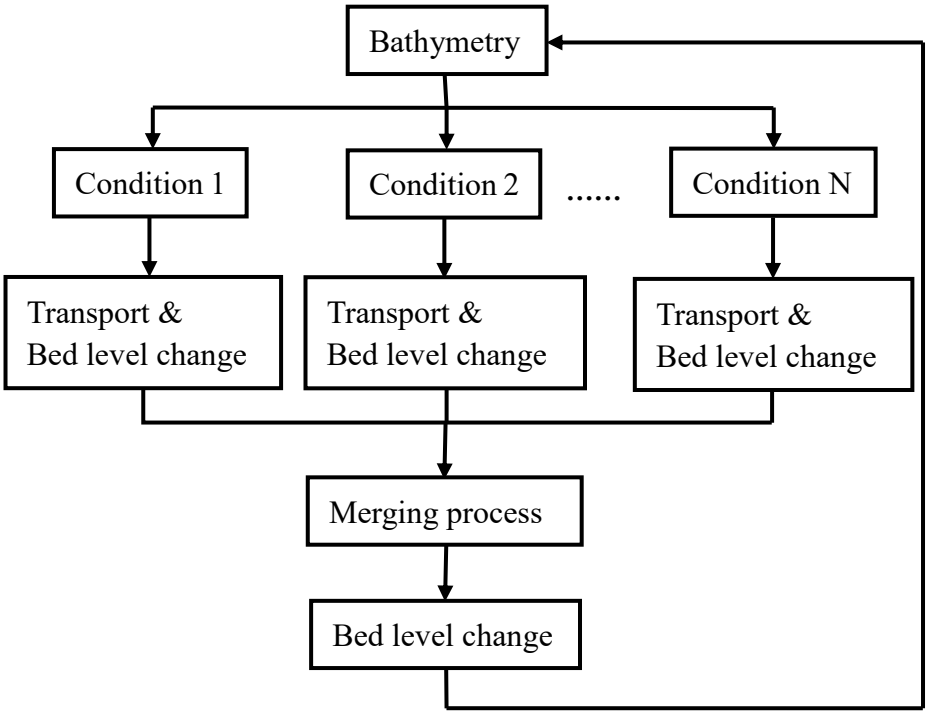

Fig.6.6 Flow scheme of Mor-Merge (after Roelvink, 2006)

The full discharge series can be divided into a number of discrete classes by discharge level. Individual discharges falling within each class are then averaged to a "mean discharge" for each discharge level. The "mean discharges" can be used as upstream boundary conditions for the model. The observed discharge at Datong station (the tidal limit) is used to determine the "mean discharges" at the upstream boundary of the Yangtze Estuary model. The Mor-Merge (MM) technique proposed by Roelvink (2006) is adopted. As is shown in Figure 6.6, if the time scale of each condition is small relatively to the morphological time scale, these conditions may occur simultaneously on the same bathymetry. The conditions can be considered as different discharge levels for the Yangtze Estuary model. The simulation of the Yangtze Estuary morphodynamic model can be split into a number of parallel processes, which all represent different conditions, i.e. discharge levels. The parallel simulations share the same bathymetry, which is updated by the weighted sum of the bottom changes due to each condition at computational time step. The simulation continues with the updated bathymetry. For the Yangtze Estuary model, the sediment load corresponding with the various discharge classes is assumed to be represented by the SSC corresponding with the mean discharge of that range. Thus, the non-linear character of the variation of the SSC with the discharge within each class is ignored.

On top of this, morphological acceleration can be achieved with the "MorFac" technique. This provides the possibility of medium-term (or long-term) simulation of morphological changes within reasonable computation times.

6.3 Mor-Merge Morphodynamic model for the Yangtze Estuary

6.3.1 Model set-up

There is a large distance from the upstream boundary of the Yangtze Estuary at Datong to its mouth. The sedimentation and erosion occurring within this long section have not been well documented. Previous research (Yun, 2004) points out that the sediment concentration at Xuliujing is slightly less than at Datong. Due to the uncertainty about the amount of sediment stored or eroded in this section, the exchange of sediment between bed and water body in this section is excluded, by assuming critical bed shear stress of erosion infinitively large and critical bed shear stress of deposition infinitively small for the sediment fraction of clay and fine silt range (Gao, 2008). Therefore, all sediment traveling downstream from Datong reaches Xuliujing.

The abovementioned process-based Yangtze Estuary model is applied to simulate the bathymetry change with various values of MorFac. A spin-up period of about 15 days is applied in each simulation to get rid of the influence of the initial conditions. Before this period, the model is used to simulate two years of flow with the long term monthly-averaged river discharge from upstream. In order to obtain the proper initial distribution of salinity and SSC in the model domain, the results from the latter year with the corresponding discharge from upstream can be used as the initial conditions at the start time of the spin-up period. The bed level and the bottom compositions are kept constant during this spin-up period.

6.3.2 Quasi real time simulation vs. Mor-Merge approach (1998-1999)

In order to optimize the schematization of river discharge, two types of simulations have been carried out, and their results have been compared to each other. One simulation is the quasi real time (QRT) simulation, using a realistic discharge time series at the upstream boundary with the astronomic tides at the open sea boundary. The other simulation is the MM simulation, which uses multiple "mean discharges" from upstream and tides from the sea with the MorFac technique applied.

The period of 1998-01-01 to 1999-12-31 is selected for the QRT simulation. The river discharge in this period is shown in Figure 6.7, in which we can observe the seasonal variation (dry–wet–dry) occurring within each year. Note that two remarkable river flood events (peak discharge > 80,000 m^3/s) occurred in Jul., 1998 and Jul., 1999. The observed daily mean SSC is also shown in Figure 6.7. Over these two years, the observed river runoff at Datong was about 2,281 billon m^3 and the sediment load was about 718 million tons. These observed discharge and SSC data are prescribed as upstream boundary conditions to represent the real fluvial forcing for QRT simulation in this two-year period.

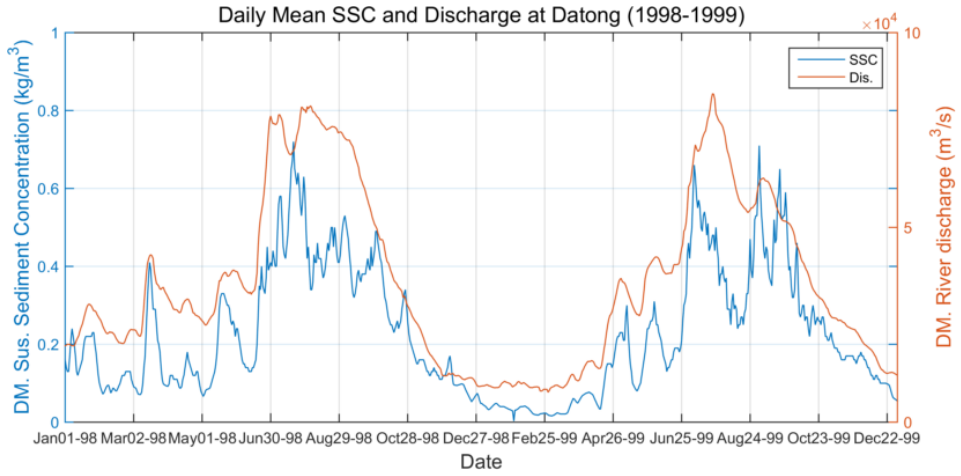

Fig.6.7 Daily mean SSC and discharge at Datong in 1998 and 1999

Table 6.2 provides the discharge levels used to represent the realistic fluvial forcing in the MM approach. We can find from this table that five different MM cases are defined with 1, 2, 4, 6, and 8 discharge level(s) with the associated SSC. The hydrodynamic simulation period is about 15 days, which approximates a morphological simulation period of 2 years by applying the MorFac of 48. One extra MM simulation with six discharge levels is also carried out for a period of 30 days with the MorFac of 24.

The 2-year (1998–1999) erosion and sedimentation patterns from the QRT simulation and from the MM simulation with six discharge levels are shown in Figures 6.8 and 6.9. The results for MM simulations with other discharge levels are similar to those of the simulation with six discharge levels. From Figures 6.8 and 6.9, we can observe that the overall distribution of sedimentation and erosion pattern simulated by the MM model is similar to that produced by the QRT model.

Table 6.2a Discharge levels at Datong in 1998 and 1999 (Single Q)

Discharge levels(m^3/s)	Mean
Occurrence (days)	730
Mean Discharge (m^3/s)	36000
SSC (kg/m^3)	0.312

Table 6.2b Discharge levels at Datong in 1998 and 1999 (Two Q)

Discharge levels(m^3/s)	<30000	>30000
Occurrence (days)	351	379
Mean Discharge (m^3/s)	18000	53000
SSC (kg/m^3)	0.138	0.367

Table 6.2c Discharge levels at Datong in 1998 and 1999 (Four Q)

Discharge levels (m^3/s)	<20000	20000~40000	40000~60000	>60000
Occurrence (days)	196	286	106	142
Mean Discharge (m^3/s)	12000	30000	49000	72000
SSC (kg/m^3)	0.090	0.196	0.348	0.441

Table 6.2d Discharge levels at Datong in 1998 and 1999 (Six Q*)

Discharge levels(m^3/s)	<25000	25000 ~35000	35000 ~45000	45000 ~55000	55000 ~65000	>65000
Occurrence (days)	264	156	99	46	49	116
Mean Discharge (m^3/s)	15000	30000	39000	51000	60000	75000
SSC (kg/m^3)	0.113	0.193	0.246	0.379	0.402	0.447

*Two simulations with six discharge levels applying MorFac of 48/24 for 15/30 days

Table 6.2e Discharge levels at Datong in 1998 and 1999 (Eight Q)

Discharge levels(m^3/s)	<15000	15000~ 25000	25000~ 35000	35000~ 45000	45000~ 55000	55000~ 65000	65000~ 75000	>75000
Occurrence (days)	155	109	156	99	46	49	55	61
Mean Discharge (m^3/s)	11000	21000	30000	39000	51000	60000	71000	78000
SSC (kg/m^3)	0.070	0.143	0.193	0.246	0.379	0.402	0.444	0.450

A comparison between the QRT and MM results using values of erosion and sedimentation in the model domain is shown in Figure 6.10 and Table 6.3. The results of two simulations are in good agreement, with a correlation coefficient of about 0.90–0.92. The slope of the best fit line is about 0.90–0.98, which means that the MM model somehow underestimates erosion and sedimentation rates compared to the QRT model.

From Table 6.3, it can be observed that using more discharge levels results in higher correlation between MM and QRT model results. However, the effective acceleration of the MM approach decreases with an increase in the number of discharge levels. Therefore, schematization with six discharge levels is considered a practical choice for a morphodynamic model of the Yangtze Estuary.

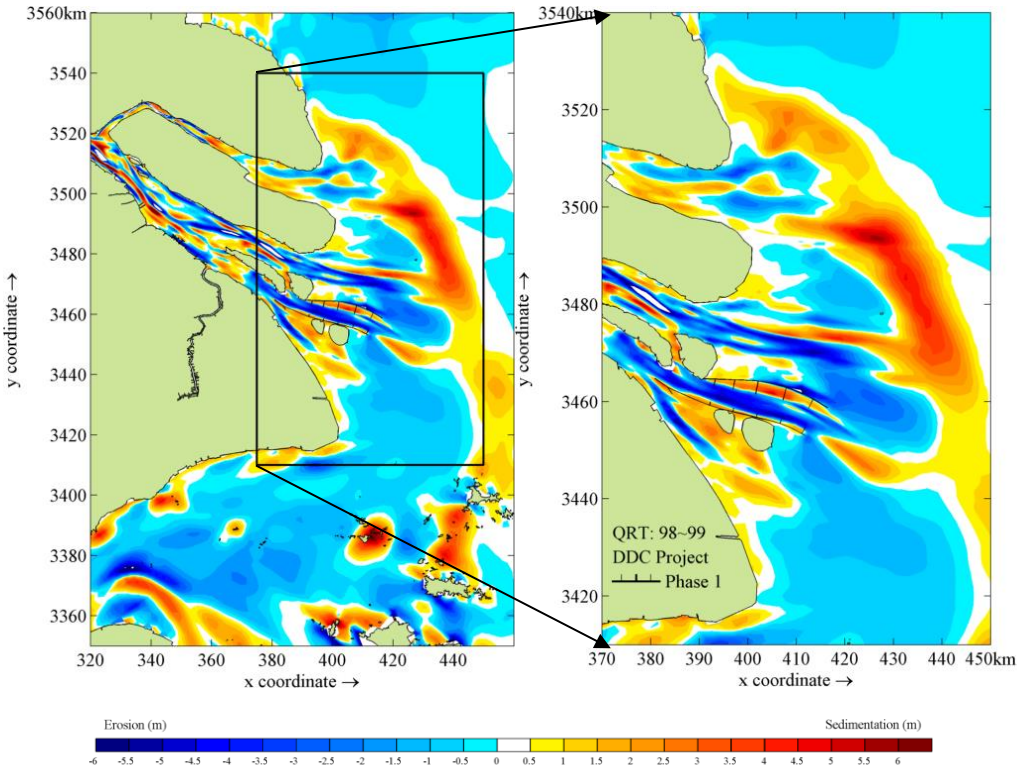

Fig.6.8 Simulated bed level change in 2 years under quasi real-time situation (1998-01-01 to 1999-12-31)

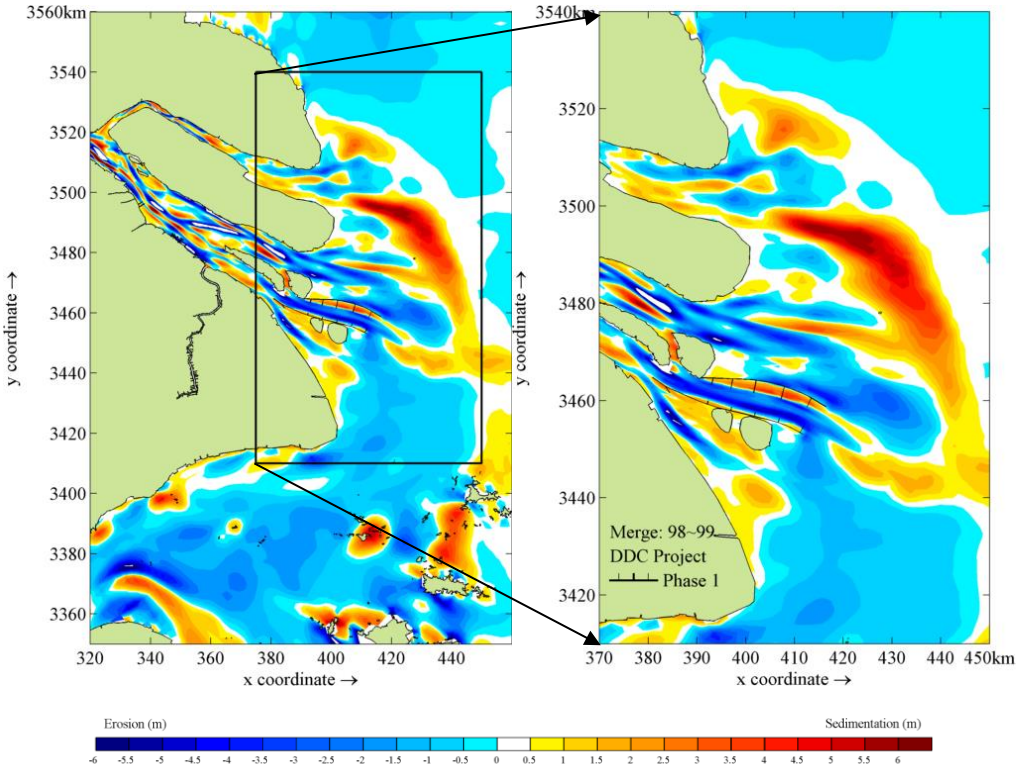

Fig.6.9 Simulated bed level change by merging results of 6 discharge levels (15 days with morphological factor of 48)

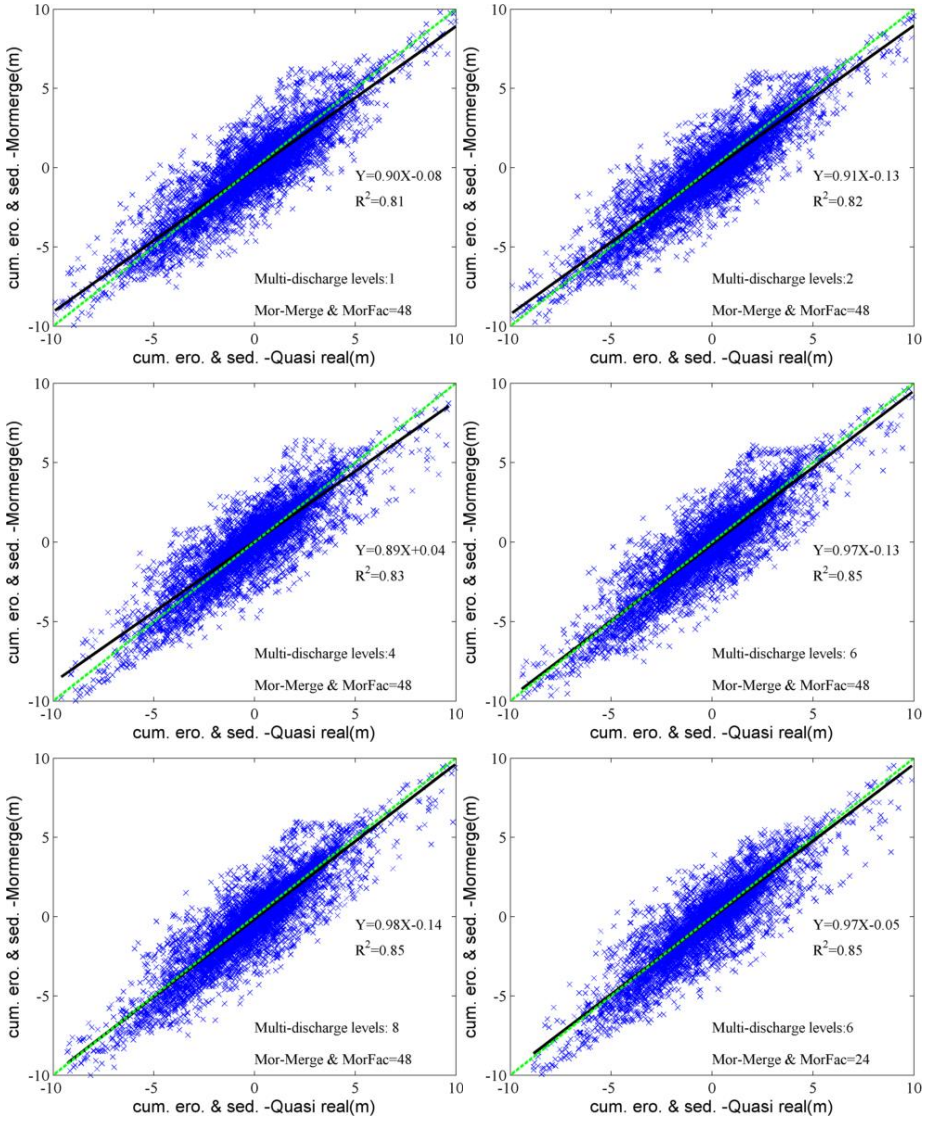

Fig.6.10 Relationship of simulated cumulative erosion and sedimentation between QRT (X-axis) and MM (Y-axis) simulation results with 1, 2, 4, 6, and 8 "mean discharges" from upstream over a period of 2 years, 1998-01-01 to 1999-12-31 (green dashed line: 1:1 match; black line: best fit; blue cross: erosion/sedimentation at individual point)

Table 6.3 Correlation of model results between MM and QRT for the Yangtze Estuary (1998–1999)

Number of discharge levels	R^2	Relationship	Effective acceleration
1	0.80	Y=0.90X-0.08	48
2	0.82	Y=0.91X-0.13	24
4	0.84	Y=0.89X+0.04	12
6	0.85	Y=0.97X-0.13	8
8	0.85	Y=0.98X-0.04	6
6b*	0.85	Y=0.97X-0.05	4

* MorFac=24 with simulation period of 30 days.

6.3.3 Morphodynamic modelling of the Yangtze Estuary (1965–1986)

In this section, the MM approach is further used for hindcasting the bathymetry change from 1965 to 1986. The Yangtze Estuary bathymetries in 1965 and 1986 have been digitized with the maps obtained from the Shanghai Waterway Bureau (Figure 6.11). The discharge series measured at Datong station between 1965 and 1986 is used to determine the upstream boundary conditions for the morphological model of the estuary. Measured daily discharge and SSC during this period are shown in Figure 6.12. Based on the discharge and SSC data shown in Figure 6.12, six discharge levels from 15,000 m^3/s to 55,000 m^3/s with an interval of 10,000 m^3/s are defined. The occurrence of each level and the corresponding SSC are presented in Table 6.4.

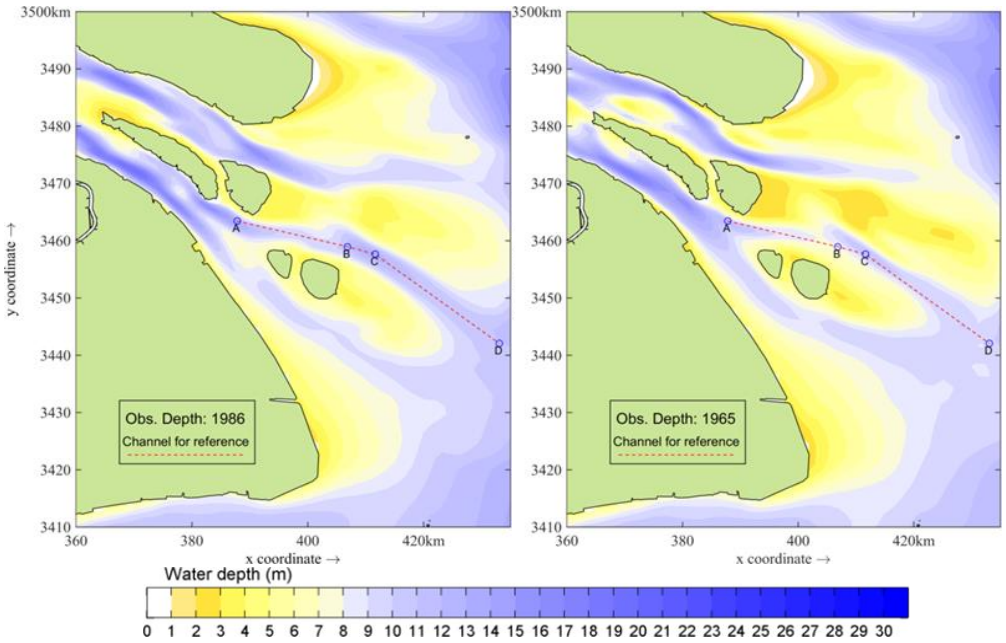

Fig.6.11 Bathymetry maps of the Yangtze Estuary in 1965 (left) and 1986 (right)

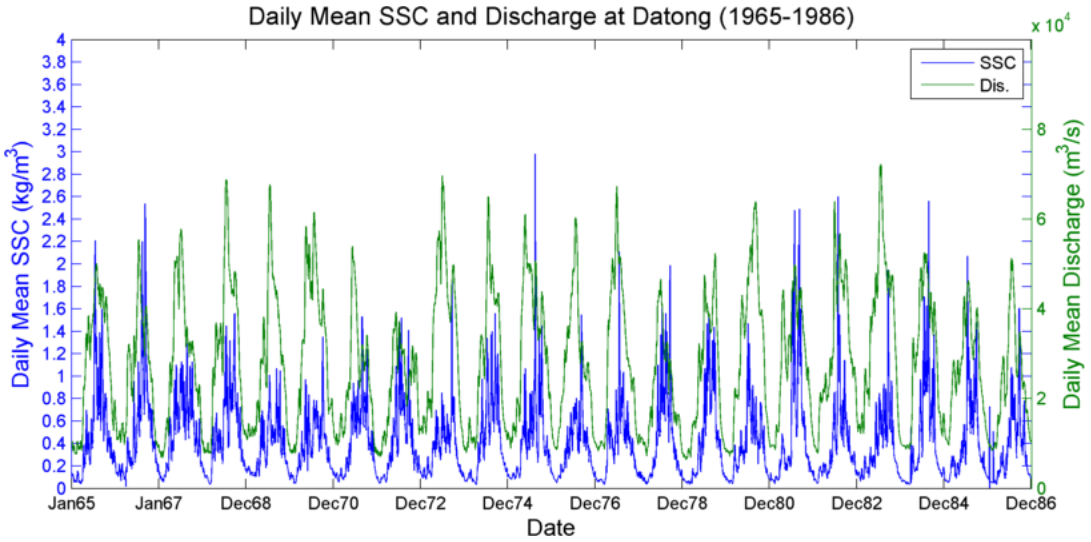

Fig.6.12 Daily mean SSC and daily mean discharge at Datong (1965–1986)

Table 6.4 Schematic discharge and SSC at Datong (1965–1986)

Discharge levels(m^3/s)	<15000	15000 ~25000	25000 ~35000	35000 ~45000	45000 ~55000	>55000
Occurrence (days)	2288	1516	1640	1399	887	305
Mean Discharge (m^3/s)	10800	20200	29900	40200	48900	60900
SSC (kg/m^3)	0.115	0.261	0.471	0.661	0.738	0.667

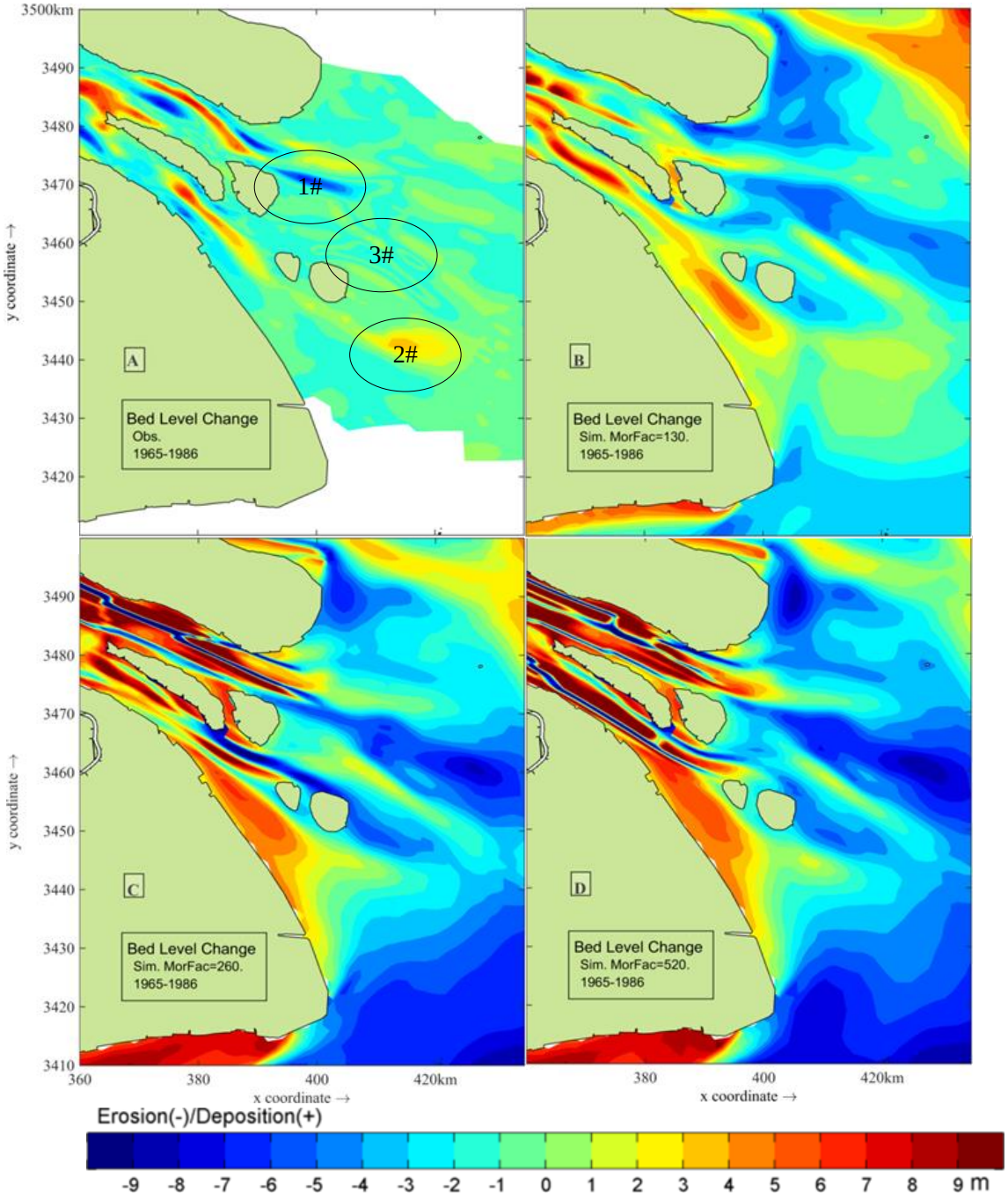

Fig.6.13 Observed (A) and simulated (B: MorFac=130; C: Morfac=260; D: Morfac=520) erosion and sedimentation around the mouth bar of the Yangtze Estuary (1965–1986) with well mixed bed

Simulation results of morphological changes the period 1965-1986 are obtained by implementing the morphological model for a 15-day period with a MorFac of 520, a 30-day period with a MorFac of 260 and a 60-day period with a MorFac of 130. The computed and observed erosion and deposition maps for the period from 1965 to 1986 are shown in Figure 6.13. It shows that the feature of erosion and sedimentation in the Yangtze Estuary is qualitatively reproduced by model with MorFac 130 (panel B). For example, the observed erosion in the middle part of the NC (indicated by 1# in Figure 6.13 panel A) is properly reproduced. Another major morphological change is the sedimentation around the lower part of the Jiuduansha Shoal (2#), which is also reasonably simulated by the model. It also can be observed from Figure 6.13 that the model result with larger MorFac (panel C: MorFac=260; panel D: MorFac=520) shows elongated features of erosion/deposition in the NC and SC, as is unrealistic from the observation. The magnitude of erosion/deposition of the model result with larger MorFac is too larger than that observed.

The simulated erosion and sedimentation along the access channel (see location in Figure 6.11) are compared with the measurement in Figures 6.14. One of the major morphological changes of interest along the channel is deposition in the middle reach (Section BC to CD; 3#) and erosion in the other parts (Yun, 2004). Tan et al. (2009) also report that the same feature of erosion and sedimentation varies along the channel, based on an analysis of multi-years data on back-siltation and dredging. It should be noted that the continuous maintenance dredging has been applied to middle and lower reach of the channel (Tan et al., 2009). From Figure 6.14, we can find that the modeled deposition in section BC of the channel differs from the measurement. This can be explained by the continuous maintenance dredging (at 3#) activities in this channel during this period, which are not included in the model. The observed erosion in the upper part of the North Channel is properly reproduced by the model.

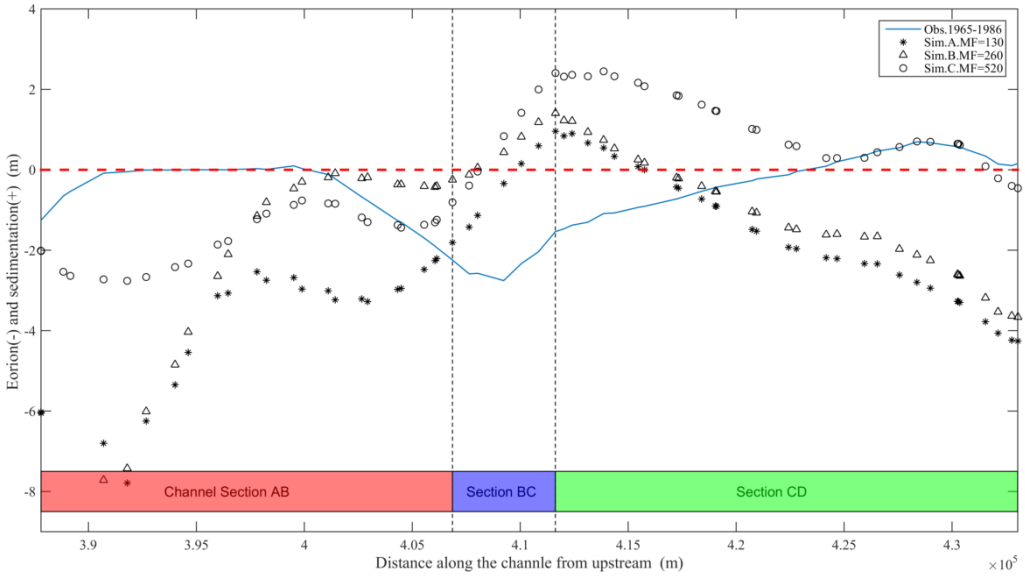

Fig.14 Observed and simulated erosion and deposition along the access channel in the North passage of the Yangtze Estuary (Simulation with well mixed bed)

6.4 Discussion and conclusion

6.4.1 Discussion

6.4.1.1 Choose of Multi-discharge levels

In this study discharge input reduction with six discharge levels is recommended for the morphodynamic model of the Yangtze Estuary. Obviously, the more discharge levels are used, the less efficient the MM model is. However, the results also show that the more discharge levels that are used, the better the agreement between the MM simulation and the QRT simulation. In practice, the number of discharge levels used for morphological model of an estuary is simply a matter of balancing computational effort and accuracy.

6.4.1.2 Bed stratigraphy model

The proposed morphodynamic model of the Yangtze Estuary adopts an assumption of well mixture of three fractions (1:1:1) at the bed due to lack of bed information. Liu et al. (2010) propose the sand-mud mixture distribution in the estuary based on the measurement of bed sample fractions. This means the bed is often made up of a range of sediment types and sizes. In such case the modelled erosion rate will be affected. If the bed stratigraphy is modelled in detail, it is assumed that the erosion rate is proportional to the availability of the sediment fraction in the upper layer of the bed stratigraphy. Therefore, the present model is further applied to simulate the morphodynamics in the estuary with bed stratigraphy included.

The layer system (Deltares, 2014) is applied to accounting the bed composition in the model. The upper layer is considered to be the transport layer where sediment is deposited and picked up. Lower layers simply store deposited sediment. In total 75 layers are used in the model, each 0.20 m thick. The initial composition is determined based on the results of Liu et al. (2010) and Luan et al. (2017). Figures 6.15 and 6.16 show the modeled erosion and sedimentation in the estuary and along the channel with bed stratigraphy included.

It can be seen from Figures 6.15 that the modeled erosion and deposition with bed stratigraphy included differs from the well-mixed bed result (Figure 6.13). The model results with larger MorFac are more moderate in comparison with those results with well mixed bed, e.g. the erosion magnitude along the access channel. The unrealistic feature of elongated erosion/deposition in the NC and SC predicted by well mixed bed model disappear. It also can be observed from Figure 6.16 that the results with MorFac 130 seem to be more pronounces, except in Section CD.

Therefore, to include bed composition in the model improved the morphological model results for the Yangtze Estuary model. The present model using the recent bed sample data (Liu et al., 2010; Luan et al.,2017) to represent the bed composition in the Yangtze Estuary, as differs from the situation at the start time of the hindcast. Thus, the

difference between the model results, not matter of the well mixed bed or bed stratigraphy included, and the observation can be expected. It is highly recommended to account the proper bed composition in the application of morphodynamic modelling for the Yangtze Estuary.

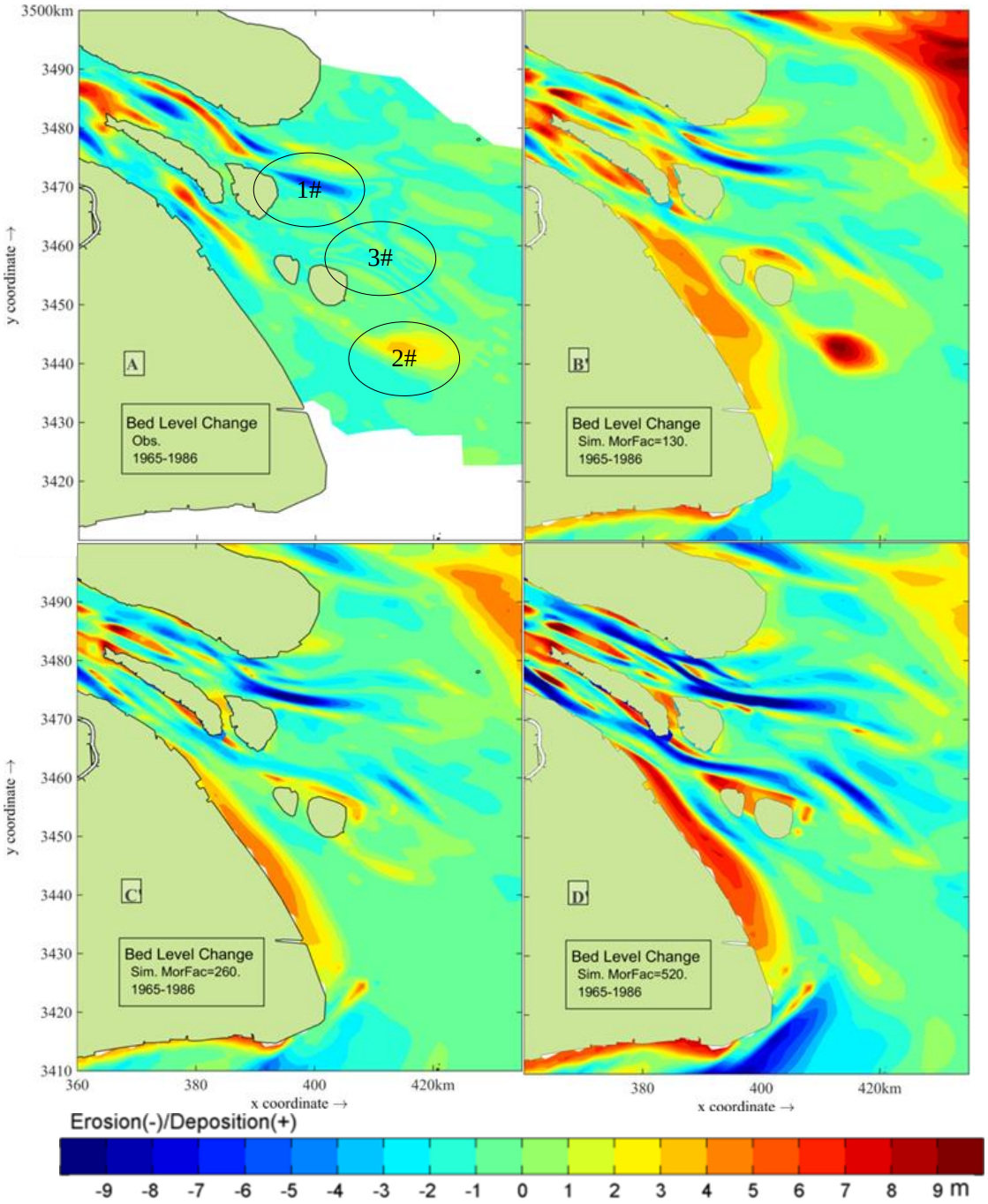

Fig.6.15 Observed (A) and simulated (B': MorFac=130; C': Morfac=260; D': Morfac=520) erosion and sedimentation around the mouth bar of the Yangtze Estuary (1965–1986) with bed stratigraphy

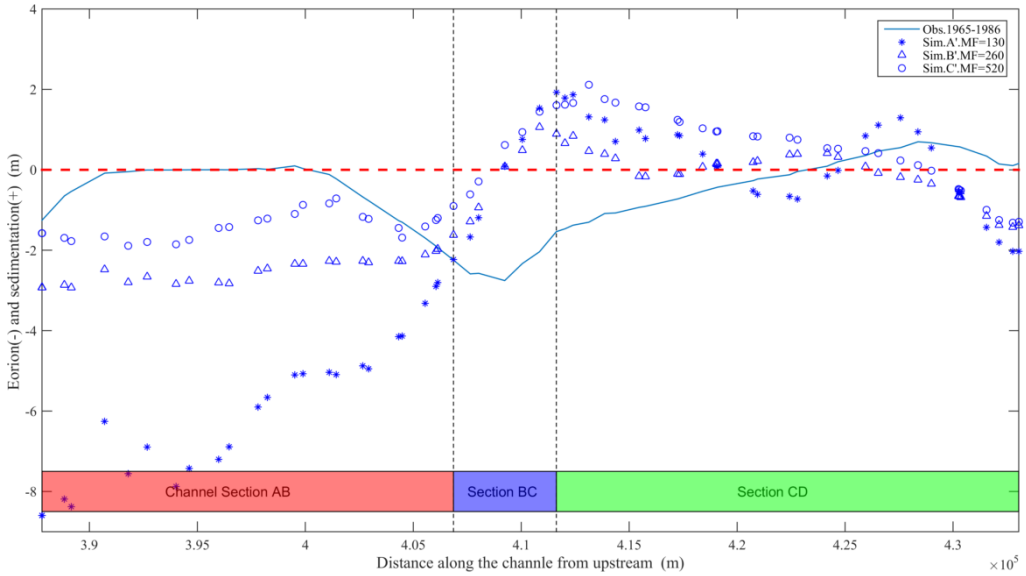

Fig.6.16 Observed and simulated erosion and deposition along the access channel in the North passage of the Yangtze Estuary (Simulation with bed stratigraphy)

6.4.1.3 MorFac for jointed input reduction

The proposed morphodynamic model of the Yangtze Estuary adopts a combined input reduction technique, with multi-discharge levels over a time span of a spring-neap tidal cycle. If a different time span is used, the MorFac for a morphological model can be determined accordingly. In this study three MorFac-values (520, 260 and 130) are used to hindcast the morphological change of the Yangtze Estuary in the period of 1965-1986. The model results vary in magnitude, as well as in some feature of the sedimentation/erosion pattern. It reveals that larger MorFac-values are not suitable for this type of estuarine morphodynamic study. It also indicates that the proposed model is not perfect and demands further improvement, for instance in the determination of the MorFac value.

6.4.1.4 Choose of processes of relevance

At present the morphodynamic model of the Yangtze Estuary includes two major drivers, discharge and tide. Some morphological change may be dominated by episodic events, e.g. typhoons, floods. Especially for the shoals at the river mouth, the influence of wave conditions on the morphological change of the estuary may also be important. Thus, the combination of tide, river input, and wave forcing, as well as individual floods or storms, in morphodynamic modelling needs further investigation. It is also noted that the MM method is better suited for modelling of long-term (decades or longer) periods than for short-term periods (season, year). The reason for this is that the time sequence of input conditions, which may be important for short-term simulations, cannot be taken into account in the MM approach.

6.4.2 Conclusion and Remarks

The investigation of input reduction methods for the morphodynamic model of the Yangtze Estuary shows that the classic "representative tide" approaches are not appropriate for estuarine cases with large fluvial discharges. The full spring-neap tidal cycle must be used to represent the tidal forcing.

The MM approach with multi-discharge levels is an alternative for morphodynamic modelling of the Yangtze Estuary. The MM model reasonably captures the morphological features when compared to the results of the QRT simulation and observed reality. In other words, with the present MM method, the simulation of medium-term morphological changes in estuaries is feasible.

The hindcast of the MM model of the Yangtze Estuary for the period of 1965-1986 remind us that the morphodynamic modelling for estuaries demands more efforts before practical application. One is the determination of the MorFac parameter. It reveals that larger MorFac is not in favor for the estuary morphodynamic models. The bottom condition, i.e. the bed composition, is sensitive for the model result. Comprehensive survey and detail study on the distribution of sediment fractions are required.

7 Conclusions and Recommendations

The aim of this research is to obtain more quantitative knowledge on sediment transport and morphodynamic processes in estuaries, especially the mouth bar area of the Yangtze Estuary. A process-based numerical model of the Yangtze Estuary is used to study the sediment transport due to various combinations of physical processes/mechanisms. The model results help increasing the fundamental understanding of the behavior, evolution and underlying physical processes of the Yangtze Estuary.

The present model is driven by river discharge, tides, wind and waves. The analytical expression for long-term net coarse sediment transport (Van de Kreeke and Robaczewska, 1993) is further expanded to the estuarine environment with large mean flow due to river run-off. Model input reduction for combinations of tide and discharge is investigated. A parallel morphodynamic model approach with multiple discharge levels is proposed. Thus, the practical target of the study, to develop and test improved modelling approach for the prediction of sediment transport and morphology of the mouth bar area of the Yangtze Estuary, has been achieved.

In order to achieve the aim mentioned above, three specific objectives were set with three research questions formulated in Chapter 1. Conclusions related to these objectives are summarized in the next sections.

7.1 Forcing and mechanisms of sediment transport in the mouth bar area

Research question: Which forcing processes/mechanisms relevant to the sediment transport need to be included in the morphological model of the Yangtze Estuary?

In order to identify the relevant processes/mechanisms results, existing literatures was studied and data from observation in the Yangtze Estuary were analyzed. A process-based model for the Yangtze Estuary was set up to study the sediment transport subject to various combinations of forcing processes/mechanisms. The model was first calibrated and validated against observation data of hydrodynamics and transport of substance (salinity and sediment) under different conditions, e.g. spring/neap tide in dry/wet seasons (Chapter 3). Two cross-sections were identified as up- and downstream controlling boundaries for sediment import/export to/from the mouth bar area of the Yangtze Estuary. Model results of the sediment budget in the mouth bar area before and after construction of the Three Gorges Dam were achieved by applying long-term mean upstream boundary conditions (discharge and SSC). These results were also validated with bathymetry observation in periods of 1990-2003 and 2003-2007. Model simulations were performed with individual physical processes excluded in order to identify which processes dominate the sediment transport in the mouth bar area (Chapter 4).

Comparison of model results for different scenarios reveals that including ***salinity*** is a prerequisite for sediment deposition in the mouth bar area of the Yangtze Estuary, in addition to the forcing by river discharge and tides. Fine cohesive sediments in the clay

and fine silt ranges are the main components of suspended sediment. ***Flocculation*** of fine cohesive sediment enhancing the sediment deposition, is also indispensable.

Wind and wave forces may influence the sediment flux towards the mouth bar area without changing the general pattern. They can increase the amount of sediment trapped in the mouth bar area not more than 23%.

The amount of sediment trapped in the mouth bar is highly related to the discharge and SSC from the river, yielding sedimentation in the wet season and erosion in the dry season. As the river's flow regime changes (e.g. due to regulation of discharge and sediment load from upstream due to the TGD), the general erosion/deposition pattern remains the same. But there is a clear decreasing trend in the total amount of deposition since the construction of the TGD, together with other projects inducing the decreasing trend in the riverine sediment transport. At present the deposition amount in the mouth bar area is only 1/3 of that before.

The model results of the flat bed test, i.e. with the mouth bar removed, also show similar characteristics of erosion/deposition characteristics in the mouth bar area. It indicates that the deposition of sediment there is due to the balance of driving forces instead of the mouth bar itself.

Therefore, to simulate the sediment transport in the mouth bar area of the Yangtze Estuary the process-based model should include salinity, fine cohesive sediment transport and flocculation. The necessity of including salinity-induced density currents implies that the sediment transport model needs to be three-dimensional.

7.2 Model input reduction for combinations of discharge and tide

Research question: To what extent can the complexity of the processes/mechanisms underlying the morphological development of the Yangtze Estuary be reduced?

The analytical expression for residual coarse sediment transport of Van de Kreeke and Robaczewska (1993), which is used as a method of tidal input reduction for estuarine morphodynamic models, was extended to estuaries with non-negligible river input. The new analytical expression demonstrates that the river discharge may play a significant role in estuaries. It indicates that the cyclic tide only with M_2 and its overtides (M_4, M_6) is insufficient to drive a morphodynamic models of this type of estuary. The tidal components were derived from process-based model results under different discharge conditions. These components were further applied in the present analytical expression for long-term net sediment transport in search of a 'representative tide'. The result shows that the 'representative tide' in the dry season differs from that in the wet season. In other words, a single representative tide does not exist for the Yangtze Estuary (Chapter 5).

As a consequence, full tidal forcing (i.e. full spring-neap cycle) is required for the morphodynamic model of the Yangtze Estuary. Similar to the idea for representative tide with average spring/neap amplitude ratio proposed by Roelvink and Reniers (2012),

the full spring-neap tidal cycle with average net spring/neap sediment transport ratio can be selected. The proposed analytical expression can be used to quickly assess the net sediment transport with the important tidal current components available.

As the tidal boundary condition cannot be simplified further, another way of input reduction for the combination of discharge and tidal forcing is required. In this study the river discharge is represented by a multiple discharge levels with different weights. First the full discharge series is divided into a number of discharge intervals. The mean discharge of each interval is used as upstream boundary condition. The number of discharge intervals is a compromise between computational effort and accuracy. The present study suggests that 6 discharge levels suffice for the morphodynamic model of the Yangtze Estuary. The morphodynamic models are therefore driven by a combination of 6 river discharges with a full spring-neap tidal cycle at the open sea boundary, using the Mor-Merge method (Chapter 6).

7.3 Morphodynamic model for the Yangtze Estuary

Research question: How can morphodynamic models be applied practically to the Yangtze Estuary?

A three-dimensional model including salinity, fine cohesive sediment and flocculation is required to properly simulate the sediment transport in the mouth bar area of the Yangtze Estuary (Chapter 4). The computational effort for this type of model limits the simulated time span to periods shorter than the morphological timescale of the estuary as a whole. Model input reduction helps to reduce the effort by coupling a limited number of river discharge levels with a spring-neap tidal cycle at open sea. The model is run following the so-called Mor-Merge approach: at each morphological time step several independent morphodynamic models with different river discharges are run in parallel, starting from the same bathymetry. Subsequently, the bathymetry is updated by the weighted sum of bottom changes from each individual run. A morphological acceleration technique is applied for each model multiplying the sediment fluxes to and from the bed by a constant factor, MorFac, at each hydrodynamic time-step. Different MorFacs have been tested to achieve the proper acceleration for the morphodynamic model (Chapter 6).

The model was applied to simulate the bathymetry change in 1998-1999 and 1965-1986. Model results of Mor-Merge approach for 1998-1999 were compared with quasi-real-time (QRT) simulation results for the same period. The two results show high correlation of the bathymetry change (Chapter 6). The observed bathymetric change in 1965-1986 is further used to validate the model. It reveals that the present model captures the major features of morphological change in this period fairly well.

Therefore, it is concluded that the present approach is feasible for intermediate-term simulation of morphological change in the Yangtze Estuary. However, additional efforts, e.g. MorFac determination and bed composition distribution, are needed before such models can be used in practice.

7.4 Recommendations

In summary, the morphodynamic modelling presented in this thesis gives insight into how to set up an estuarine morphological model in case of a high river discharge, lick in the Yangtze Estuary. Based on the analysis on physical processes/mechanisms relevant to the mouth bar formation in the Yangtze Estuary, it provides a simple, but effective method for intermediate-term simulation of morphological change in the Yangtze Estuary. This result might benefit the modelling other estuaries similar to the Yangtze Estuary.

However, the present research still has its limitations and the model concept needs to be further improved. Some important physical processes may still be missing in the present model. For example, episodic events (e.g. typhoons) may play an important role in the siltation of the navigation channel and in shoreface erosion at the seaward end of Jiuduansha Shoal and Hengsha Shoal (Yun, 2004). The combination of tide, river input and wave forcing, as well as the effects of individual flood or storm events, need to be further investigated. Nevertheless, the present model itself can serve in such studies as a “numerical laboratory”. Results of the present study indicate that taking the initial bottom stratigraphy into account can alter the computed morphological development. Apparently, the initial distribution of sediment composition at the bed is an important issue. Future studies and field observations on bed composition are therefore recommended. In addition, the human interference (e.g. dredging and construction work of the DDC project, the reclamation of the Hengsha Shoal, the construction of Qingcaosha fresh water reservoir) is so active that the effects of the changing natural condition and engineering work can be hardly distinguished. The present model can be used to assess the impacts under above mentioned scenarios.

References

Aubrey, D. G. (1986). Hydrodynamic Controls on Sediment Transport in Well-Mixed Bays and Estuaries. *Physics of Shallow Estuaries and Bays*, Vol. 16, 245-258.

Bagnold, R.A., (1966). An approach to sediment problem from general phsics. *Geological Survey Professional Paper*, 422-1.

Baker, V. R. (1977). Stream-channel response to floods, with examples from central Texas, *Geological Society of American Bulletin*, 1057-1071.

Bernaedes M. E. C., Davidson, M. A., Dyer, K. R., & George, K. J. (2006). Towards medium-term (order of months) morphodynamic modelling of the Teign estuary, UK, *Ocean Dynamics*, Vol 56, 186-197.

Boon, J.D. & Byrne, R.J. (1981). On basin hypsometry and the morphodynamic response of coastal inlet systems. *Marine Geology*, 27–48.

Bretschneider, C.L. (1963) A one-dimensional gravity wave spectrum. *In: Proceedings of a conference on ocean wave spectra*, Prentice-Hall, Englewood Cliffs, USA, pp41-56.

Cameron W. M., & Pritchard, D. W. (1963). Estuaries. In M. N. Hill (editor): *The Sea*, John Wiley and Sons, New York, Vol: 2, 306-324.

Cao, Z. D., & Wang, Y. H. (1993). Numerical modeling of hydrodynamics and sediment transport. *Tianjing University Press* (in Chinese).

Cayocca, F. (2001). Long-term morphological modeling of a tidal inlet: the Arcachon Basin Franc, *Coastal engineering*, 42: 115-142.

Changjiang Sediment Bulletin. (2001-2017). *Changjiang Press* (in Chinese).

Chen, J. Y. (1957). Notes on the development of the Yangtze Estuary. *Acta Geographica Sinica*, Vol. 23(3), 241-253.

Chen, J. Y., Yu, Z. Y., & Yun, C. X. (1959). Morphological development of the Changjiang Delta. *Acta Geographica Sinica*, Vol. 25(3), 201-220.

Chen, J. Y., Yun, C. X., Xu, H. G., & Dong, Y. F. (1979). The Developmental Model of the Chang Jiang River Estuary during last 2000 years. *Acta Geographica Sinica*, Vol. 1(1), 103-111.

Chen, Z.S. (1998). Bays of China, *China Ocean Press*, Vol. 14, ISBN 7-5027-4323-5.

Chu, A., Tai, J. A., Y, Y. T., & Zhang, W. (2005). Wave field along the Jiangsu Coast. *technique report of Hohai University and Water resource Bureau of Jiangsu* (in Chinese).

Chu, A., Wang Z.B. and De Vriend H.J. (2009). Process-based for the Yangtze Estuary, *Proc. Coastal Dynamic*, Tokyo.

Chu, A., Wang Z.B., De Vriend H.J and Stive M.J.F. (2010). A process-based approach to sediment transport in the Yangtze Estuary, *Proc. ICCE*, Shanghai.

Chu, A., Wang Z.B., De Vriend H.J and Tai J.A. (2013). Modeling processes controlling sediment transport at the mouth bar of the Yangtze Estuary, *Proc. IAHR word congress*, Chengdu.

Chu, A., Wang, Z., de Vriend, H. J., & Tai, J. (2018). Parallel Morphodynamic Modelling for the Yangtze Estuary. *Journal of Coastal Research*, 85, 641-645. doi:10.2112/si85-129.1.

Dai, Z. J., Du, J. Z., Chu, A., & Zhang, X. L. (2011). Sediment characteristics in the North Branch of the Yangtze Estuary based on radioisotope tracers. *Environmental Earth Sciences*, Vol: 62(8), 1629-1634.

Dai, Z. J., Chu, A., Li, W. H., Li, J. F., & Wu, H. L. (2013). Has Suspended Sediment Concentration Near the Mouth Bar of the Yangtze (Changjiang) Estuary Been Declining in Recent Years? *Journal of Coastal Research*, Vol:29(4), 809-818.

Dai, Z., Liu, J.T., Wei, W., Chen, J., 2014. Detection of the Three Gorges Dam influence on the Changjiang

(Yangtze River) submerged delta. *Nature Sci. Rep*. 4, 6600, DOI:10.1038/srep06600.

Dastgheib, A. (2012). Long-term Process-based Morphological Modeling of Large Tidal Basins, *PhD dissertation*, UNESCO-IHE.

Deltares (2014), Delft3D-Flow: Simulation of multi-dimensional hydrodynamic flows and transport phenomena, including sediments, *User manual*, Hydro-Morphodynamics, Delft, Netherlands.

De Vriend, H. J., Zyserman, J., Nicholson, J., Roelvink, J. A., P.Pechon, & Southgate, H. N. (1993a). Medium-term 2DH coastal area modelling. *Coastal engineering*, Vol. 21, 193-224.

De Vriend, H. J., Capobinaco, M., Chesher, T., De Swart, H. E., Latteux, B., & Stive, M. J. F. (1993b). Approach to long-term modelling of coastal morphology: a review, *Coastal engineering*, 21, 225-269.

De Vries, M. (1973). River-bed variation-aggradation and degradation, Int. Seminar on Hydraulics of Alluial Streams, *IAHR*, New Delhi, India.

Ding, P. X., & Shi, F. (2000). Prediction Model for the Erosion and Accretion in the South Passage of the Yangtze Estuary. *Research report*, East China Normal University.

Dobrochinski, J.P.H., 2009. Wave climate reduction and schematization for morphological modelling, *MSc Thesis*, Delft University of Technology, Univali University, Brazil.

Dou, X. P. (1997). Numerical model for the total load in the Yangtze Estuary. *Technique report*, Nanjing Hydraulic research institute.

Dronkers, J. (1984). Import of Fine Marine Sediment in Tidal Basins. *Netherlands Journal of Sea Research*, 10, 83-105.

Dronkers, J. (1986). Tidal asymmetry and estuarine morphology. *Netherlands Journal of Sea Research*, Vol: 20(2-3), 117-131.

Dronkers, J. (2005). Dynamics of Coastal Systems, *Advanced Series on Ocean Engineering*, Vol. 25, World Scientific, Singapore.

Du, P. J. (2007). Sediment Transport Research in Yangtze Estuary and Hangzhou Bay. *PhD dissertation*, East China Normal University.

Dalrymple, R. W., Zaitlin, B. A., & Boyd, R. (1992). Estuarine facies models: conceptual basis and stratigraphic implications. *Journal of Sedimentary Petrology*, 62, 1130-1146.

Dyer K. R., 1997, Estuaries: a physical introduction, 2nd Ed., *John Wiley and Sons*.

Edmonds, D. A., & Slingerland, R. L. (2007). Mechanics of river mouth bar formation: Implications for the morphodynamics of delta distributary networks. *Journal of Geophysical Research*, Vol. 112(F02304), 1-14.

Eisma, D. (1998). Intertidal Deposits: River Mouth, Tidal Flats and Coastal Lagoons. *CRC Press*, Boca Raton, Florida, 459pp.

Elias, E. (2006). Morphodynamics of Texel Inlet. *PhD dissertation*, Delft University of Technology.

Fan, D. D., Guo, Y. X., Wang, P., & Shi, J. Z. (2006). Cross-shore variation in morphodynamics processes of an open-coast mudflat in the Changjiang Delta, China: With an storm impacts. *Continental Shelf Research*, 26, 517-538.

Fang, G. H., & Yang, J. F. (1987). Numerical simulation for east and south in the East China Sea. *Acta Oceanologica Sinica*, Vol. 9(4).

Friedrichs, C.T., and D.G. Aubrey (1988), Non-linear tidal distortion in shallow well-mixed estuaries: a synthesis, Estuarine, *Coastal and Shelf Science*, 27, 521-545.

Friedrichs, C.T. & Aubrey, D.G. (1994). Tidal propagation in strongly convergent channels. Journal of *Geophysical Research*, Vol. 99 (C2), 3321–3336.

Galappatti, G. and Vreugdenhil, C.B. (1985). A depth-integrated model for suspended sediment transport, *Journal*

of Hydraulic Research, Vol. 23(4): 359-377.

Gao, M. (2008). A Pre-feasibility Study of Navigation Channel Regulation Works in North Channel, Yangtze Estuary. *MSc Thesis*, UNESCO-IHE.

Gelfenbaum, G., Roelvink, J. A., Meijs, M., & Ruggiero, P. (2003). process-based morphological molding of Grays Harbor inlet at decadal time scales. in: proceedings of *Coastal Sediments* '03, ASCE, Clearwater Beach, Florida.

Gong, Z., Wang, Z., Stive, M. J. F., Zhang, C., & Chu, A. (2012). Process-Based Morphodynamic Modeling of a Schematized Mudflat Dominated by a Long-Shore Tidal Current at the Central Jiangsu Coast, China. *Journal of Coastal Research*, 285, 1381-1392. doi:10.2112/jcoastres-d-12-00001.1.

Groen, P. (1967). On the residual transport of suspended matter by an alternating tidal current. *Netherlands Journal of Sea Research*, 3(4), 564-574.

Grunnet, N.M., Walstra, D. J. R. and Ruessink, B.G. (2004). Process-based modelling of a shoreface nourishment, *Coastal Engineering*, Vol 51: 581-607.

Guan, X. W., Chen, Y. Z., Lin, Y. A., & Li, Y. (1992). Field micro-obsevation on the sediment flocs in the Changjiang Estuary. *Journal of Sediment Research*, Vol. 3, 54-59.

Guo, L., & He, Q. (2011). Freshwater flocculation of suspended sediments in the Yangtze River, China. *Ocean Dynamics*, 61(2-3), 371-386. doi:10.1007/s10236-011-0391-x.

Guo, L., M. van der Wegen, J. A. Roelvink,and Q. He. (2014). The role of river flow and tidal asymmetry on 1-D estuarine morphodynamics, *J. Geophys. Res. Earth Surf.*, 119, 2315–2334, doi:10.1002/2014JF003110.

Guo, L., M. van der Wegen, D. Roelvink, and Q. He. (2015). Exploration of the impact of seasonal river discharge variation on long-term estuarine morphodynamic behavior, *Coastal Engineering*, 95, 105–116, http://dx.doi.org/10.1016/j.coastaleng.2014.10.006.

Guo, L., M. van der Wegen, Z. B. Wang, D. Roelvink, and Q. He (2016). Exploring the impacts of multiple tidal constituents and varying river flow on long-term, large-scale estuarine morphodynamics by means of a 1-D model, J. *Geophys. Res. Earth Su*rf., 121, 1000–1022, doi:10.1002/2016JF003821.

Han, Z. C., Dai, Z. H., & Li, G. B. (2003). Regulation and exploitation of Qiantang Estuary. *China Water & Power Press.*

Hasselmann, K., Barnett, T. P., Bouws, E., Carlson, H., Cartwright, D. E., Enke, K., Walden, H. (1973). Measurements of wind-wave growth and swell decay during the Joint North Sea Wave Project (JONSWAP). *Deutches Hydrographisches Institut*.

Hu, F. X., Hu, H., Gu, G. C., Su, C., & Gu, X. J. (1995). Salinity fronts in the Changjiang River Estuary. *Oceanologia ET Limnology Sinica Supplement*, 26(5), 23-31.

Hu, K., Ding, P. X., Wang, Z. B., & Yang, S. L. (2009). A 2D/3D hydrodynamic and sediment transport model for the Yangtze Estuary, China. *Journal of Marine System*, Vol: 77(1-2), 114-136.

Huang, G. (2007). Study on the Character of Flow and Sediment Exchange and Transport between Changjiang Estuary and Hangzhou Bay. *Msc Thesis*, East China Normal University.

Hoitink, A.J.F., Hoekstra, P. & Van Maren, D.S. (2003). Flow asymmetry associated with astronomical tides: Implications for the residual transport to sediment. *Journal Geophysical Research*, Vol. 108 (C10), 3315.

Kong, Y., He, S., Ding, P., & Hu, K., (2004). Characteristics of temporal and spatial variation of salinity and their indicating signif icance in the Changjiang Estuary. *Acta Geographica Sinica*, Vol. 26 No.4, 9-18.

Krone R.B., (1962). Flume Studies of the Transport of Sediment In Estuarial Shoaling Processes. *Final Report, Hydraulic Engineering Laboratory and Sanitary Engineering Research Laboratory*, Berkely, CA; prepared for US Army Engineering District, San Francisco, San Francisco, CA, under US Army

Contract No. DA-04-203.

Krone R.B., (1963). A Study of Rheological Properties of Estuarial Sediments. *Technical Bulletin No. 7, Committee on Tidal Hydraulics, Corps of Engineering, US Army Engineer Waterways Experiment Station*, Vicksburg, MS.

Kuang, C. P., Liu, X., Gu, J., Guo, Y. K., Huang, S. C., Liu, S. G., . . . Sun, B. (2013). Numerical prediction of medium-term tidal flat evolution in the Yangtze Estuary: Impacts of the Three Gorges project. *Continental Shelf Research*, 52, 12-26.

Lanzoni, S. & Seminara, G., (1998). On tide propagation in convergent estuaries. *Journal of Geophysical Research*, C103, 30793–30812.

Lanzoni, S., and Seminara, G., (2002). Long-term evolution and morphodynamic equilibrium to tidal channels, *Journal of Geophysical Research*, 107, C13001, doi:10.1029/2000JC000468.

Latteux, B. (1995). Techniques for long-term morphological simulation under tidal action, *Marine Geology*, Vol: 126(1-4), 129-141.

Lely, M. (2007). Hydraulic roughness in sediment-laden flow. *Msc Thesis*, Delft University of Technology.

Lesser, G.R. (2009). An approach to medium-term coastal morphological modelling, *PhD thesis, Delft University of Technology*, ISBN 978-0-415-55668-2.

Lesser, G. R., Roelvink, J. A., Kester, J. V., & Stelling, G. S. (2004). Development and validation of a three-dimensional morphological model. *Coastal engineering*, Vol: 51(8-9), 883-91.

Li, M. G. (2006). A review on mathematical models of sediment in coastal and estuarine water. *The Ocean engineering*, Vol.24(1), 139-154.

Lin, C. K. (1984). A study on the source and quantity of sediment at the Yangtze River Estuary. *Journal of Sediment Researc*h, Vol.2, 22-32.

Lin, Y. A., Tang, R. Y., Li, Y., Dong, H. L., Guan, X. W., & Chen, Y. Z. (1995). Biogeochemical Characteristics of Biogenic elements and its relationship to the flocculation in the Yangtze Estuary. *Acta Oceanologica Sinica*, Vol. 17(5), 65-72.

Liu H., He Q., Wang Z. B., Weltje G. J., & Zhang, J. (2010). Dynamics and spatial variability of near-bottom sediment exchange in the Yangtze Estuary, Estuarine, *Coastal and Shelf Science*, Vol. 86, 322-330.

Liu, J. (1997). Coastal sediment movement and morphology *Technique report*, Nanjing Hydraulic research institute。

Luan Hua Long, Ping Xing Ding, Zheng Bing Wang & Jian Zhong Ge (2017). Process-based morphodynamic modeling of the Yangtze Estuary at a decadal timescale: Controls on estuarine evolution and future trends, *Geomorphology*, doi: 10.1016/j.geomorph.2017.04.016.

Luo, X. F. (2003). numerical modeling for salnity in the Yangtze Estuary. *PhD dissertation*, Nanjing hydraulic research Institute.

Marine Atlas of East China Sea (1992). *China Ocean Press* (in Chinese).

Milliman, J. D., Shen, H. T., Yang, Z. S., & Meade, R. H. (1985). Transport and deposition of river sediment in the Changjiang estuary and adjacent continental shelf. *Continental Shelf Research*, Vol: 4(1-2), 37-45.

Partheniades, E., (1962). A study of erosion and deposition of cohesive soil in salt water. *PhD Thesis*, University of California, Berkely, California, USA.

Partheniades, E., (1965). Erosion and Deposition of Cohesive Soils, *Journal of the Hydraulic Division*, ASCE, no. HY1, vol 91.

Pawlowicz, R., Beardsley B., Lentz S., (2002). Classical tidal harmonic analysis with error analysis in MATLAB using T_TIDE. *Computers & Geosciences*, 28, 9. doi:DOI: 10.1016/S0098-3004(02)00013-4.

Perillo, G. M. E. (1995). Geomorphology and Sedimentology of Estuaries. *Development in Sedimentology*, 53,

Elsevier.

Pingree, R.D. & Griffiths, D.K. (1979). Sand transport paths around the British Isles resulting from M2 and M4 tidal interactions. *Journal of the Marine Biological Association of the U.K*., 59" 497-513.

Postma, H. (1967). Sediment transport and sedimentation in the estuarine environment. In, *Estuaries,* edited by G.H. Lauff, AAAS, Washington, 158-179.

Ranasinghe, R., and C. Pattiaratchi. (2000). Tidal inlet velocity asymmetry in diurnal regimes, *Continental Shelf Research*, 20, 2347-2366.

Ridderinkhof, H. (1997). The effect of tidal asymmetries on net transport of sediments in the Ems Dollard estuary. *Journal of Coastal Research*, 41–48.

Roelvink, J. A., & Van Banning, G. K. F. M. (1994). Design and development of Delft3D and application to coastal morphodynamics. *Hydoinformatics*, Vol: 94, 451-455.

Roelvink J.A. (2006). Coastal morphodynamic evolution techniques, *Coastal engineering*, Vol: 53(2-3), 277-287.

Roelvink J.A., R., A.J.H.M. (2012). A guide to coastal morphology modeling, *Advances in Coastal and Ocean Engineering*, World Scientific Publishing Company, Singapore.

Ross, D. A. (1995). Introduction to Oceanography. *Harper Collins College Publishers*, New York.

Rouse, H., 1938. Experiments on the mechanics of sediment suspension. *Proceedings of the Fifth International Congress for Applied Mechanics*, Cambridge, Massachusetts, 550–554.

Sanford, L. P. (2008). Modeling a dynamically varying mixed sediment bed with erosion, deposition, bioturbation, consolidation, and armoring. *Computers & Geosciences*, 34(10), 1263-1283. doi:10.1016/ j.cageo. 2008.02.011

Schuttelaars, H.M. & De Swart, H.E. (2000). Multiple morpho-dynamic equilibria in tidal embayments. *Journal of Geophysical Researc*h, C 105, 24105–24118.

Shao,S.L.(1994) Converting of accumulation frequency of wave height, *Port Engineering Technology*, No.3, 12-13 (in Chinese).

Shen, H. T., He, S. L., Pan, D. A., & Li, J. F. (1992). A study of turbidity maximum in the Changjiang Estuary, . *Acta Geographica Sinica*, vlo:47(5), 472-479.

Shen, H. T., Wu, J. X., Wang, P. C., Wu, H. L., Liu, X. C., Fu, R. B., & Huang, Q. H. (2001). Material flux of the Changjiang Estuary. *China Ocean Press* (in Chinese).

Shi, Z., Zhou, H. J., Eitterim, S. L., & Winterwerp, J. C. (2004). Settling velocities of fine suspended particles in the Changjiang Estuary, China. *Journal of Asian Earth Sciences*, Vol:22, 245-251.

Song, D.H., X.H. Wang, A.E. Kiss, and X.W. Bao (2011), The contribution of tidal asymmetry by different combinations of tidal constituents, *Journal of Geophysical Research*, 116, C12007, doi:10.1029 /2011JC007270.

Speer, P.E. & Aubrey, D.G. (1985). A study of non-lineartidal propagation in shallow inlet/estuarine systems, Part II: theory. *Estuarine Coastal and Shelf Science*, 21,207–224.

Steijn R.C. (1992). Input filtering techniques for complex morphological models, *Delft Hydraulics, Report*.

Stevens, M. A., Simmons, D. B., & Richardson, E. V. (1975). Non-equilibrium river form, *Journal of the Hydraulic Division*, ASCE, Vol. 101(5), 557-566.

Su, J. L., & Wang, K. S. (1986). The Suspended Sediment Balance in Changjiang Estuary. *Estuarine, Coastal and Shelf Science*, Vol. 23(1986), 81-98.

Tan, Z. W., Fan, Q. J., Zheng, W. Y., & Zhu, J. F. (2009). Analysis of reasons for the siltation in North Passage of Yangtze Estuary. *Port & Waterway Engineering*, No. 6, 91-102.

Tang, J. (2007). Characteristics of fine cohesive sediment's flocculation in the Changjiang Estuary and its adjacent sea area. *Msc Thesis*, East China Normal University.

Teisson, C., Ockenden, M., Le Hie, P., Kranenburg, C., & Hamm, L. (1993). Cohesive sediment transport processes. *Coastal engineering,* Vol. 21, 129-162.

Tonnon, P. K., Rijn, L. C. V., & Walstra, D. J. R. (2007). The morphodynamic modelling of tidal sand waves on the shoreface. *Costal Engineering*, Vol. 54(4), 279-296.

Van de Kreeke, J., & Robaczewska, K. (1993). Tide-induced residual transport of coarse sediment application to the ems estuary. *Netherlands Journal of Sea Research*, 31(3), 209-220.

Van de Kreeke, J. & Dunsbergen, D.W. (2000). Tidal asymmetry and sediment transport in the Frisian Inlet. In: Yanagi, T. (Ed.), Interactions Between Estuaries, Coastal Seas and Shelf Seas. Terra Scientific Publishing Company, Tokyo, 2000.

Van der Spek, A.J.F. (1997). Tidal asymmetry and long-term evolution of Holocene tidal basins in the Netherlands: simulation of paleo-tides in the Schelde estuary. *Marine Geology*, 71–90.

Van der Wegen, M. (2010). Modeling morphodynamics evolution in alluvial estuaries, *PhD dissertation*, UNESCO-IHE.

van der Wegen, M., Jaffe, B., Foxgrover, A., & Roelvink, D. (2016). Mudflat Morphodynamics and the Impact of Sea Level Rise in South San Francisco Bay. *Estuaries and Coasts*, 40(1), 37-49. doi:10.1007/s12237-016-0129-6.

Van Kessel, T., Winterwerp, H., Van Prooijen, B., Van Ledden, M., & Borst, W. (2011). Modelling the seasonal dynamics of SPM with a simple algorithm for the buffering of fines in a sandy seabed. *Continental Shelf Research*, 31(10), S124-S134. doi:10.1016/j.csr.2010.04.008

Van Ledden, M. (2003). Sand-Mud segregation in estuaries and tidal basins. *PhD dissertation,* Delft University of Technology.

Van Rijn, L.C. (1986). Sediment transport, Part II: Suspended load transport. *Journal of Hydraulic Engineering,* Vol. 110(11), 1613-1641.

Van Rijn, L. C. (1993). Principles of sediment transport in rivers, estuaries and coastal seas. *AQUA Publication*, Amsterdam.

Van Rijn, L. C. (2000). General View on Sand Transport by Currents and Waves: Data Analysis and Engineering Modeling for Uniform and Graded Sand TRANSPOR2000 and CROSMOR2000 Models. *Report*, WL Delft Hydraulics.

Van Rijn, L. C. (2007a). Unified View of Sediment Transport by Currents and Waves. I: Initiation of Motion, Bed Roughness, and Bed-Load Transport. *Journal of the Hydraulic Division*, ASCE, Vol. 13(6), 649-667.

Van Rijn, L. C. (2007b). Unified View of Sediment Transport by Currents and Waves. II: Suspended Transport. *Journal of the Hydraulic Division*, ASCE, Vol. 133(6), 668-689.

Van Rijn, L. C., Walstra, D. J. R., & M., V. O. (2007). Unified View of Sediment Transport by Currents and Waves. IV: Application of Morphodynamic Model. *Journal of the Hydraulic Division*, ASCE, Vol. 133(7), 776-793.

Van Vuren, S. (2005). Stochastic modelling of river morphodynamics, *PhD dissertation*, Delft University of Technology.

Van Straaten, L. M. J. U. & Kunen, P.H. (1957), Accumulation of fine-grained sediments in the Dutch Wadden Sea, *Geologie en Mijnbouw*, 19 329-354.

Wang, Y. H., Ridd, P. V., Wu, H. L., Wu, J. X., & Shen, H. T. (2007). Long-term morphodynamics evolution and equilibrium mechanism of a flood channel in the Yangtze Estuary (China). *Geomorphology*, Vol. 99, 130-138.

Wang, Z. B. (1992). Theoretical analysis on depth-integrated modelling of suspended sediment transport, *Journal of Hydraulic Research*, Vol. 30(3): 403-421.

Wang, Z. B. (1994). Hangzhou Bay Environmental Study Hydrodynamic Modeling. *Repor*t, WL Delft Hydraulics.

Wang, Z. B., Jeuken, M. C. J. L., & De Vriend, H. J. (1999). Tidal asymmetry and residual sediment transport in estuaries. *Report*, WL Delft Hydraulics.

Wei, W., Dai, Z., Mei, X., Liu, J. P., Gao, S., & Li, S. (2017). Shoal morphodynamics of the Changjiang (Yangtze) estuary: Influences from river damming, estuarine hydraulic engineering and reclamation projects. *Marine Geology*, 386, 32-43. doi:10.1016/j.margeo.2017.02.013.

Winterwerp, J. C. (2001). Stratification effects by cohesive and non-cohesive sediment. *Journal of Geophysical Research*, Vol. 106(C10), 559-574.

Winterwerp J. C., & Van Kesteren W. G. M., (2004). Introduction to the Physics of Cohesive Sediment in the Marine Environment. *Developments in Sedimentology*, Vol. 56, 2004, 466 p.

Woodworth, P.L., D.L. Blackman, D.T. Pugh, and J.M. Massie (2005), On the role of diurnal tides in contributing to asymmetries in tidal probability distribution function in areas of predominantly semi-diurnal tide, *Estuarine, Coastal and Shelf Science*, 64(2-3), 235-240.

Wu, H., Zhu, J. R., Chen, B. R., & Chen, Y. Z. (2006). Quantitative relationship of runoff and tide to saltwater spilling over from the North Branch in the Changjiang Estuary: A numerical study. Estuarine, *Coastal and Shelf Science*, Vol. 69, 125-132.

Xu, F. M., & Zhang, C. K. (2004). Study of the effect of storm wave on rapid deposition of the Yangtze River Estuary channel. *Journal of hydrodynamics*, Vol. 19(2), 137-143.

Yang, S. L., Ding, P. X., & Chen, S. L. (2001). Changes in progradation rate of the tidal flats at the mouth of the Changjiang žYangtze/ River, China. *Geomorphology*, Vol. 38(2001), 167-180.

Yang, S. L., Belkinb, I. M., Belkinac, A. I., Zhao, Q. Y., Zhu, J., & Ding, P. X. (2003). Delta response to decline in sediment supply from the Yangtze River: evidence of the recent four decades and expectations for the next half-century. Estuarine, *Coastal and Shelf Science*, Vol. 57(4), 689-699.

Yang, S. L., Zhang, J., Zhu, J., Smith, J. P., Dai, S. B., Gao, A., & Li, P. (2005). Impact of dam on the Yangtze River sediment supply to the sea and delta intertidal wetland response. *Journal of Geophysical Research*, Vol. 110(F03006), 1-12.

Yang, S. L., Li, M., Dai, S. B., Liu, Z., Zhang, J., & Ding, P. X. (2006). Drastic decrease in sediment supply from the Yangtze River and its challenge to coastal wetland management. *Geophysical research letters*, vol. 33, 1-4.

Yi, J. H., & Ye, X. X. (1983). 2DH numerical model of the salinity in the Yangtze Estuary. *Technique report for the waterway management of the Yangtze Estuary*.

Yun, C.X. (2004). Recent development of the Changjiang Estuary, *China Ocean Press*, ISBN 7-5027-6219-1.

Zhang, J.L., 1995, Numerical model for storm surge forecast, Numerical model for forecasting astronomic tide and storm surge, The Ministry of Water Resources China, *technique report* No.2 (In Chinese).

Zhang, R., (1997). River dynamics, Lecture note, *China Water & Power Press* (in Chinese).

Zhao, J., Guo, L., He, Q., Wang, Z. B., van Maren, D. S., & Wang, X. (2018). An analysis on half century morphological changes in the Changjiang Estuary: Spatial variability under natural processes and human intervention. *Journal of Marine Systems*, 181, 25-36. doi: 10.1016/j.jmarsys.2018.01.007.

Zhang, W. (2005). Numerical Modeling of Tides Wave in Margin Seas near China. *Msc Thesis*, Hohai University.

List of Figures

List of Tables

List of Main Symbols

Symbol	Unit	Description
A	[m^2]	Cross section area
a	[m]	Reference height as defined by Van Rijn
C	[kg/m3]	Mass concentration
C	[$m^{1/2}/s$]	Chézy coefficient
C_a	[kg/m^3]	Mass concentration at reference height a
c_b	[kg/m^3]	Average near-bed sediment concentration
d	[m]	Sediment grain diameter
D	[$kg/m^2/s$]	Deposition flux
D_{50}	[µm]	Mean sediment diameter
E	[$kg/m^2/s$]	Erosion flux
f	[-]	Coefficient for sediment transport formula
g	[m/s^2]	Acceleration of gravity
h	[m]	Water depth
$H_{1/10}$	[m]	Average height of 10 highest waves in a wave train
H_s	[m]	Significant wave height
M	[$kg/m^2/s$]	User-specified erosion parameter
n	[$s/m^{1/3}$]	Manning coefficient
N	[-]	Number of the other tidal constituents
P	[m^3]	Tidal prism
R	[-]	Coefficient for linear regression analysis
s	[-]	Specific sediment gravity (=2.65)
S	[kg/s]	Sediment transport rate
T	[°C]	Temperature
$\bar{u}$	[m/s]	Depth averaged velocity
u_i	[m/s]	Amplitude of the other tidal current constituents
u_*	[m/s]	Bed friction velocity
u_{M0}	[m/s]	Eulerian residual flow
u_{M2}	[m/s]	Amplitude of M_2 tidal current constituent
w	[m/s]	Sediment fall velocity
α	[°]	Phase of S_2 relative to φ_{M2}
α_1	[°]	Phase of S_2 relative to φ_{M2}
α_2	[°]	Phase of N_2 relative to φ_{M2}
α_3	[°]	Phase of MS_4 relative to φ_{M2+S2}
α_4	[°]	Phase of MN_4 relative to φ_{M2+N2}
α_5	[°]	Phase of K_1 relative to $\varphi_{M2}/2$
α_6	[°]	Phase of O_1 relative to $\varphi_{M2}/2$
β	[-]	Constant (Rouse profile)
β	[°]	Phase of M_4 relative to φ_{M2}
γ	[°]	Phase of M_6 relative to φ_{M2}
γ	[kg/m^3]	Volume weight of water

γ_s	[kg/m^3]	Volume weight of sediment
ε_i	[-]	Normalized tidal current constituent ***i*** by M_2
ε_{M0}	[-]	Normalized Eulerian residual flow by M_2 tidal current constituent
φ_{bo}	[-]	Biological and organic material
$\varphi_{cohesive}$	[-]	Cohesive particle-particle interaction effects
φ_i	[°]	Phase of tidal current constituent ***i*** relative to M_2
φ_{M2}	[°]	Phase of M_2 tidal current constituent
$\varphi_{packing}$	[-]	Packing effects
$\Delta\sigma$	[°/hour]	Beat frequency between ω_{M2} and ω_{S2}
$\Delta\sigma1$	[°/hour]	Beat frequency between ω_{M2} and ω_{S2}
$\Delta\sigma2$	[°/hour]	Beat frequency between ω_{M2} and ω_{N2}
$\Delta\sigma3$	[°/hour]	Beat frequency of $\omega_{M2}/2$ and ω_{K1}
ω_i	[°/hour]	Angular frequency of the other tidal current constituents
ω_{M2}	[°/hour]	Angular frequency of M_2
ω_s	[m/s]	Sediment settling velocity in still water
ω_s	[m/s]	(hindered) settling velocity
κ	[-]	von Karman constant (=0.4)
ν	[m^2/s]	Kinematic viscosity
$\tau_{c,b}$	[N/m^2]	Bed shear stress due to current
$\tau_{cr,e}$	[N/m^2]	Critical shear stress for erosion
$\tau_{cr,d}$	[N/m^2]	Critical shear stress for deposition
$\tau_{cr,o}$	[N/m^2]	Critical shear stress for erosion of cohesive particle

Acknowledgements

This PhD research has been carried out from 2008-2019 at the Department of Civil Engineering and Geoscience of Delft University of Technology (DTU) and at the College of Harbor, Coastal and Offshore Engineering of Hohai University (HHU, China). The National Nature Science Foundation of China (NSFC grant No. 51620105005) and the National R&D Projects of China (No. 2017YFC0405401) financially supported this research at HHU for the period 2018-2019. The Lamminga Fund of DTU (No. Lamm-19-05-pv) facilitated me to come back to Delft for finalizing and defending the PhD thesis. In the period 2013-2017 the work was partly financed by the Sim.coast project (2014.01-2014.10). The China Scholarship Council (CSC) fully financed the work at DTU in the period 2008-2012 with co-financial support from the Lamminga Fund and KNAW (No. PSA-SA-E-02).

During my PhD research in Delft, I was privileged to work with and get support from a large community of scientists and professionals. I would like to thank a lot of persons, hoping to forget nobody. The duration of the work is so long that many things have been changed. Especially, most of those persons now have different positions and titles with respect to the moment when they first appeared on the sense. Therefore, I would not mention any title or qualification on purpose. I feel that it is easier to list them in the order of their appearance,

The first person that I want to thank is Huib de Vriend (Deltares and DTU). He gave me the opportunity to start to do research in the Netherlands. He was my supervisor of my Master thesis and later became my first official PhD supervisor. He kept contributing to the thesis by making correction and providing constructive comments, as has done more than enough as a promotor. However, due to my personal circumstance my study was delayed too long after his retirement. I regret very much that he cannot sit as my promotor at my defence. I am grateful for his efforts and attentions and I want to heartily thank to him.

I thank Changkuan Zhang (HHU), who initiated me in the subject of research work in coastal seas and estuaries. He was an enthusiastic supervisor for my Master & PhD study and work at HHU. He has high expectation to me and keeps supporting me with no thought of rewards, although he might be disappointed by my low research progress. I also regret that the work made him waiting too long to attend my defence as a committee member, as it is too risky for him to travel overseas.

My direct supervisor, Zhengbing Wang, deserves particular thanks. He was an exceptionally good supervisor of my Master thesis and inspired me to start this PhD. I am grateful for many scientific discussions we have had during my PhD work. He also patiently taught me how to address scientific problems and write scientific papers. With his impressive personality and wide experience, he became the example to follow and made me an enthusiastic estuarine engineer and researcher. He kept encouraging me and gave decisive push to complete this PhD thesis after so many years.

Marcel Stive deserves special thanks. I think all our CSC students have to thank to those professors, especially him, for the effort to get extra fund from DTU to finance our works. He is also an enthusiastic mentor to all the young researchers, as he conveyed us his passion for

research.

I am grateful to Stefan Aarninkhof not only for taking the promotor position for my defence but also for sharing his experience to finalize the PhD research during his work. His example gave me the decisive push to complete this work.

Furthermore, I want to express my thanks to Yongping Chen (HHU). His financial support by SimoCoast project allowed me stay at Delft in 2014, when I made an important progress in my work. Also, he took good care of me when I worked at HHU in recent years.

A number of professionals contributed to the work through their participation in fruitful discussions. They are Dano Roelvink, Han Winterwerp, Leo van Rijn, Huib de Swart, Dirk-Jan Walstra, Mick van der Wegen, Bram van Prooijen, Bas van Maren and Zhijun Dai. I am indebted to Jacobus van der Kreeke and four other anonymous reviewers for their critical reviews that helped to improve the papers in this thesis. I want to express my thanks to Mariette van Tilburg for the translation of Dutch summary and to Jiacheng Zhou for the language check.

The Master students who contributed to this work deserve a big 'thank you'. They are Bo Jiang (2015, DTU), Danghan Xie (2017, HHU), Tianyi Zhou (2018, HHU) and Yi Xu (2019, HHU).

Also many friends contributed indirectly. I cannot list all the colleagues at DTU and HHU. Some of them deserve great thanks, because I could share my everyday life with them. First thanks to my three office mates, Matthieu, Sierd and Martijn for their helping, hosting and jokes, especially for the big wooden boat on my desk. They made me feel at home when being at work. And some other colleagues, Marije, Meno, Judith, Joao, Roeland, Mark, Ronald, Saulo, Cees, Franca, Bas, Jaap, Gerben, Wei, Hong, Peng, Min, Zhan, Fan, Hua, Lu, Gengsheng, Qinghua, Yu, Shun, Wei, Ziru, Liang, Dongfeng, Leicheng, Yuanyang, Zhi, Stefen, Jianfeng, Jingjing and many others. Without this group of friends, the Delft rainy and cold days would have been even darker.

In my personal life I am grateful to family and friend, who provided support, perhaps unknowingly. They sometimes inquired my research progress and sometimes did not mention it at all wisely. I am grateful to my parents, Youming and Xiaomei, my brother, Biao, and my sister, Hui, for the inspiring and supporting atmosphere. Last but not least I would like to thank my wife and my kid for their loving support, especially during the last two years of finishing, and for just being there for me.

Curriculum Vita

Ao Chu was born on May 14th, 1976 in Shanghai, China. He grew up in Pudong, a Shanghai suburb, where he completed primary school, middle school and high school by 1994. He started his study on Coastal Engineering at Hohai University in September 1994. After he graduated as a BSc in July 1998, he has been employed as an academic staff at College of Harbor, Coastal and Offshore Engineering at Hohai University. From July 1999 to June 2000 he was temporarily transferred from Hohai University to Changjiang Water Resources Committee, where he worked as an engineer and was involved in designing and supervising the construction of the ship-lock of the Three Gorges Dam. He went to Delft in October 2000 for his Master study at UNESCO-IHE. He got his MSc in May 2002 with the thesis about the extreme hydrodynamics of the Yangtze Estuary. He went back to Hohai University and worked there until 2007. He started his PhD research in 2008, at Delft University of Technology, Faculty of Civil Engineering and Geoscience, Department of Hydraulic Engineering. He full-time worked on his PhD research of morphodynamics of the Yangtze Estuary at Delft until 2012. Meanwhile he was still employed by Hohai University. He went back to his job at Hohai University in 2012 with the draft thesis. He worked at Hohai University focusing on the researches relevant to his PhD work on the Yangtze Estuary. He was involved in one 973 Project, one Science and Technology Support Project and two National R&D Projects of China. At the same time, he kept working on his PhD work at spare time resulting in this thesis.

List of author's publications

Journal papers

Chu, A., Wang, Z., de Vriend, H. J., & Tai, J. (2018). Parallel Morphodynamic Modelling for the Yangtze Estuary. *Journal of Coastal Research*, 85, 641-645. doi:10.2112/si85-129.1 (this thesis, part of Chapter 6)

Zhu Y.L, Chen W.L, Chu A. (2018). The analytical model of estuarine tidally averaged quasi-steady salinity, *Oceanologia et Limnologia Sinic*, Pages 541-550, vol 49, No.3.

Chu A., Wang Z.B. and De Vriend H.J. (2015), Analysis on residual coarse sediment transport in estuaries, Estuarine, Coastal and Shelf Science, Pages 194–205 (this thesis, Chapter 5)

Gong, Z., Wang, Z., Stive, M. J. F., Zhang, C., & Chu, A. (2012). Process-Based Morphodynamic Modeling of a Schematized Mudflat Dominated by a Long-Shore Tidal Current at the Central Jiangsu Coast, China. *Journal of Coastal Research*, 285, 1381-1392. doi:10.2112/jcoastres-d-12-00001.1.

Dai Z.J., Chu A., Li W.H., Wu H.L., 2012, Has suspended sediment concentration near the mouth bar of the Yangtze (Changjiang) Estuary been declining in recent years? Journal of Coastal Research, doi: 10.2112/JCOASTRES-D-11-00200.1.

Dai Z.J., Chu A., Stive M.J.F., Yao H.Y., 2012, Impact of the Three Gorges Dam overruled by an extreme climate hazard, Natural Hazards Review, doi: http://dx.doi.org/10.1061/(ASCE)NH.1527-6996.0000081

Dai Z.J., Chu A., Stive M.J.F., Li J.F., 2011, Is the Three Georges Dam the cause behind the 2006 extreme low suspended sediment discharge into the Yangtze (Changjiang) estuary? Hydrological Sciences Journal 56(7): 1280-1288

Dai Z.J., Du J.Z., Chu A., Zhang X.L., 2011, Sediment characteristics in the North Branch of the Yangtze Estuary based on radioisotope tracers. Environmental Earth Sciences 62: 1629-11634.

Dai Z.J., Chu A., Stive M.J.F., Zhang X.L., Yan H., 2011, Unusual salinity conditions in the Yangtze Estuary in 2006: impacts of an extreme drought or of the Three Gorges Dam? Ambio, doi: 10.1007/s13280-011-0148-2.

Dai Z.J., Du J.Z., Chu A., Li J.F., Chen J.Y. and. Zhang X.L, 2010, Groundwater discharge to the Changjiang River, China, during the drought season of 2006: effects of the extreme drought and the impoundment of the Three Gorges Dam. Hydrogeology Journal 18: 359-369.

Dai Z.J., Chu A., Du J.Z., Stive M.J.F., and Yan H., 2010, Assessment of extreme drought and human interference on baseflow of the Yangtze River, Hydrological Processes 24: 749-757.

Manuscripts in preparations/under review

Chu A., Wang Z.B. and De Vriend H.J., Morphodynamic Modelling for the Yangtze Estuary – A Mor-Merge Approach with Multi-Discharge Levels, submitted to Estuarine Coastal & Shelf Science

Chu A. Xu Y. Wang Z.B. and Chen Y.P, Analytical model of tidally net total-load sediment transport, submitted to ICS2020.

Conference proceedings/(published)abstracts/presentations

Chu A., Tai J. and Tan Y., (2018). Effect of Storm Surge Barrier at the North Branch on the Extreme High Water Level in Yangtze Estuary, Proc. ISOPE2018, Sapporo, Japan.

Chu A. and Tai J. (2015). Analytical approach to long-term coarse sediment transport in estuaries, IAHR Den Hague (abstract)

Chu A. Tai J. and Gu S., (2014). Influence of the Three Gorges Dam on Sediment Budget at Mouth Bar of the Yangtze Estuary' Proc PACOMS, 2014 (presentation).

Chu A., Wang Z.B., De Vriend H.J and Tai J.A. (2013). Modeling processes controlling sediment transport at the mouth bar of the Yangtze Estuary, Proc. IAHR word congress, Chengdu. (this thesis, part of Chapter 4)

Grasmeijer B., Chu A., van Rijn L. (2011). Application and comparison of two different fine cohesive sediment transport models in delft3d. Proc. Coastal Sediments 2011, Miami.

Chu A., Wang Z.B., De Vriend H.J and Stive M.J.F. (2010). A process-based approach to sediment transport in the Yangtze Estuary, Proc. ICCE, Shanghai. (this thesis, part of Chapter 4)

Chu A., Wang Z.B. and De Vriend H.J. (2009). Process-based for the Yangtze Estuary, Proc. Coastal Dynamic, Tokyo. (this thesis, part of Chapter 3)